UNIVERSITY OF SOUTHAMPTON

FACULTY OF MEDICINE

Cancer sciences

Understanding the role for Fc gamma receptors in response to anti-CD20 monoclonal antibody therapy

by

Thomas R. W. Tipton

Thesis for the degree of Doctor of Philosophy

September 2015

UNIVERSITY OF SOUTHAMPTON

ABSTRACT

FACULTY OF MEDICINE

Cancer Sciences

Thesis for the degree of Doctor of Philosophy

Understanding the role for Fc gamma receptors in response to anti-CD20 monoclonal antibody therapy

Research into cancer therapeutics has utilized the antigen specificity of antibodies to provide targeted cancer treatments. One notable therapeutic is rituximab, a chimeric human IgG1 antibody that has specificity to the CD20 protein on the surface of B cells. This antibody is currently used in the treatment of leukaemia and lymphoma. However, due to reasons not fully understood patients often relapse and become resistant to therapy. Therefore an increasingly important area of research is to uncover the key mechanisms of action of anti-CD20 antibodies.

It has been demonstrated that antibody Fc: FcγR interactions are critical for effective anti-CD20 antibody dependent cellular cytotoxicity (ADCC). During this project the role of Fc: FcγR interactions and their ability to mediate anti-CD20 mediated B cell depletion was explored. We assessed two different types of anti-CD20 antibody: type I, rituximab has been shown to have high levels of antibody:antigen internalisation following CD20 engagement. This process has been termed antigenic modulation. In contrast, type II, obinutuzumab do not display a high level of antigenic modulation. We assessed the ability of rituximab and obinutuzumab to deplete normal and malignant B cells. Additionally, macrophages and NK cells have both been implicated as key FcγR expressing effector cells. Therefore, we assessed rituximab and obinutuzumab using *in vitro* macrophage or NK cell mediated ADCC assays and looked at the impact antigenic modulation had on effector cell activity. *In vivo* analysis revealed that obinutuzumab give more sustained B cell depletion compared to

rituximab. Furthermore, we demonstrate that this sustained depletion is due to a lack of antigenic modulation preventing NK cell and macrophage mediated ADCC. In contrast rituximab undergoes significant internalisation preventing both NK cell and macrophage mediated ADCC.

In addition, it has been well documented that the tumour microenvironment will affect the phenotype of the surrounding stroma, particularly macrophages. Established tumours are typically associated with low levels of apoptosis. Therefore, we investigated the impact dysregulated apoptosis had on the ability of macrophages to orchestrate ADCC. Using apoptosis resistant Vav Bcl-2 mice, as well as other apoptosis defective strains, we demonstrate that there is a decrease in the activatory to inhibitory FcγR ratio on effector cell subsets. This was largely due to an increase in inhibitory FcγRIIb. Subsequent analysis revealed that an increase in FcγRIIb may be due to the autoimmune-like phenotype of the Vav Bcl-2 mouse.

This knowledge will be beneficial to future consideration of antibody selection and provides further avenues of research into antibody and FcγR interactions.

Table of Contents

List of tables

List of figures

DECLARATION OF AUTHORSHIP

I, Thomas Tipton.....[please print name]

declare that this thesis and the work presented in it are my own and has been generated by me as the result of my own original research.

[title of thesis] ..Understanding the role for Fc gamma receptors in response to anti-CD20 monoclonal antibody therapy
.....

I confirm that:

1. This work was done wholly or mainly while in candidature for a research degree at this University;
2. Where any part of this thesis has previously been submitted for a degree or any other qualification at this University or any other institution, this has been clearly stated;
3. Where I have consulted the published work of others, this is always clearly attributed;
4. Where I have quoted from the work of others, the source is always given. With the exception of such quotations, this thesis is entirely my own work;
5. I have acknowledged all main sources of help;
6. Where the thesis is based on work done by myself jointly with others, I have made clear exactly what was done by others and what I have contributed myself;
7. [Delete as appropriate] None of this work has been published before submission [or] Parts of this work have been published as: [please list references below]:

Signed:.....

Date:.....

Acknowledgements

I would like to thank my supervisors professor Mark Cragg and Dr Stephen Beers for help and assistance throughout this project. They have been both very patient and enthusiastic throughout.

I would also like to acknowledge Dr Stephen Beers for preliminary data produced using the Vav Bcl-2 mouse and for *In vivo* B cell depletion studies shown in **Figure 3-1**. Additional thanks are extended to Ian Mockridge for acquiring SPR data and to Dr Ruth French for generating data in **Figure 4-1**.

Thanks go to the leukaemia and lymphoma research foundation for providing funding throughout this project.

I would also like to extend my gratitude to the past and present members of the Tenovus research facility for their help and kindness in providing tea, cake and training.

Finally, I would like to thank my wife Laura for her help and support throughout the last four years.

Definitions and Abbreviations

A:I	Activatory to inhibitory ratio
AID	Activation induced cytidine deaminase
APAF1	Apoptotic protease activating factor 1
APC	Allophycocyanin
BAI1	Brain specific angiogenesis inhibitor 1
Bcl-2	B-cell lymphoma-2
BCR	B cell receptor
BH	Bcl-2 homology
BLR1	Burkitt's lymphoma receptor 1
BMDM	Bone marrow derived macrophages
bp	Base pairs
c(T)	Threshold cycle
calcein-AM	Acetoxymethyl ester
CARD	Caspase recruitment domains
cDNA	Complementary DNA
CDR	Complementary determining region sequences
CFSE	5(6)-carboxyfluorescein
CHO	Chinese hamster ovary
CHOP	Cyclophosphamide, doxorubicin, vincristine and prednisone
CLL	Chronic lymphocytic leukaemias
CLP	Common lymphoid progenitor
CMP	Common myeloid progenitor

CMP	Common myeloid progenitors
Cr-51	Chromium-51
CRD	Cysteine rich domains
CSF-1	Colony stimulating factor 1
CVF	Cobra venom factor
D	Diversity
DD	Death domain
DED	Death effector domains
DEL	Duck egg lysozyme
DISC	Death inducing signalling complex
DLBCL	Diffuse large B cell lymphoma
dsDNA	Double stranded DNA
Eμ	Immunoglobulin heavy chain enhancer
EBI2	Epstein –Barr virus-induced gene 2
EDC	1-ethyl-3 (3-dimethylaminopropyl)-carbodimide
Egr	Early growth response
ELISA	Enzyme linked immunosorbent assays
EMPs	Erythro-myeloid progenitors
F	Phenylalanine
Fab	Fraction antigen binding
FADD	Fas associated death domain
Fc	Fraction constant
FcRn	Neonatal Fc receptor

FCS	Foetal calf serum
FcγR	Fc gamma receptor
FDA	Food and drug administration
FDC	Follicular dendritic cells
FITC	Fluorescein
GEF	Guanine nucleotide exchange factor
GFP	Green fluorescent protein
hCD20	Human CD20 Tg
HCl	Hydrochloric acid
HEL	Hen egg lysozyme
HMGB1	High mobility group box 1 protein
HSC	Haematopoietic stem cell
IC	Immune complex
IFNγ	Interferon gamma
IL	Interleukin
ITAM	Immunoreceptor tyrosine-based activation motifs
ITAM	Intracellular tyrosine activation motif
ITIM	Immunoreceptor tyrosine-based inhibitory motif
J	Joining
LPC	lysophosphatidylcholine
LPS	Lipopolysaccharide
LPS	lipopolysaccharide
LTF	lactoferricin

mAb	Monoclonal antibodies
mAb	Monoclonal antibody
MAC	Membrane attack complex
MACS	Magnetic automated cell sorter
M-CSF	Macrophage colony stimulating factor
MDM	Monocyte derived macrophages
MDP	Macrophage/DC precursor
MDSC	Myeloid derived suppressor cells
MerTK	Mer tyrosine kinase
MGF-E8	EGF factor 8
MHC	Major histocompatibility complex
MHCII	Major histocompatibility complex class 2
mIL-2	Murine IL-2
MMP	Multipotent progenitor
mNK	Murine NK
MOMP	Mitochondrial membrane permeabilization
MPS	Mononuclear phagocyte system
MS	Multiple sclerosis
MZ	Marginal zone
NED	N-(1-napthyl)ethylene-diamine dichloride
NFκB	NF kappa B
NHL	Non-Hodgkin`s lymphomas
NHS	N-hydroxysuccinimide

NK	Natural killer
NO	Nitric oxide
OPD	o-phenylenediamine dihydrochloride
PALS	Periarticuolar lymphoid sheath
PAMP	Pathogen associated molecular patterns
PBMC	Peripheral blood mononucleocytes
PBS	Phosphate buffered saline
PCR	Polymerase chain reaction
pDC	Plasmacytoid dendritic cells
PE	R-. Phycoerythrin
PI	Propidium iodide
PMSF	Aprotinin and phenyl-methl-sulphonly
PNGaseF	Peptide -N-Glycosidase F
Pre-BCR	Pre B cell receptor
PRR	Pattern recognition receptors
PS	Phosphatidylserine
RA	Rheumatoid arthritis
RAGE	Receptor for advanced glycation end products
RT	Room temperature
RU	Response units
S1P	Sphingosine 1-phosphate
S1P-R1-5	Sphingosine 1 phosphate receptors 1-5
SEC	Size exclusion chromatography

SFK	Scr family kinases
SH2	Src homology 2
SHIP	SH2-containing inositol polyphosphate 5-phosphate
SHM	Somatic hypermutation
SLC	Surrogate light chain
SLE	Systemic lupus erythematosus
SLS	Scientific laboratory services
SPR	Surface plasmon resonance
SYK	Spleen tyrosine kinase
T:E	Targets to effectors
T1	Transitional 1
T2	Transitional 2
TAM	Tumour associated macrophages
TAM	Tyro-Axl-Mer
TCR	T cell receptor
TD	Thymus dependent
TdT	Deoxynucleotide transferase
TGFβ	Transforming growth factor β
TI	Thymus independent
TIM4/1	T cell immunoglobulin and mucin domain containing molecule 4 and 1
TLR	Toll like receptors
TNFR	Tumour necrosis factor receptor

TNFR1	TNF-receptor 1
TNFRSF	Tumour necrosis factor receptor super family
TRAIL-1,	TNF related apoptosis inducing ligand receptor 1
TRAIL-2	TNF related apoptosis inducing ligand receptor 2
V	Valine
V	Variable
VEGF	Vascular endothelial growth factor
WHO	World health organisation
WT	Wild type
Y	Tyrosine
YS	Yolk sac

Chapter 1: General Introduction

1.1 Background information

The World Health Organisation (WHO) states that cancer is one of the leading causes of morbidity and mortality [1]. In 2012 there were 8.2 million cancer related deaths worldwide and 14 million new cases, a number which is expected to rise to 22 million by 2030 [1]. Cancers are thought to arise from a single malignant clone and much research over the past 50 years has focused on the cellular changes associated with tumorigenesis. This research has been extensively reviewed by Hanahan & Weinberg in 2000 and again 2011 [2, 3]. In their original 2000 paper it was proposed that there are 6 capabilities that need to be acquired by a cell if it is to form a successful tumour. These characteristics are; sustained proliferative signalling, evasion of growth suppressors, metastasis, replicative immortality, induction of angiogenesis and resistance to cell death [2]. However, by 2011 they added to these six capabilities to include the emerging hallmarks of avoiding immune destruction and deregulating cellular energetics [3].

These hallmarks of cancer are thought to be present in all developing tumours and current research is looking to exploit one or more as drug targets [3]. This project is interested in resistance to cell death and how this hallmark influences cells of the surrounding tumour microenvironment. Specifically, it is focussed on cancers of a haematological origin, termed blood cancers. Blood cancers come in the form of leukaemia, lymphoma or myeloma and develop from normal blood precursors. Leukaemia's are present in the circulating blood whereas lymphoma and myeloma are tumours found typically in the secondary lymph node organs of the spleen, lymph nodes or bone marrow [4].

Follicular lymphoma (FL) is one such haematological malignancy. FL is the second most diagnosed lymphoma in Europe and the US, with those diagnosed having a mean age of 60 years [5]. Typically, FL presents with asymptomatic lymphadenopathy (enlargement of lymph nodes) with involvement of the bone marrow in 70 % of patients [5]. This lymphadenopathy results from an expanding B cell population within the germinal centre of a lymph node [6]. FL is of interest because it is typically associated with a resistance to cell death

that is achieved via a chromosomal translocation, t(14;18), which puts transcription of the anti-apoptotic Bcl-2 protein under the control of the B cell heavy chain enhancer. This results in dysregulated overexpression of Bcl-2 and abated apoptosis [5, 6]. This translocation is found in the majority of FL's [5, 6].

Current therapeutics for leukaemia, lymphoma and myelomas involve cytotoxic agents, immunotherapeutic drugs and/or surgery [7]. The choice of treatment is primarily dependent upon the type of blood cancer. Conventional chemotherapy, in the form of cytotoxic drugs or radiotherapy, target dividing cells and is successful at treating more aggressive highly proliferative cancers [8]. Recent research has focused on the use of immunotherapeutic drugs to treat these diseases. A branch of which are monoclonal antibodies (mAb) and it is this type of treatment that our group is primarily focused on developing. To understand how mAb are produced and how leukaemia and lymphoma develop it is important to understand how B cells progress from immature to antibody secreting plasma cells.

1.2 B cell lymphopoiesis

1.2.1 The discovery of B cells

In the late 19th century it was unknown whether it was the humoral or cellular compartments of the body which provided the majority of protection against disease [9]. The discovery by Von Behring and Kitasato that immunity to diphtheria and tetanus is due to antibodies against their endotoxins provided strong evidence for a humoral based theory of acquired immunity [10]. In the mid-20th century there were two competing theories on antibody formation [9]. Niels Jerne in 1955 was accredited with the natural selection theory of antibody formation [9]. This idea was based on Ehrlichs side chain theory and suggests that antibodies of every kind of specificity are present in human sera and upon chance interaction with their antigen they are sequestered to a target cell which then produce copies of this antibody [9]. Around the same time the competing theory of clonal selection was put forward by Talmage and Burnet, this suggested that antigen specific responses arise from a clone of cells all with the same antigen specific cell surface receptor [9]. Although widely adopted it would take a number of years for the clonal selection hypothesis to be proven by Max Cooper [11]. The work of Max Cooper in 1966 identified B lymphocytes as the cells that produced antibody and thus confirmed the clonal selection theory of antibody formation. In this study they irradiated and removed the bursa of newly hatched chickens and noted that these chickens consistently developed agammaglobulinemia. However, if the chickens were infused with non-irradiated bursa cells immunoglobulin production was restored, the cells responsible for this were later termed B cells [12].

1.2.2 Early B cell development

All haematological cells develop from pluripotent haematopoietic stem cells (HSC), which are produced in human foetal liver at 7.5 weeks gestation and in the bone marrow from weeks 14-17 [13-15]. The earliest B cell lineage commitments occur when multipotent progenitor (MMP) cells differentiate to either the common lymphoid progenitor (CLP) or common myeloid progenitor (CMP) lineages, dependent upon the transcription factors Ikaros or PU.1 respectively [16]. Commitment to the B cell lineage involves up regulation of the transcription factors E2A, EBF and Pax5. Importantly, these proteins work to increase levels of the somatic recombination enzymes RAG1 and RAG2 [16]. Diversity amongst B cell receptors is thought to be in the region of 10^{11} specificities and it is somatic recombination of joining (J), diversity (D) and variable (V) genes within the immunoglobulin heavy and light chain loci along with the substitution of random nucleotides via the enzyme terminal deoxynucleotidyl transferase (TdT), termed junctional diversity, that is responsible for the initial B cell receptor (BCR) diversity amongst immature B cells. This recombination gives rise to a unique set of heavy and light chain variable domains [14, 15]. Early B cell development occurs via a number of well-defined check points (**Figure 1-1**). The first committed B cells are termed early pro B cells and it is at this stage where rearrangement of joining (J_H) and Diversity (D_H) gene segments at the immunoglobulin heavy chain locus on chromosome 14 occur [15]. Progression to late pro B cell requires the recombination of the earlier recombined DJ_H gene segments with a Variable (V_H) gene segment, followed by joining to the μ constant region to give a complete heavy chain [14, 15].

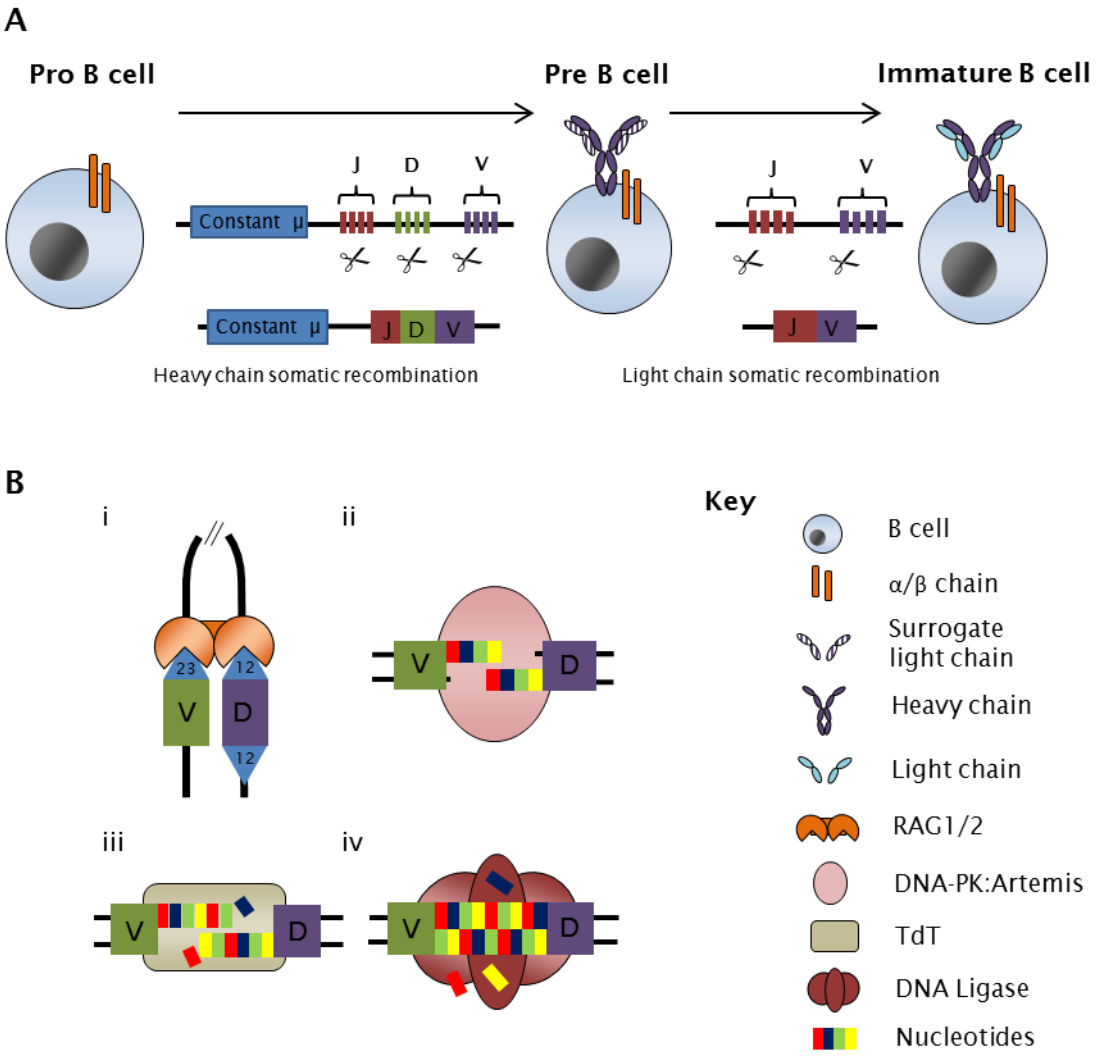

Figure 1-1: Early B cell development and generation of the BCR

(**A**) The Pro B cell phase of B cell development, the recombination of heavy chain VDJ gene segments are undertaken to make a unique heavy chain protein. During the Pre B cell phase light chain VJ gene segments rearrange and join with the heavy chain to create an immature B cell with a functional BCR. (**B**) Further diversity in the BCR is achieved through the addition of random nucleotides to the "gaps" between V, D and J genes once they are joined. i) Rag1/2 makes a double stranded DNA breaks, lining up the desired V, D or J gene and leaving two hairpin loops. ii) DNA-PK: Artemis opens DNA hairpin loops. iii) TdT randomly adds nucleotides to the ends of these hairpin loops. iv) DNA ligases join the two coding ends introducing junctional diversity.

Pre B cells can be sub-divided into large pre B cells and small pre B cells [15]. Large pre B cells contain two rearranged μ heavy chains (one for each allele), as a result the cell needs to undergo allelic exclusion whereby the first allele to generate a pre B cell receptor (pre-BCR) signals to prevent rearrangement and transcription of the other allele [15]. The pre-BCR at the Pre B cell surface

consists of the heterodimer CD79a (Igα), CD79b (Igβ) along with λ5, VpreB and a complete μ heavy chain [16, 17]. Igα, Igβ form the signalling component of the B cell receptor and each has an associated intracellular tyrosine activation motif (ITAM) that can recruit src family kinases (SFK) and non SFK such as spleen tyrosine kinase (SYK) to initiate downstream signalling [17]. λ5 and VpreB form the surrogate light chain (SLC) which is essentially a "dummy" light chain and ensures that any heavy chain produced is able to associate with any future light chain that is generated. Throughout the life of a B cell, constant low level tonic signalling is required to evade apoptosis and any pre B cell clone that fails to produce functional Igα, Igβ or SLC will be deleted due to a lack of tonic signalling and initiation of apoptosis through an ill-defined mechanism [17, 18].

Following pre-BCR signalling large pre B cells undergo numerous rounds of cell division before becoming resting small pre B cells [14]. At this point there will be a cluster of B cells expressing the same heavy chain, therefore rearrangement of the light chain leads to further diversity [15]. Small pre B cells initiate rearrangement of their immunoglobulin light chain [15]. Light chain rearrangement only occurs between variable (V_L) and joining (J_L) gene segments at the immunoglobulin light chain locus. There are two loci for light chain gene rearrangement one on chromosome 2 and the other on chromosome 22, these are termed kappa (κ) and lambda (λ) respectively. In human and mouse the κ locus rearranges first and so most functional antibody is of the κ isotype this is especially true in the mouse where 95% of B cells are κ expressing [19, 20]. Once the small pre B cell has successfully rearranged its light chains and expresses an intact surface Igμ (IgM) molecule as a functional BCR it can be classified as an immature B cell [15, 16].

Before immature B cells leave the bone marrow for the periphery they are screened for reactivity to self-antigens in a process known as receptor editing. This is an important stage, as it is a clear check point in the maintenance of B cell tolerance. Receptor editing was first described, independently, by two groups. First, Gay *et al* in 1993 demonstrated that mice encoded with transgenes, which gave them antibody specific to double stranded DNA (dsDNA), rearranged their light chains and could escape clonal deletion. Secondly, at the same time Tiegs *et al* generated transgenic mice expressing

antibody (anti-H-$2^{k/b}$) which is specific for a major histocompatibility complex (MHC) class of antigen, the H-2^k or H-2^b haplotype. When these transgenic mice were mated with mice expressing the H-2^k or H-2^b haplotype offspring had B cells positive for H-2^k or H-2^b but they were absent from the periphery. Furthermore these positive B cells continued to undergo light chain rearrangement in the bone marrow [21, 22].

The removal of B cells in the bone marrow, to eliminate those that have a BCR that recognises a host antigen, is referred to as central tolerance whereas B cells that evade this checkpoint can be removed at a later date, in the spleen, in a process referred to as peripheral tolerance [15]. Central tolerance is a very important check point in B cell development and loss of central tolerance can lead to the generation of auto reactive B cell clones and development of autoimmune disease through the generation of antibodies with specificity to host antigens, termed autoantibodies [15]. B cells that are found to have activity against host antigens are inactivated either through deletion by apoptosis or by disabling the B cell so that it is anergic and unresponsive to the host antigen. This is thought to be achieved via positive signalling through the BCR in the absence of co-stimulation [14, 18]. This was demonstrated in the 1980s by Goodnow *et al* whose group generated two types of transgenic mice, the first expressed Hen egg lysozyme (HEL) under the control of a constitutively expressing promoter which is active throughout the lifetime of the mouse. The second mouse expressed transgenic B cell receptors with high affinity for HEL. When these mice were mated they generated offspring that had functionally silenced anti-HEL B cells, this was due to the transgenic B cells recognising HEL as a host antigen and sending positive signals through the BCR in the absence of co-stimulation [23]. Later this same group demonstrated that anergy or deletion is due to recognition of monovalent soluble antigen or multivalent membrane bound antigen, respectively. In this study they generated transgenic mice that expressed either soluble or membrane bound HEL. They then mated these mice with transgenic mice that had high affinity HEL specific B cells. Offspring from both membrane bound and soluble HEL mice contained no anti-HEL antibody. However, the offspring from membrane bound HEL mice contained no anti HEL B cells (deletion) whereas the offspring from the mice that expressed soluble HEL contained anti-HEL B cells that were anergic and non-responsive [24].

1.2.3 Late B cell development

Late B cell development also occurs through a number of well-defined checkpoints (**Figure 1-2**). Immature B cells from the bone marrow express high levels of surface IgM and are classed as transitional 1 (T1) B cells, T1 B cells have a half-life of ~3 days and subsequently migrate to the spleen for maturation [15, 25]. Within the spleen these B cells first arrive at the marginal zone sinus then move towards the periarticuolar lymphoid sheath (PALS) and then to the B cell follicle [25]. Migration involves a number of different signalling proteins, termed chemokines. One important chemokine receptor for migration to the B cell follicle is Burkitt's lymphoma receptor 1 (BLR1, CD185, CXC-R5) and mice lacking BLR1 show decreased migration of B cells to splenic follicles [26].

Within the follicle immature B cells progress towards becoming transitional 2 (T2) B cells. The result of this transition is expression of a functional B cell co-receptor, CD21 (complement receptor 2). This is the point at which the immature B cell becomes a mature B cell [15]. Mature B cells can be sub divided into three groups; these are B1, B2 and marginal zone (MZ). Their differential generation largely depends upon downstream signalling through the BCR [27]. The majority of B cells will become conventional B2 follicular B cells and their continued survival in the follicle is dependent upon B cell activating factor (BAFF, BLyS). BAFF is produced by follicular dendritic cells (FDC) which are interspersed throughout the primary follicle and provide vital support to resident B cells. Defects in either BAFF or the B cell receptor for BAFF (BAFF-R) result in an absence of progression through T1 and T2 and so production of mature B cells is retarded [25]. In addition, overexpression of BAFF can lead to B cell hyperplasia and autoimmune disease presumably due to increased B cell trafficking, maturation and antibody production [15, 28]. The final stage of B cell progression is dependent upon BCR activation by its cognate ligand. Activation may lead to the generation of high affinity soluble antibody and differentiation into long term memory effector cells [15].

1.2.4 B cell activation

Mature B cells have a half-life of 3-8 weeks and will circulate throughout the lymphatic system until they come into contact with antigen recognised by their unique BCR [15]. To activate B cells the cooperation of co-receptors is paramount. This was demonstrated by Barrington *et al* who showed that B cell co-receptors such as CD21 promote cell survival upon BCR activation [29]. This work used HEL antigen specific B cells crossed with $CD21^{-/-}$ mice. They showed that mice lacking CD21 were unable to become activated upon infusion of Duck egg lysozyme (DEL) (for which the B cells have lower affinity) and were likely eliminated by apoptosis [29].

The most important function of B cells is the production of soluble antibody. To become fully activated and acquire this capacity the majority of B cells require interaction with $CD4^+$ T-helper cells. This is referred to as thymus dependent (TD) activation, since it is dependent on T cell production in the thymus. B cells that require the help of $CD4^+$ T cells generally give rise to higher affinity and class switched antibody [15]. Naïve $CD4^+$ T cells migrate between secondary lymphoid organs. Within each lymph node these cells will screen the surface of resident dendritic cells looking for antigen specific to their T cell receptor (TCR). Once a $CD4^+$ T cell recognises this antigen it will move to the outer T zones where it can interact with B cells that have migrated to the edge of the primary lymphoid follicle in response to antigen recognition. This site of B and T cell interaction is known as the primary focus (**Figure 1-2**) [15]. Once B cells engage antigen through their BCR they will internalise it and process it to generate shortened peptides which then associated with MHC class-2 (MHCII) proteins. This will lead to the expression of peptide bound MHCII proteins on the cell surface. These MHCII peptides bind $CD4^+$ T cells which have a TCR that is specific to that of the internally processed and presented peptide. Binding to this peptide will then activate the T cell [15, 30].

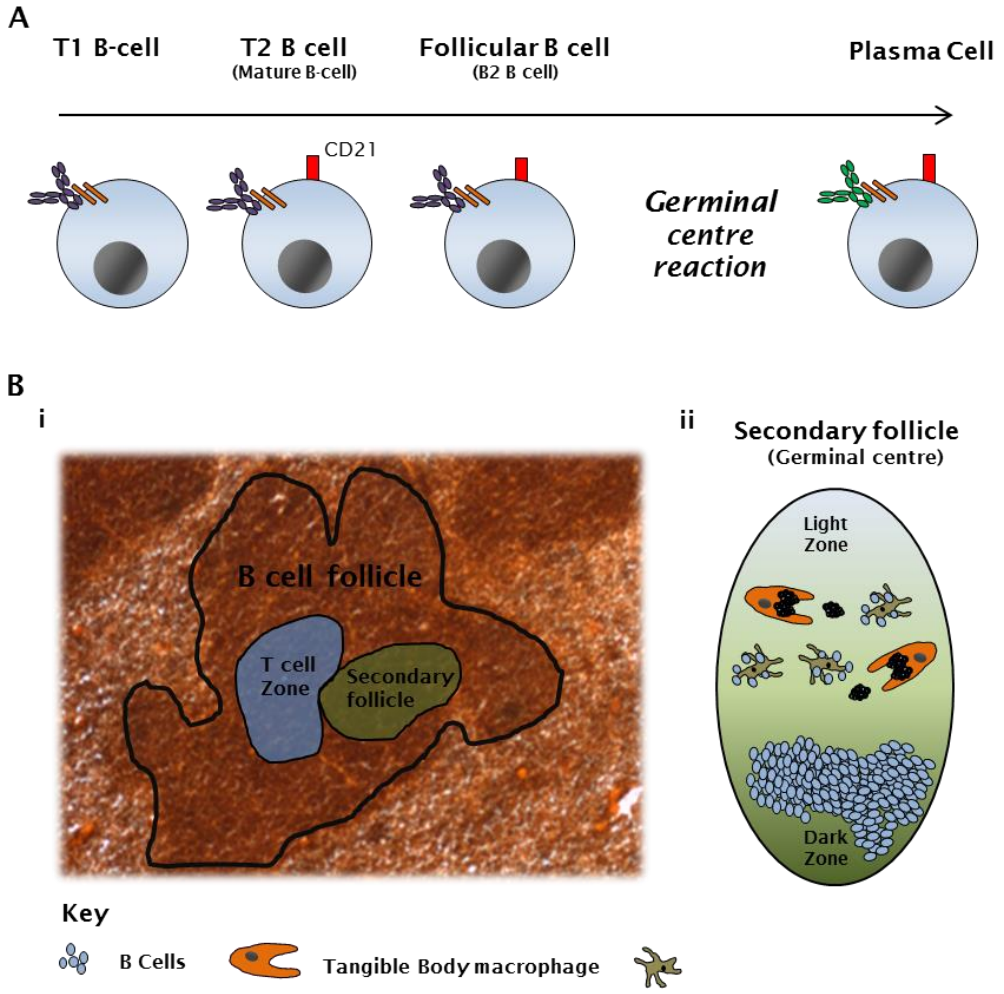

Figure 1-2 B cell maturation and activation.

(**A**) Immature B cells leave the bone marrow as transitional T1 B cells and upon expression of CD21 become mature T2 cells. Migration to the B cell follicles of lymph nodes may result in activation via the germinal centre reaction and differentiation into plasma and long lived memory B cells. (**B**) H&E staining of a wild type murine spleen, showing the B cell follicle and extra follicular zone. Naïve, mature B cells circulate throughout the lymphatic system, upon activation by antigen they migrate to the edge of the T cell zone and with the help of $CD4^+$ T cells establish a secondary follicle (germinal centre). Within the germinal centre B cells undergo proliferation in the dark zone and somatic hypermutation/ class switching in the light zone. Plasmablasts escape the germinal centre and either establish a new germinal centre or migrate to the extra follicular zone where they secrete antibodies. Micrograph taken from the spleen section of a C57BL/6 mouse, H&E staining.

At the primary focus key receptor interactions occur [31, 32]. B cells express the tumour necrosis factor receptor super family (TNFRSF) proteins CD40 and CD30 and $CD4^+$ helper T cells express CD40L and CD30L. When CD30 and

CD40 are bound they will lead to downstream activation of NF kappa B (NFκB) and B cell activation. Early work by Fanslow *et al* demonstrated that CD40 ligation is important for B cell proliferation [33]. Here they generated soluble CD40 and placed it in solution with B cells. When they activated these B cells, through anti-IgM agents, they found that the cells proliferated in response to anti-CD40 antibody. However, when soluble CD40 was present there was reduced proliferation, presumably due to competitive inhibition [33].

When B and T cells proliferate at the edge of the primary follicle they develop their own unique structure known as the secondary follicle [32]. The secondary follicle has two distinct zones, based on its histological appearance, the light zone & dark zone. The light zone contains the majority of FDC and $CD4^+$ T cells whereas the dark zone contains the majority of proliferating B cells. B cells within the Light zone are known as centrocytes and do not readily proliferate whereas B cells within the dark zone are known as centroblasts and are actively proliferating [34]. $CD4^+$ T-helper cells secrete cytokines Interleukin 4, 15 and 6 (IL-4, IL-15 and IL-6) which influence B cell proliferation, somatic hypermutation and class switching [35]. Finally, activated B cells will migrate to the extra follicular areas where they will rapidly expand and differentiate into plasmablasts and plasma cells. Migration of plasmablasts is reliant upon chemokine receptors CXCR5, CXCR4 and Epstein –Barr virus-induced gene 2 (EBI2). Plasmablasts that are $EBI2^-$, $CXCR5^+$ and $CXCR4^+$ remain within B cell follicles and can establish a new germinal centre [36]. Plasmablasts that are $EBI2^+$, $CXCR5^-$, $CXCR4^+$ migrate to the extra follicular zone where they secrete antibody. These plasmablasts then migrate to the bone marrow where they continue antibody production and become long lived plasma cells or migrate to the lymphoid organs to become short lived plasma cells. These plasma cells will have low levels of proliferation and high levels of antibody synthesis [15, 32]. A population of memory B cells will also arise from the germinal centre reaction. These cells reside in the lymphoid organs and blood stream. Memory B cells can be characterised by expression of the co stimulatory molecule CD27 and CD138 (Syndecan-1) and they respond quickly upon reinfection to secrete large amounts of antibody [15, 37].

B cell activation independent of $CD4^+$ T cell help is known as thymus independent (TI) activation. There are two types of TI activation known as TI-1 and TI-2. TI-1 activation involves B cells having a BCR which recognise common

bacterial constituents such as Lipopolysaccharide (LPS) or bacterial DNA [31]. All B cells will respond to these components through toll like receptors (TLR) which are innate pattern recognition receptors. However, B cells which have a BCR that also recognises a common bacterial component will be able to initiate an antibody response at much lower concentrations of agonist [15]. TI-2 antigens consist mainly of bacterial capsular polysaccharides and it is predominantly B1 and MZ B cells that response to these antigens. Response to TI antigens provides a quick source of antibody, although, this antibody will be of lower affinity and an IgM isotype as it has not gone through the maturation process [15].

1.2.4.1 Somatic hypermutation and isotype class switching

Somatic hypermutation (SHM) occurs during B cell activation, in the germinal centre. It is the method of fine tuning the variable regions of the BCR to maximise target antigen binding affinity and is the final level of BCR diversification [15]. This process introduces single point mutations throughout the antibody variable regions at a high frequency (~$1x10^{4}$ base pairs) with the aim to improve antigen binding affinity. Work by Jacob *et al* provided the first evidence for somatic hypermutation [38]. This group used polymerase chain reaction (PCR) to amplify the heavy chain variable region DNA isolated from germinal centres or the PALS of vaccinated mice. They observed a higher mutation frequency or rearranged V region genes in the germinal centres of vaccinated mice compared to the PALS [38]. Later it was discovered that the enzyme activation induced cytidine deaminase (AID) is upregulated upon BCR engagement and is responsible for mutation of the variable genes [15, 39]. This enzyme works by removing an amine group from cytosine thus turning cytosine into uracil. Since guanine pairs with cytosine this creates a mismatch which upon DNA replication can be repaired to give a thymine: adenine pairing [39].

As reviewed by Pereira, Kelly & Cyster non-favourable mutations lead to the deletion of the B cell clone, whereas favourable mutations will be selected for via B cell binding to antigen presented on FDCs [40]. The process of selecting B cells with receptors of the greatest affinity is known as affinity maturation and involves the B cell moving from the dark zone of the germinal centre where it has been dividing and undergoing somatic hypermutation to the light zones

where it will interact with FDCs presenting antigen. If the B cell fails to bind the presented antigen and does not re-enter the dark zone it will undergo apoptosis and will be engulfed by tangible body macrophages. This model of B cell migration is known as cyclic re-entry [15, 40].

Antibody class switching is another important process that takes place during the germinal centre reaction. There are 5 primary antibody classes in humans. These are Igα(A), Igδ(D), Igε(E), Igγ(G) and Igμ(M) and each class has its own specific functions. Class switching occurs in response to cytokines produced by $CD4^+$ T cells during B cell activation, for example in the mouse IL-4 promotes a IgG1 isotype whereas interferon gamma (IFNγ) promotes a mouse IgG2a isotype [15]. The molecular mechanisms of class switching again involve the enzyme AID and results in pairing the heavy chain variable region with the desired heavy chain constant region. This is reliant upon switch regions in the germ line DNA [15, 41]. Antibody class switching relies upon switch regions which are segments of repetitive DNA that lie between the different constant region code. The enzyme AID will make double stranded DNA brakes in these regions removing the intervening DNA and re-joining with the next switch region, there is a switch region for each constant region [41]. In order for B cells to class switch one switch region must pair up with the desired switch region and in doing so deletes the genetic material in-between. As such B cells that undergo class switching do so sequentially and cannot revert back to their previous isotype [15, 42, 43].

1.2.5 Follicular lymphoma tumorigenesis

In terms of tumorigenesis It is at the pro B cell developmental stage (during VDJ_H recombination) where the majority of follicular lymphomas are thought to obtain their characteristic t(14;18) translocation [6]. This translocation will take place on the non-functional allele and is thought to occur at a frequency of $1x10^{3-4}$ B cells in normal individuals [44]. The t(14;18) translocation places the Bcl-2 gene on chromosome 18 under the control of the Eμ enhancer, which is located between the Constant (C) μ coding sequence and the J_H gene cluster on chromosome 14. Functionally this acts to increase transcription of constitutive Bcl-2 which has anti-apoptotic capabilities (discussed in section **1.3**) therefore prolonging cell survival [44, 45]. Although uncertain it is thought that the majority of FL cases express surface IgD with 20-30 % undergoing class

switching to an IgA or IgG isotype. In addition, the majority of FLs will be undergoing SHM with the incidence being higher in isotype switched cells, reflecting what would occur in the normal B cell [6]. An inability for cells to undergo sufficient apoptosis is an important hallmark of this disease.

1.3 Apoptosis

There are billions of cells in the human body, millions of which die every day. The majority of these cells are processed, causing no adverse side effects to the host in the process known as apoptosis. The term apoptosis was originally coined by Kerr, Wyllie and Currie in their 1972 review on cell death. The morphological features of apoptosis proceed as follows: Firstly the cell chromatin and nucleus condense and the cell breaks up into a number of membrane bound fragments; Secondly these fragments, termed apoptotic bodies, are removed either through shedding via epithelial lined surfaces or via ingestion by neighbouring or professional phagocytic cells [46].

Yuan *et al* identified that cysteine proteases (caspases) are important to the mechanisms underlying apoptosis [47]. By the mid-1990s it was known that there is a cascade of caspase cleavages which bring about the morphological changes seen in apoptosis. However, it was unknown what mechanisms triggered this caspase cascade. Liu *et al* showed that cytochrome c, a protein which normally resides in the mitochondrial membrane is crucial to apoptosis [48]. Since these discoveries work has progressed to categorise two apoptotic pathways; the mitochondrial and death receptor pathways, these are also known as the intrinsic and extrinsic pathways, respectively (**Figure 1-3**) [49, 50].

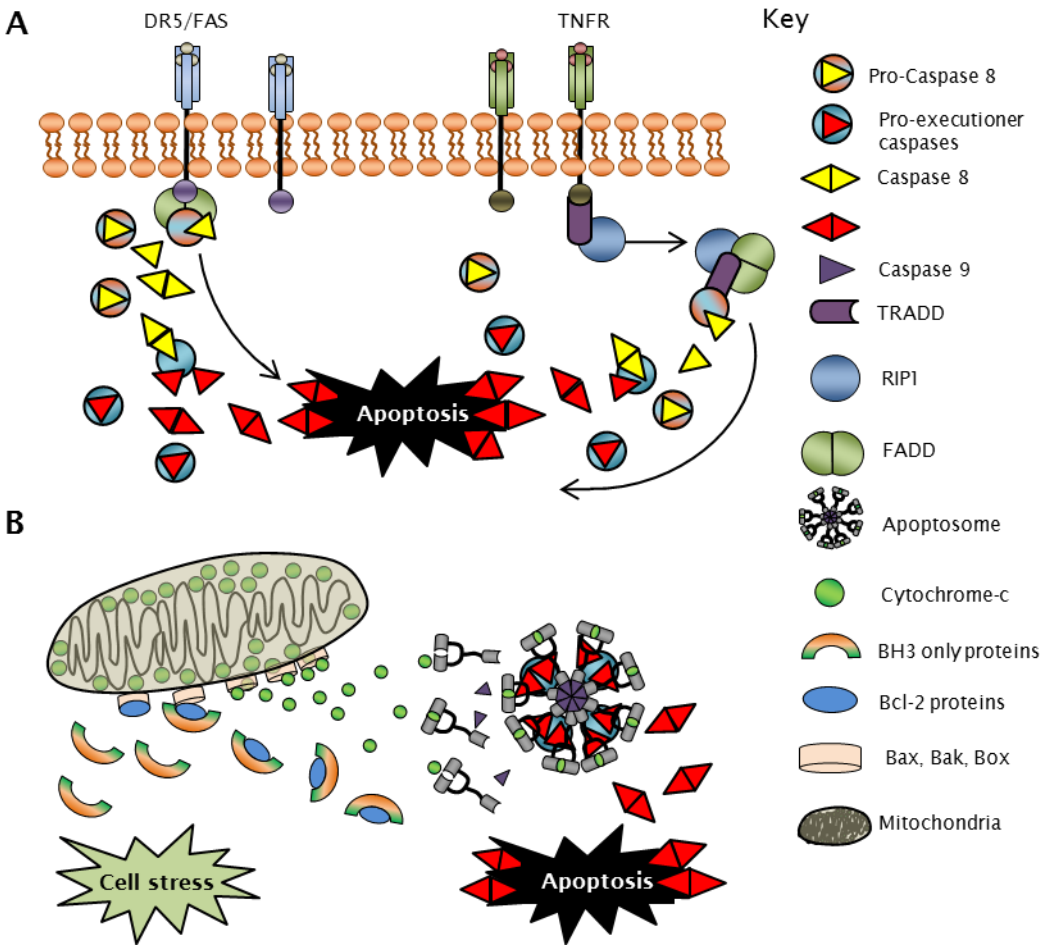

Figure 1-3: The intrinsic and extrinsic pathways of apoptosis

(**A**) The extrinsic pathway is initiated via cell surface ligation of death receptors, this leads to the activation of caspase 8 and downstream activation of executioner caspases 3 and 7 again leading to a structured disassembly of the cell. (**B**) The intrinsic pathway is elicited in response to cell stress and involves the activation of Bcl-2 proteins which together regulate MOMP. Following MOMP there is assembly of the apoptosome and downstream activation of caspases which effectively cleave cellular proteins leading to a structured disassembly of the cell.

1.3.1 Mitochondrial pathway

Intracellular stresses induce the mitochondrial pathway. The key step in this pathway is outer mitochondrial membrane permeabilization (MOMP). This was demonstrated by Goldstein *et al* who used cytochrome c conjugated to green fluorescent protein (GFP) to show that there is release of cytochrome c from the mitochondrial membrane and that this precedes phosphatidylserine (PS) exposure on the apoptotic cell surface [51]. Cytochrome c associates with

apoptotic protease activating factor 1 (APAF1). APAF1 was identified by Zou *et al* as a human protein with homology to *C. Elegans* protein CED-4. APAF1 in conjunction with cytochrome c leads to the activation of caspase 3 [52]. Soon after it was demonstrated that the initiator caspase 9 is needed to bind to APAF1: cytochrome c complexes and dimerise before there can be activation of downstream caspases. This cytochrome c: APAF1: caspase 9 complex was later termed the apoptosome [49, 53-56].

Caspases activated downstream of the apoptosome are caspases 3, 6 and 7. Together these are known as the executioner caspases. As reviewed by Lamkanfi *et al*, the executioner caspases work by cleaving after aspartic residues and this directly or indirectly brings about the morphological changes seen in apoptosis [57]. Caspases are evolutionarily conserved proteins which can also function in activation of pro-inflammatory cytokines. Caspases are endopeptidases that hydrolase peptide bonds only after certain aspartic acid residues in the substrate. This makes the dismantling of the cell a controlled process [58]. Caspases 1, 2, 4, 5, 9, 11 and 12 contain caspase recruitment domains (CARDs) whereas caspases 8 and 10 contain death effector domains (DED). Both of these caspase pro domains are essentially structurally related death folds which recruit adaptor proteins that activate the caspase by allowing it to dimerise [57].

Regulation of MOMP is critical to the activation of the executioner caspases. As a result regulation of MOMP is tightly controlled. Research over the past 30 years has unveiled the mechanisms by which MOMP is regulated upon exposure to apoptotic stimuli. As mentioned a classical feature of FL is the t14;18 translocation which puts the protein Bcl-2 under the promotion of the immunoglobulin heavy chain enhancer (Eμ). Whilst investigating Bcl-2 as a potential oncogene for FL Vaux, Cory & Adams showed that in Eμ Myc transgenic mice transfection of Bcl-2 led to elevated incidence of B cell tumorigenesis. However, if Bcl-2 was transfected into the non c-Myc effected myeloid or lymphoid cells the cells persisted in a non-replicative stage of growth. This identified Bcl-2 as an oncogene with importance for cell survival [59]. Later, it was discovered that Bcl-2 associates with the mitochondria to bring about inhibition of apoptosis. This was shown using confocal microscopy and subcellular fraction analysis [49, 60]. The next breakthrough came when it was proven that Bcl-2 prevented apoptosis by blocking the release of

cytochrome c from the mitochondria, thus placing it as a key regulator of MOMP [61, 62].

Whilst work into the role of Bcl-2 in apoptosis continued, it became clear that Bcl-2 was part of a wider family that regulates MOMP. The Bcl-2 family of proteins contain 2 subgroups these are pro-apoptotic and anti-apoptotic. Anti-apoptotic family members consist of Bcl-2, Bcl-X_L, Bcl-w, Mcl-1, A1 and Bcl-B. These family members share three or four Bcl-2 homology (BH) domains (BH1-4). Pro-apoptotic family members can be further sub-divided into executioner and BH3 only members. Executioner members consist of Bax, Bak and Bok and contain two –three BH domains. The BH3-only family members consist of Bad, Bik, Bid, Bim, Noxa and Puma and they contain only one BH domain (BH3) [63]. How these proteins work to bring about disruption of the outer mitochondrial membrane has not yet been fully resolved, but the current understanding is detailed below.

Oltvai, Milliman & Korsmeyer showed that overexpression of Bax accelerates apoptosis and that Bcl-2 can associate with Bax. This research lead to the original rheostat model which states that there is a balance between Bcl-2 and Bax proteins and that this balance regulates MOMP [64, 65]. However, the rheostat model did not explain how cells can tolerate high levels of Bax proteins or what role the later discovered BH3 only proteins had in programmed cell death [66]. Letai *et al* then demonstrated the importance of the BH3 only proteins. They found that BH3 proteins such as Bid and Bim were capable of activating Bak and Bax as well as neutralising Bcl-2. Whereas less potent BH3 proteins such as bad and Bik will only neutralise Bcl-2, on thereby increasing the level of apoptosis. This formed the basis of the direct activator/suppressor model of apoptosis. In effect the BH3-only proteins either directly activate Bax and Bak or indirectly activate Bax and Bak by neutralising anti-apoptotic family members such as Bcl-2 [67].

Willis *et al* then highlighted the different interactions between Bcl-2 family members. Upon activation of the BH3 only proteins Bcl-2 proteins are displaced from the mitochondrial membrane and cell death ensues. However, some Bcl-2 proteins are only displaced by certain BH3 proteins for example Mcl-1 will only bind to Noxa. Therefore if a certain drug or stimuli only up regulated Noxa cell death may not ensue due to the fact that other Bcl-2 proteins such as Bcl-X_L

which do not bind to Noxa will keep Bax and Bax from causing MOMP. Essentially, there is limited redundancy between BH3 proteins that bind to Bcl-2 proteins. The most potent BH3 only proteins are Bim, Bid and Puma since they bind to all the anti-apoptotic Bcl-2 proteins [49, 68].

1.3.2 Death receptor pathway

The other major route to apoptosis is through external signalling via death receptors. As reviewed by Guicciardi & Gores, death receptors are members of the tumour necrosis factor receptor (TNFR) superfamily [69]. The members of this family contain sequence homology in their extracellular domains typically with the presence of up to six cysteine rich domains (CRDs) and members contain a specific cytoplasmic sequence known as the death domain (DD). In humans the most well studied death receptors are Fas and its external ligand Fas-L, TNF-receptor 1 (TNFR1) and TNF related apoptosis inducing ligand receptor 1 and 2 (TRAIL-1, TRAIL-2). Activation of Fas, TRAIL-1 or TRAIL-2 will generally result in cell death whereas activation of TNFR1 will induce cytokine production, inflammation and cell survival. If unable to do this TNFR-1 will initiate cell death. The ligand to these death receptors are generally membrane bound and referred to as death ligands [69].

Upon cell surface ligation of Fas the intracellular adaptor protein Fas associated death domain (FADD) binds to the DD on Fas. FADD has its own DED which binds to pro-caspase 8 (FLICE). This signalling complex is known as a death inducing signalling complex (DISC). Pro caspase 8 is proteolytically cleaved into active caspase 8, which is released from the DISC as a heterodimer that migrates into the cytosol and activates the executioner caspase 3 thus initiating the caspase cascade and cell death. Signalling by TRAIL-1 and TRAIL-2 follow this similar pattern of activation [70, 71]. It was shown that in order to signal for apoptosis TNFR1 must associate with TNF receptor associated death domain (TRADD), RIP1 and TRAF2 and that this will signal activation of NFκB and the prevention of apoptosis through the FLICE inhibitor $FLIP_L$. However, if there is a failure in activation of NFκB TRADD and RIP1 will associate with FADD and caspase 8 and so apoptosis will ensue [72]. Death receptor signalling can also induce MOMP through FLICE cleaving Bid to tBid. tBid then migrates to the mitochondrial membrane where it will displace the anti-apoptotic family

members and activate Bak and Bak thus leading to MOMP and cell death [49, 73, 74].

1.4 Anti-CD20 monoclonal antibody therapy

1.4.1 History of monoclonal antibodies

The ability to produce antibodies of a desired and single specificity, known as monoclonal antibodies (mAb) has only relatively recently been achieved. The seminal work on antibody production was by Kohler & Milstein in 1975. This group made a hybrid cell line which secreted soluble antibody specific for sheep red blood cells. This was achieved using Sendai virus to fuse murine melanoma B cells and mouse splenic B cells [75]. This became the traditional method of mAb production for many years and is still used today. Although useful it does not generate fully humanised mAb, which is important since many mechanisms of mAb action rely on functional humanised Fc regions.

A more recent method of production involves the use of phage display libraries of antibody variable regions. Here, PCR is used to expand random heavy and light chain variable regions from DNA extracted from whole splenocytes. These heavy and light chain genes are then cloned into bacteriophages to create a fusion protein, containing bacteriophage coat protein and immunoglobulin variable region. These fusion proteins make up the phage display library. Bacteriophage numbers are increased and the bacteriophage exposed to a given antigen. The bacteriophage with the desired variable region is selected by its ability to bind to its complementary antigen. The successful variable region genes can then be removed and inserted into other antibody plasmids with the desired fully human frameworks and isotype these are then used to create a functional protein by insertion into a specific cell line [15, 76]. This method has the advantage that it may use human DNA and so produce fully humanised antibody. Other methods of antibody production involve the use of transgenic mice which are genetically altered to produce humanised antibody using an artificial chromosome. In these mice endogenous heavy chain is deleted through targeted mutations of D regions, disabling the production of IgM. This is in combination with the addition of a number of transgenes encoding human V, D and J segments [15, 77, 78].

1.4.2 The structure and function of immunoglobulins

As described above there are 5 classes of immunoglobulin (**Figure 1-4**). The majority of mAb produced for therapeutic use are of the human IgG isotype and one of the key benefits of IgG is its superior half-life compared to other isotypes [79]. This half-life is achieved through binding to the neonatal Fc receptor (FcRn). The structure of IgG consists of two heavy and light polypeptide chains joined together by disulphide bonds. Binding through the fraction antigen binding (Fab) is non-covalent and takes place at the three hypervariable regions found at the tip of each heavy and light variable domain. The fraction constant (Fc) region is responsible for the recruitment of effector cells and the activation of the serum protein complement cascade.

In humans there are 4 subclasses of IgG named by their diminishing concentration in the serum (IgG1-4). Although over 90% identical at the amino acid level, each IgG subclass will have distinctive properties. The most abundant isotype is IgG1 which is typically seen in response to soluble and membrane bound proteins [80]. IgG2 is typically seen in response to carbohydrate antigens and is typically seen in response to bacterial polysaccharides. IgG3 appears to be the most efficient class at eliciting pro inflammatory and effector responses although benefit is tempered by its reduced half-life compared to the other isotypes. This is thought to be due to intracellular competition for FcRn with the other IgG classes [81-83]. Mice have three major IgG subclasses. These are IgG1, IgG2 and IgG3. In addition to this there are two subclasses of IgG2, these are IgG2a/c and IgG2b. Importantly, C57BL/6 mice produce IgG2c whereas BALB/C mice produce IgG2a and research has shown that antibodies specific for IgG2a will not cross react with IgG2c [84].

Antibodies typically mediate their effector function by binding to soluble toxins, neutralising their pathogenic effects or by engaging Fc gamma receptors (FcγR) on cytotoxic effector cells such as macrophage and neutrophils. Effector actions are heavily reliant upon IgG1 glycosylation of the C_H2 domain at Asn-297 [85]. Glycosylation at this point acts to give a defined conformation in the Fc hinge region, allowing for binding to FcγR [86]. Substitution of Asn with Ala at position 297 resulted in significant loss of Fc and C1q binding [86].

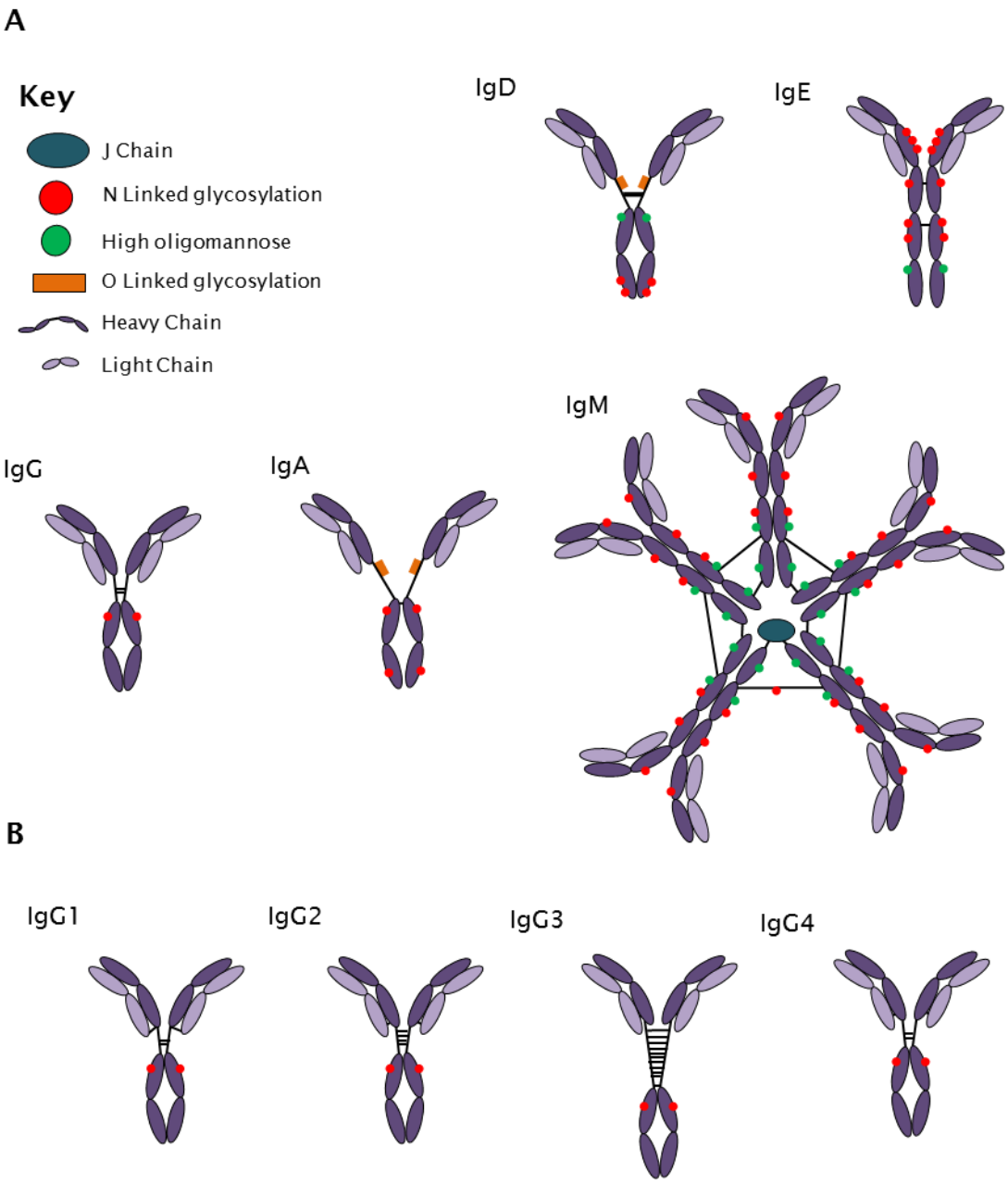

Figure 1-4: The structure of Human IgG

(**A**) Immunoglobulins consist of two pairs of polypeptide chain these are the heavy and light chains (dark and light purple respectively). There are 5 distinct classes; IgM, IgD, IgA, IgG and IgE each with distinct functional characteristics and varying levels of glycosylation. (**B**) IgG makes up the majority of circulating and functional antibody. There are 4 subclasses of IgG with slightly different functions, the major structural differences in these isotypes comes from the different sized hinge regions.

1.4.3 Anti-CD20 monoclonal antibodies

Anti-CD20 monoclonal antibodies have become an established treatment for many B cell malignancies, additionally they are currently being looked at as a treatment for auto immune diseases such as rheumatoid arthritis (RA), multiple sclerosis (MS) and systemic lupus erythematosus (SLE) [7, 87, 88]. The first CD20 antibody, originally termed B1, was identified in the 1980s by Stashenko *et al* using this monoclonal antibody the group determined that CD20 is present on approximately 9 % of circulating lymphocytes and 95 % of B cells within the blood and lymphoid organs [89]. In addition, this same group later found that CD20 is expressed on over 80 % non-Hodgkin`s lymphomas (NHL) and 95 % of chronic lymphocytic leukaemias (CLL) making it a useful biomarker of B cell malignancies [90]. Subsequently, CD20 has become an effective target for mAb therapy especially in combination with traditional chemotherapy [91]. In 1997 Rituximab (Mabthera®) became the first licenced mAb for treatment in oncology and was demonstrated to be clinically beneficial for patients with NHL [92]. However, resistance to rituximab is common and since its introduction a number of modified anti-CD20 mAb have come to market with the aim of improving clinical efficacy. The major difference in the next generation anti-CD20 mAb is progressive humanisation and glycomodification [93-95].

1.4.3.1 Type I & II anti-CD20 monoclonal antibodies

Anti-CD20 antibodies can be broadly classified as either type I or II. This classification comes from the observation that some anti-CD20 mAb were more efficient at activating complement whereas others were poor at activating complement but could induce a non-apoptotic form of cell death termed homotypic adhesion [91, 96-98]. These classifications were made when it was found that complement activity correlated with re-distribution of CD20 into plasma membrane lipid rafts [98]. Type I antibodies were able to re-distribute CD20 into lipid rafts and potently activate C1, the first component of the complement cascade. Whereas type II antibodies showed efficacy when using only the $F(ab)_2$ fragments [98]. It was later shown that this non apoptotic form of cell death involved activation of lysosomes which lead to the loss of plasma membrane integrity [96].

1.4.4 Mechanisms of action by anti-CD20 mAb

There are three proposed mechanisms of action for the efficacy of anti-CD20 mAb. These are complement dependent cytotoxicity (CDC), antibody dependent cellular cytotoxicity (ADCC) and programed cell death (PCD), (**Figure 1-5**) [88, 94, 95].

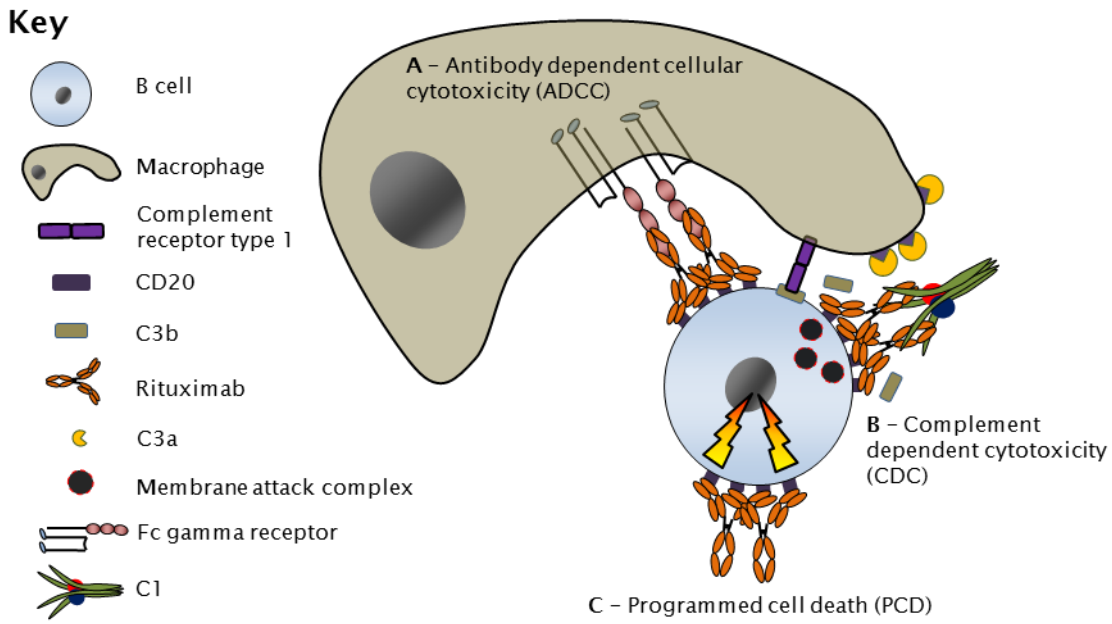

Figure 1-5: Proposed mechanisms of action of anti-CD20 monoclonal antibodies

(**A**) Antibody dependent cellular cytotoxicity (ADCC), effector cells including macrophages recognise and kill rituximab coated B cells via Fc:FcγR interactions. (**B**) Complement dependent cytotoxicity (CDC), complement component C1 will bind to the Fc region of clustered rituximab on the B cell surface. This will result in activation of the complement cascade and direct lysis of the target B cell through formation of the membrane attack complex. Additionally the formation of C3b acts as an opsonin form phagocytic cells such as macrophages whereas C3a and C5a act to establish a pro inflammatory environment. (**C**) Programmed cell death (PCD) involves the cross linking of antibody leading to intracellular signalling for the initiation of apoptosis through as yet undefined mechanisms.

1.4.4.1 Programmed cell death

PCD in response to anti-CD20 antibodies has been observed in a number of different lymphoma cell lines. With type I antibodies it is thought to be dependent on mAb cross linking to generate signals to bring about apoptosis via the mitochondrial pathway [94]. Work by Byrd *et al* observed that a proportion of CLL patients receiving rituximab treatment showed *in vivo* activation of caspase 9 and 3 as well as poly(ADP-ribose) polymerase (PARP) cleavage in leukemic cells. Also, the anti-apoptotic proteins XIAP and Mcl-1 were down regulated on circulating leukemic cells which suggests a potential mechanism of resistance to anti-CD20 mAb [99]. In addition work by Stolz *et al* found that rituximab directly triggered apoptosis via the mitochondrial pathway in NHL cell lines and that expression of Bcl-X_L confers resistance against rituximab treatment [100]. However, there is as yet no conclusive proof that *in vivo* antibody therapy kills via PCD.

Chan *et al* showed that cell death induced by rituximab is independent of caspase activation and upon redistribution of CD20 into Triton-X 100 insoluble lipid rafts. Since this form of cell death was independent of caspase activation it suggested a non-apoptotic form of cell death [101]. Furthermore, Ivanov *et al* showed that type II antibodies evoked homotypic adhesion which was independent of caspases and Bcl-2 proteins, this was also a lysosome dependent pathway [96].

1.4.4.2 Complement dependent cytotoxicity

CDC is initiated when C1q binds to juxtaposed Fc regions of antibody. C1q binding initiates the complement cascade, leading to the generation of C3b which has a highly active thioester bond that allows covalent binding to hydroxyl groups. Therefore, if C3b is not in close proximity to carbohydrates or proteins conveying hydroxyl groups it will become hydrolysed by the surrounding environment to form inactive C3b(H_20) [102]. Activation of the complement cascade will bring about lysis of the target via formation of the membrane attack complex (MAC). This complex consists of C5b binding to C6 and C7, this complex then inserts itself in the phospholipid bilayer of a cell.

Next, C8 and C9 will further bind to this complex creating the MAC. This causes permeabilisation of the target cell. The role of CDC in B cell depletion is controversial with some studies suggesting CDC is important to B cell depletion and others suggesting that CDC is in fact detrimental [103].

Work by Golay *et al,* using an *in vivo* B lymphoma murine model found that natural killer (NK) cells and neutrophil depletion had no significant effect on antibody therapy. Neither did macrophage depletion by clodronate coated liposomes. However, depletion of complement component C2 through the use of cobra venom factor (CVF), which activates all available complement, resulted in a significant reduction in the ability of rituximab to control tumour *in vivo* [104]. In contrast, work by Wang *et al* suggests that complement is in fact detrimental to antibody therapy. In this study they used NK cells as the ADCC effector cells and analysed their phenotype in response to rituximab coated lymphoma cells. This was in the presence of complement sufficient or inactivated serum. They found that normal serum failed to induce an activated NK phenotype and hypothesised that complement products such as C3b block FcγR interactions [105]. Further work supporting a role for CDC came from C1q polymorphisms. Here, Racila *et al* genotyped patients with follicular lymphoma for either C1q 276A or C1q 276G, they found that patient homozygous for 276A showed beneficial response to rituximab therapy compared to heterozygous or C1q 276G homozygous patients [106, 107]. Other studies attempting to elucidate the contribution of complement as an effector mechanism conclude that complement is neither a benefit or a hindrance and suggest that ADCC mediated by effector cell FcγRs is most important to an effective anti- CD20 mAb response [103, 108, 109].

1.4.4.3 Antibody dependent cellular cytotoxicity

It is now emerging that the most important mechanism of B cell depletion in response to anti-CD20 therapy is ADCC mediated by FcγR expressing effector cells. Seminal work by Clynes *et al* highlighted the importance of activatory and inhibitory FcγRs [110]. In this study transgenic mice were made which failed to express the common γ chain, had no FcγRIIb or a combination of both knockouts. It was then demonstrated that mice lacking inhibitory FcγRIIb had enhanced elimination of opsonised targets, whereas mice deficient for the common γ chain showed a diminished response to antibody therapy [110].

Subsequently, using macrophage and/or FcγR deficient mice it has been reported that monocytes are the major effector cells and that T cells and NK cells are not critical to therapy [110, 111]. Recent *in vivo* work by Albanesi *et al* showed that TA99 antibody therapy for the B16 metastatic melanoma cell line relied predominantly on two murine FcγR: I and III [112]. In contrast work by Otten *et al* suggests that murine FcγRI and IV are critical to therapy. This was shown using an FcγRIV blocking antibody (9E9) in combination with FcγRI$^{-/-}$ mice. Collectively the data is in agreement that effector cells mediated by FcγR are critical to successful antibody therapy. However, it is not clear what contribution each FcγR provides or which are the dominant effector cell subsets.

Evidence supporting the role of ADCC in humans comes from clinical data showing that patients with FcγR polymorphisms respond differently to treatment. It was found that if FcγRIIIa contained a valine (V) at position 158 it bound IgG1 with a threefold higher affinity than if it contained a phenylalanine (F) [113]. Work then confirmed that patients with the FcγRIIIa V/V phenotype showed stronger NK cell dependent ADCC and an improved response rate to rituximab treatment [114].

1.4.5 Resistance to anti-CD20 therapy

It has been noted that following Rituximab treatment many chronic lymphatic leukaemia (CLL) patients have undetectable CD20 on the B cell surface. This was thought to be due to masking of the CD20 protein by rituximab, however, Jilani *et al* showed this not to be the case [115, 116]. They demonstrated that CD20 and rituximab binding was down regulated on various B cell surfaces and that this was transient, with CD20 expression detectable again following 24 hours recovery [116]. Following this, work by Kennedy *et al* showed that with the standard high dose of rituximab, complement is rapidly consumed and levels of CD20 on circulating B cells are diminished [117]. This same lab suggested that cytotoxic effector systems are quickly exhausted in response to high doses of mAb and that effector cells 'shave' CD20 from the target cell in a trogocytosis like fashion [118-121].

In contrast, work by Beers *et al* demonstrates that there is rapid antigen: antibody complex internalisation, termed antigenic modulation, by type I

compared to type II mAb and that there are differing rates of antigenic modulation on various cell lines and primary cells with diffuse large B cell lymphoma (DLBCL) being resistant and CLL cells being highly modulating, follicular lymphoma cells typically modulate slowly but some show rapid internalisation [109, 122]. Shaving and antibody modulation may both contribute to resistance to antibody therapy and future work looks to dissect both these mechanisms.

1.5 The role of Fcγ receptors in antibody therapy

1.5.1 Introduction to Fc gamma receptors

FcγR mediated effector mechanisms appear to be the most important in anti-CD20 mAb therapy, therefore it is important to discuss these receptors in more detail. There are four FcγRs in the mouse (**Figure 1-6**); FcγRI, FcγRIIb, FcγRIII and FcγRIV [123]. Importantly FcγIIb is an inhibitory receptor and contains an immunoreceptor tyrosine-based inhibitory motif (ITIM). In contrast, the other receptors are activatory and signal through immunoreceptor tyrosine-based activation motifs (ITAM), through their association with the γ chain.

In humans there are six FcγR; FcγRI, FcγRIIa, FcγRIIb, FcγRIIc, FcγRIIIa and FcγRIIIb. In humans, like mice, FcγIIb functions through an ITIM whilst the other receptors function through ITAMs [124]. Different immunological cells express different FcγRs. B cells express only the inhibitory FcγRIIb. However, in mice and humans there are two isoforms of FcγRIIb: B1 and B2 which differ in a small amount of intracellular sequence, here Brooks *et al* showed that alternative splicing resulted in a lack of 19 ammino acids at the terminal end of the B2 isoform [125]. B cells predominantly express the longer B1 isoform [124-126]. NK cells only express FcγRIIIa in humans and FcγRIII in mice, whereas macrophages in both mice and humans express the full range of FcγR [124, 127].

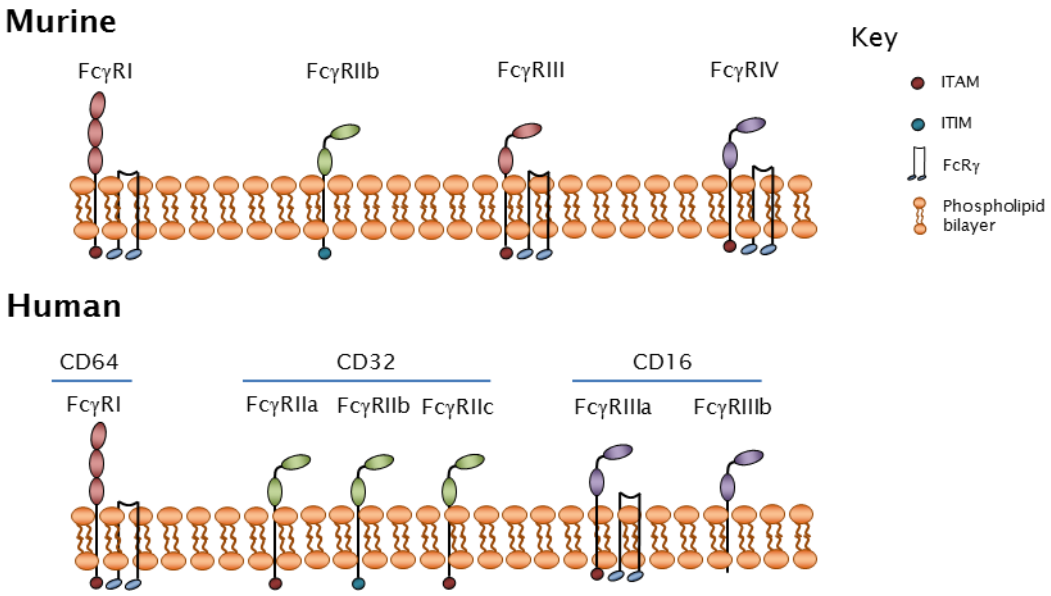

Figure 1-6: Murine and human FcγR

Murine cells contain four FcγRs whereas human cells contain six. Engagement of FcγRIIb in both cases leads to inhibition of effector mechanisms. In contrast, Engagement of FcγRI, III or IV in mice and FcγRI, IIa, IIc or IIIa in humans leads to activation of cellular effector mechanisms. Additionally, murine FcγRI and IV are high affinity receptors and can bind monomeric IgG where as FcγRIIb and FcγRIII are low affinity receptors and will only bind to immune complexed IgG. In humans FcγRI has high affinity for IgG1.

The FcγRs have different binding affinities for IgG. This high or low affinity depends on IgG isotype and whether antibody is monomeric or aggregated in the form of immune complex (IC). Work by Hamaguchi *et al* demonstrated in a mouse model that IgG1 interacted with low affinity murine FcγRIII and that mouse IgG2a had high affinity for mouse FcγRI. They showed this using a combination of FcγR deficient mice and FcγR blocking antibodies [128]. FcγRIV, in mice, was only recently described and shown to be expressed on macrophages. FcγRIV has affinity for mouse IgG2a/c and IgG2b. Mouse IgGI does not bind FcγRIV [123].

As reviewed by Nimmerjahn & Ravetch the expression level of the inhibitory FcγRIIb and the glycosylation state of the antibody constant region are major factors in the interaction between target and effector cells [129]. Research is looking to increase the binding affinity, of therapeutic antibodies, to activatory FcγRs. This can be achieved through glyco-modification of the antibody constant region. In order to bind FcγRs circulating immunoglobulin needs to be

glycosylated at Asn-297 (for human IgG), this effectively changes the conformation of the Fc fragment so that it can bind the FcγR. Much research into next generation CD20 mAb has focused on engineering of this Fc glycan [130]. One such antibody is obinutuzumab (GA101, Gazyva™). Following removal of fucose from the sugar chain attached to Asn-297, a greater binding affinity to human FcγRIIIa was observed. This increased affinity has been ascribed in part to a sugar interaction that is derived from ASP-162 on the FcγR. Obinutuzumab has recently been assessed in clinical trials and is now recommended for clinical use in the treatment of CLL [129, 131].

1.5.2 Signalling by Fc gamma receptors

As eluded to above, FcγRs signal via ITAM and ITIM domains (**Figure 1-7**). These domains can be differetnciated by their amino acid sequence, ITAM receptors contain a specific motif consisting of Y-X-X-(L/I)-$X_{-(6-8)-}$Y-X-X-(L/I). They signal through recruitment of SFK such as Lyn which phosphorylate the tyrosine (Y) residues on the ITAM receptor. This phosphorylation allows for docking of Syk or Zap70 kinase which in turn recruit the adapter proteins LAT and SLP-76. These adapter proteins signal through MAPK, NFκB, AP1 and NFAT to elicit new gene transcription. Work is still ongoing to understand the context specific cellular responses downstream of ITAM signaling [132].

ITIM receptors inhibit signaling activity. They contain a specific 6 amino acid sequence (I/V/L/S)-X-Y-X-X-(L/V). Clustering of these receptors by crosslinking of FcγRs will promote phosporylation of the tyrosine groups by an SFK as is the case in ITAM signaling. However, this phophorylation leads to the recruitment of cytoplasmic phophatases having Src homology 2 (SH2) domains. There are two types of SH2 phosphatases which are recruited. The first is a tyrosine phosphatase SHP-1, the second, an inositol phospahatase SH2-containing inositol polyphosphate 5-phosphatase (SHIP). Recruitment by the ITIM of either SHP-1 or SHIP will lead to distinct alterations in downstrem signaling pathways. SHP-1 will cause dephophorylation by removing the tyrosine phosphate from BTK and SYK, inhibiting the PLCγ2 pathway. Whereas, SHIP will remove the phosphate from phosphatidylinositol 3,4-trisphosphate (PIP_3) to generate phosphatidylinositol 3,4-bisphosphate (PIP_2). This essentialy stops recruitment of intracellular signaling molecules at the cell membrane [133]. In

macrophages this inhibits cytoskeletal actin rearangement and phagocytosis [134]. In B cells ITIM signaling by FcγRIIb acts to regulate B cell activation.

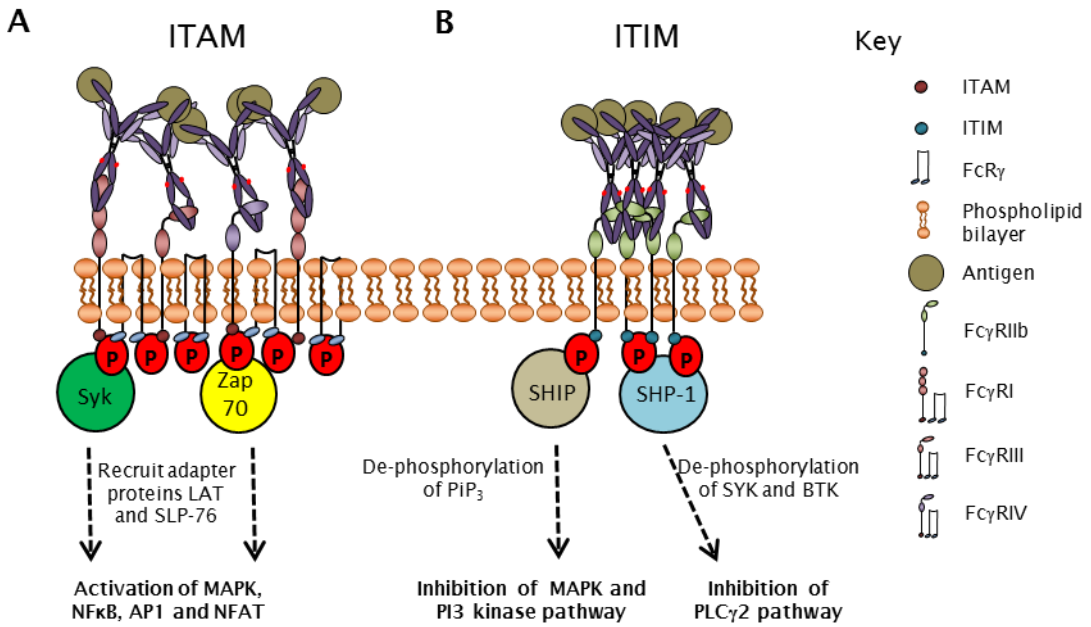

Figure 1-7 ITAM and ITIM signalling by FcγR

(**A**) ITIM signalling by activatory FcγR, clustering of ITAM receptors results in phosphorylation by SFK. Tyrosine kinases such as Syk and Zap 70 are recruited to the clustered ITAM receptor by virtue of SH2 domains. These kinases then act to phosphorylate adapter proteins LAT and SLP-76, leading to the downstream activation of cellular pathways. (**B**) ITIM signalling by inhibitory FcγRIIb, clustering of ITIM receptors results in phosphorylation by SFK. The phosphatases SHIP and SHP-1 are recruited to the clustered ITIM receptor by virtue of SH-2 domains, this results in de-phosphorylation of tyrosine kinases such as Syk, resulting in inhibition of downstream cellular pathways involved in activation.

1.6 Macrophages

Macrophage FcγR mediated phagocytosis has been shown to be critical to anti-CD20 therapy [109, 110, 135, 136]. The manipulation of macrophages is also being investigated to treat numerous cancers. Macrophages are a class of professional phagocytic cell first described by Elie Metchnikoff in 1884 [9]. These cells were later found to derive from monocytes which themselves, like B cells, derive from haematopoietic stem cells. As reviewed by Taylor *et al* there is an incredibly large amount of heterogeneity amongst macrophages and distinct macrophage subsets can be found in the liver (Kupffer cells), lung (alveolar macrophages), nervous system (microglia) and epidermis (Langerhans cells) [137, 138]. The precise generation and renewal of these macrophage subsets has not yet been fully determined [139].

1.6.1 The mononuclear phagocytic system

Van Furth & Cohn first described macrophages as originating from monocytes in the bone marrow. This conclusion originated from labelling experiments which incorporated thymidine-^{3}H into murine monocytes. It was found that these monocytes rapidly divided only in the bone marrow and in response to new born calf serum inoculation, peritoneum monocytes migrated to this site to become peritoneal macrophages [140]. This demonstrated that the development of monocytes occurs in the bone marrow and like B cell development requires progression through a number of check points [139]. As reviewed by Geissmann *et al*, macrophages, monocytes and dendritic cells, which make up the mononuclear phagocyte system (MPS), develop from common myeloid progenitors (CMP) which like the CLP develop from pluripotent haematopoietic stem cells [139, 141]. Important to the progression of HSCs towards a CMP is the transcription factor PU.1 [142]. PU.1 works by overriding transcription factors that would otherwise determine a separate cell fate and by promoting early growth response (Egr) transcription factors which promote monocyte/macrophage development [141].

The first myeloid cell subset to show distinct lineage is the macrophage/DC precursor (MDP). This subset is distinguished from the granulocyte/macrophage progenitor by its expression of the receptor colony

stimulating factor 1 (CSF-1) and the chemokine receptor CX3CR1 [141]. Dai *et al* highlighted the importance of CSF-1 to monocyte development. This group inactivated the murine CSF-1 receptor gene and found that mice lacking this receptor had dramatically reduced numbers of monocytes and showed a similar but more severe phenotype to osteopetrotic (op/op) mice (which lack the CSF-1 protein) [143]. Two types of monocyte are commonly generated from the MDP, $Ly6C^-$ cells give rise to alveolar macrophages whilst $Ly6C^+$ cells give rise to inflammatory monocytes/macrophages, MDSS and inflammatory DCs [139]. These monocytes will migrate from the bone marrow to tissue upon signalling by chemokine receptors such as CX3CR1 in response to environmental pro-inflammatory stimuli. In contrast to bone marrow derived monocyte and macrophage there are a tissue specific population, known as tissue resident macrophages.

Tissue resident macrophages are phagocytic cells thought to be predominantly involved in the clearance of apoptotic cells and the production of growth factors [139]. It is not yet fully understood how tissue macrophages develop. Work by Schulz *et al* described two early myeloid lineages in the mouse which arise from HSC, one is dependent upon PU.1 and the transcription factor Myb whilst the other, which originated from the yolk sac (YS), is dependent upon PU.1 but is independent of Myb. This work was the first to show that non-bone marrow derived macrophages make up part of the MPS system [144]. More recent work by the same group has established that in the mouse yolk sac tissue resident macrophages originate from a $Tie2^+$ cellular pathway generating $Csf1r^+$ erythro-myeloid progenitors (EMPs) and that these are distinct from HSCs [145]. Interestingly by 10 weeks gestation these yolk sac derived EMP cells colonise the foetal liver, giving rise to EMP derived erythrocytes, granulocytes, macrophages and monocytes. However, all but the macrophage population are replaced by HSC derived cells by 17 weeks gestation. However, studies based on foetal transfer of precursors suggest that in the long term Langerhans and alveolar macrophages are not derived from yolk sac precursors [146, 147].

1.6.2 Phagocytosis and inflammation

Phagocytosis is a dynamic process constantly changing in response to signals received during the engulfment process [148]. The molecular mechanisms defining the rearrangement of the phagocytes cytoskeleton and engulfment of the target are still being defined [149]. The mechanisms of phagocytosis have been reviewed by Flannagan, Jaumouille & Grinstein [134]. Phagocytosis is attributed to ingestion of large >0.5 μm particles and is an active process, needing recognition by cell surface receptors, primarily FcγR and TLR [134]. There is large variation in the types of cell that undertake phagocytosis with epithelial, endothelial and fibroblast cells being capable of phagocytosing apoptotic cells but unable to ingest microorganisms [134]. Following phagocytosis of necrotic or pathogenic material, macrophages will generally participate in a pro-inflammatory response. These responses are defined by the presence of pain swelling, redness and heat at the site of the infection. This reflects the changes in the local vasculature as it tries to slow the spread of potentially dangerous material [15].

The first stage in phagocytosis by macrophages is recognition of the target. This involves a host of cell surface receptors termed pattern recognition receptors (PRR) which recognise pathogen associated molecular patterns (PAMP), such receptors include Dectin-1 and the TLRs. The importance of Toll was first described by Lemaitre *et al* who showed that activation of the extracellular Toll ligand in Drosophila lead to expression of antifungal peptides and that if this Toll signalling pathway was knocked out then there was a dramatic reduction in survival following fungal infection [150]. Human homologues of Toll are therefore referred to as the Toll like receptors. The first TLR to be discovered was TLR4 which was later found to recognise lipopolysaccharide (LPS), a common constituent on bacterial cell walls [151, 152]. Upon binding to PAMPs dimerisation of TLRs will lead to the recruitment of an adaptor protein MyD88. Downstream this leads to the translocation of the nuclear transcription factor NFκB and production of pro-inflammatory cytokines such as TNFα and IL-12 [152].

Necrotic cells typically induce inflammation [153]. Work by Chen *et al* demonstrated that MyD88 also plays a role in the pro-inflammatory response to necrotic material. Here they injected freeze thaw treated cells into MyD88

deficient mice. These mice were therefore unable to activate NFκB in response to TLR signalling and had reduced recruitment of neutrophils. This was largely dependent on the IL-1 receptor and not the TLRs, as in the case of defence against microbes [154].

Research is now looking to identify non cytokine molecules that will elicit inflammation [153]. One such protein is high mobility group box 1 protein (HMGB1) which was shown to induce inflammation when released from necrotic cells. Once outside the cell HMGB1 will bind to the receptor for advanced glycation end products (RAGE) on the effector cell. Interestingly, HMGB1 is not released from apoptotic cells even when they have formed secondary necrotic bodies [155].

Another major contributor to the pro-inflammatory response against pathogens are the complement proteins C3a and C5a which are released in response to the breakdown of C3 and C5. These complement breakdown products act as pro-inflammatory mediators which recruit effector cells to the site of inflammation [156]. Interestingly, C5a and FcγR activation has been shown to be bi-directional, whereby engagement of the C5a receptor on the macrophage (CD88) sets the threshold for FcγR activation. Indeed, engagement of activatory or inhibitory FcγRs will modulate downstream C5a responses [85, 157, 158].

1.6.3 Phagocytosis of apoptotic cells

As recently reviewed by Hochreiter-Hufford & Ravichandran the clearance of apoptotic cells is the final stage of the apoptotic program and the key hallmark in this process is the absence of inflammation. During apoptosis the dying cell will release 'find me' and 'eat me' signals which lead to the recognition, response and removal of the apoptotic cell. Recognition signals include lysophosphatidylcholine (LPC), Cx3CL1 (fractalkine), the nucleotides ATP and UTP whereas the 'eat me' signal predominantly comes from phosphatidylserine (PS) (**Figure 1-8**) [159]. The process of apoptotic cell engulfment is generally associated with the release of anti-inflammatory cytokines such as TGF-β and IL-10. These cytokines act to create an immunologically silent response thus protecting the cell from inflammation and autoimmune responses [159-162].

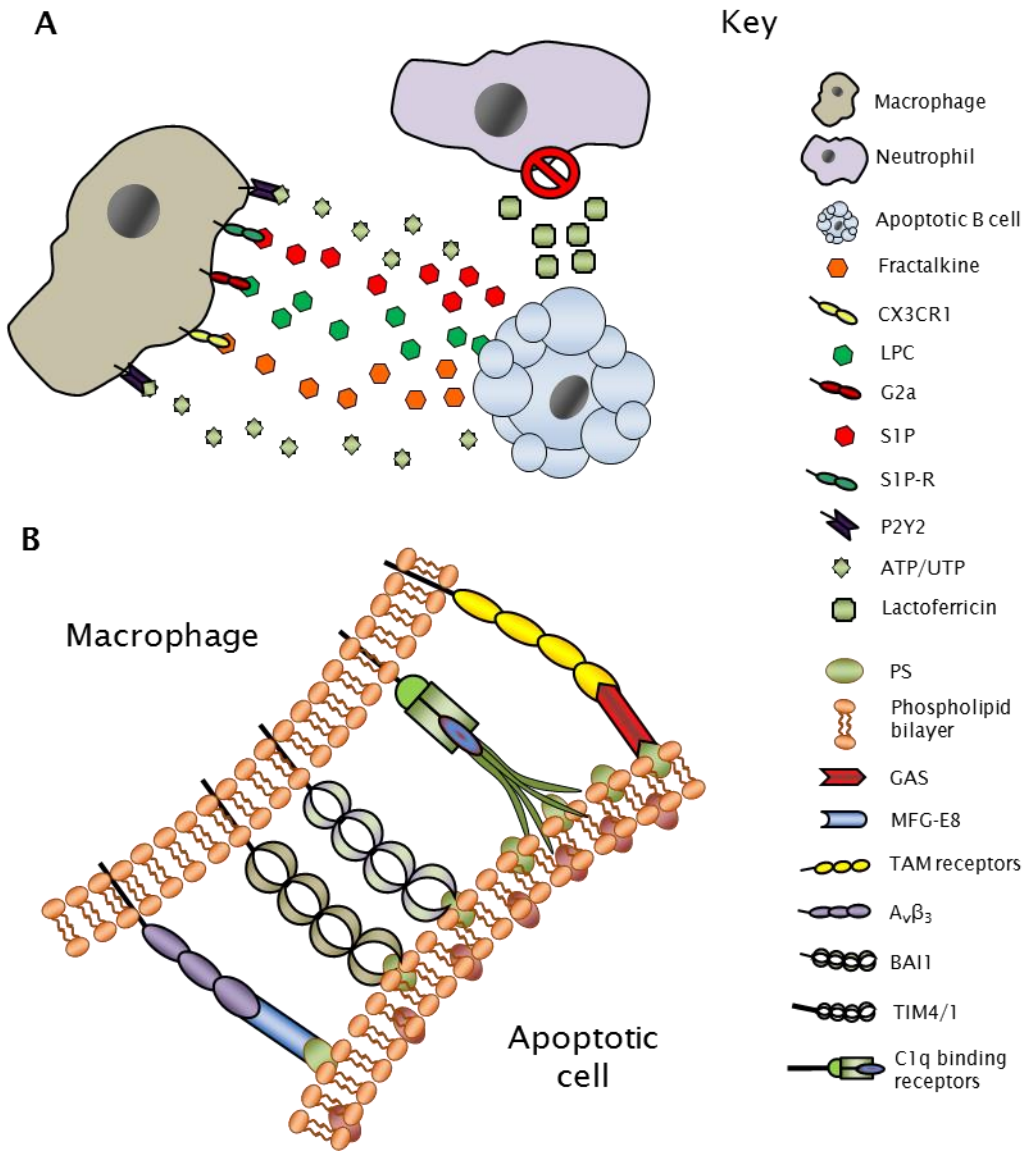

Figure 1-8: 'Find me' and 'Eat me' signals

Phagocytosis of apoptotic cells involves 'find me signals' that produce a chemotactic gradient for macrophages to follow then 'eat me' signals which facilitate the uptake of apoptotic cells. 'find me signals consist of ATP/UTP, S1P, fractalkine and LPC whereas phosphatidylserine comprises the major 'eat me' signal. Engulfed apoptotic material is degraded in $Lamp1^+$ lysosomes.

1.6.3.1 'Find me' signals

Fractalkine is a chemokine and intracellular adhesion molecule. Its release from the apoptotic cell as a 'find me' signal for macrophages is dependent upon caspases and Bcl-2. This was achieved by using Bcl-2 or pan caspase inhibitors such as z-VAD-fmk, which resulted in the loss of detectable fractalkine from

the cell surface [163]. Macrophages deficient for the fractalkine receptor (CX3CR1) do not migrate to secondary lymphoid organs, which under normal circumstances would contain large numbers of macrophages due to the high levels of apoptosis [163]. LPC was identified as a chemoattractant by Lauber *et al* who subsequently showed that the release of LPC was dependent upon caspase 3 activation [164]. The receptor for LPC which can be found on macrophages is G2a which is a G protein coupled receptor [164, 165]. Sphingosine 1-phosphate (S1P) is another lipid which acts as a 'find me' signal that is secreted by apoptotic cells. It functions by binding to sphingosine 1 phosphate receptors 1-5 (S1P-R1-5) on macrophages [159]. Elliott *et al* showed nucleotides to be an important class of find me signal secreted from apoptotic cells. This group showed that the nucleotides ATP and UTP are released in a caspase dependent manner and that when purified they elicit monocyte migration. In addition they show that treatment of apoptotic cell supernatants with apyrase (which hydrolyses ATP to AMP) diminishes the supernatant`s ability to attract monocytes. The phagocytic cell receptor for ATP and UTP was found to be a purinergic G protein coupled receptor, $P2Y_2$. It was shown that mice lacking the $P2Y_2$ receptor had significantly impaired monocyte and macrophage recruitment in response to apoptotic supernatants. *In vivo* it was found that mice lacking $P2Y_2$ had a reduced ability to clear apoptotic cells over wild type counterparts [166]. In addition, 'keep out' signals deter neutrophils and other phagocytic cells that may cause a pro inflammatory response from engulfing an apoptotic cell. One such keep out signal is lactoferricin (LTF) which was shown to selectively inhibit granulocytes but not monocytes through regulation of granulocyte signalling pathways which control adhesion and motility [167].

1.6.3.2 'Eat me' signals

Once attracted to an apoptotic cell professional phagocytes will react to certain 'eat me' signals which determine whether the cell needs to be ingested or not. The best studied 'eat me' signal is the exposure of PS on the apoptotic cell surface and Fadok *et al* showed that phagocytosis of apoptotic cells was inhibited in the presence of PS liposomes [168]. The mechanisms by which PS is exposed on the apoptotic cell are still being defined, although it appears to be caspase dependent and involve the TMEM16 family of calcium channels which were shown to mediate phospholipid scrambling [159]. There are a

number of receptors on the phagocytic cell that recognise exposed PS on the apoptotic cell. The Tyro-Axl-Mer (TAM) family of receptors, recognise exposed PS indirectly via the protein Gas6. These intermediate bridging proteins appear to be quite common in the recognition of apoptotic 'eat me' signals [159, 169]. Another such bridging molecule is milk fat globule EGF factor 8 (MGF-E8). Hanayama *et al* showed that MGF-E8 can be secreted from macrophages and will bind to PS [170]. Additionally the integrin receptor $\alpha_v\beta_3$ will recognise MGF-E8 and macrophages with elevated levels of $\alpha_v\beta_3$ show an enhanced ability to phagocytose apoptotic cells [170]. A final bridging molecule for the recognition of PS is calreticulin which Gardai *et al* showed to associate with exposed PS on apoptotic cells. It was also shown that calreticulin is up regulated on the cell surface of apoptotic cells [171].

Phagocytic cell receptors that directly recognise exposed PS include brain specific angiogenesis inhibitor 1 (BAI1). BAI1 was found to be a receptor upstream of the engulfment cell motility / detector of cytokines (ELMO/DOCK180/Rac) protein module which acts as a guanine nucleotide exchange factor (GEF) for the GTPase Rac. BAI1 was found to bind directly with PS to bring about this signalling which leads to phagocytosis [172]. The T cell immunoglobulin and mucin domain containing molecule 4 and 1 (TIM4/1) are transmembrane proteins that also bind directly to PS as shown through the use of anti TIM4/1 antibodies which blocked phagocytosis. However, it does not appear that they are directly involved in phagocytosis but have a role in tethering the apoptotic cell to the phagocyte [159, 173]. The importance of each 'find me' and 'eat me' signal and the receptors that sense them are still to be elucidated, although, it seems apparent that PS is critical to the effective phagocytosis of apoptotic cells.

The complement component C1q also acts as a bridging molecule between apoptotic and effector cells. C1q binds to apoptotic cells by its globular heads and will connect with a number of C1q binding ligands on effector macrophages and monocytes [174]. The systemic loss of C1q has been shown to have a significant impact on the formation of auto immune diseases and is frequently observed alongside SLE. Upon bridging apoptotic and effector cell, C1q has been shown to have a role in the anti-inflammatory response involving the uptake of apoptotic cells [175]. Work by Benoit *et al* demonstrated that

C1q remains bound to apoptotic lymphocytes during the phagocytic process and that C1q is responsible for altering signalling processes resulting in an increase of anti-inflammatory cytokines; IL-10, IL-27, IL-33, IL-37 and inhibition of NLRP3-dependent cleavage of caspase-1. This inhibition of caspase-1 cleavage will negatively impact on inflammasome formation and the increase seen in IL-33 may polarise macrophages to an alternatively activated phenotype [175]. It was also recently demonstrated that binding of C1q to apoptotic cells promoted the expression of Mer tyrosine kinase (MerTK) on macrophages, this receptor is also involved in the clearance of apoptotic cells and is mostly found on M2c polarised cells [176]. It is thought that C1q not only binds to apoptotic cells but also to immune complex. This prevents the immune complex interacting through FcγR with plasmacytoid dendritic cells (pDC) which would otherwise produce large amounts of pro-inflammatory INFα.

1.6.4 Macrophage Phenotype and polarisation

An important feature of macrophages is their extreme level of plasticity, being able to engulf and degrade undesired material but also promote growth and repair damaged tissue. This high level of heterogeneity has made the macrophage population hard to characterise as many phenotypic markers such as CD11b, F4/80, MHCII are found on a variety of different subsets. Although there are specific markers which can identify a macrophage population it is often a combination of markers and their expression level which is used to define the macrophage subset. To better define the variation in macrophage functions, cell subsets have been broadly defined as being either M1 or M2 like although this classification is losing favour as macrophages can fall anywhere along the spectrum of M1-M2. Macrophages are heavily influenced by their local environments. Pro-inflammatory cytokines such as IFNγ, which are generated in response to TLR engagement will polarise macrophages to a classically activated (M1-like) phenotype and in contrast many anti-inflammatory cytokines such as IL-13 and IL-4 will polarise macrophages to an alternative (M2-like) or wound healing phenotype [177].

Macrophages are known to become classically activated in response to two signals. The first is IFNγ which in combination with bacterial components such as LPS will prime the macrophage for activation [178]. The second signal comes in the form of endogenous TNFα which is produced by the macrophage

in response to TLR signalling. Both signals together result in the classical activation which is notably marked by an increase in nitric oxide (NO) synthesis, in mice [178]. Upon activation M1 macrophages will migrate to the site of inflammation and act to facilitate a pro-inflammatory response and engulf any pathogens present. They do this in a number of ways, M1 macrophages will have reduced levels of mannose receptor (CD206) and, inhibitory FcγRIIb [178, 179]. The enhanced killing by M1 macrophages is brought about by the increased levels of NO which act to degrade pathogens in the phagosome. In addition, iron and tryptophan are restricted from the phagosome and this hinders any intracellular pathogen growth [178]. Within tissues classically activated macrophages will associated with Th1 $CD4^+$ T cells to form granulomas which are highly pro-inflammatory and can cause local tissue destruction. Interestingly, tuberculosis infection which is associated with granuloma formation in the lungs typically results in carcinomas which are generated as a result of the high levels of local inflammation and tissue destruction [178, 180].

M2 macrophages are characterised as IL-12^{low}, IL-23^{low} and $IL10^{high}$ expressing cells [181]. M2 macrophages are linked with the recruitment of leukocytes, anti-inflammatory responses, tissue repair, allergic responses, resistance to helminth infection and tumour progression. In general they are associated with humoral Th2 responses [181]. Although, under physiological conditions macrophages are on a continuum of activation ranging from M1 to M2 and it was Mantovani et al who suggested further differentiation into M2a, M2b and M2c [182]. M2a macrophages are generally associated with regulated expression of pro-inflammatory cytokines IL-1, TNF and IL-6. It was also noted that M2 macrophages fail to produce NO due to elevated production of arginase. In addition M2 macrophages are generally poor at MHCII antigen presentation and can actively dampen T cell proliferation [178]. M2b macrophages are polarised by exposure to select TLR agonists. These macrophages are associated with an increase in pro-inflammatory cytokines and regulation of Th2 $CD4^+$ T cells and antibody production, whereas M2c macrophages are associated with increased IL10 production and have been shown to have an enhanced response to anti CD20 therapy [182, 183].

Macrophages are also heavily involved in tumorigenesis survival and growth. In order for a tumour to effectively establish itself it is heavily reliant upon its microenvironment. Stein *et al* reported that the anti-inflammatory cytokine IL-4 enhanced macrophage levels of CD206 and this was the first time the alternative (M2) activation of macrophages had been described [184]. Alternatively activated macrophages are an important part of this tumour microenvironment and can contribute growth factors and immune suppression. These macrophages can constitute myeloid derived suppressor cells (MDSC) which lead to tumour associated macrophages (TAM). These cells show similar characteristics to alternatively activated M2 macrophages in that they aid cell growth/tissue repair and in general suppress a pro-inflammatory response [185-187]. As reviewed by Allavena & Mantovani TAMs show similar properties to MDSC in that they promote angiogenesis and suppress adaptive immune responses [188]. Work by De Nardo *et al* demonstrated that IL-4 producing $CD4^+$ T cells indirectly enhanced metastasis by promoting polarisation to a TAM phenotype, which in turn enhanced epidermal growth factor signalling [189]. Upon entering the tumour microenvironment monocytes can differentiate into macrophages in response to M-CSF which is secreted by tumour cells and in combination with other suppressive cytokines such as IL-10 can skew macrophages to a TAM phenotype [188]. The perceived wound healing by macrophages in the context of tumours will only help in disease progression. This is why cancers have sometimes been referred to as never healing wounds [190]. Ways in which M2/TAM macrophages aid tumour progression are: increased arginase-1 and vascular endothelial growth factor (VEGF), decreased MHCII and NO synthesis, increased synthesis of IL-10 and transforming growth factor β (TGFβ) and decreased synthesis of IL-12 [188].

Tissue resident macrophages are self-renewing and do not develop in the bone marrow form an important macrophage population involved in tissue homeostasis and tumour progression. These cells are also subject to polarisation by the tumour microenvironment. Following the M1-M2 paradigm tissue resident macrophages are very broadly thought of as M2-like due to their wound healing capabilities and engulfment of apoptotic debris and maintenance of tissue homeostasis. However this varies from tissue to tissue and niche specific environments, furthermore in disease settings there is no distinction between recruited inflammatory macrophages and tissue resident

macrophages [191]. It has been reported that tissue resident macrophages will accumulate in and around the tumour as it develops from an early stage, due to the tumour secreting cytokines, including IL-4 and IL-13 which will polarise tissue resident macrophages to an alternatively activated M2/TAM-like state. Therefore, in contrast to classically activated inflammatory macrophages tissue resident macrophages will aid tumour growth. Insufficient immunosurveillance by tissue resident macrophages will lead to reduced recruitment of inflammatory monocytes and neutrophils thus aiding tumour progression. The importance of macrophages to tumour progression was shown through clodronate liposome depletion studies which resulted in reduced tumour growth [192, 193]. Therefore, a large area of future research is to better understand the monocyte and tissue macrophage activation as well as the tumour microenvironment in order to skew the phenotype to one appropriate (M1-like) to augment immunosurveillance and antibody therapies such as rituximab.

1.6.5 Macrophages and anti CD20 therapy

The activatory to inhibitory ratio (A:I) of FcγRs on effector cells is an important consideration for antibody therapy and is dependent upon numerous internal and external factors [194, 195]. For example it is known that some cytokines can skew the expression of FcγRs on macrophages and that the same cytokines are up regulated by apoptotic cells [157, 196]. Therefore, it may well be that skewing of macrophages by apoptotic cells affects the macrophages ability to phagocytose antibody targeted cells and that the addition of M1 skewing agonists may reverse this defect.

It is traditionally thought that classically activated M1 macrophages are best suited to depletion of anti-CD20 mAb coated cells. However, work by Leidi *et al* showed that human monocyte derived macrophages (MDM) polarised with IL-10 to give an M2c phenotype demonstrated increased killing of Rituximab opsonised leukemic targets compared to classically LPS/IFNγ (M1) polarised MDMs [183]. These authors also suggested that phagocytosis was not affected by CD20 levels or by FcγR polymorphism at 158 (Val/Phe) of FcγRIIIa but that phagocytosis was inhibited by excess immunoglobulins [183]. Interestingly polarisation with IL-10 increased expression of all FcγR whereas polarisation

with IL-4/13 decreased levels of FcγRI and FcγRIII [183]. In addition, it was demonstrated that moderate levels (400-1300 pg/ml) of IL-10 could be collected from the supernatant of the human leukemic Raji cells.

There are documented links between apoptosis and IL-10 production showing that inhibition of IL-10 leads to a reduction in Bcl-2 and sensitisation to cytotoxic drugs, suggesting that IL-10 is used as a pro-survival mechanism [197, 198]. The fact that tumours have been shown to produce IL-10 would appear at odds with the evidence that M2c polarised macrophages are effective at depleting Rituximab labelled B cells and requires further investigation. Recently work by Lawlor *et al* showed that the overexpression of Bcl-2 in the Vav Bcl-2 mouse led to an increase in the $Ly6C^{Lo}$ population of monocytes and an increase in the inhibitory FcγRIIb receptor on macrophages. Importantly, this was independent of IgG levels [199]. This may suggest that endogenous, elevated, levels of Bcl-2 in monocytes/macrophages work to increase levels of FcγRIIb. This would present an interesting avenue of research as it may also be true for B cells and as discussed above FcγRIIb is detrimental to antibody therapy. In contrast, work by Fudala *et al* showed in the lung that IL-8 ICs engaged with FcγRIIa to enhance Bcl-X_L levels in neutrophils and this acted to abate apoptosis, suggesting a link between IC, defective apoptosis and FcγR expression [44].

1.7 Mouse Models

Throughout this project a number of mouse models which represent different states of dysregulated apoptosis were used, of particular interest are the Vav Bcl-2 and Eμ Myc models. This is because they represent contrasting levels of cell death.

1.7.1 Vav Bcl-2 mouse

The Vav Bcl-2 mouse is very similar to what is seen in FL i.e. up regulation of Bcl-2 [200]. Ogilvy *et al* developed Vav Bcl-2 mice by targeted expression of the human Bcl-2 gene using the Vav promoter. This induced expression of Bcl-2 in all nucleated cells of the haematopoietic lineage [201]. Egle showed that Vav Bcl-2 mice develop germinal centre hyperplasia followed by FL like symptoms at ~10 months. Younger mice have larger germinal centres and an increased

number of circulating B cells. In addition, Vav Bcl-2 mice develop auto immune like kidney disease [202]. Interestingly, Eμ Bcl-2 mice which mimic the t(14;18) translocation and have increased Bcl-2 expression throughout the B cell lineage only, do not go on to develop follicular lymphoma like symptoms [202].

1.7.2 Eμ Myc mouse

Myc is a transcription factor necessary for the production of numerous proteins involved in cell cycle progression. The importance of Myc dysregulation is reflected by the fact that ~70 % of human cancers show Myc activation [203]. The Eμ Myc mouse model aimed to mimic Burkitt's lymphoma by introducing a t(8;14) translocation which places c-Myc under the control of the heavy chain enhancer. Eμ Myc mice present with increased numbers of pre-B cells. However, there is no increase in the number of mature B cells, this is due to effective apoptosis of pre-B cells, resulting from increased levels of the pro apoptotic protein puma [204]. Eμ Myc mice will eventually succumb to lymphomagenesis, this is brought about through mutations in P53 leading to subversion of pro apoptotic machinery [204-206]. Before the onset of lymphomagenesis we can use Eμ Myc mice as a model of elevated apoptosis.

1.8 Hypothesis and aims

It has been well documented that the depletion of target B cells in response to anti-CD20 antibodies is reliant upon FcγR interactions [110, 122] and that macrophages are likely to be the key effector cell involved in targeted B cell depletion [135, 136]. The surrounding microenvironment has been shown to impact on the activation status and FcγR expression of macrophages. Shushakova *et al* demonstrated that the generation of a pro-inflammatory response towards alveolar macrophages using IC resulted in modulation of FcγRIII by complement component C5a [157]. Under normal conditions there are large levels of systemic apoptosis every day. Lymphocytes in particular have high levels of apoptosis primarily due to the manner in which they are generated and function in an immune response. Macrophages are largely responsible for the clearance of apoptotic cells and the uptake of phagocytic cells is likely to have consequences for macrophage function and phenotype [162, 207-209].

Therefore, we hypothesise that macrophages are responsible for the majority of B cell depletion that occurs in response to anti-CD20 therapy and that alternate rates of apoptosis will impact on anti-CD20 therapy. Specifically, that low levels of systemic apoptosis such as those seen in the Vav Bcl-2 mouse will be detrimental to therapy. The lack of systemic apoptosis will educate macrophages to an alternatively activated phenotype. The FcγR repertoire of the macrophage will be altered in such a way as to give a decreased A:I ratio resulting in diminished phagocytic potential.

The aim of the current study was to investigate this hypothesis. The FcγR expression of various apoptosis resistant mice and the ability of macrophages to deplete anti-CD20 opsonised B cells was focused upon to address the following questions:

1. Are macrophages or NK cells the dominant effector cell, responsible for anti-CD20 mediated B cell depletion?

2. Do different rates and levels of apoptosis impact on anti-CD20 therapy?

3. Are there differences in the FcγR expression levels on apoptosis dysregulated effector cells?

4. In what way does abated apoptosis inhibit macrophage phagocytosis of anti-CD20 opsonised B cells?

Chapter 2: Materials and Methods

2.1 Primary CLL samples

Ethical approval for the use of clinical samples was obtained by the Southampton University Hospitals NHS Trust from the Southampton and South West Hampshire Research Ethics Committee (COREC 228/02/t). Informed consent was provided in accordance with the declaration of Helsinki.

2.2 Animals

Mice were bred and maintained in local facilities in accordance with home office guidelines. Experiments were cleared through local ethical committees and performed under Home Office licences PPL30/2451 and PPL30/2964. In-Bred C57BL/6 or BALB/c mice were obtained from Charles River Laboratories (Margate, Kent). Eμ Myc mice were supplied by Adrian Ochensberins (Bern, Swizerland) and were maintained on the C57BL/6 strain. Human CD20 Tg (hCD20) mice were obtained from Prof. Mark Shlomchik (Yale, USA) and were maintained on either a C57BL/6 or BALB/c background mFcγRI, IIb and III$^{-/-}$ mice were obtained from Dr. Sjef Verbeek, Leiden University (Leiden, the Netherlands). mFcγR$^{-/+}$ mice were obtained from the European Conditional Mouse Mutagenesis Program (Munich, Germany) and were intercrossed to obtain the homozygous knock out phenotype [210]. FcγRI/IIb/II/IV$^{-/-}$ (FcγR null) mice were generated and obtained from Dr. Sjef Verbeek, Leiden University (Leiden, the Netherlands) and were maintained on a C57BL/6 or BALB/c background [210]. Serum from autoimmune Murphy Roths Large (MRL$^{lpr/lpr}$) mice was obtained from Dr Jessica Teeling (University of Southampton). Vav Bcl-2, puma$^{-/-}$ and Bim$^{-/-}$ mice were obtained from Prof. Andreas Strasser (Melbourne, Australia) and were maintained on a C57BL/6 background. Both the FcγRIIb$^{-/-}$ and hCD20 mice were backcrossed by Dr Stephen Beers onto the BALB/c background and maintained in house.

2.2.1 Animal genotyping

2.2.1.1 hCD20 mice

C57BL/6 or BALB/c mice were ear tagged for identification and ~100 µl of peripheral blood obtained, by tail vein puncture, for genotyping purposes. Blood (20 µl) was opsonised with antibodies to human CD20-FITC (Ritm2a) and mouse CD19-PE (1D3). Samples were incubated for 20 minutes on ice before being subjected to red cell lysing buffer (AbD Serotec, Kidlington, UK) and washed in phosphate buffered saline (PBS) supplemented with 10 % BSA and 10 mM Sodium Azide, from now on known as FACS wash. Samples were acquired on either a FACS Scan™ or FACS Caliber™ flow cytometer (Becton Dickinson, Oxford, UK). Example positive and negative FACS plots can be found in (**Appendix 1**).

2.2.1.2 Vav Bcl-2 mice

C57BL/6 mice were ear tagged for identification and ~100 µl of peripheral blood was obtained, by tail vein puncture, for genotyping purposes. Blood (20 µl) was diluted 1:4 with PBS and cell number was quantified using a Coulter particle counter Z1 (Coulter Electronics, Luton, UK). Vav Bcl-2 mice have a higher total cell number compared to WT mice. If cell counts returned an uncertain result then genotyping was performed using intracellular staining for human Bcl-2. For this 25 µl of blood was fixed using 0.5 ml paraformaldehyde/PBS for 10 minutes at room temperature (RT). The sample was then washed in FACS wash and permeabilised with 80 % methanol (0.5 ml/tube) for 10-30 minutes at -20 °C. Samples were then washed in FACS buffer and stained with anti-human Bcl-2-FITC (BD Pharmingen, clone 124) in 0.3 % saponin (Sigma Aldrich, Dorset, UK). Samples were incubated on ice for 30 minutes and then washed in FACS wash containing 0.3% saponin. Samples were acquired on either a FACS Scan™ or FACS Caliber™ flow cytometer. Example cell counts, positive and negative FACS plots can be found in (**Appendix 2**).

2.2.1.3 Eµ MYC mice

C57BL/6 mice were ear tagged for identification and mouse tissue from the ear tagging process was digested in 100 µl of 50 mM Trisma pH 8.9 (Sigma

Aldrich, Dorset, UK), 12.5 mM magnesium chloride ($MgCl_2$) (Sigma Aldrich, Dorset, UK), 0.5 % Tween-20 (Sigma Aldrich, Dorset, UK) and 20 mg/ml Proteinase K (Sigma Aldrich, Dorset, UK), from now on known as DNA isolation buffer. Samples were incubated overnight at 55 °C.

Genomic DNA was assessed by PCR using the following primers;

5' Myc primer (myc1): CAGCTGGCGTAATAGCGAAGAG

3' Myc primer (myc2): CTGTGACTGGTGAGTACTCAACC

The PCR master mix for each samples contained 1 µl 5' primer (forward primer) (100 ng/ml), 1 µl 3' primer (reverse primer) (100 ng/ml), 16 µl sterile deionised water (dH_2O), 5 µl 5X green GoTaq buffer (Promega, Southampton, UK), 0.5 µl Go Tag DNA polymerase (Promega, Southampton, UK), 0.5 µl dNTPs (Promega, Southampton, UK) and 1 µl of purified DNA. PCR was performed using a PTC-100 programmable thermal controller (MJ research, Waltham, USA) and the following program; 1) 94 °C for 4 minutes, 2) 94 °C for 40 seconds, 3) 55 °C for 30 seconds, 4) 72 °C for 60 seconds, 5) repeat steps 2-4 for 30 cycles, 6) 72 °C for 5 minutes. The resulting PCR fragment is 900 base pairs (bp) long. PCR products were resolved on a 0.7% agarose gel enriched with a 1:20,000 GelRed nucleic acid stain (Cambridge Bioscience, Cambridge, UK) and the samples were analysed by gel electrophoresis, 170V for ~30 minutes. Results were visualised by exposing the agarose gel to UV light using the GelDoc system (Bio-Rad, Hemel Hempstead, UK).

2.3 Antibodies

A number of anti CD20 and isotype control mAb were used throughout this thesis. Clinical grade rituximab (hIgG1) was obtained from Southampton General Hospital oncology pharmacy. Herceptin was used as an isotype control for hIgG1 and was also obtained from Southampton General Hospital oncology pharmacy. Ofatumumab was made in house from patent published sequence. Obinutuzumab was obtained from Dr. Christian Klein, Roche™ (West Sussex, UK). Antibody engineered versions of Rituximab, Ofatumumab and Obinutuzumab variants incorporating a mIgG2a or mIgG1 were made in house by Dr Claude Chan, as was the mIgG2a isotype control WR17. These antibodies

were produced from the supernatants of stably transfected CHO-k1 cells. All antibodies were purified on protein A columns and purity was assessed by electrophoresis (Beckman EP system; Beckman), lack of aggregation was confirmed by SEC HPLC and all preparations confirmed endotoxin low (<1 ng/mg protein) using the Endosafe-PTS system (Charles River Laboratories).These experiments were performed by Mrs Chris A Penfold and Dr Jini H Kim.

2.4 Tissue culture

All tissue culture was carried out using class II safety cabinets and molecular grade reagents. Cell quantification was achieved using a Coulter particle counter Z1.

2.4.1 Murine L929 cells

Murine L929 cells were cultured in RPMI-1640 (Life Technologies, Paisley, UK) enriched with 10% heat inactivated foetal calf serum (FCS) (Lonza Biologics PLC, Slough, UK), 2 mM glutamine (Life Technologies, Paisley, UK), 1 mM pyruvate (Life Technologies, Paisley, UK), 57.2 µM 2-mercaptoethanol (Sigma Aldrich, Dorset, UK), 100 µg/ml penicillin (Life Technologies, Paisley, UK) and 100 µg/ml streptomycin (Life Technologies, Paisley, UK), from now on known as complete media. Cells were cultured at 37 °C (5 % CO_2) in tissue culture flasks. Supernatant was collect once cells were confluent and filter sterilised using a Millex 0.22 µM PES membrane filter (Fisher Scientific, Loughborough, UK). Samples were stored at -20 °C until needed.

2.4.2 Murine bone marrow derived macrophages

Bone marrow derived macrophages (BMDM) were prepared by euthanizing mice with CO_2 followed by cervical dislocation. With scissors, the hind legs of the mouse were removed and placed into ice cold PBS (Lonza Biologics PLC, Slough, UK). Muscle tissue was removed from the hind legs and the bone marrow flushed, with PBS, into a 50 ml conical tube (Fisher Scientific, Loughborough, UK) using a 20 ml syringe and 25 gauge needle. Bone marrow was passed through a 100 µm cell strainer (Scientific laboratory services (SLS), Hessle, UK) to make a single cell suspension. This suspension

was transferred to a 50 ml conical tube and centrifuged for 5 minutes at 458 g, RT.

Cells were then resuspended in complete media. Splenocytes were diluted to $1x10^6$ cells/ml and aliquoted 4 ml/well into a 6 well tissue culture plate (Fisher Scientific, Loughborough, UK). To stimulate macrophage development, 20 % of L929 supernatant, which contains murine macrophage colony stimulating factor (M-CSF), was added to the sample. Cells were then incubated at 37 °C (5 % CO_2) in a humidified incubator. Media was changed on days 3 and 7, using a jumbo pastette (Alpha Labs, Eastleigh, UK). The 6 well plates were then washed in PBS and 5 ml of complete media containing 20 % L929 added. BMDMs were typically used for experimentation between days 7 and 10.

2.4.3 Monocyte derived macrophages

Human monocyte derived macrophages (MDM) were prepared from concentrated samples of human peripheral blood (National blood services, customer Number 5055). Human blood was placed into a 50 ml conical tube and diluted to 50 ml using PBS supplemented with 2 mM EDTA and 10 % heat inactivated FCS. Peripheral blood mononucleocytes (PBMC) were isolated using two 50 ml conical tubes by carefully layering 25 ml of pre-diluted blood onto 12.5 ml, room temperature, Lymphoprep™ (STEMCELL technologies, Cambridge, UK). Using a contained centrifuge, samples were centrifuged for 20 minutes at 800 g, RT, with the break released. Following centrifuging, the interphase layer from each tube, which contains PBMC, was removed using a 3 ml pipette and transferred to a separate 50 ml conical tube. PBMC were then washed by diluting the sample to 50 ml using PBS containing 2 mM ETDA and 10 % heat inactivated FCS and centrifuging for 5 minutes at 300 g (RT). Supernatant was discarded and wash steps repeated at least three times until there was a clear loss of platelets. Finally, cells were resuspended to $1x10^7$ cells/ml in RPMI-1640 medium enriched with 1 % human AB serum (In-house), 2 mM glutamine, 1 mM pyruvate, 100 µg/ml penicillin and 100 µg/ml streptomycin, from now on known as R10 medium. Into a 6 well tissue culture plate 2 ml of cells ($1x10^7$ cells/ml) were placed and incubated for 2 hours at 37 °C, to allow cells to adhere. Cells were then washed at least two times, so that there was a semi-confluent monolayer of cells adhered to the bottom of each

well, and resuspend in 2 ml R10 medium. Cells were incubated overnight and the following day 200 ng/well of M-CSF (In-house) was added. R10 media enriched with 200 ng/well M-CSF was replenished on days 3 and 6 and MDMs were typically used in functional assays between days 7-10.

2.4.4 Murine natural killer cells

A single cell suspension of splenocytes was prepared by euthanizing a C57BL/6 mouse followed by removal of the spleen which was then disassociated and passed through a 100 µm cell strainer (Fisher Scientific, Loughborough, UK). This single cell suspension was collected and centrifuged at 458g for 5 minutes, RT, after which the supernatant was discarded and the cells resuspended in ~10 ml PBS. The cell suspension was then passed through a 100 µm cell strainer before being processed using a magnetic automated cell sorter (MACS) murine NK (mNK) cell isolation kit (Miltenyi Biotech, Surrey, UK), according to the manufacturer's instructions. This is a negative selection kit which uses a primary biotin-antibody cocktail; CD4 (L3T4, rat IgG2b), CD5 (Ly-1, rat IgG2a), CD8a (Ly-2, rat IgG2a), CD19 (rat IgG2a), Ly-6G (Gr-1, rat IgG2b), Ter-119 (rat IgG2b). These antibodies target all cell populations present except NK cells. Anti-biotin microbeads were then added, these microbeads are conjugated to a monoclonal anti-biotin antibody (Bio3—18E7.2, mouse IgG1) and so will bind to the primary antibodies. Sample was then passed through a MACS LS column (Miltenyi Biotech, Surrey, UK) where magnetically labelled non-NK cells are retained on the column in the magnetic field of a midiMACS separator (Miltenyi Biotech, Surrey, UK).

Isolated mNK cells were resuspended to a concentration of $1x10^6$ cells/ml in complete media. Recombinant murine IL-2 (Peprotech, London, UK) was then added (200 ng/ml). IL-2 facilitates NK cell proliferation by binding to the IL-2R on NK cells which triggers downstream signalling for proliferation [211]. NK cells were transferred to a 48 well tissue culture plate (Fisher Scientific, Loughborough, UK) 1 ml/well and incubated at 37 °C and 5 % CO_2. Media was changed on day 4 by collecting the media from each well and adjusting the concentration of mNK cell to $1x10^6$ cells/ml. Murine IL-2 (200 ng/ml) was then added back into the medium. The cell suspension was then transferred back to a 48 well plate or to either a 24 well or 6 well plate depending on the volume of media used. mNK cells proliferated rapidly and

additional media containing 200 ng IL-2 was added every 1-2 days. NK cells were typically used during the third week of growth since this provided adequate numbers for experimentation.

2.5 Antibody effector function assays

All data was obtained using either a FACS Canto™ II or FACS Caliber™ flow cytometer (Becton Dickinson, Oxford, UK) and data was analysed using FCS express (De Novo Software, Glendale, CA) FACS Diva (Becton Dickinson, Oxford, UK), Microsoft Excel (Microsoft, USA) and GraphPad Prism 6 (GraphPad Software, Inc., La Jolla, CA) software.

2.5.1 Murine ADCP assay

To remove adherent BMDM cells, (between days 7-11 post-harvest) 1-2 ml warm Trypsin/EDTA (Life Technologies, Paisley, UK) was added for 15 minutes at 37 °C (5 % CO_2). Following incubation cells were removed from the bottom of their 6 well plate using a cell scraper (Fisher Scientific, Loughborough, UK) and diluted in complete media before being centrifuged for 5 minutes at 458 g (RT). Cells were then resuspended in 10 ml complete media and quantified. Cells were adjusted to $5x10^5$ cells/ml using complete media containing 20 % L929 then 100 µl/well ($5x10^4$ cells/well) transferred to a 96 well flat bottom plate. Water or PBS was added to the outside wells of the 96 well plate to prevent loss of sample due to evaporation ('edge effect'). Cells were incubated at 37 °C (5 % CO_2) until needed, typically 1-2 days later.

Target hCD20 B cells were obtained by euthanizing C57BL/6 or BALB/c mouse and removal of the spleen into ice cold PBS. The spleen was disassociated using a 100 µm cell strainer and the rubber end of a 2 ml syringe. Sample was centrifuged for 5 minutes at 458 g (RT) and then passed through a 100 µm cell strainer a second time. B cells were isolated using a Miltenyi MACS murine B cell isolation kit (Miltenyi Biotech, Surrey, UK) following manufacturer's instructions. This kit works on the same principles as the mNK cell isolation kit described in **2.4.4** however antibodies are directed against; CD43 (Ly48, rat IgG2a), CD4 (L3T4, rat IgG2b) and Ter-119 (rat IgG2b). Following B cell isolation cells were centrifuged for 5 minutes at 458 g, RT and then

resuspended at $1x10^7$ cells/ml in PBS. B cells were stained with 5(6)-carboxyfluorescein (CFSE) (5 μM) (Sigma Aldrich, Dorset, UK) and incubated in the dark at RT for 10 minutes. Following CFSE staining samples were incubated with an equivalent volume of heat inactivated FCS for 1 minute to stop the reaction. Samples were then diluted in complete media before being centrifuged for 5 minutes at 458 g (RT). Following centrifugation samples were resuspended to $2.5x10^6$ cells/ml in complete media.

Target B cells were opsonised with desired anti-CD20 mAb at 10 μg/ml unless specified. Samples were incubated for 30 minutes at 4 °C. Following antibody opsonisation target B cells were washed in FACS wash. Supernatant was discarded and samples were resuspended to $2.5x10^6$ cells/ml in complete media. Next, BMDMs were washed in PBS and the supernatant removed. Then 100 μl of B cells were added to the relevant wells and samples incubated for 30 minutes at 37 °C (5 % CO_2). Following co-culture, F4/80-APC antibody (Serotech, UK) (CI:A3-1) was added to the relevant wells in order to identify the macrophage population. Samples were incubated at room temperature for 15 minutes before being placed on ice. All wells were washed using a multichannel pipette with 200 μl warm FACS wash then 200 μl ice cold FACS wash. Samples were rested for 10 minutes before being transferred to FACS tubes. Samples were then acquired on a FACS Caliber™ flow cytometer. Phagocytosis was calculated as the percentage of $CSFE^+$, $F4/80^+$ events within The $F4/80^+$ positive population. $F480^+$ events are gated on a forward and side scatter high population which are inclusive of granulocytes but not lymphocytes.

2.5.2 Murine ADCC assay

Target hCD20 B Cells were isolated from mouse spleen cells using a B cell isolation kit (Miltenyi Biotech, Surrey, UK) as previously described in **2.5.1**. Isolated B cells were resuspended to a concentration of $1x10^7$ cells/ml and then stained with 10 μl/ml of acetoxymethyl ester (calcein-AM) (Life Technologies, Paisley, UK). When inside a live cell calcein-AM is converted to calcein by intracellular esterases allowing its retention. Upon lysis of B cells by effector cells calcein is released into the supernatant and is detectable at 530 nm when excited at 495 nm. Target hCD20 B cells were incubated with calcein-AM at 37 °C for 1 hour with agitation every 15 minutes. Following incubation

the reaction was inhibited by addition of an equivalent volume of heat inactivated FCS. To remove excess calcein-AM, cells were centrifuged at 458 g for 5 minutes (RT) and were washed three times in PBS containing 10 % heat inactivated FCS.

Target hCD20 B cells were resuspended in complete media to a concentration of $2x10^6$ cells/ml. Next, a 96 well round bottom plate (Fisher Scientific, Loughborough, UK) was prepared by adding 50 µl of complete media containing the relevant mAb at the desired concentration to each of the desired wells. 50 µl of target hCD20 B cells were then added to each of the relevant wells and incubated for 30 minutes (4 °C). Effector NK cells were harvested and resuspended in complete media to a concentration of $1x10^7$ cells/ml and 100 µl of NK cells added to target hCD20 B cells, this gave a 1:10 ratio of targets to effectors (T:E) ratio. Samples were then centrifuged at 300 g for 3 minutes (RT) and incubated at 37 °C for 2 hours.

Following this incubation, samples were centrifuged for 3 minutes at 300 g. Next, 75 µl of supernatant from each relevant sample was transferred to a Greiner CELLSTAR 96 well plate (Sigma Aldrich, Dorset, UK). It was important at this stage not to disturb the cell pellet since B cells containing calcein would falsely increase the background fluorescence. Sample data was acquired on a Varioskan™ Flash plate reader (Thermo scientific, UK), with excitation at 495 nm. In addition to this 100 µl of remaining sample was transferred to a FACS tube (SLS, Hessle, UK) and stained with NK1.1-APC (PK136) (eBiosciences, UK) for 15 minutes at room temperature. Samples were washed in FACS wash and examined by flow cytometry.

2.5.3 Human ADCP assay

Human MDM cells were generated as described in **2.4.3**. Human ADCP assay was performed in a manner equivalent to that described in **2.5.1**. Briefly, on day 8-10 MDM were harvested by repeated agitation with ice cold PBS and 100 µl was plated out into a 96 well microtitre plate at $1x10^5$ cells/ml. Target B cells, typically human CLL samples were stained with CFSE (5 µM) for 15 minutes at RT. An equivalent volume of heat inactivated FCS was added. Samples were washed and resuspended in complete media. Target B cells were then co-cultured with MDM at a 1:5 T:E ratio at 37 °C for 1 hour. To highlight

the MDM population samples were stained with CD16-APC. Samples were then washed and acquired on a flow cytometer.

2.5.4 Human ADCC

Human PBMC cells were generated as described in **2.4.3**. Human ADCC assay was performed in a manner equivalent to that described in **2.5.2**. Briefly; target B cells, typically Primary CLL stained with calcein-AM (5 μM). Effector cells were PBMCs isolated from whole blood as described in **2.4.3**. Target B cells were co-cultured with effector cells at a 1:50 T:E ratio. Samples were co-cultured for 4 hours at 37 °C. Samples were then centrifuged and 75 μl of supernatant was analysed for fluorescence as described in **2.5.2**.

2.6 Macrophage polarisation

Macrophages were polarised to either an M1 or M2 phenotype. Confirmation of macrophage polarisation was obtained by observing a 'change' in cell morphology, characterization of phenotypic changes by flow cytometry or by measurements of NO/Arginase activity. All results were analysed using Microsoft Excel and GraphPad Prism 6 software.

2.6.1 M1 polarisation

To obtain an M1 polarisation BMDM, in complete media, were incubated with IFNγ (2 ng/ml) (Peprotech, Southampton, UK) and LPS (100 ng/ml) (Sigma Aldrich, Dorset, UK) for 24 or 48 hours.

2.6.2 M2 polarisation

To obtain an M2a polarisation BMDMs were incubated with murine IL-4 (10 ng/ml) (Peprotech, Southampton, UK) and IL-13 (10 ng/ml) (Peprotech, Southampton, UK) for 24 or 48 hours. To obtain an M2c polarisation BMDMs were incubated with murine IL-10 (10 ng/ml) (Peprotech, Southampton, UK) for 24 or 48 hours.

2.6.3 Detection of NO

To detect murine macrophage M1 polarisation measurements of NO were taken. Macrophages, when activated make use of reactive oxygen species to inactivate their targets, therefore reactive oxygen species such as NO will be elevated in classically activated M1 macrophages. In a 96 well plate 100 µl of cell culture supernatant to be tested was added. A standard curve of sodium nitrate ($NaNO_3$) (250-0 µM) was prepared in RPMI-1640 supplemented with 10 % FCS and 100 µl added to the 96 well test plate. In dH_20 a mixture of 0.1 % N-(1-napthyl)ethylene-diamine dichloride (NED), 1 % Sulfanilamide and 5 % phosphoric acid was made and 100 µl added to each standard and test sample. Samples were incubated for 10 minutes at RT. Absorbance at 570 nm was then taken using an EPOCH microplate spectrophotometer (BioTek instuments, Inc., Winooski, USA). Results were interpreted from the standard curve and expressed as µM using Microsoft Excel software. Functionally this assay works through N_2 associating with sulphanilamide to form diazotized sulphanilamide. The presence of phosphoric acid gives a low pH which allows the coupling of diazotized sulphanilamide with NED to form a reddish azo compound that can be detected by spectrometry at 570 nm. All reagents were purchased from Sigma Aldrich, Dorset, UK unless otherwise stated.

2.6.4 Detection of M2 macrophages

When macrophages are M2 polarised they produce elevated levels of arginase-1 which is associated with suppression of Th2 cytokine-driven inflammation. Arginase levels were measured indirectly since urea was measured as a product of arginase activation. Cells of interest were lysed using 25 µl of 0.1 % Triton X-100 in 50 mM Tris-HCL containing 0.1 mg/ml of pepstatin A, aprotinin and phenyl-methl-sulphonly (PMSF) and allowing samples to incubated for 30 minutes at RT. To activate any arginase present 25 µl of 10 mM manganease chloride ($MnCl_2$), 50 mM Tris-HCL pH7.5 was added and samples incubated for 10 minutes at 55 °C. To activate any arginase present 50 µl of L-arginine (0.5 M) was added and samples incubated for 60 minutes at 37 °C. L-arginase will be hydrolysed to ornithine + urea by any surrounding arginase. This reaction was stopped through the addition of 400 µl sulphuric acid (H_2O_4) (2.5 M) and 85 % Phosphoric acid (H_3PO_4). A standard curve of urea was generated (30-0

µg/ml) and 100 µl added to the 96 well test plate. Finally, 25 µl of ethanol containing 7% α-isonitroso-propiophenone was added and samples incubated for 45 minutes at 100 °C. 7% α-isonitroso-propiophenone will react with urea to form a coloured product that can be read using spectrophotometry at 570 nm. Samples were acquired using an EPOCH microplate spectrophotometer. Calculation of arginase levels was determined using a standard curve of a known urea concentration and results were expressed as µg/ml. All reagents were purchased from Sigma Aldrich, Dorset, UK.

2.7 Adoptive transfer assay

Wild type and hCD20 transgenic mice were euthanized and the spleens removed in ice cold PBS. Spleens were kept separate and were disassociated using a 100 µm cell strainer and the rubber end of a 2 ml syringe. WT and hCD20 splenocytes were adjusted to a concentration of $1x10^7$ cells/ml in PBS. WT splenocytes (non-target; nT) were stained with 0.5 µM CFSE whereas hCD20 splenocytes (target; T) were stained with 5 µM CFSE for 15 minutes at RT. FCS of the same volume was then added for 1 minute to quench further labelling. A 1:1 mixture of WT and hCD20 splenocytes was made and $5x10^6$ cells of this mix were injected i.v. into the desired recipient mice. 24 hours post injection each mouse was administered 10 or 50 µg (i.v.) of the desired anti-CD20 antibody or irrelevant control (WR17).

The following day experimental mice were euthanized using CO_2 and the spleens removed in ice cold PBS. Spleens were kept separate and were disassociated using a 100 µm cell strainer and the rubber end of a 2 ml syringe. Cell suspensions were centrifuged at 458 g for 5 minutes (RT) the cell supernatant discarded and sample resuspended in PBS before being passed through another cell strainer to remove any remaining debris. Samples were again centrifuged at 458 g and resuspended in ~2 ml PBS. Splenocytes (200 µl) were added to the appropriate FACS tubes and stained (10 µg/ml) with anti CD19-APC (1D3, eBioscience). Samples were then acquired on a FACS Canto™ flow cytometer.

The target to non-target ratio (T:nT ratio) was calculated as:

T:nT= % T/ % nT

This was normalised for each experiment as:

Normalised T:nT = T:nT/(average of WR17 treated T:nT)

2.7.1 Clodronate liposome production

In some experiments clodronate liposomes were used to deplete the macrophage population prior to adoptive transfer assays. Preparation of clodronate liposomes was carried out in a fume hood. Clodronate liposomes were produced by dissolving 8 mg cholesterol (Sigma Aldrich, Dorset, UK) into 10 ml chloroform (Sigma Aldrich, Dorset, UK) using a 50 ml glass centrifuge tube. Next, 860 µl (86 mg) of Phosphatidylcholine (PC) (Sigma Aldrich, Dorset, UK) at 1 mg/ml was added to sample. The chloroform phase was removed by gently blowing Nitrogen gas into the tube over ~ 1-2 hours. The phospholipid film was dispersed in 10 ml of PBS or clodronate (Sigma Aldrich, Dorset, UK) solution containing 2.5 g clodronate in 10 ml dH_20 (0.6 M). It takes ~ 30 minutes to 1 hour of resuspension with intermediate sonication to fully disperse the liposomes. Non-encapsulated clodronate was removed by centrifugation (10,000 g) for 15 minutes at 4 °C using an ultra-centrifuge. Clodronate liposomes form a milky band on top of a relatively clear solution, whereas the PBS fraction pellets at the bottom of the centrifuge tube. The PBS and clodronate fractions were collected and resuspended in PBS. This wash step was repeated 4 times to ensure that all chloroform had been removed before use *in vivo*. Liposomes were resuspended in PBS and stored under nitrogen in a parafilm sealed tube at 4 °C for up to two weeks. For *in vivo* depletion of splenic macrophages mice were injected twice with 200 µl (i.v.) of liposome 48 hours apart. Depletion occurred within 24 hours and lasted up to 7 days.

2.8 Antigenic modulation assay

In a 96 well flat bottom plate 200 µl of cells at 1 x 10^6 cells/ml were incubated at 37 °C (5 % CO_2) for 0.5, 2 or 4 hours with Alexa-488 labelled anti-CD20 antibody (5 µg/ml). Cells were harvested and washed twice by adding 3 ml FACS wash and centrifuging at 458 g for 5 minutes (RT). Cells were resuspended in 200 µl of PBS then 100 µl of cells was transferred to a FACS

tube and left as untreated, this was the non-quenched sample. Another 100 µl was transferred to a FACS tube and 2.5 µl of anti-Alexa-488 mAb (Life technologies, Paisley, UK) was added, this is the quenched sample. Analysis of non-quenched and quenched samples was performed on a FACS Scan™ flow cytometer. Data for the non-quenched and quenched values were reported as MFI of FL-1 and results were expressed as a percentage of fluorescence of the non-quenched sample:

$$\% \text{ Quenching} = \frac{((\text{non-quenched-background}) - (\text{quenched-background}))}{(\text{non-quenched} - \text{background})} \times 100$$

2.9 *In vivo* B cell depletion experiments

C57BL/6 or BALB/c mice (3-5 mice per group), 8-14 weeks old, were treated i.v. with 250 ug of irrelevant or anti-CD20 antibody. The percentage of circulating B cells was monitored over 100 days by flow cytometry. To determine the percentage of circulating B cells, peripheral blood (~100 µl) was obtained through tail vein puncture. This blood was stained with anti-CD19-APC (1D3) and B220-PerCP (RA3-6B2). Samples were then acquired on a FACS Caliber™ flow cytometer. Data was analysed using Microsoft Excel and GraphPad Prism software.

2.10 Enzyme linked immunosorbant assays

Enzyme linked immunosorbent assays (ELISA) were used to detect the human and murine IgG levels as well as immune complexe. Data was analysed using ReaderFit™, Microsoft Excel and GraphPad Prism 6 software.

2.10.1 Human IgG detection

Human immunoglobulin in plasma was measured by first coating a 96 well immunomaxisorb ELISA plate (Fisher Scientific, Loughborough, UK) with 100 µl rabbit anti-human polyclonal IgG (In-house) at 25 µg/ml in ELISA coating buffer (15 mM Sodium Carbonate, 28.5 mM Sodium Bicarbonate). Plates were covered and incubated for 1 hour at 37 °C then at 4 °C overnight. The following day this coating solution was removed by inversion of the plate and blotting on

paper towel then 100 µl of PBS/1 % BSA was added to each relevant well. Plates were incubated at RT for 1 hour to block any non-specific binding. Following this plates were washed 3 times in PBS/0.05 % tween, using a SKANWash plate washer (MTX lab systems, Inc., Vienna, USA).

Polyclonal human IgG1 was used to generate a standard curve (10 – 0 µg/ml) and 100 µl added to the test plate. Plasma samples were initially diluted 1:2,000 from neat plasma and then serially diluted 1:2 across the plate. Samples were incubated at RT for 90 minutes. Following incubation, samples were washed 5 times using the SKANWash plate washer. Goat anti-human HRP antibody (Stratech Scientific, Ltd., Suffolk, UK) was then prepared in PBS/ 1 % BSA and 100 µl added at a 1:2,000 dilution to each relevant well. Samples were incubated for 90 minutes at RT.

Enzyme substrate was prepared by dissolving an o-phenylenediamine dihydrochloride (OPD) tablet (Sigma Aldrich, Dorset, UK) in 24.7 ml of ELISA citrate (19.2g/L citric acid). When dissolved 25.3 ml ELISA phosphate (28.4g/L Sodium Phosphate) and 50 ml dH_20 were added. Enzyme substrate was stored in the dark and just before use 40 µl of 30% hydrogen peroxide (H_2O_2) was added. Following the incubation with secondary HRP conjugated antibody the samples were washed 5 times using the SKANWash plate washer and 100 µl of enzyme substrate added. Samples were then incubated in the dark at room temperature for 30 minutes, to allow colour development. To stop the reaction 50 µl of 2.5 M Sulphuric acid was added. Samples were read using an EPOCH microplate spectrophotometer, measuring absorbance at 490 nm. Plasma concentration of antibody was calculated using the standard curve and reported as µg/ml.

2.10.2 Murine IgG detection

The detection of murine IgG was performed as described in **2.10.1** with the following changes; Coating antibody was rabbit anti-mouse IgG (in-house), detection antibody was rabbit anti-mouse IgG HRP (Stratech Scientific, Ltd., Suffolk, UK), polyclonal murine IgG (Cambridge Bioscience, Cambridge, UK) was used as a standard.

2.10.3 Murine IgG subset detection

The detection of murine IgG isotypes was performed as described in **2.10.1** with the following changes: Goat anti-mouse IgG (Cambridge Bioscience, Cambridge, UK) was used to coat ELISA plates at 25 µg/ml. Antibody isotype was detected in serum samples using either Goat anti-mouse IgG2c-HRP, IgG1-HRP or IgG2b-HRP, all purchased from Cambridge Bioscience, Cambridge, UK. All secondary antibodies were used at 1:5000 dilutions. Standard curves of either a mouse IgG1 (3G8), IgG2c (18B12) or IgG2b (F2-2) were produced using control mAb of known concentrations.

2.10.4 Immune complex detection

The detection of immune complex was adapted from the ELISA method in **2.10.1** and previous publications [212, 213]. Rather than using an antibody to capture immune complex, human C1q full length Protein (Abcam®, Cambridge, UK) was used. C1q was resuspended in ELISA coating buffer to a concentration of 2.5 µg/ml and 100 µl used to coat each well of a 96 well microtitre plate. ELISA plates were probed with serum samples of various dilutions and detection of immune complex was achieved using a Goat anti-mouse IgG-HRP antibody. Heat aggregated WR17 was used as a standard and monomeric WR17 was used as a negative control these were both of a mouse IgG2a isotype.

2.11 Surface plasmon resonance

Surface plasmon resonance (SPR) analysis was achieved using Biacore™ T-100 analyser (GE Healthcare, Buckinghamshire, UK). mAb (10 µg/ml) in 10 mM Sodium acetate pH 5.5 was immobilised to 1000 response units (RU) to a CM5 sensor chip (GE Healthcare, Buckinghamshire, UK). This was achieved using the amine coupling kit from Biacore™ (GE Healthcare, Buckinghamshire, UK). Briefly, mAb was covalently bound to the carboxymethylated dextran matrix on the sensor chip by amine coupling at a flow rate of 5 µl/min. This involved coupling a carboxy group in the dextran matrix to an amine group on the mAb. The surface of the chip was exposed to a 1:1 ratio of N-hydroxysuccinimide (NHS) and 1-ethyl-3 (3-dimethylaminopropyl)-carbodimide (EDC) coupling solutions for 6 minutes. This converts the carboxymethyl

groups to ester groups that react easily with amines. Hydrochloric acid (HCl) was run over the surface of the chip for 6 minutes to block all uncoupled ester groups. The surface was then rinsed with 0.1 M glycine HCL buffer (pH 2.5) for 3 minutes to remove any non-specifically bound proteins. In order to measure FcγR binding affinity, soluble FcγR (R&D systems, Abingdon, UK) were used at various concentrations (200-20 nM) in 1 x HBS-EP$^+$ buffer (GE Healthcare, Buckinghamshire, UK) at 30 µl/min, with 300 seconds association and 600 seconds dissociation. Affinity constants were derived by analysis of association and dissociation using a 1:1 binding model using bioevaluation software (GE Healthcare, Buckinghamshire, UK).

2.12 Size exclusion chromatography

Size exclusion chromatography (SEC) was performed using two 1.6 x 94.3 cm Superdex™ 200 columns (GE Healthcare, Buckinghamshire, UK) and a 2138 UVICORD S detector (LKB Bromma, Sweden). mAb was acquired at a speed of 0.3 ml/min over a 16-24 hour period. The buffer used to acquire sample contained Tris 0.2 M (pH8), HCL 0.1 M and EDTA 10 mM from now on known as TE8 running buffer. Fractions were collected at 15 minute intervals and each fraction contained 4 ml of sample. Results were recorded onto graph paper using a 22-10 1 channel recorder (LKB Bromma, Sweden). The desired fractions were pooled and mAb was concentrated to greater than 2 mg/ml using Amicon Ultra centrifuge units (Millipore, Watford, UK). Centrifuge tubes were prepared by centrifugation with ~3 ml PBS at 3202 g for 10 minutes. Sample was then loaded and centrifuged at 3202 g for 30 minutes to 1 hour. Sample was collected and stored long term at -20 °C.

2.13 Antibody dialysis

Antibody dialysis was performed to exchange the buffer which antibody was solubilised in. To dialyse antibody into PBS Slide-A-Lyzer™ dialysis cassettes (Life technologies, Paisley, UK) were used. These were first pre-soaked in PBS before the mAb to be dialysed was injected into the cassette using a needle and syringe and the cassette placed into PBS. This was at a 1:1,000 dilution i.e.

1 ml mAb in cassette into 1000 ml PBS. Dialysis cassettes were left on a magnetic stirrer to equilibrate in at room temperature. Buffer was exchanged every 2-3 hours with a minimum of three exchanges. The mAb was removed from the cassette using a needle and syringe and quantified using a Nanodrop ND-1000 (Fisher Scientific, Loughborough, UK) and passed through a 0.22 µM filter prior to use.

2.14 Generation of immune complex

Whole IgG was prepared in PBS at a concentration greater than 5 mg/ml. samples were heat aggregated at 65 °C for 30 minutes. Confirmation of heat aggregation was obtained using a ZORBAX G250 HPLC column (Agilent Technologies, UK). Separation of aggregated IgG and non-aggregated monomeric IgG was achieved by SEC as described in **2.11**. Following SEC samples were concentrated and dialysed into PBS. Samples were stored short term at -20 °C.

2.15 Antibody deglycosylation

Deglycosylation of mAb was performed using PNGase F (Promega, Southampton, UK) which removes all glycan residues from Asn-297. Antibody was dialysed into PBS then 0.05 units of PNGase F /µg of antibody was added. Sample was incubated overnight (~20 hours) at 37 °C. Confirmation of deglycosylation was achieved using SDS Page gel, electrophoresis analysis. Whereby, 5 µg of 2 ME reduced mAb was loaded into a NuPage 10 % Bis Tris gel (Life Technologies, Paisley, UK) and acquired at 220 V, 30-60 minutes. Deglycosylated product shows a fractionally lower band to WT product. Successful deglycosylation was also confirmed using SPR as described in **2.11** by looking at the binding affinity to host FcγR. Excess PNGase F was removed from antibody by SEC as described in **2.12**.

2.16 Detection of murine FcγR by flow cytometry

Cells ($1x10^6$), typically murine splenocytes or bone marrow, were stained for 30 minutes on ice with 1 µl of each of the following antibodies; anti-mouse CD11b-PE (M1/70), F4/80-APC (CI:A3-1), Ly6G-PEcy7 (RB6-8C5), Ly6C PerCP

Cy5.5 (HK1.4), CD19-APC eFluor780 (1D3), CD3-BD Horizon 500 (500A2) (Becton Dickinson, Oxford, UK) and NK1.1 eFluor 450 (pk136), antibodies were from eBioscience, UK, unless otherwise stated. Cells were also stained with 10 µg/ml In-house, FITC conjugated, anti-mouse FcγRI (AT159-1 $F(ab)_2$), FcγRIIb (AT130-2 N297A) FcγRIII (AT154-2 $F(ab)_2$) or FcγRIV (AT130 $F(ab)_2$). Irrelevant $F(ab)_2$ was used as a control antibody. Cells were then washed in red blood cell lysis buffer and centrifuged at 458 g for 5 minutes (RT). Supernatant was discarded and cells washed in 3 ml FACS wash and centrifuged at 458 g for 5 minutes (RT) to remove excess antibody and red blood cell lysis buffer. Samples were then acquired on a FACS Canto™ II flow cytometer. Data was analysed using FCS express, Microsoft Excel and GraphPad Prism 6 software. For each FcγR stained sample; neutrophils, monocytes, macrophages, B cells, NK cells and T cells were gated upon and the geometric mean of FL-1 (FITC) reported. These values were transformed, for each sample, by multiplying the activatory receptor values for FL-1 together and then dividing them by the FL-1 value for the inhibitory receptor this was then expressed as a ratio compared to the non-treated control mouse (A:I ratio).

2.17 Quantification of FcγR mRNA

BMDM cells were treated for 48 hours with aggregated or monomeric IgG (WR17). BMDM (>$1x10^6$ cells) were harvested and pelleted via centrifugation at 180 g for 5 minutes (4 °C). Total cellular RNA was purified through use of the Purelink RNA mini-kit (Life technologies, Paisley, UK), following manufacturer's instructions. Complementary DNA (cDNA) synthesis was then undertaken using the Superscript first strand synthesis system (Life Technologies, Paisley, UK) following manufacturer's instructions. cDNA was then diluted 1:3 in nuclease-free water and 0.5 µl (~3 ng) mixed with: 4 µl RNase-free H_2O, 5 µl platinum quantitative PCR supermix-UND (Life Technologies, Paisley, UK) and 0.5 µl FcγR gene-specific Taqman FAM-TAMRA probe. Acquisition of data was performed using a CFX96™ real time detection system (Bio-Rad, USA) and CFX manager software (Bio-Rad, USA). Data was analysed in Microsoft Excel and GraphPad Prism 6. The number of cycles required for the fluorescent signal to reach a pre-determined value is known as the threshold cycle (c(T)) and is directly proportional to the amount of starting material. cT values were calculated automatically by CFX software and transformed in Microsoft excel by

expressing the cT for each FcγR as a ratio of the NT material, this was known as the normalised ΔΔ Ct.

2.18 Murine B cell subset immunophenotyping

To look for mature B cells C57BL/6 or BALB/c splenocytes were stained for 20 minutes on ice with 1 µl of the following antibodies: CD19-APC (1D3), B220-PerCP (RA3-6B2) (Bio Legend, UK), CD21-PE cy7 (8D9), CD23-PE (B3B4), IgM-APC (II/41), CD38-PB (90). Immature B cells in murine bone marrow were identified by staining with CD19-APC (1D3), B220-PerCP (RA3-6B2), IgM-APC (II/41), IgD-PB (11-26c), CD43-PE (S7). All antibodies were from eBioscience, UK, unless otherwise stated. Samples were additionally stained with 10 µg/ml In-house, FITC conjugated, FcγRIIb (AT130-2 N297A). Samples were washed in red blood cell lysing buffer and centrifuged at 458 g for 5 minutes (RT). Supernatant was discarded and samples were washed in 3 ml FACS wash and centrifuged at 458 g for 5 minutes (RT) to remove excess antibody and RBC lysis buffer. Samples were acquired on a FACS Canto™ II flow cytometer and data was analysed using FCS express, Microsoft Excel and GraphPad Prism 6 software. The geometric mean for FL-1 was reported for pro B cells, pre B cells, immature B cells, follicular B cells, mature B cells, marginal zone B cells and germinal centre B cells.

2.19 Antibody quantification

Cells were stained with anti-CD20 mAb (10 µg/ml) for 20 minutes at 4 °C. Samples were then washed in FACS wash and centrifuged at 458 g (5 minutes, RT) to remove excess mAb. Cells were then stained with Goat anti-mouse or human IgG-PE (Stratech Scientific, Ltd. UK) for 20 minutes at 4 °C. Samples were washed in FACS wash and centrifuged at 458 g for 5 minutes (RT) to remove excess antibody. Samples were acquired on a FACS Scan™ flow cytometer. In order to quantify the amount of antibody on the cell surface QuantiBRITE™ beads (Becton Dickinson, Oxford, UK) were acquired on the same flow cytometer immediately after acquisition of cells. QuantiBRITE™ beads are various sized beads containing a known number of PE molecules/bead. This will reflect the number of mAb on the cell surface assuming a 1:1 ratio of PE to mAb. Data was analysed using Microsoft Excel

and GraphPad Prism software. The MFI of FL-2 (PE) was transformed into the number of PE molecules per cell (#PE/cell) as follows:

Sample MFI / Bead MFI x Bead #PE/cell

2.20 In vitro apoptosis assay

Annexin V was produced and FITC conjugated in-house. Propidium iodide (PI) (Sigma Aldrich, Dorset, UK) was reconstituted in dH_20. Both are non-membrane permeable and can be used to detect cell death and apoptosis. During the early stages of apoptosis PS will flip from the inner to the outer cell membrane. Annexin V will bind to PS as it is exposed on the cell membrane thus highlighting any apoptotic cells. PI will intercalate into the DNA of cells that have permeabilised membranes, so have gone beyond the initial stages of apoptosis. By using both Annexin V and PI both early stage apoptotic and late stage apoptotic/necrotic cells can be identified.

Cells of interest were resuspended to $1x10^6$ cells/ml then a stock solution containing Annexin V-FITC (16 µg/ml) and PI (90 µg/ml) was made in 100 mM HEPES, 1.4 M Sodium chloride and 25 mM calcium chloride, from now on known as 10x binding buffer. This mixture was added to the required sample 1:10 so that the final concentration of Annexin V and PI was 1.6 µg/ml and 9 µg/ml respectively. Samples were incubated in the dark at RT for 15 minutes. Samples were assessed by flow cytometry using either a FACS Scan™ or FACS Caliber™ machine. Cells undergoing apoptosis were identified as FL-1 positive events, FL-1 and FL-2 positive events indicated late stage apoptotic/necrotic cells and an absence of FL-1 or FL-2 fluorescence indicated that cells were viable.

2.21 Statistical analysis

All statistical tests were performed using GraphPad Prism 6 software. All data were analysed by one-way ANOVA or two-way ANOVA, with multiple comparison tests where appropriate.

Chapter 3: Antigenic modulation impacts on ADCC and ADCP effector mechanisms

3.1 Introduction

Rituximab was first approved for clinical use during 1997 following several successful clinical studies McLaughlin *et al* investigated its potential as a single use agent. They treated relapsed or low grade FL patients over a number of days totalling four intravenous doses, each of 375 mg/m^2. They found that just under half of the 166 patients enlisted responded with a median time to progression of 13 months, which was comparable with the success of single agent chemotherapy at the time [214]. Furthermore, when combined with standard chemotherapy, a cocktail containing cyclophosphamide, doxorubicin, vincristine and prednisone (CHOP) rituximab was found to significantly prolong event free survival in the treatment of elderly patients with diffuse large B cell lymphoma [215]. Today rituximab is used as a first line treatment in combination with CHOP chemotherapy for the treatment of several types of NHL [95].

Following on from the success of rituximab are the next generation anti-CD20 antibodies including ofatumumab and obinutuzumab. Ofatumumab was developed in an effort to generate more potent anti-CD20 reagents and was made using human immunoglobulin transgenic mice [77]. These mice have targeted disruption of the endogenous murine heavy and light κ chain genes which is brought about by deletion of the heavy chain J gene and the light chain κ constant and J gene segments. These deletions were accomplished in combination with the introduction of human transgenes which contain fragments of the human heavy and light κ chain immunoglobulin loci [78]. The introduced human heavy chain transgene included 4V, 16D and 6J gene segments as well as the Cμ and Cγ regions. The introduced light chain transgenes included 4Vκ and 5Jκ gene segments as well as the Cκ gene region.

There was also an additional transgene containing extra Vκ light chain gene segments [78]. Of the anti-CD20 antibodies generated in these mice 2F2 (ofatumumab) showed a slower cell dissociation rate (off rate) and enhanced CDC, due to increased C1q activation and was able to lyse a number of rituximab resistant CLL targets. Ofatumumab also showed type I antibody characteristics in that it successfully redistributed CD20 into Triton X-100 insoluble lipid rafts [77]. It was subsequently found using epitope mapping studies and peptide screening that ofatumumab and all the other anti-CD20 mAb raised in the Immunoglobulin transgenic mouse recognise a unique region of CD20 away from that detected by rituximab and other anti-human CD20 mAb [216]. In 2009 ofatumumab was approved by the food and drug administration (FDA) for clinical use in fludarabine resistant CLL patients [217, 218].

Obinutuzumab (GA101, GAZYVA®) was developed in 2010 by Mossner *et al* to address the problem of resistance associated with anti-CD20 therapeutics. The key differences with obinutuzumab compared to other anti-CD20 antibodies in the clinic are its type II nature and its Fc glycomodification, designed to enhance FcγRIIIa affinity [219]. These changes were achieved by grafting the complementary determining region sequences (CDR) from the murine anti-CD20 mAb B-ly1 onto a human framework. Glycoengineering of the antibody was achieved using the glutamine synthetase expression system, whereby Chinese hamster ovary (CHO) cells were engineered to overexpress the recombinant glycosylation enzymes β-1, 4-N-acetyl-glucosaminyltransferase III and Golgi α-mannosidase II. Overexpression led to an accumulation of antibody glycoforms containing bisected non-fucosylated oligosaccharides attached to Asn-297. This process essentially defucosylated the Fc portion of the antibody which resulted in enhanced binding to FcγRIIIa [219, 220].

Laboratory experiments revealed obiunutuzumab to show type II antibody characteristics: it was unable to stabilise CD20 molecules into Triton X-100 resistant lipid rafts; it showed diminished CDC and also enhanced homotypic adhesion of B cells *in vitro* [219]. Subsequently, Golay *et al* showed that obinutuzumab also has an increased affinity for FcγRIIIb and that this was important for neutrophil mediated B cell depletion [221]. Obinutuzumab was recently approved for first-line treatment in patients with CLL, following

successful clinical trials comparing chlorambucil plus either rituximab or obinutuzumab. It was found that treatment with obinutuzumab significantly improved progression free survival over that of rituximab although greater adverse events, typically involving neutropenia were observed when treating with obinutuzumab [131].

Despite their widespread use in the clinic the mechanisms behind how anti-CD20 mAb deliver their therapeutic benefit are still being investigated. As highlighted in the chapter 1 rituximab and other anti-CD20 mAb are proposed to operate through three effector functions; PCD, ADCC and CDC [88, 94, 95]. Further to this, the field is now largely contented that FcγR are absolutely critical to effective antibody therapy [110, 113, 114]. For most mAb what is still debated is to what extent different cell types expressing FcγR contribute to B cell depletion, namely whether effector outcome is predominantly governed by ADCC and NK cells or ADCP and macrophages and it is this question which will be addressed throughout this chapter.

In both mice and humans, multiple cell types express FcγR with variable expression patterns. B cells express only the inhibitory FcγRIIb, with the exception of a minor proportion of the human population who express an open reading frame for FcγRIIc [222]. NK cells express only FcγRIIIa and macrophages, neutrophils and monocytes variably express the full repertoire of FcγR [127]. The contribution of NK cells has largely been inferred from *in vitro* studies using human blood, which has a bias for containing NK cells compared to macrophages. Experiments have also showed that human IgG1 binds more strongly to homozygous FcγRIIIa-158V rather than 158F and that patients with two copies of the high affinity allele associated with a better response in clinical trials [223]. Although and as stated in these papers, it should be recognised that macrophages, monocytes and neutrophils also express FcγRIIIa and so these polymorphisms will also affect their function too.

Further evidence for the possible therapeutic contribution of NK cells came from a phase one clinical trial into the use of IL-2 as a co-therapeutic with rituximab, this found that there was increased clinical response as the number of NK cells increased and that elevated levels of ADCC ensued following IL-2 therapy [224]. Also, B lymphoma cells have been shown to escape rituximab targeted deletion through the up regulation of HLA class I antigens a process

that would increase activatory killer immunoglobulin like (KIR) mediated suppression of NK cells [225]. Finally, a separate body of work has investigated the use of co-stimulatory antibodies against CD137 (41-BB) which is a co-stimulatory receptor upregulated on activated NK and memory T cells. The addition of CD137 resulted in the up-regulation of NK cell degranulation and tumour cell lysis [226-228]. Similar results have now been shown with anti-KIR antibodies which target the receptors expressed on NK cells [229].

Although NK cells have been seen as the main cytotoxic effector, an increasing body of work now supports macrophages as the most important effector cell subset. Data for this has largely come from the systemic depletion of macrophages in mice using clodronate containing liposomes which can result in an inability to deplete anti-CD20 opsonised B cells *in vivo* [122, 135, 136]. Also, a recent role for neutrophils has been proposed by Albanesi *et al*, when this group depleted neutrophils using an anti-Gr1 antibody and used B16-F10 melanoma or BT474 breast carcinoma tumour models to show that neutrophils are needed for tumour rejection and that there is no role for NK cells, macrophages or monocytes [230]. Furthermore, liver kupffer cells have been cited as the major cell subset responsible for B cell phagocytosis in response to antibody therapy. Early work by Gong et al investigated the effector mechanisms required for B cell depletion in the hCD20 mouse. Here it was again found that Fc:FcγR interactions were critical and that depletion of effector cells through clodronate liposomes nullified the majority of B cell depletion. Interestingly this group also investigated the contributions of the spleen and liver to B cell depletion, they found that splenectomised mice showed no abrogation in B cell depletion and in fact had enhanced depletion, in response to anti CD20 mAb. In contrast, mice which had their blood supply to the liver severely restricted showed a profoundly reduced ability to deplete B cells in response to anti CD20 mAb. Further histological analysis revealed co localisation of $B220^{+}$ opsonised B cells and $F4/80^{+}$ effector cells [231]. This data in combination with recent intravital imaging [136] highlights the importance of the liver in B cell depletion.

Despite the success of anti-CD20 antibodies, patients often become resistant to therapy and relapse. Acute resistance can be associated with loss of CD20 from the cell surface, particularly in the case of CLL. Work by Jilani *et al*

highlighted that CD20 can become down modulated following treatment with rituximab and that this was not due to rituximab masking the detection of CD20 following therapy [116]. Successively, our group has shown that antigenic modulation, whereby CD20 antibody/antigen complexes are internalised after type I mAb binding impacts on the efficacy of anti-CD20 antibodies. This is accelerated by FcγRIIb expression [122, 232, 233].

A competing theory for the loss of CD20 from the cell surface is through trogocytosis of antibody and antigen from the cell surface, termed the shaving reaction. Work by Kennedy *et al* in 2004 showed that there is a rapid consumption of complement following the standard high dose (375 mg/m^2) of rituximab. Further to this, the rapid reduction in B cell numbers was seen to be transient with the returning B cells having significantly reduced CD20 on the cell surface. This led to the idea that antigen antibody complexes are removed from the target cell by effectors [117]. Expanding on this work in 2006, Beum *et al* showed that THP-1 monocytes and PBMCs incubated with opsonised B cells had demonstrable levels of antibody:CD20 complex on the cell surface of effector cells and that inhibition of FcγR signal transduction or the use of a F(ab_2) antibody prevented this process from occurring [120]. Subsequent experimentation revealed that this process is mediated by FcγRI [120].

In this chapter we wished to further investigate which effector cells are important for human anti-CD20 mAb therapy and whether antigenic modulation is having an impact on killing by these effector cells. We demonstrate that antigenic modulation impacts upon ADCP and ADCC in both the mouse and human systems *in vitro* and that ADCP is the dominant effector mechanism of B cell depletion, mediated by anti-CD20 mAb, in the mouse. These data explain the greater efficacy of type II antibodies *in vivo* in mice, and have implications for future antibody selection and development in humans.

3.2 Investigation into the impact of antibody type and class on B cell depletion

Previous work by Beers *et al* has demonstrated the superior depleting ability of the type II anti-CD20 mAb tositumumab over that of Ritm2a in human CD20 Tg mice [109, 122]. These antibodies were both of a mouse IgG2a isotype which has been well documented to be optimal for depletion studies in mice [128]. To determine the efficacy of human IgG1 antibodies in B cell depletion comparisons were made between clinically relevant rituximab, ofatumumab and obinutuzumab (glycomodified and non-glycomodified) with class switched mouse IgG2a versions in systemic long term *in vivo* depletions (**Figure 3-1**). For clarity obinutuzumab (OBZ, GA101) is the clinical reagent which has been glycomodified so as to improve FcγRIIIa binding whereas obinutuzumab-gly (OBZ-gly, BHH2hIgG1) is a parental human IgG1 version which has not been glycomodified and so has comparable Fc binding properties to that of rituximab. Throughout these depletion studies mice were bled periodically and the blood stained with antibodies against CD19 and B220 to detect B cells. Following acquisition by flow cytometry B cells were regarded as being CD19 and B220 positive events and these were gated upon. Results are reported as the percentage of B cells compared to time 0; time 0 was the percentage of B cells in the circulation prior to treatment with therapeutic antibody. We found that for all antibody isotypes tested the type II antibodies provided prolonged B cell depletion compared to type I antibodies (**Figure 3-1b vs Figure 3-1c**). Additionally, at least with regards to the type I antibodies, the mouse IgG2a versions outperformed the human IgG1 versions (**Figure 3-1c**).

Since they have been shown to have different affinities for activatory and inhibitory mouse FcγRs [128] comparisons were also made between mouse IgG2a and IgG1 versions of rituximab and obinutuzumab (**Figure 3-1d**). These results demonstrated that for both rituximab and obinutuzumab the IgG2a versions of these antibodies out-performed IgG1. Since isotype matched type I and II antibodies performed differently with regards to B cell depletion capacity this suggested that there were inherent differences between the type I and II antibodies ability to deplete B cells. The next set of experiments aimed to

probe why it might be that type II antibodies were outperforming type I anti-CD20 antibodies in terms of prolonged B cell depletion.

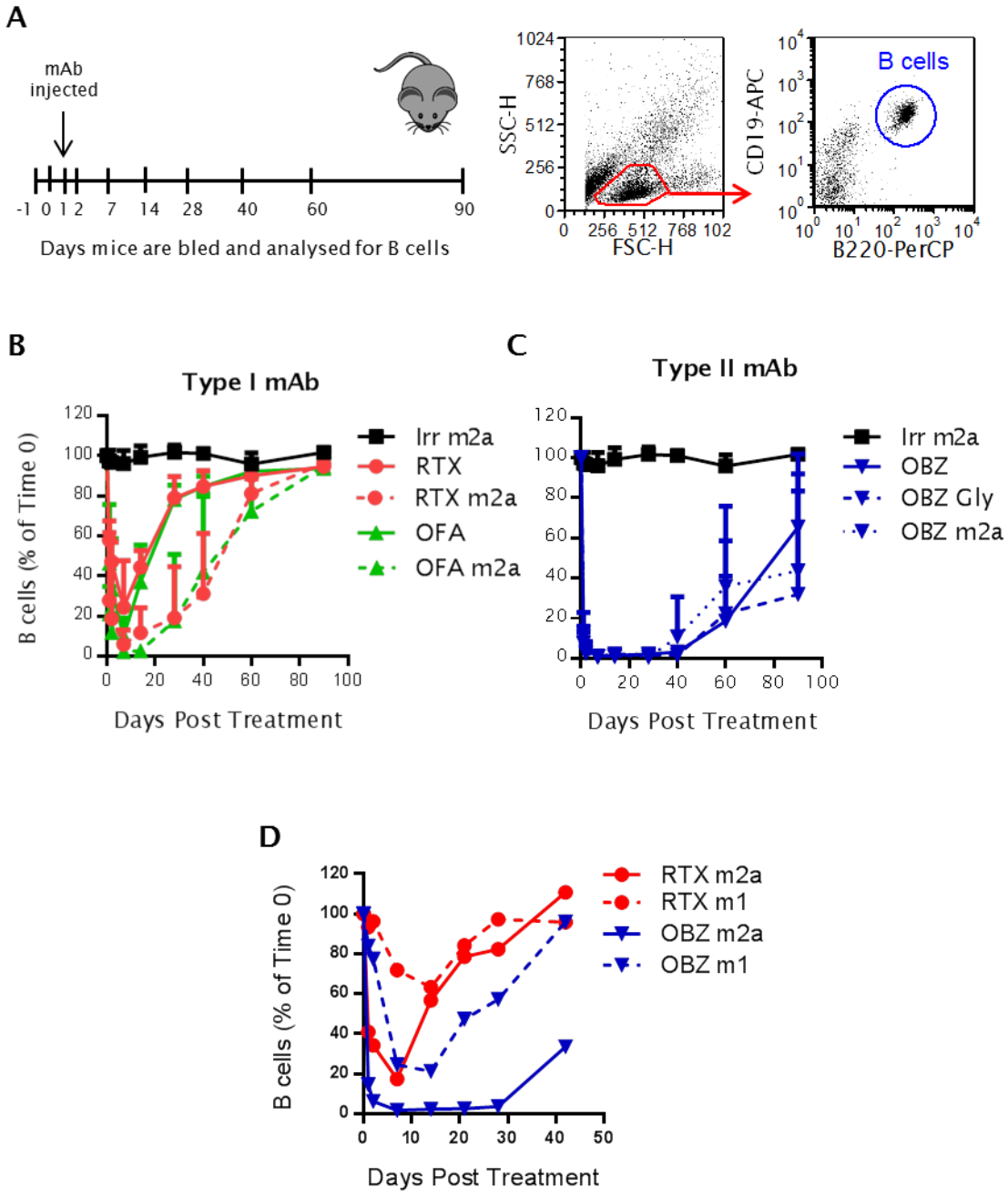

Figure 3-1 *In vivo* depletion using type I and II antibodies of various isotype

(**A**) Schematic representation of *in vivo* B cell depletion studies, mice were bled before injection of therapeutic antibody then again after, periodically, for 90 days. Blood was stained and B cells were determined as $B220^{+}$ and $CD19^{+}$ by flow cytometry. The percentages of B cells remaining compared to pre-treatment results are reported. (**B-C**) Transgenic hCD20 mice were administered 250 µg anti-CD20 by tail-vein injection and the percentage of circulating B220, $CD19^{+}$ B cells measured over 90 days (N=4). (**D**) Transgenic hCD20 mice were administered 250 µg anti-CD20 by tail-vein injection and

the percentage of circulating B220, $CD19^+$ B cells measured over 40 days (N=3). Experiments in **B** - **D** were performed by Dr Stephen Beers.

A possible explanation for the differences between type I and II antibodies seen in **Figure 3-1** could be a difference in FcγR binding affinity between isotype matched type I and II antibodies. To test this hypothesis SPR analysis was used, as described in **2.11**, to measure the binding affinity of rituximab and obinutuzumab Fc regions of human IgG1, mouse IgG2a and mouse IgG1 isotype against mouse FcγRI - IV (**Figure 3-2**).

Results from **Figure 3-2** and **Table 1** revealed that mouse IgG1 from both rituximab and obinutuzumab had no detectable affinity for FcγRI and FcγRIV but moderate affinity to FcγRIIb and FcγRIII. The mouse IgG2a versions of rituximab, ofatumumab and obinutuzumab had high affinity for FcγRI and FcγRIV, little affinity for FcγRIIb and moderate affinity for FcγRIII, in keeping with the published literature [128]. Finally, the clinically relevant hIgG1 versions of these antibody displayed similar characteristics to the mouse IgG2a versions: They had high affinity for FcγRI and FcγRIV and little affinity for FcγRIIb. However, in contrast to mouse IgG2a the human IgG1 isotypes displayed little to no affinity for FcγRIII. Taken together these studies revealed that no observed difference in Fc binding affinity to murine FcγR was found between type I and II antibodies of the same isotype and these results therefore failed to explain why the type II antibodies consistently outperform the type I reagents throughout *in vivo* depletions presented in **Figure 3-1**.

Table 1: KD values following SPR analysis of anti- CD20 antibodies

KD values were determined by dividing the dissociation rate (Kd) by the association rate (Ka) as measured from sensorgams in **Figure 3-2** using Biacore analysis software.

Antibody	mFcγRI KD (M)	mFcγRII KD (M)	mFcγRIII KD (M)	mFcγRIV KD (M)
RTX m2a	$3.7x10^{-8}$	ND	$2.83x10^{-6}$	$2.67x10^{-8}$
OBZ m2a	$3.21x10^{-8}$	ND	$1.07x10^{-7}$	$2.27x10^{-8}$
OFA m2a	$3.93x10^{-8}$	ND	$1.28x10^{-7}$	$2.56x10^{-8}$
RTX m1	No Binding	$4.5x10^{-7}$	$2.33x10^{-7}$	No Binding
OBZ m1	No Binding	$5.98x10^{-7}$	$1.77x10^{-7}$	No Binding
RTX	2.0410^{-7}	ND	$3.04x10^{-7}$	$9.96x10^{-8}$
OBZ	4.0910^{-7}	ND	$8.92x10^{-7}$	$4.03x10^{-8}$
OBZ gly	2.6310^{-7}	ND	$2.16x10^{-6}$	2.6710^{-7}

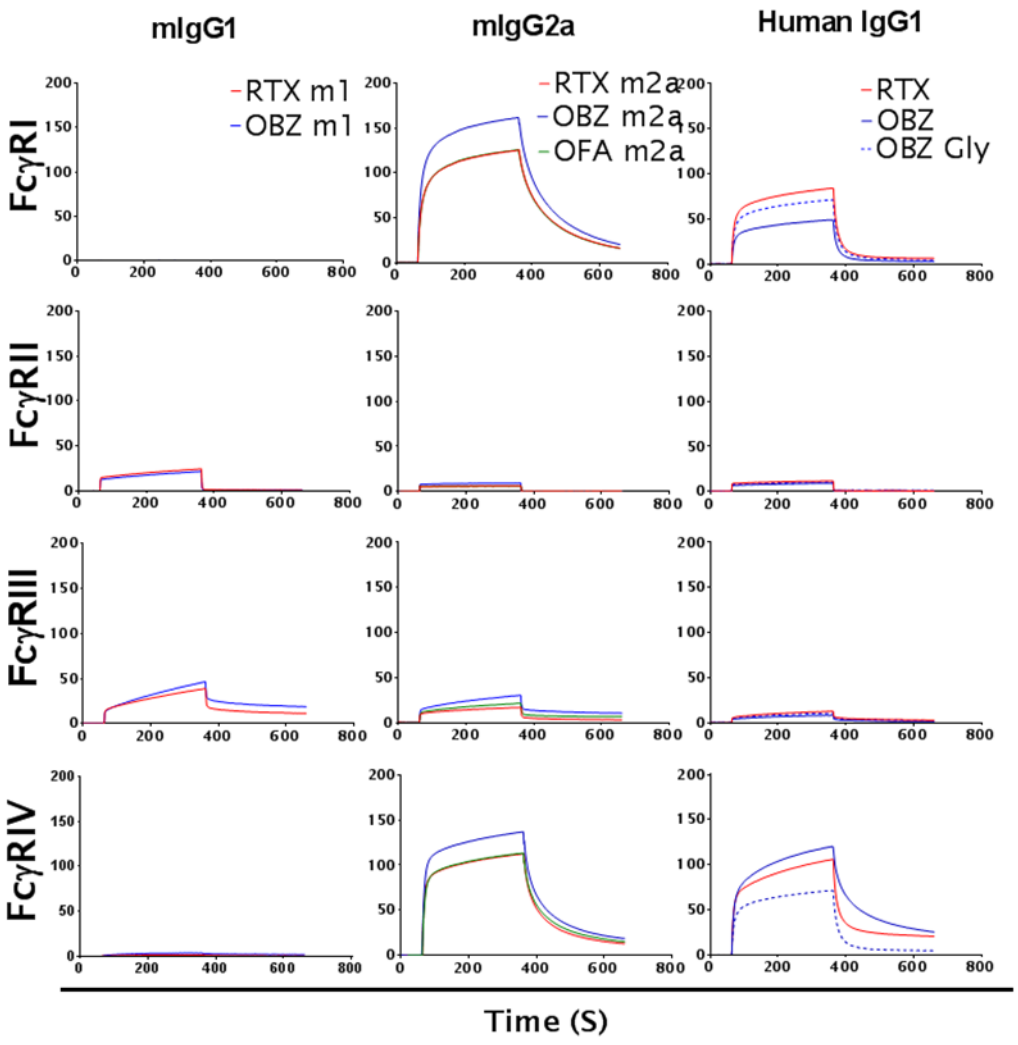

Figure 3-2 Anti-CD20 antibody binding affinities to murine FcγR

SPR analysis of human anti-CD20 mAb (hIgG1, mIgG1 and mIgG2a) binding to mouse FcγRI - IV. mAb was immobilised at 2000 RU onto a CM5 sensor chip. Recombinant, soluble, FcγR protein was passed over mAb at 200 nM. Association was measured for 300 seconds and dissociation measured for 600 seconds. Sensorgrams are shown.

Another possible explanation for the superior B cell depleting propensity of the type II reagents could be a difference in their ability to bind CD20. It has been reported that type I antibodies bind to a greater extent on the B cell surface compared to type II antibodies [77, 98]. In fact studies have put this binding at a 2:1 ratio in favour of type I, rituximab. To explore this, hCD20 Tg B cells were opsonised with either type I or II antibody of various isotype and then the immediately bound antibody was detected using an anti-mouse Fc $F(ab)_2$ mAb, conjugated to PE. To quantify the number of PE molecules on the cell surface

BD Quantibrite beads were used. This reagent contains various sized beads with a known number of PE molecules per bead. Based on these known quantities calculations of the mean number of PE molecules per cell can be made, assuming a 1:1 PE to antibody ratio (**Figure 3-3**).

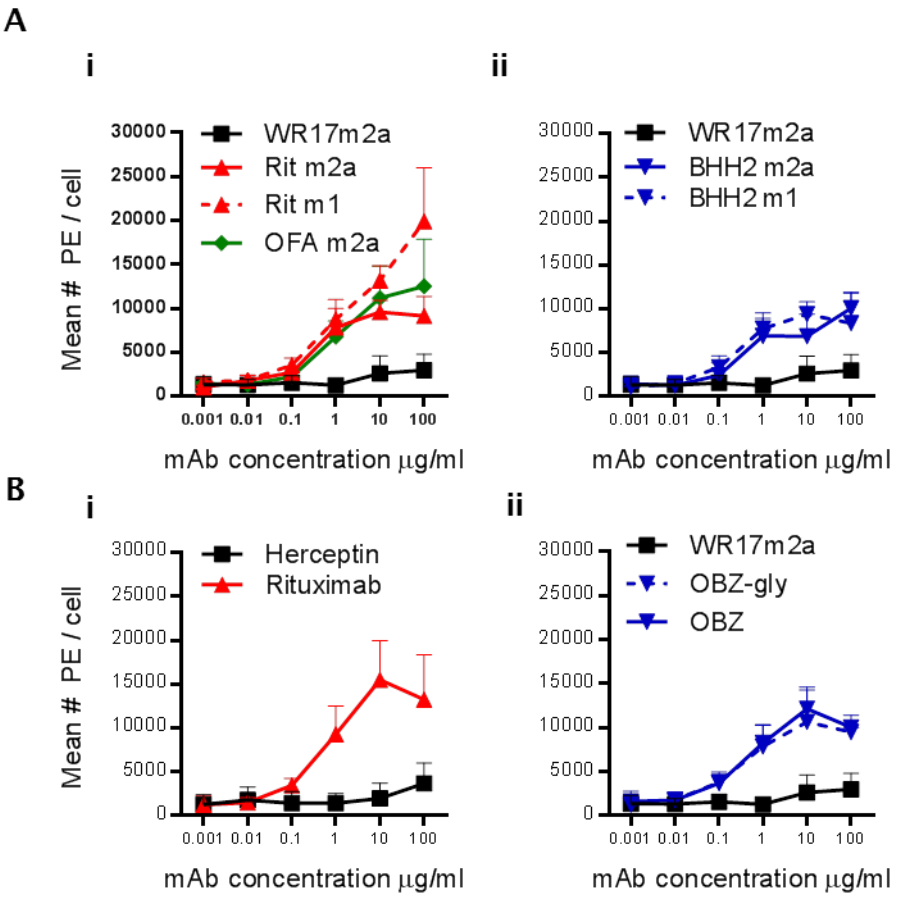

Figure 3-3: Cell surface quantification of type I and II antibodies on hCD20 Tg B cells

(**A**) Binding comparison of mouse IgG1 and IgG2a, type I and II anti-CD20 mAb to transgenic C57BL/6 hCD20 B cells. Cells were opsonised with 0.001 - 100 µg/ml anti-CD20 mAb for 30 minutes on ice. Red blood cells were lysed and samples were analysed by flow cytometry. The mean number of PE molecules per cell was quantified by indirect staining with anti-mouse or anti-human Fc PE conjugated $F(ab)_2$ and comparison of the Geo-MFI with BD Quantibrite beads. (**B**) Binding comparison of type I and II human IgG1 antibodies on mouse hCD20 Tg B cells. Staining was carried out as described in **A**. N=3 +/- SD.

From **Figure 3-3** it can be seen that the type I antibodies of all isotypes tested bind at least to the same extent as the type II antibodies. The type I antibodies do appear to bind to a greater extent on the B cell surface compared to the type II antibodies although results are variable for different mAb and isotypes. Additionally, there was no difference in the amount of CD20 binding between glycomodified and non glycomodified obinutuzumab.

Thus far it has been demonstrated that the clinically relevant type II antibody obinutuzumab outperforms the type I antibody rituximab regardless of it being glycomodified or not. It was subsequently demonstrated that this is not due to a difference in Fc:FcγR binding affinity or due to the amount of antibody bound to the B cell surface. Antibody consumption could provide an explanation for the differences in B cell depletion seen and lend support to the idea that antigenic modulation is responsible for improved type II therapeutic outcome. Therefore the circulating hIgG1 levels were tested from mice treated with the clinically relevant hIgG1 antibodies used in **Figure 3-1** using a standard anti-human IgG ELISA method (**Figure 3-4**)

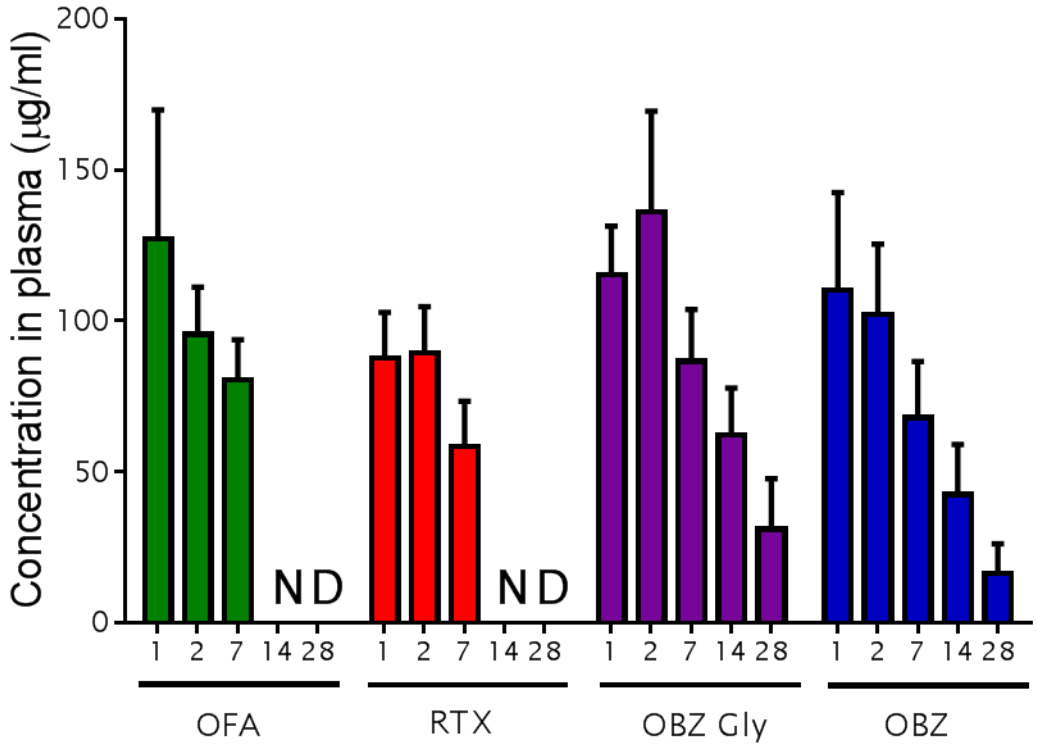

Figure 3-4 Detection of hIgG1 antibody following treatment with anti-CD20 reagents

The concentration of hIgG1 antibody in sera of mice previously treated with rituximab, ofatumumab, obinutuzumab or obinutuzumab-gly hIgG1 determined by ELISA. 96 well ELISA plates were coated with 25 µg/ml Rabbit anti-human IgG. Plasma was initially diluted 1:500 and then serially diluted across the plate. Bound IgG1 was detected using a 1:2000 dilution of Rabbit anti-human IgG1-HRP. Results were converted to a concentration (µg/ml) using a standard curve of human IgG1. N = 4 +/- SD. ND= not detectable.

From **Figure 3-4** it can be seen that type I antibodies had a shorter plasma half-life compared to type II reagents, possibly due to B cell dependent internalisation of antibody which has been previously reported upon [122, 232, 233]. The reduced quantity of type I antibody available is likely to impact upon effector cell mechanisms ADCC and ADCP. However, CDC would likely also be effected. Therefore to investigate the importance of CDC adoptive transfer experiments were performed using complement deficient C3 knock out mice. **Figure 3-5** shows representative examples of the adoptive transfer assay. Due to the large number of transgenic species (Vav Bcl-2, FcγRI-IV$^{-/-}$, puma$^{-/-}$ Bim-/-) used throughout this thesis it would be unfeasible to cross all mice to an

hCD20 Tg background for use in systemic depletion studies. Therefore an adoptive transfer method was undertaken to assess the ability of various Tg mice to deplete hCD20 opsonised B cells.

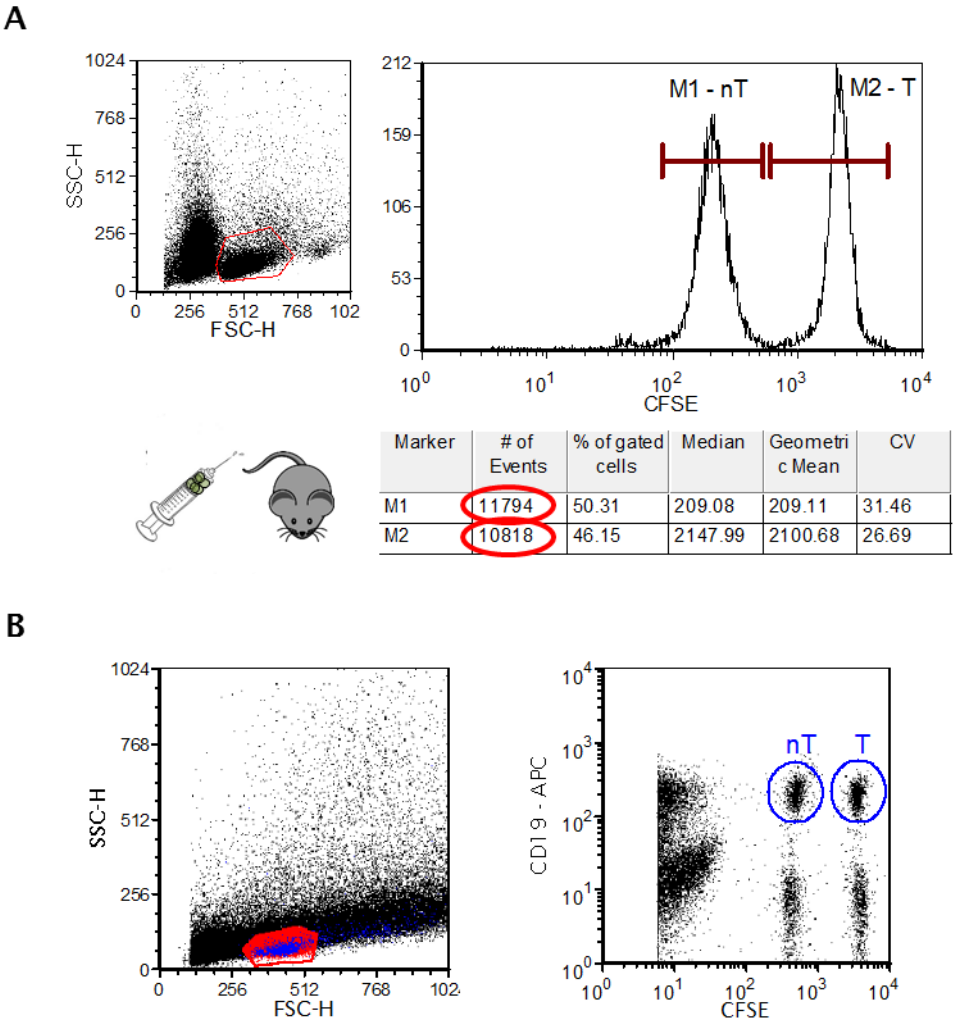

Figure 3-5 Example of an adoptive transfer experiment

Target (T) hCD20 and non-target (nT) WT splenocytes were isolated and dissociated to give a single cell suspension. They were then differentially stained with CFSE (nT-5 nM & T-5 μM) before being mixed together at a 1:1 ratio. (**A**) Representative FACS plot showing typical SSC and FSC and a histogram plot detecting CFSE fluorescence following 1:1 mixing (before injection). (**B**) Representative FACS plot showing the high and low CFSE stained $CD19^{+}$ B cells following removal and disassociation of the spleen. To reduce the file size, a threshold was placed on the CFSE (FL-1) fluorescence parameter (set to 200 MFI).

Previous work has shown a lack of role for CDC when using mIgG2a antibodies *in vivo* [122]. To test the role of CDC when using clinically relevant hIgG1

antibodies genetically modified mice which lack the classical complement component C3 (C3 KO mice) were used. Adoptive transfer experiments using these mice in combination with rituximab or obinutuzumab were conducted (**Figure 3-6**). Results from individual adoptive transfer assays can be variable, in terms of the maximal level of depletion reached. However, trends are always consistent, therefore, results were normalised to their corresponding irrelevant control. For example if the wild type irrelevant control gave a reading of 0.5 and with therapeutic antibody a reading of 0.4 the former would be divided by the later to give a normalised T:nT ratio of 0.8.

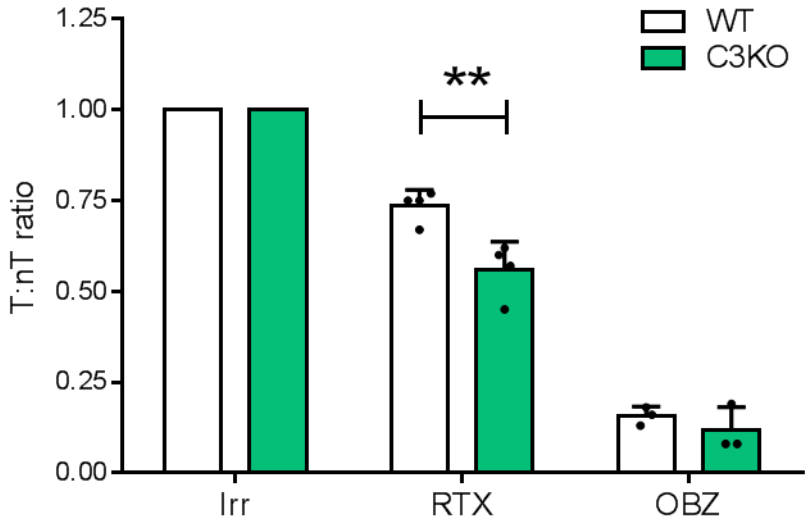

Figure 3-6 B cell depletion in WT or complement deficient mice

Adoptive transfer experiments were performed using C57BL/6 mice. WT or C3 KO mice were injected intravenously with 10 µg rituximab or obinutuzumab, both of a human IgG1 isotype. Spleens were harvested 24 hours later and analysed by flow cytometry for CFSE fluorescence as shown in **Figure 3-5**. Samples have been normalised to the irrelevant control for each strain of mouse. N=3 (OBZ), N=4 (RTX)+/- SD. Statistical analysis performed using two-way ANOVA.

From **Figure 3-6** it can be seen that the ability to deplete anti-CD20 mAb opsonised B cells is not inhibited in complement deficient mice. In fact, C3KO mice given Ritm2a showed significantly elevated levels of depletion compared to the WT mouse. Previously, our group has shown that complement and apoptosis are redundant effector mechanisms in depleting hCD20 B cells with

mouse IgG2a anti-CD20 mAb. In contrast, depletion of macrophages with clodronate or treatment of γ chain$^{-/-}$ mice arrested B cell depletion [122]. Experiments using C3 KO mice have confirmed these results for human IgG1 mAb. Given these confirmatory findings, the differential effects of FcγR-mediated ADCC and ADCP on B cell depletion using clinical CLL samples and hCD20 mice were investigated. Human ADCC and ADCP assays were already in place and so to allow a comparison between mouse and human ADCC assays a murine ADCC assay was adapted for use.

3.3 Adaptation of a novel calcein based assay for detection of murine ADCC

Successful ADCC assays require three components; specifically labelled target cells, therapeutic antibody and an effector cell population. Traditional ADCC assays have used radioactive chromium-51 (Cr^{-51}) to label the target cell population. For example Moga *et al* used this assay in combination with human PBMC or isolated NK cells with primary CLL cells as targets to demonstrate that IL-15 can be used in combination with rituximab to enhance ADCC [234]. Briefly, target cells are labelled with Cr^{-51} and then opsonised with antibody, they are then co-cultured with effector cells typically at a 10:1 E:T ratio.

Although a robust assay, alternative methods for measuring ADCC are being sought. This is primarily due to the safety concerns of using radioactive Cr^{-51} but also it would be attractive to have a flow cytometry compatible assay that would allow for further analysis of target and effector subsets [235]. To meet this need the calcein-AM method of labelling target cells has been adapted for use in combination with human effector cells, typically PBMC. Calcein-AM was chosen over other fluorescent dyes such as CFSE due to its superior retention by the cell leading to less cross-staining of other cells. This is due to Calcein-AM being an intracellular dye. Once inside the cell calcein-AM is converted to calcein through intracellular esterase and the fluorescent calcein product is retained within the cell until the cell is lysed by the effector population. Calcein is then released into the supernatant [235, 236].

We wanted to adapt this calcein based assay for use with murine target and effector cells. The major problem associated with murine ADCC assay is an inability to generate sufficient numbers of effector cell. Therefore the feasibility of culturing isolated murine NK cells, *ex vivo,* using high levels of murine IL-2 (mIL-2) was investigated (**Figure 3-7**).

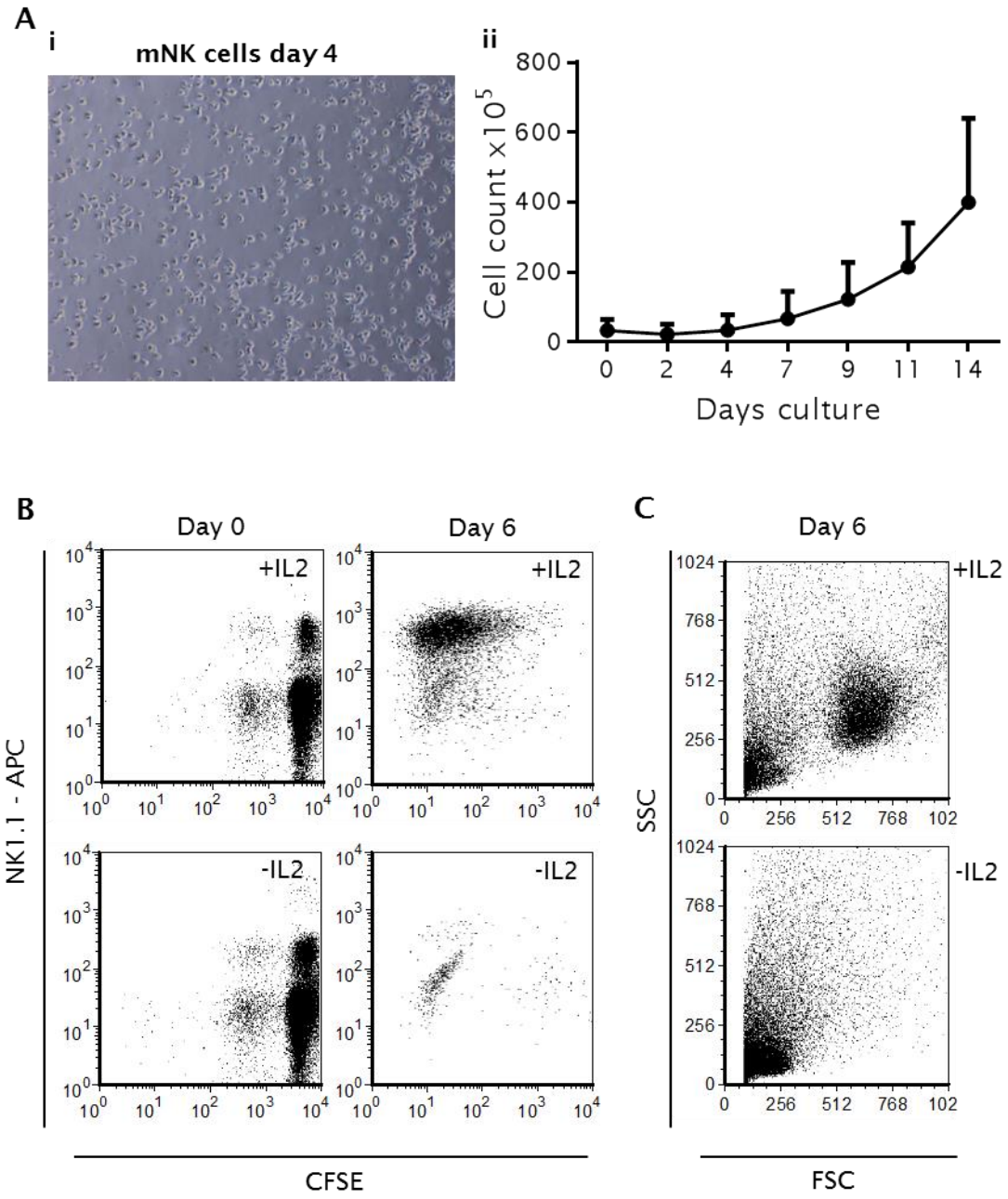

Figure 3-7 *Ex vivo* cultured murine NK cells

Murine NK cells were isolated from C57BL/6 splenocytes using a Miltenyi murine NK cell isolation kit. Murine NK cells were cultured in complete media supplemented with 200 ng/ml recombinant murine IL-2. (**A**) i, Representative micrograph of murine NK cells following 4 days culture. ii, Growth curve of murine NK cells, cells were counted at regular intervals over 14 days culture (N=3+/- SD). (**B**) CFSE proliferation assay demonstrating the need for IL-2 in the culture medium. WT NK cells were isolated, cells were then CFSE stained (5 μM) and put into culture either with or without murine IL-2 (200 ng/ml) the level of CFSE fluorescence was measure on days 0, 3 and 6. (**C**) Representative SSC and FSC FACS plots from NK cell culture with and without IL-2, again demonstrating the need for IL-2 in the culture medium.

From Figure 3-7 it can be seen that these ex vivo mNK cells appear morphologically similar to other lymphocytes such as B cells; under the microscope they appear small, round and shiny. Cell counts taken periodically highlight that during the first week of culture these cells appear to be relatively slow growing and take a week to reach appreciable numbers. This is likely due to the very low number of cells which are isolated from splenocytes (~1-3 x 106 cells). However, during the second week of culture numbers rapidly increase until day 14, by which time there are ~ 5x107 cells which is sufficient for use in immunological assays. Finally the absolute requirement for mIL-2 during the culture process is shown by CFSE proliferation assays. In the absence of mIL-2 there was no expansion of the NK1.1 population whereas in the presence of mIL-2 a clear NK1.1 positive population had expanded which is also detectable by FSC and SSC. Since Miltenyi isolation kits may not be sufficiently selective and may include a small number of macrophages there was a need to use IL2 to not only expand but to also further enrich this cell population.

Overall it was demonstrated that isolated NK cells from murine splenocytes could be cultured and expanded. Furthermore, this process was absolutely dependent on the high concentrations of mIL-2. Previous work has documented the need for cytokine supplements when culturing mNK cells. Toomey *et al* highlighted the importance of cytokines such as IL-2 and IL-15 in the culture medium and report on enhanced growth when used in combination with IL-21 [211]. Other groups have also cultured mNK cells *ex vivo* in the presence of mIL-2 and in complete RPMI media [237]. To confirm that these cells were indeed NK cells their phenotype was assessed by flow cytometry following isolation and after 14 days culture. Common NK cell markers NK1.1 and NKG2D were looked for as well as activation markers FcγRIII and CD69. The absence of other abundant lymphoid cells such as B and T cells was confirmed by staining samples for the common lymphoid markers CD3 and CD19 (**Figure 3-8**).

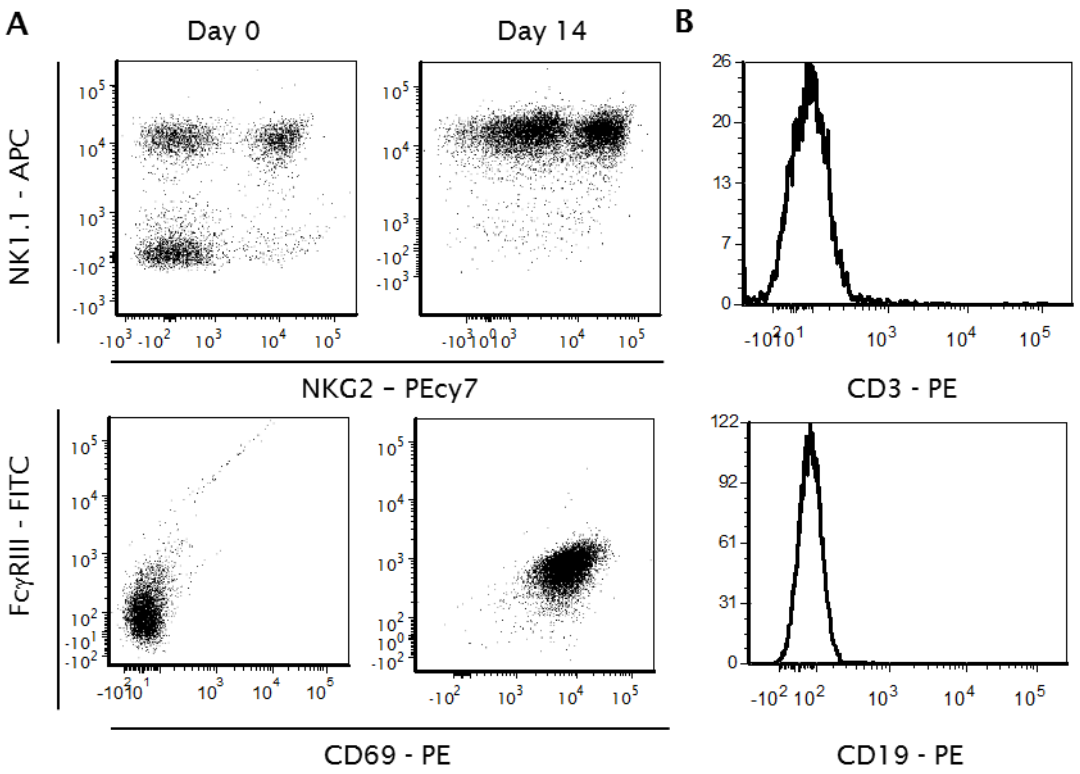

Figure 3-8 Phenotypic analysis of e*x vivo* cultured murine NK cells

(**A**) Representative FACS plots from C57BL/6 murine NK cells following isolation and 14 days culture in complete media containing 200 ng/ml IL-2. NK cells were stained ($1x10^6$ cells) for the activation markers CD69 and FcγRIII (AT154-2 $F(ab)_2$) as well as the NK cell markers NK1.1 and NKG2D. (**B**) Representative histograms showing murine NK cells ($1x10^6$ cells) stained (1 µl/test) for the lymphocyte markers CD3 (T cells) and CD19 (B cells).

Figure 3-8 demonstrates that cultured cells can be classed as NK cell like as they express the NK cell lineage markers NK1.1 and NKG2D. Additionally they failed to express the other lymphoid cell markers CD19 and CD3 and so were not B or T cells.

Through *ex* vivo cell culture sufficient numbers of murine NK cells could be obtained and these cells were next used in calcein based ADCC assays. Firstly, the number of B cells needed to give a good signal to noise was determined. In duplicate, B cells from C57BL/6 mice were isolated, calcein-AM stained and adjusted to an initial concentration of $10x10^5$ cells/well. Samples were then serially diluted 1:2 across the plate. Half the samples were lysed to give a maximum lysis reading and the level of fluorescence measured (**Figure 3-9a**). It was found that $2.5\ x10^4$ B cells were sufficient to distinguish lysed B cells from

the non-lysed background. However, from these results it was decided that $1x10^5$ B cells would be taken forward into future experiments. This was because large numbers of effector cells are used in ADCC assays, therefore this lower number of target cells would mean less effector cells are needed.

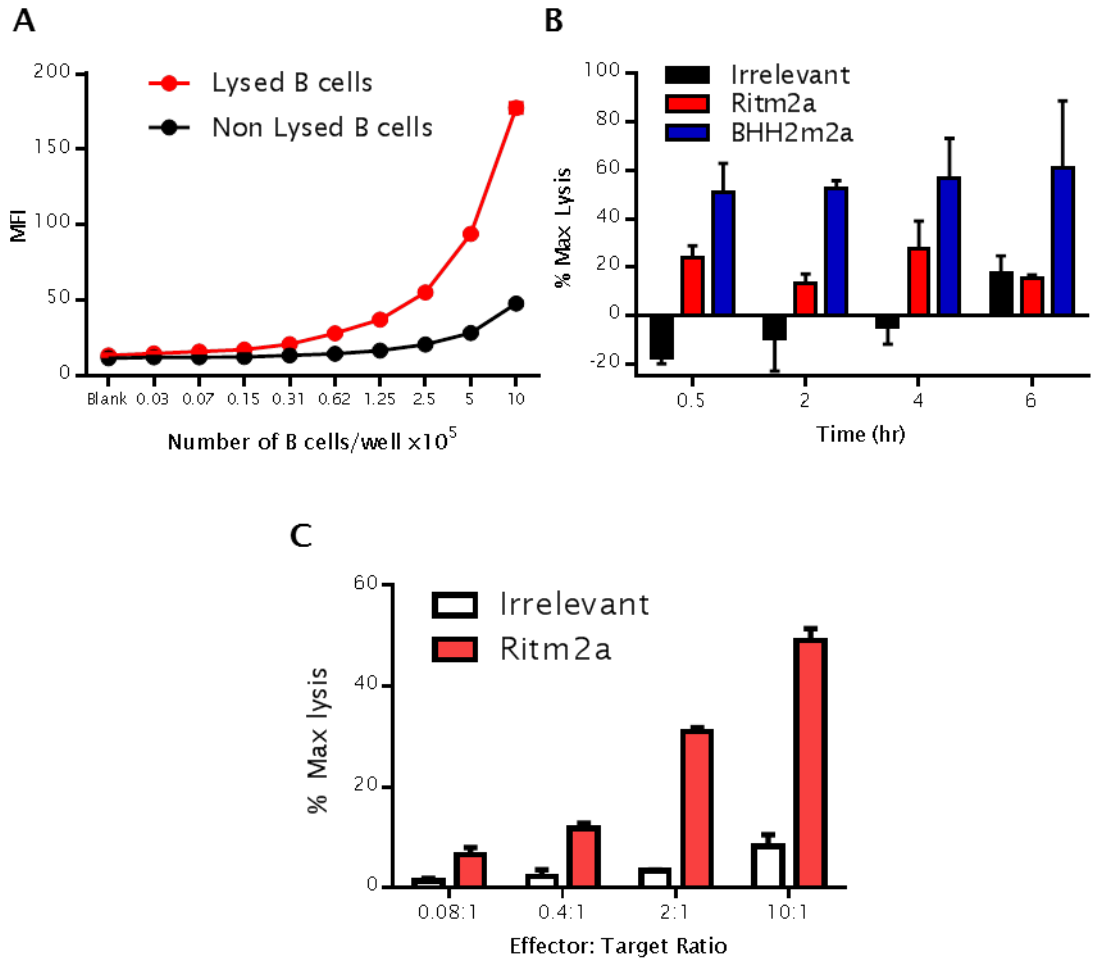

Figure 3-9 experimental set up for calcein based ADCC assays using murine effector cells

(**A**) B cells from C57BL/6 mice were isolated and stained with calcein-AM. In duplicate B cells were plated out initially at $1x10^6$ cells/well. Samples were then diluted 1:2 across the plate. Half the samples were then lysed with Triton X (4 %). (**B**) Isolated B cells from C57BL/6 mice were calcein-AM stained and added to murine mNK effector which were at an E:T ratio of 10:1 for between 2 and 6 hours. (**C**) Target B cells ($1x10^5$) were co-cultured at various E:T ratios with *ex vivo* cultured murine NK cells at an E:T ratio of 10:1 for 2 hours.

Based on 1 $x10^5$ B cells/well the target and effector co-culture time was investigated. For this experiment an E:T ratio of 10:1 was chosen and the ability of mNK cells to lyse B cells after 30 minutes 2, 4 or 6 hours co-culture was ascertained. From **Figure 3-9b** it can be seen that ADCC could be detected at all the time points tested and that the OBZm2a type II antibody displayed higher levels of ADCC compared to the Ritm2a type I antibody. From these results it was decided that a two hour co-culture period would be used. This was because there was little difference between 0.5, 2, 4 and 6 hour co-culture period. Finally, the optimal E:T ratio was determined. Investigations used an E:T ratio ranging from 0.08 - 10:1 in combination with $1x10^5$ B cells. From **Figure 3-9c** it can be seen that an E:T ratio above 0.4:1 was sufficient to detect killing of labelled B cells however results were clearer when using an E:T of 2:1 and highest maximal lysis was seen when using an E:T of 10:1. Therefore, from these results an E:T ratio of 10:1 was taken forward into future ADCC experiments.

Once validated the murine ADCC assay was subsequently used to address questions with regards to type I and II antibodies, antigenic modulation and the importance of effector cell subsets. One of the benefits of using the calcein-AM method of ADCC analysis is the ability to acquire samples on the flow cytometer. To determine if this was feasible experiments were performed in which the amount of type I or II antibody needed to kill B cells was titrated. Sample was then acquired on the flow cytometer. Results were reported as the remaining percentage of B cells following treatment, therefore antibodies that fail to engage ADCC will have a higher percentage of remaining B cells than those that do (**Figure 3-10**).

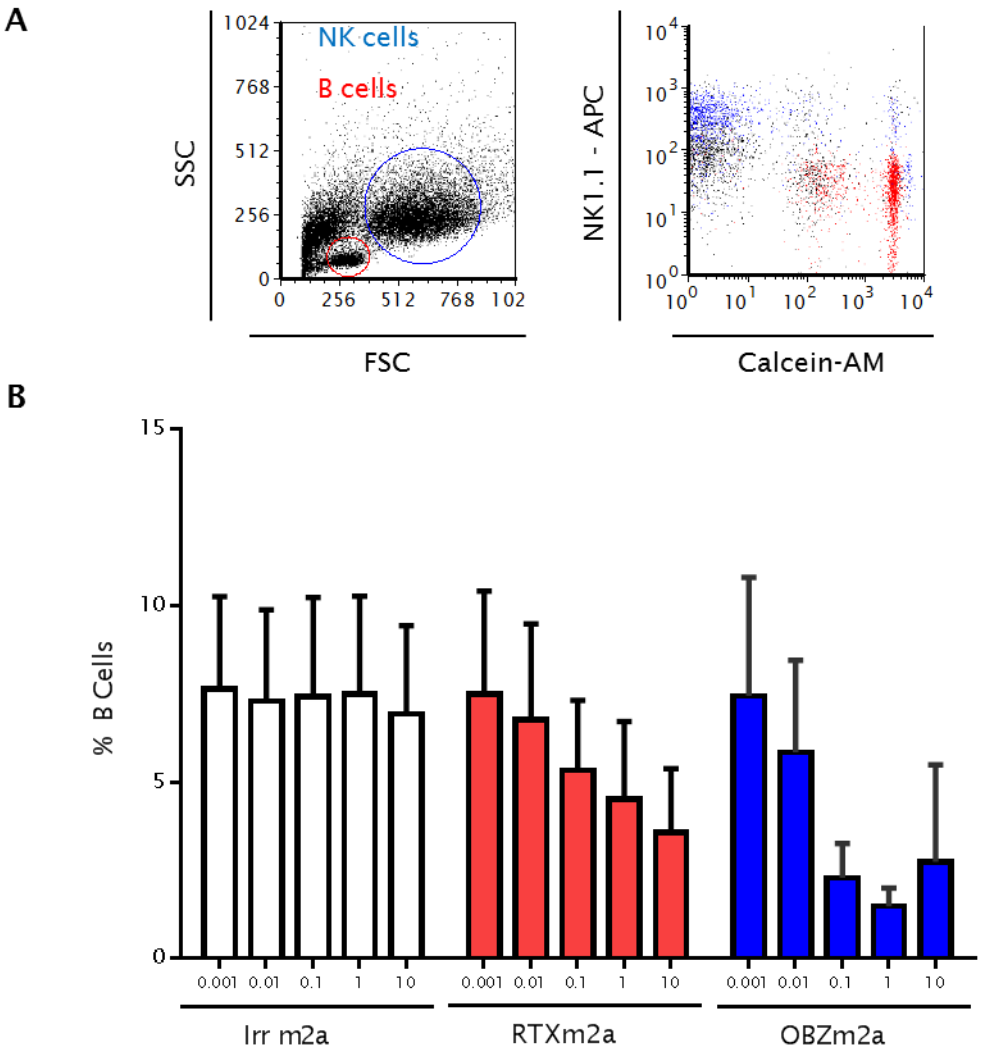

Figure 3-10 Acquisition of murine ADCC samples on the flow cytometer

Isolated B cells from C57BL/6 mice were calcein-AM stained (5 μM) and opsonised with various concentrations of anti-CD20 mAb (10-0.001 μg/ml). Target B cells ($1x10^5$ cells/well) were co-cultured with mouse NK effector cells at a 10:1 E:T ratio. Following acquisition of fluorescence data samples were stained with NK1.1 (1 μl) then acquired on the flow cytometer. (**A**) Representative FACS plot of acquired data NK cells=Blue, B cells=Red. (**B**) Type I and II antibody was titrated and analysed by flow cytometry. N=3+/-SD.

From **Figure 3.10** it can be seen that B cells and NK cells can be distinguished by FSC and SSC, additionally NK1.1 staining reveals the mouse NK cell population, whereas calcein-AM detection highlights the remaining B cells. Interestingly, there appear to be some double positive NK1.1 and Calcein events perhaps suggesting these cells are engaging with each other. Analyses of these results reveal that IgG2a version of obinutuzumab to be more potent

than IgG2a rituximab and this is in keeping with cell lysis results **Figure 3-9b**. This data demonstrates that results can be gleaned from acquiring samples on the flow cytometer and both murine NK effector and B cell targets can be detected. Now that a murine based ADCC assay had been developed the ADCC ability of type I and II antibodies of various isotypes was investigated.

3.4 Assessment of murine and human ADCC activity in response to anti-CD20 mAb

Earlier findings (**Figure 3-9**b and **Figure 3-10**) and published data [122] report that type II antibodies have a greater ability to deplete B cells *in vivo* compared to type I antibodies. Furthermore, this was independent of whether the antibody was a mouse IgG1, IgG2a or human IgG1 isotype. In order to explore why type II antibodies outperform type I antibodies the differential ability to activate ADCC and ADCP was investigated. Initially, mAb with a mouse IgG isotype were used in murine ADCC assays, and mAb of human IgG1 isotype were used in human ADCC assays (**Figure 3-11**).

From **Figure 3-11** it can be seen that the two type I antibodies, rituximab and ofatumumab perform very similarly with 10 µg/ml sufficient to elicit maximal ADCC and any cytotoxic response absent at 0.01 µg/ml. This was true when using both murine and human assay formats. With regard to type II antibodies, these outperformed type I antibodies at all concentrations measured and appeared to be more potent than type I antibodies as they titrated out ~10 fold lower level (0.001 µg/ml).

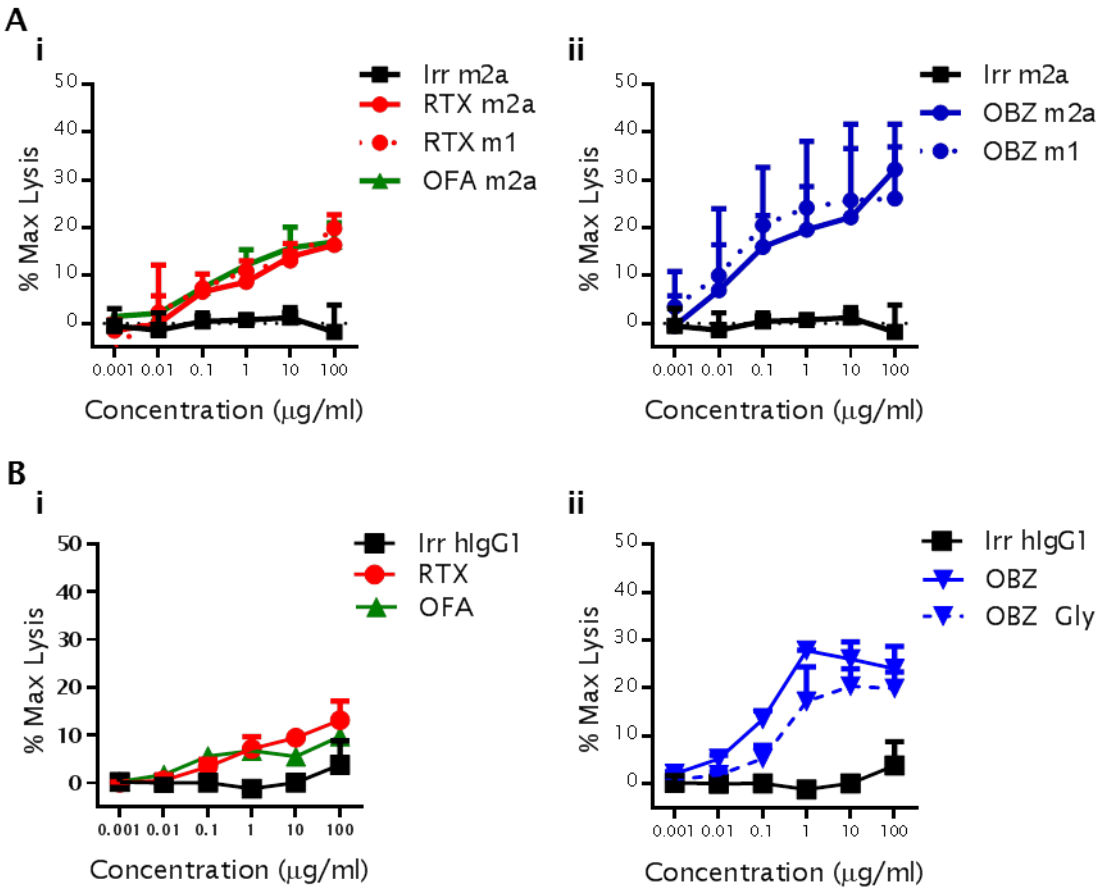

Figure 3-11 Titration of type I and II antibodies or various isotype in ADCC assays

(**A**) Murine ADCC assays titrating type I (i) and II (ii) mouse IgG1 and IgG2a antibodies. hCD20 Tg B cells were isolated from C57BL/6 mice, these were calcein-AM stained (5 μM) and $1x10^5$ B cells were co-cultured with $1x10^6$ *ex vivo* cultured murine NK cells for 2 hours. Sample supernatant was then analysed for fluorescence, with excitation at 490 nm and the percentage maximum lysis determined based on the maximum lyses obtained using Triton X (4 %). (**B**) Human ADCC assays using human CLL target cells and PBMC effectors, titrating human IgG1 type I (i) and II (ii) anti-CD20 antibodies. Primary CLL samples were thawed and stained with calcein-AM, $8x10^4$ cells were then co cultured with $4x10^6$ PBMC, this gave a E:T ratio of 50:1. Samples were incubated for 4 hours before sample supernatant was analysed for fluorescence, with excitation at 490 nm. The percentage maximum lysis was calculated as described for **A**. N=3 +/- SD.

The increased ADCC activity seen with type II antibodies was not due to altered glycosylation since both obinutuzumab mouse IgG1 and IgG2a were both wild type mAb and not defucosylated. This observation that type II antibodies outperform type I in terms of ADCC is perhaps surprising given the relative binding levels determined earlier (**Figure 3-3**). The superior activity of the type II antibody were further confirmed using a FcγRIIIa ADCC Bio-reporter assay,

which measures the extent of FcγRIIIa engagement (**Figure 3-12**). From this experiment it can again be seen that the type II antibodies appear to be more potent than the type I. Although using this Bio-reporter assay mAb appear to give signal at much lower concentrations compared to our ADCC assays, this is likely due to the fact that this assay system assesses signalling and FcγR engagement whereas ADCC assays assess cytotoxicity and effector outcome.

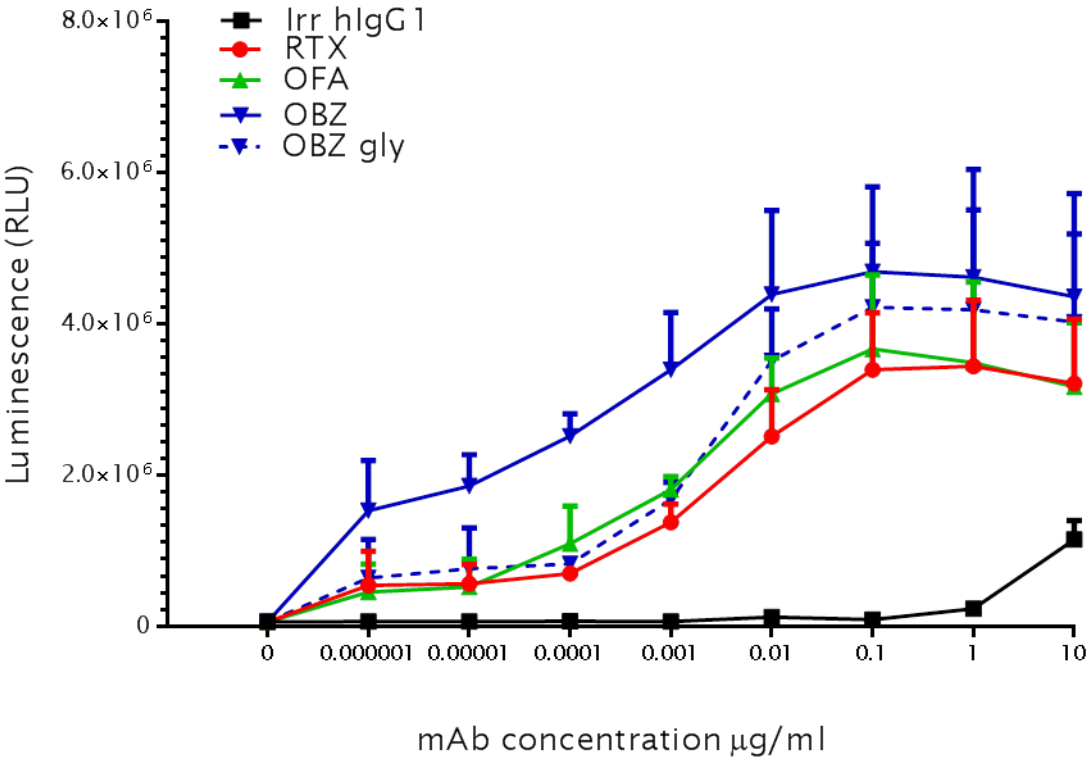

Figure 3-12 Engagement of human FcγRIIIa using a novel ADCC bio-reporter assay

Target B cells were opsonised with antibody at various concentrations (10-0.000001 µg/ml). Method was performed as described in manufacturer's instructions. Briefly, Target B cells were then incubated with Promega target cells (Jurkat) which had been transfected to express solely FcγRIIIa with a luciferase reporter downstream of the signal module. Following 4 hours co-culture of target and effector cells sample supernatant was assayed for luminescence. N=1+/- SEM.

Now that the effective dose range for ADCC experiments had been determined, direct comparisons between type I and II mouse IgG1, IgG2a and human IgG1 mAb were undertaken. In these studies isolated hCD20 B cells were opsonised with 10 µg/ml mAb (**Figure 3-13**). Equivalent levels of ADCC between IgG2a

and mouse IgG1 antibodies were observed. Interestingly, human IgG1 mAb gave very poor levels of ADCC, even though they depleted B cells when used *in vivo* (**Figure 3-1**). The FcγR binding affinities indicated that in contrast to mouse IgG1 and IgG2a isotypes, human IgG1 had negligible affinity for FcγRIII, but high affinity for mouse FcγRI and FcγRIV (**Figure 3-2**). As mNK cells only express FcγRIII [124], these data explain the inability of human IgG1 mAb to elicit substantial ADCC with mouse effectors. Moreover, coupled with the depletions observed in hCD20 Tg mice they demonstrate that ADCC is not the dominant effector cell mechanism depleting B cells in the mouse.

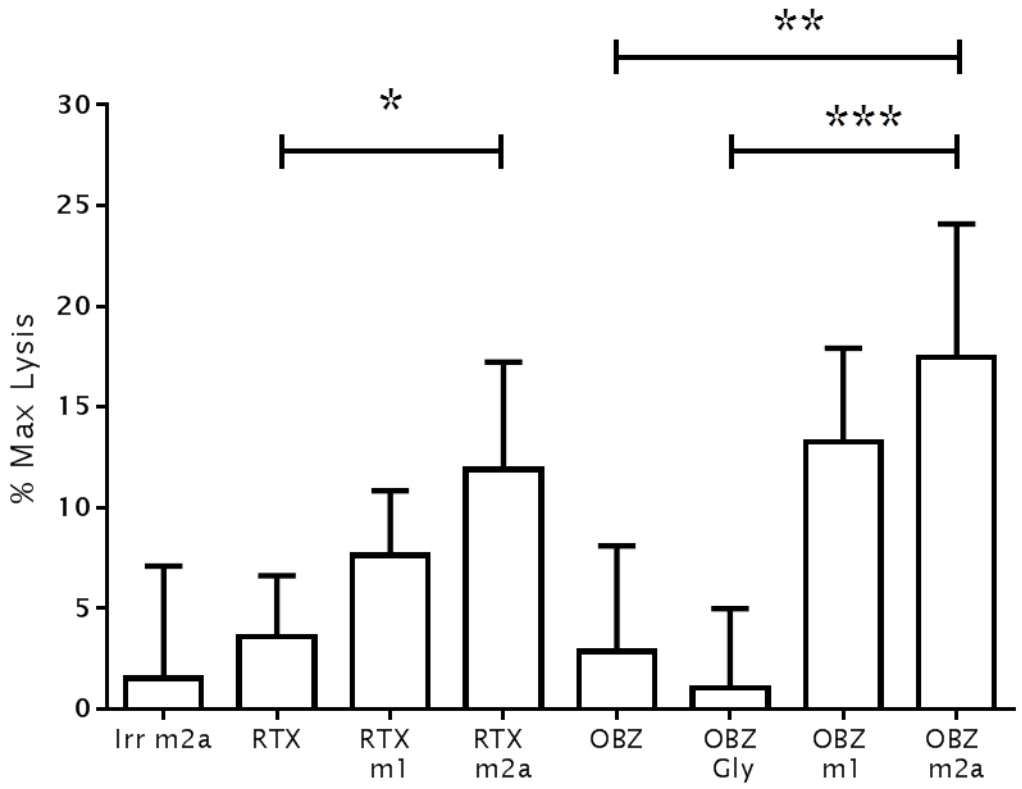

Figure 3-13 Murine ADCC assay comparing type I and II antibodies of various isotype

Transgenic hCD20 murine B cells were loaded with calcein-AM (5 μM) and opsonised with anti-CD20 mAb. B cells ($1x10^5$ cells/well) were co-cultured with murine NK cells ($1x10^6$ cells/well) for 2 hours at an effector to target ratio of 10:1. Supernatant was assayed for calcein release, with excitation at 490 nm. N=3 +/-SD. Statistical analyses were carried out using one-way ANOVA with multiple comparisons and significance was accepted at *$p < 0.05$, **$p < 0.01$ and *** $p < 0.001$.

3.5 Assessment of murine and human ADCP activity in response to anti-CD20 antibodies

As described in chapter 1, macrophages have been recently implicated as the key effector population in antibody-mediated depletion [108, 122, 135, 136]. Since ADCC failed to adequately explain our *in vivo* results the abilities of type I and II antibodies to mediate ADCP were measured. First, the importance of macrophages was confirmed when using clinically relevant hIgG1 antibodies by performing adoptive transfer experiments in which macrophages were systemically depleted using clodronate containing liposomes. Liposomes will be ingested and digested by macrophages causing the release and accumulation of clodronate inside the cell. At a certain intracellular concentration, clodronate will induce apoptosis [238].

Administration of two i.v. doses (200 µl) of clodronate liposomes successfully depleted the macrophage population in C57BL/6 mice **Figure 3-14**. Based on the total number of cells it appeared that the monocyte and neutrophil populations were relatively unaffected, which could be due to rapid generation and repopulation from the bone marrow. Following depletion of macrophages, adoptive transfer studies demonstrated that type I and II anti-CD20 antibodies were unable to deplete target B cells in clodronate deficient mice compared to wild type counterparts. However, there remained a modest reduction in the T:nT ratio of B cells when using obinutuzumab in combination with clodronate liposomes, indicating an activity independent of macrophages. This may reflect the type II nature of the antibody and its enhanced ability to elicit PCD.

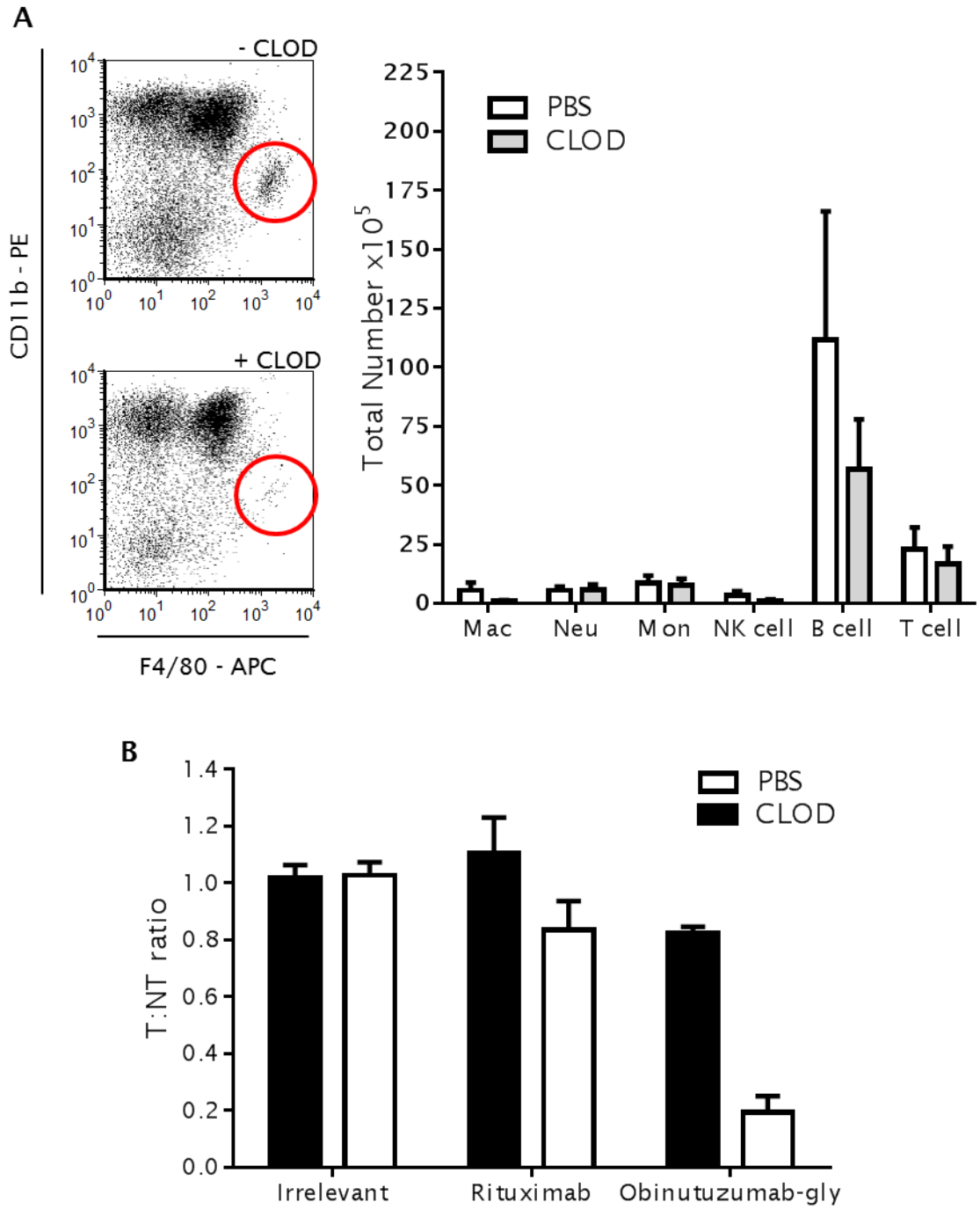

Figure 3-14 Depletion of macrophages using clodronate liposomes

(**A**) Representative FACS plots showing the lack of a macrophage population (red circles) when depleting with colodronate liposomes (48 hours post treatment). (**B**) Age matched C57BL/6 mice received two 200 µl injections of clodronate or PBS containing liposomes (i.v.) one 48 and the other 24 hours prior of therapeutic antibody. Isolated splenocytes were stained with CFSE, target (5 µM) and non-target (5 nM), mixed 1:1 and injected i.v. ($5x10^6$ cells) 24 hours prior to treatment with therapeutic antibody. Irrelevant or therapeutic antibodies (10 µg) were injected i.v. 24 hours after treatment spleens were harvested, stained with CD19-APC and analysed by flow cytometry. N=3 +/- SD.

Having re-affirmed the importance of macrophages in the depletion of target B cells by anti-CD20 mAb, the ability of type I and II antibodies of various isotypes to deplete B cells was determined using *in vitro* ADCP assays. For these assays bone marrow was isolated from the hind legs of C57BL/6 mice and cultured for 8-12 days in complete media containing M-CSF, as described in the materials and methods (**2.4.2**). Following culture of BMDMs *in vitro* ADCP assays were performed. **Figure 3-15** shows the development of bone marrow monocytes to BMDM over 7 days. Cells start off as small round and shiny, similar in appearance to lymphocytes. By day 3 they have become fully adherent and have begun to elongate and by day 7 they are fully differentiated and show pronounced elongation.

Figure 3-15 also shows representative examples of data obtained when conducting phagocytosis assays. The FSC and SSC are able to distinguish the BMDM population (due to these cells being large and granular) which is gated upon (red quadrant). Within this population macrophages are further defined as being F4/80 positive cells and macrophages which have phagocytosed B cells are dually F4/80 and CFSE positive. Phagocytosis is expressed as a percentage of the CFSE positive events within the F4/80 positive gate and representative data from **Figure 3-15** shows that an anti-CD20 antibody, Ritm2a (10 µg/ml), will elicit around 40 % phagocytosis compared to an irrelevant control of the same isotype which will elicit around 10 % phagocytosis.

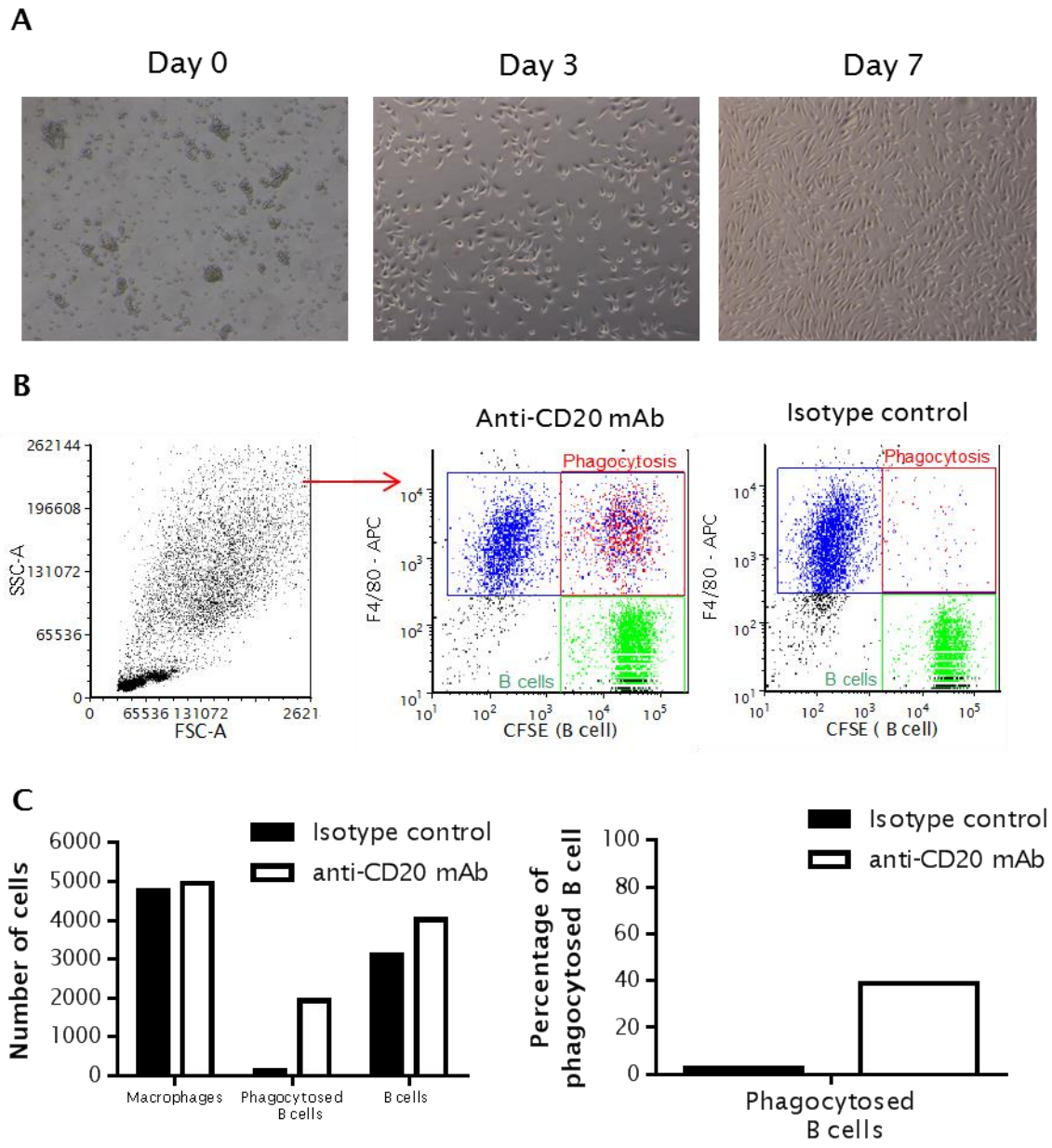

Figure 3-15 ADCP experimental set up

(**A**) Representative micrographs from *in vitro* cultured BMDMs on the day of harvest, day 3 and day 7. In phagocytosis experiments BMDMs were used from day 7 onwards. (**B**) Representative FACS plots from a single ADCP experiment. Target hCD20 B cells were isolated and stained with CFSE (5 µM). Target B cells (2.5 x10^5 cells) were then incubated with BMDMs (5x10^4 cells). Samples are stained with F4/80-APC (2 µl/well) and analysed by flow cytometry. BMDMs and B cells can be separated based on SSC and FSC. Macrophages are FL-4 (APC) positive and non-phagocytosed B cells are FL-1 (CFSE) positive. The percentage of BMDMs that have phagocytosed B cells was gated upon based upon FL-1 (CFSE) and FL-4 co-fluorescence. (**C**) Representative result from a single ADCP assay when using an anti-CD20 mAb compared to an irrelevant control. Showing the number of cells analysed and the calculated percentage of phagocytosed B cells based on the population of macrophages as a whole.

Using this murine phagocytosis assay and the human MDM equivalent, dose response experiments were conducted to determine the working range of murine and human anti-CD20 antibodies. It was found that type I and II mIgG2a antibodies elicit phagocytosis optimally at 10 µg/ml when using BMDMs and that all phagocytic activity was lost by 0.01 µg/ml (**Figure 3-16**).

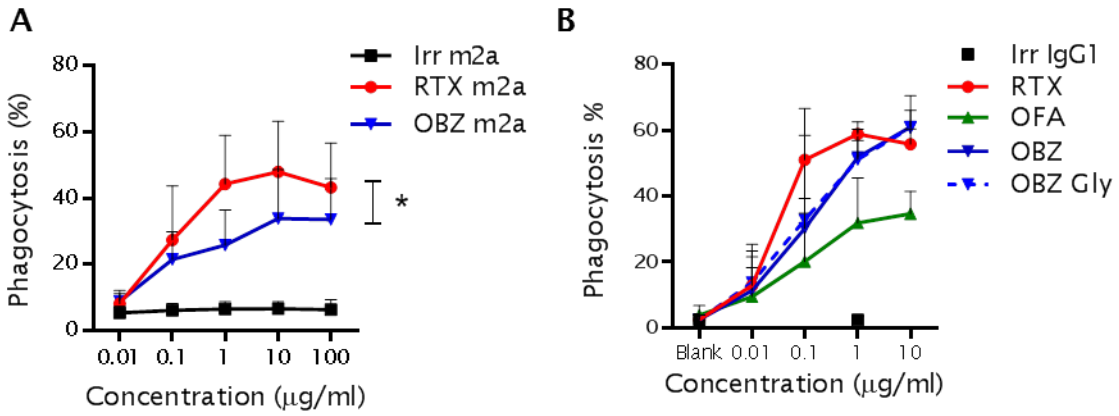

Figure 3-16 Human and murine ADCP dose response

(**A**) Murine hCD20 B cells were CSFE Stained (5 µM) before being opsonised with therapeutic antibody and co-cultured with BMDM. Cells were co-cultured for 30 minutes then stained with F4/80-APC (2 µl/well). (**B**) Primary human CLL B cells were CSFE Stained (5 µM) before being opsonised with therapeutic antibody and co-cultured with human MDM effector cells. Cells were co-cultured for 1 hour then stained with anti-CD16-APC mAb (2 µl/well). N=3 +/-SD. Statistical analysis performed using two-way ANOVA.

Human IgG1 antibodies showed a similar trend with human MDMs when depleting CLL target cells. In addition, rituximab displayed a trend towards inducing greater levels of phagocytosis than obinutuzumab when using either murine or human effector cells, perhaps reflecting the higher levels of bound antibody (**Figure 3-3**).

After determining the maximal and suboptimal doses for eliciting ADCP the impact of antibody isotype on murine ADCP assays was assessed to see if this would correlate with *in vivo* depletion studies (**Figure 3-1**). C57BL/6 hCD20 target B cells in combination with BMDM effectors were used to see how well type I and II antibody of an mouse IgG1, IgG2a or human IgG1 isotype would elicit phagocytosis at a standard dose of 10 µg/ml (**Figure 3-17**). In the case of

murine targets and effectors, with type I and II reagents, IgG2a was significantly superior to the mouse IgG1 isotype at eliciting phagocytosis and this correlated with the superior *in vivo* depletion of IgG2a antibodies over that of mouse IgG1 observed in **Figure 3-1**. Furthermore, and in contrast to ADCC data, human IgG1 antibodies showed equivalent levels of phagocytosis compared to IgG2a antibodies for both type I and II reagents, in keeping with their similar FcγR binding profiles observed in **Figure 3-2**.

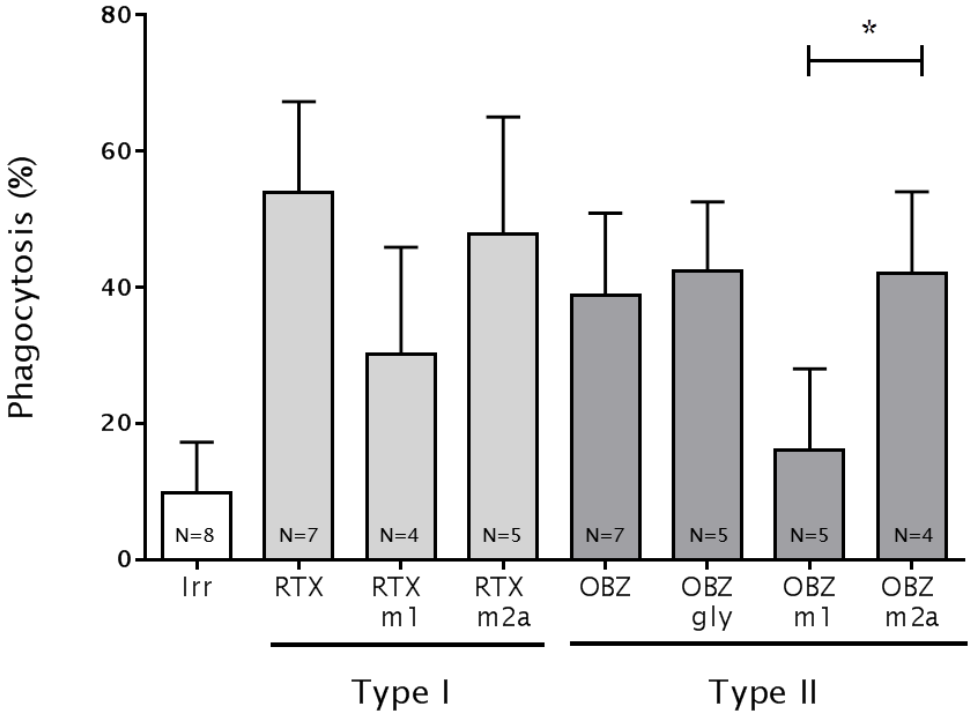

Figure 3-17 Comparison of mAb type and isotype on murine ADCP

Target hCD20 B cells were isolated from C57BL/6 mice. Cells were stained with CFSE (5 μM) and opsonised with type I or II mAb (10 μg/ml) of either a mouse IgG1, IgG2a or human IgG1 isotype. Target cells were co-cultured with BMDMs for 30 minutes at 37 °C (5 % CO_2). Samples were than stained with F4/80-APC (2 μl). Samples were acquired on the flow cytometer. N=4-8 +/- SD. Statistical analyses were carried out using one way ANOVA with multiple comparisons and significance was accepted at *$p < 0.05$.

Earlier data showed that although ADCC was not elicited by human IgG1 antibodies with murine effector cells, however these antibodies were efficacious in depleting target B cells *in vivo* (**Figure 3-13**). In contrast, data presented in **Figure 3-17** demonstrate that hIgG1 mAb were effective in ADCP assays, unlike their mouse IgG1 equivalents. Taking into account these mAb *in vivo* activities, these data indicate ADCP to be the key effector mechanism in the mouse. However, type I reagents performed better than type II reagents in ADCP assays, suggesting that type I antibodies should perform better than type II *in vivo* and this is evidently not the case (**Figure 3-1**). Based upon earlier observations *in vitro* and previous literature [109, 122], it was speculated that antigenic modulation may limit the effector functions of type I mAb. Experiments were next performed to address the impact antigenic modulation had on both ADCC and ADCP.

3.6 Antigenic modulation impacts on effector cell mechanisms

Thus far it has been demonstrated that the type II antibody obinutuzumab is superior to both rituximab and ofatumumab in its ability to deplete normal B cells *in vivo*. Furthermore, there is no difference in binding affinity for mouse FcγR between isotype matched type I and II reagents but there is a more rapid loss of detectable type I antibody in the plasma suggesting a role for antigenic modulation. The literature suggests that macrophages are important to B cell depletion in response to anti-CD20 mAb and experiment **Figure 3-17** shows that rituximab and obinutuzumab perform to a similar extent in ADCP assays. However these experiments do not take into account the potential impact of antigenic modulation. Therefore, there is a need to investigate the kinetics of antigenic modulation. This was done by opsonising hCD20 murine B cells or primary human CLL B cells with a saturating dose (10 μg/ml) of either type I or type II antibody and then detecting the amount of cell surface bound antibody following 0-6 hours mAb-ligation. This was done using a secondary anti-Fc PE conjugated reagent (**Figure 3-18**).

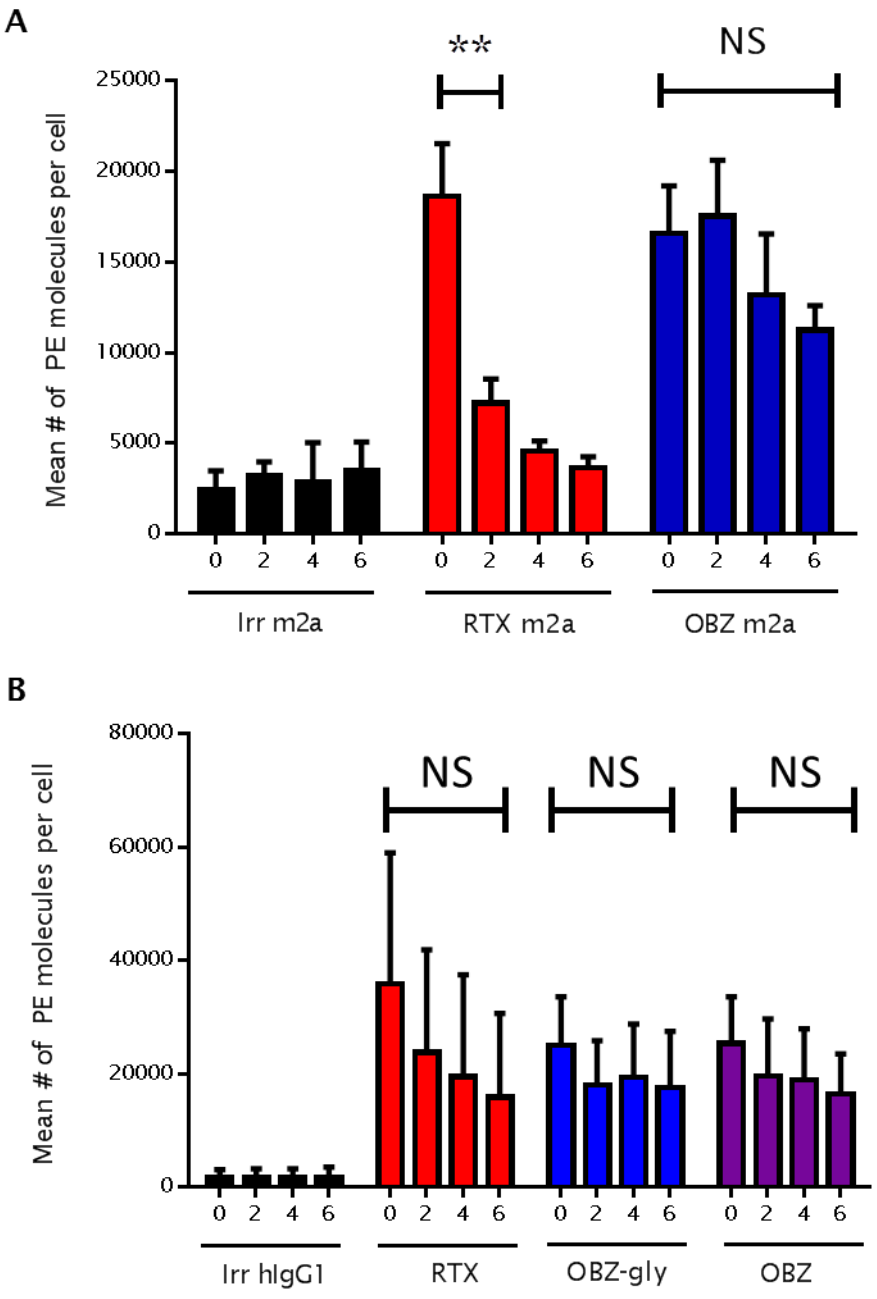

Figure 3-18 Antibody is rapidly lost from the cell surface of type I opsonised B cells

(**A**) Murine hCD20 B cells were opsonised (10 µg/ml) with anti-CD20 mAb for 30 minutes to 6 hours (4 °C). Samples were then stained for 30 minutes (4 °C) with anti-mouse Fc-PE mAb. QuantiBRITE beads and samples were acquired on a flow cytometer. (**B**) Human CLL B cells were opsonised (10 µg/ml) with anti-CD20 mAb for 30 minutes to 6 hours (4 °C). Samples were then stained for 30 minutes (4 °C) with anti-human Fc-PE mAb. QuantiBRITE beads and samples were acquired on a flow cytometer. N=3 +/- SD. Statistical analysis performed using a two-way ANOVA.

From **Figure 3-18a** it can be seen that there was a significant loss of Ritm2a from the cell surface of hCD20 B cells following 6 hours co-culture with antibody. In contrast, obinutuzumab IgG2a remained relatively unaffected and still displayed appreciable levels of antibody on the cell surface following 6 hours co-culture.

Rituximab showed a loss in detectable antibody on the cell surface of primary CLL cells following 6 hour modulation **Figure 3 18b**, however, this result did not reach significance when analysed by two-way ANOVA ($p=0.2$). This is likely due to the high levels of heterogeneity that are found from patient to patient coupled with the low number of clinical samples used ($N=3$) and it would be predicted that significance would be reached if an appropriately high number of primary CLL samples were used. The reason that the reduction of hCD20 seen on murine B cells reached significance is likely due to the inbred nature of the mouse, resulting in reduced heterogeneity between samples.

A obinutuzumab and obinutuzumab-gly showed little loss of antibody on the cell surface of primary CLL cells following 6 hour modulation. After confirming that antibody is indeed lost from the cell surface the effector mechanisms critically affected by modulation were determined. To this extent, hCD20 Tg B cells or primary human CLL cells were opsonised with antibody for 0-6h and then examined in their ability to elicit ADCC using either murine assay in combination with hCD20 Tg B cells or human ADCC assay in combination with primary CLL cells (**Figure 3-19**).

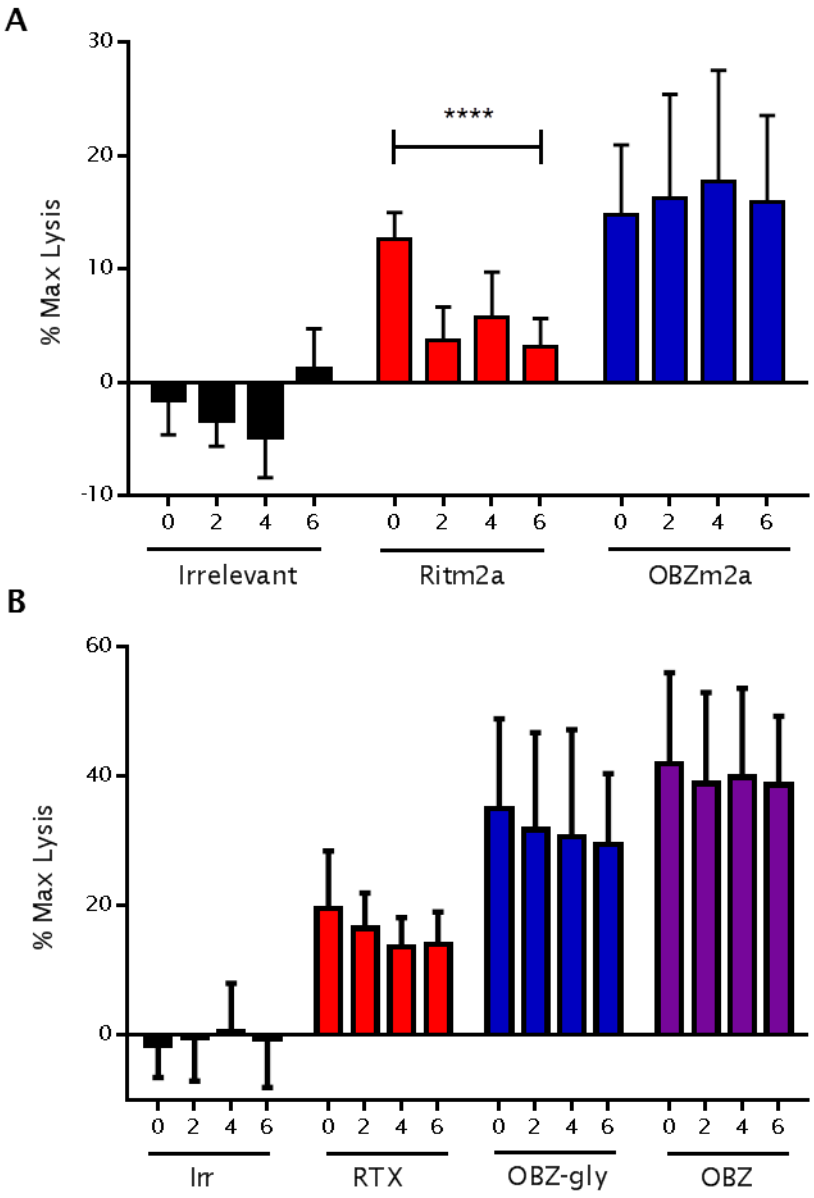

Figure 3-19 Impact of antigenic modulation on ADCC

(**A**) Target hCD20 B cells were stained with calcein-AM (5 µM). Samples were opsonised with irrelevant or anti-CD20 mAb (10 µg/ml) and allowed to undergo antigenic modulation for 30 minutes – 6 hours at 37 °C (5 % CO_2). Target ($1x10^5$ cells) and effectors ($1x10^6$ cells) were co-cultured for 2 hours at 37 °C (5 % CO_2). Fluorescence was measured with excitation at 490 nM. N=6+/-SD (**B**) Target CLL B cells were stained with calcein-AM (5 µM). Samples were opsonised with irrelevant or anti-CD20 mAb (10 µg/ml) and allowed to undergo antigenic modulation for 30 minutes – 6 hours at 37 °C (5 % CO_2). Target ($1x10^5$ cells) and effectors ($1x10^6$ cells) were co-cultured for 4 hours at 37 °C (5 % CO_2). Fluorescence was measured with excitation at 490 nM. N=3 +/-SD. Significance was assessed using a two-way ANOVA.

From **Figure 3-19** it can be seen that antigenic modulation has significantly reduced the ability of type I but not type II antibodies to facilitate ADCC when using murine targets and effector cells. This reduction, was rapid with a significant loss in ADCC after only 2 hours modulation time. In contrast, when using human target and effector cells the same dramatic loss in ADCC activity was not observed although there was a modest decrease in ADCC activity after 6 hours modulation. The differences observed with rituximab compared to Ritm2a may not be significant due to the longer (4 hour) target and effector incubation period required for the human ADCC assay, which would allow modulation to occur even in the 0 hour samples. Also, the fact that Ritm2a was lost from the cell surface to a greater extent than rituximab would have impacted upon the extent to which ADCC occurred.

Next, the impact of antigenic modulation on phagocytosis was investigated. Target hCD20 B cells in combination with murine BMDM and primary CLL cells in combination with MDM were used to assess the impact of 0-6 hour modulation on the ability to elicit ADCP (**Figure 3-20**). It was found that type I reagents were significantly (p<0.05) effected by modulation whereas type II reagents remained unaffected when using both murine and human effector cells. Compared to the murine ADCC assay the loss in effector function was not as dramatic in the murine ADCP assay.

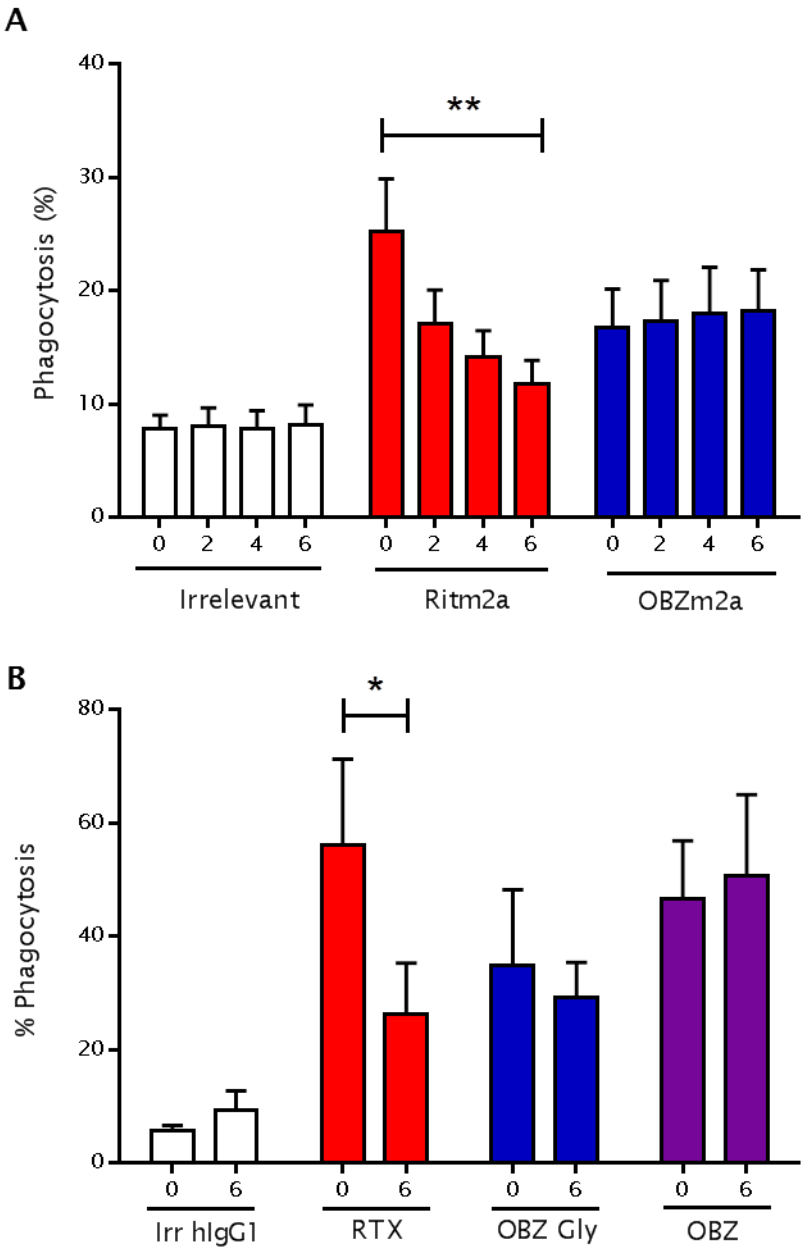

Figure 3-20 Impact of antigenic modulation on ADCP

(**A**) Target hCD20 B cells were stained with CFSE (5 µM). Samples were opsonised with irrelevant or anti-CD20 mAb (10 µg/ml) and allowed to undergo antigenic modulation for 30 minutes – 6 hours at 37 °C (5 % CO_2). Target ($2.5x10^5$ cells) and effectors ($5x10^4$ cells) were co-cultured for 30 minutes at 37 °C (5 % CO_2). Samples were stained with F4/80-APC (2 µl) and acquired on a flow cytometer. N=6+/-SD (**B**) Target CLL B cells were stained with CFSE (5 µM). Samples were opsonised with irrelevant or anti-CD20 mAb (10 µg/ml) and allowed to undergo antigenic modulation for 30 minutes – 6 hours at 37°C (5 % CO_2). Target ($2.5x10^5$ cells) and effectors ($5x10^4$ cells) were co-cultured for 1 hour at 37 °C (5 % CO_2). Samples were stained with anti-CD16 mAb (2 µl) and acquired on a flow cytometer. N=3 +/-SD. Significance was assessed using a two-way ANOVA.

These data demonstrate that antigenic modulation impacts on both ADCP and ADCC effector mechanisms. To apply these results to a more clinically relevant setting, earlier B cell depletion findings were confirmed in a relevant tumour mouse model. The recently characterised C57BL/6 Eμ-TCL-1 tumour model of CLL was used [239]. The TCL-1 gene was initially found to be overexpressed in mature T cell leukaemias and subsequently observed in B cell leukaemias. Eμ-TCL-1 mice have forced expression of the TCL-1 gene under the control of the V_H promoter-Ig(H)-Eμ enhancer. This led to forced expression of the TCL-1 gene in immature and mature B cells [239]. Eμ-TCL-1 mice were crossed with C57BL/6 hCD20 mice to generate a hCD20 x Eμ-TCL-1 tumour which could be passaged into immunocompetent hCD20 Tg mice. Tumours were passaged rather than using spontaneously generated tumours due to the long time it takes for tumour to present (~ 1 year). It was important to cross Eμ-TCL-1 mice onto the hCD20 background to avoid any rejection of tumour once passaged into hCD20 recipients. Using this model the ability of human IgG1 antibodies to deplete tumour cells and whether this also correlated with the presence of antibody in the plasma was investigated (**Figure 3-21**).

From **Figure 3-21** it can be seen that hCD20 x TCL-1 tumour B cells show significantly ($p<0.05$) prolonged depletion when treated with type II (OBZ gly) compared to type I (RTX) mAb, OBZ gly could still be detected in the plasma at 21 days whereas RTX was undetectable by day 14. This depletion was to a similar extent to that shown with normal hCD20 Tg B cells (**Figure 3-1**). The prolonged plasma half-life seen when using OBZ gly compared to RTX was again similar to results previously seen with WT material (**Figure 3-4**). Overall this data supports earlier findings when using normal B cells and again demonstrates the superior effects of type II antibodies *in vivo*, this time in a mouse tumour model of CLL.

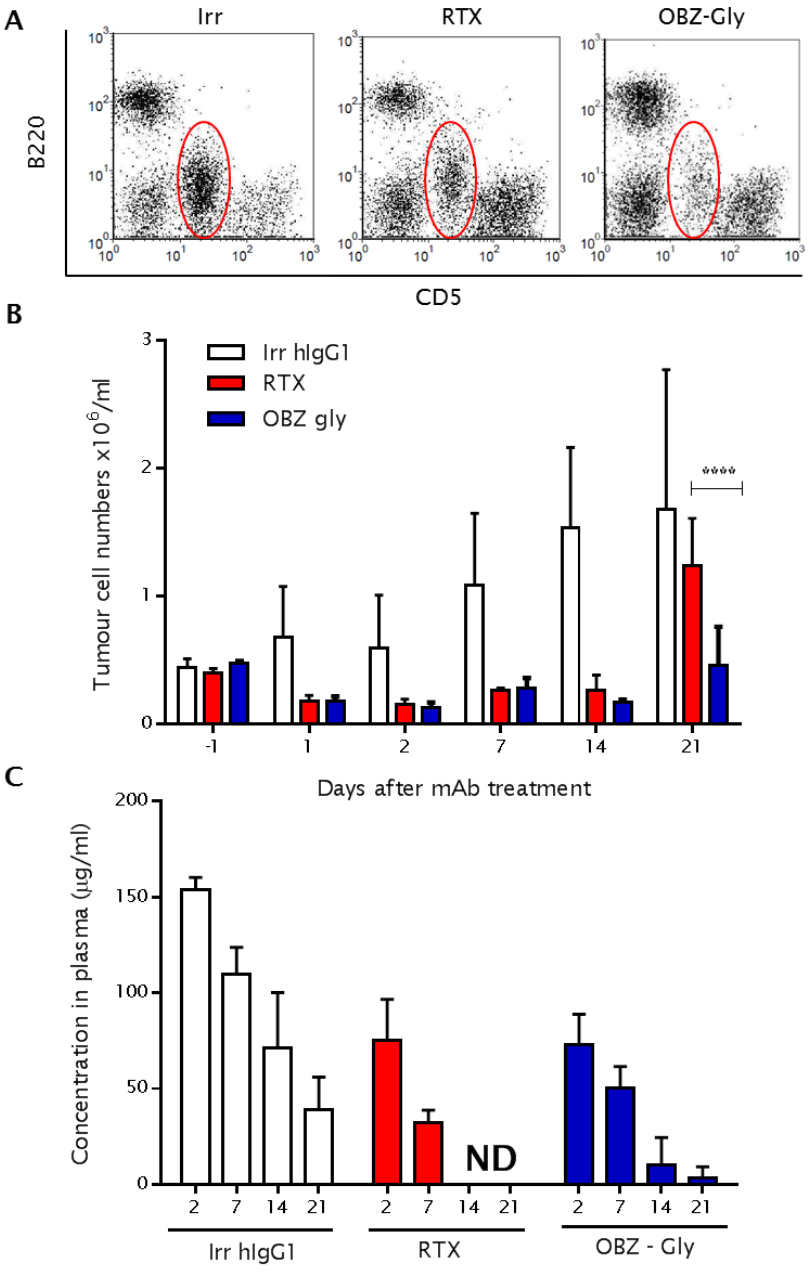

Figure 3-21 *In vivo* depletion of Eμ-TCL-1 x hCD20 Tg leukemic B cells

(**A**) Representative FACS plots showing Eμ-TCL-1 x hCD20 tumour (red circle) present 21 days post treatment with therapeutic mAb. (**B**) C57BL/6 hCD20 mice were treated i.p. with Eμ-TCL-1 x hCD20 tumour ($1x10^7$ cells). Once tumour could be detected by flow cytometry (35-42 days) mice were treated i.v. with therapeutic antibody (250 μg). The percentage of circulating tumour was monitored using flow cytometry. Peripheral blood samples were stained for B220-PerCP and CD5-PE, periodically, for 21 days. (**C**) plasma was collected 2, 7, 14 and 21 days post treatment with therapeutic antibody. Plasma was initially diluted 1:500 and then serially 1:2 across the ELISA plate. Irrelevant human IgG1 was used as a standard and results were interpreted based on extrapolation from standard curve. N=3+/- SD. Statistical analysis performed using two-way ANOVA.

3.7 Chapter discussion

Previous work by Beers *et al* has shown that mouse IgG2a versions of type II anti-CD20 antibodies will outperform type I antibodies of the same isotype and that the detrimental process of antigenic modulation takes place more rapidly with type I antibodies [109, 122]. In this chapter it has been shown that antigenic modulation is indeed detrimental to the efficacy of type I antibodies and that the reason for this is that antigenic modulation impacts upon FcγR dependent function, namely the mechanisms of ADCC and ADCP. These findings explain the observation that type II antibodies outperform type I, *in vivo,* in normal B cell depletion and tumour models. Furthermore, when using human effector cells and primary CLL samples these same effector mechanisms were similarly impacted with clinically relevant human IgG1 type I antibodies. Importantly, since human IgG1 antibodies were successful in depleting hCD20 B cells *in vivo* but showed little efficacy in murine ADCC assays it can be concluded that ADCP is the dominant effector mechanism, at least in the mouse. This conclusion is further supported by FcγR binding data **which show** that there is little affinity by human IgG antibodies for mouse FcγRIII.

Interestingly, differences were observed between the depletion of murine hCD20 B cells when using a type I hIgG1 or mIgG2a antibody (Figure 3-1). However, such differences were not seen when using type II obinutuzumab. One likely explanation for this discrepancy is the enhanced antibody consumption of type I hIgG1 over that of mIgG2a. It has been demonstrated that antigenic modulation is accelerated with type I antibodies [109] but there may be other factors that enhance the consumption of hIgG1 in the mouse and one such factor is trogocytosis. Trogocytosis is the process by which cell surface molecules are transferred from one cell to another, it occurs through a number of well-defined mechanisms. The first stage involves recognition of the target ligand, with regard to anti-CD20 therapy this would be between the antibody bound to CD20 and FcγRs on accepter cells. This recognition results in an immunological synapse followed by membrane remodelling and fusion of plasma membranes. The targeted molecules along with sections of plasma membranes are then taken up by the accepter cell and are degraded internally [240]. Trogocytosis was shown by Beum et al to be rapid with significant

removal of CD20 by THP1 monocytes within 45 minutes [241]. This study used only type I rituximab and ofatumumab and it would be very interesting to see if similar results are obtainable when using type II obinutuzumab. It would also be interesting to determine if there are any species differences between a mouse and human setting. To this end SPR data revealed mouse IgG2a and human IgG1 to have similar binding profiles for mouse FcγRI and IV, however mIgG2a had superior binding affinity for mouse FcγR (Table 1). Therefore, due to greater binding affinity, it may be expected that there is enhanced trogocytosis when using mouse IgG2a compared to hIgG1 antibodies and this would seem be at odds with the hypothesis that hIgG1 is preferentially removed from the system. An alternative explanation for the differences observed are that due to the clustering of type I antibody into lipid rafts on the cell surface an anti-hIgG1 response was formed, resulting in the active removal of hIgG1 from the system. This response would likely be more prolific when using type I compared to type II hIgG1 antibodies due to clustering which would augment binding to low affinity FcγRIIb on antigen presenting dendritic cells. This would enhance uptake and the formation of an immune response to hIgG1 when using type I antibodies but would occur to a lesser extent when using type II obinutuzumab. This mouse anti-human IgG1 response in combination with antigenic modulation and trogocytosis could be responsible for the enhanced consumption of hIgG1 over mIgG2a type I antibodies. Although further research would be needed to investigate these proposed mechanisms.

Previous work comparing clinically-relevant antibodies have demonstrated that ofatumumab and obinutuzumab are superior to rituximab in different ways; ofatumumab displays enhanced CDC and obinutuzumab enhanced ADCC and direct cell death [242, 243]. Although insightful, these experiments did not take into account the potentially detrimental effect of antigenic modulation which is shown here to have a significant impact on FcγR-dependent effector mechanisms. In contrast to the importance of ADCC/ADCP there is work supporting the role of CDC which must be accounted for. Work by van Meerten *et al* showed a strong correlation between CDC and CD20 expression, such a correlation was not seen with regards to ADCC [244]. These results would have suggested antigenic modulation to have an impact on CDC however, work presented here and by others were unable to demonstrate a role for CDC in the

mouse [122]. To investigate the possible role of antigenic modulation on CDC future work could allow antigenic modulation to occur on isolated B cells and then measure the levels of cell death following addition of a complement source such as human serum.

In contrast, work presented here and by others have been able to demonstrate the critical need for macrophages and ADCP [122, 135, 136] and it may perhaps be that the levels of CD20 compared by van Meerten *et al* did not reach a sufficiently low level to impact on FcγR mechanisms; a threshold that is crossed by significant loss of antibody due to modulation. Obinutuzumab is defucosylated so as to improve its affinity for FcγRIIIa and so augment ADCC/ADCP effector functions. These results found that obinutuzumab did indeed elicit greater levels of ADCC compared to its non defucosylated counterpart obinutuzumab-gly. This highlights the benefit of de-fucosylation and the potential of glycoengineering. However, it was found that there were equivalent levels of B cell depletion seen in the mouse when using either obinutuzumab or obinutuzumab-gly. Binding data for these antibodies reveal that there are similar affinities for FcγRI and IV although obinutuzumab did have a slower dissociation rate for FcγRIV. There may be fundamental differences in mouse and human immunology which help explain why obinutuzumab and obinutuzumab-gly show a similar ability to deplete B cells, in the mouse. Human NK cells express FcγRIIIa and this receptor shares a higher sequence identity to FcγRIV than it does to FcγRIII [123]. Since FcγRIV is not expressed on murine NK cells *in vivo* depletion results here may underestimate the role that glycomoification plays in ADCC [123, 245]. Interestingly human FcγRIIIa is glycosylated at residue Asn-162 [246] with FcγRIV glycosylated at a similar location, likely explaining why obinutuzumab has slightly different kinetics of binding to this FcγR. Based on SPR data showing the binding affinities of monomeric antibody it would be interesting to determine the interaction of multimeric immune complex human IgG1 with mouse FcγRIII and FcγRIV using a similar methodology to that described recently [247].

Human IgG1 antibodies showed negligible binding to mouse FcγRIII and therefore, as expected, human IgG1 antibodies of both type I and II had negligible activity in our murine ADCC assays. Although they did have activity

equivalent to that of IgG2a antibodies in our murine ADCP assays and *in vivo* depletion studies, together this demonstrated that ADCP is the dominant effector mechanism in the mouse. Further supporting the dominant role of ADCP in the mouse are data showing that both mouse IgG1 and IgG2a antibodies had equivalent ADCC activity but that mouse IgG1 antibodies were inferior to mouse IgG2a at ADCP and that this correlated with *in vivo* depletion results. These conclusions are further supported by recent intravital imaging experiments which show that tissue macrophages (liver kupffer cells) are critical to effective antibody therapy [135, 136].

However, when using human target and effectors in human ADCP assays obinutuzumab was as effective as obinutuzumab-gly. Based on these observations it may be that any differences seen when comparing rituximab with obinutuzumab may largely reflect the inherent differences between type I and II antibodies. Indeed recent clinical trial data demonstrated that CLL patients given chlorambucil alone or in combination with either rituximab or obinutuzumab showed that patients receiving the obinutuzumab arm of treatment had improved progression free survival and higher rates of complete response compared to those receiving rituximab. However, those receiving obinutuzumab did receive a higher dose compared to rituximab [131]. These results are complementary to what we found with regards to our hCD20 x Eμ-TCL-1 B cell depletion studies, since treatment with obinutuzumab resulted in significantly prolonged B cell depletion compared to rituximab. Furthermore, our studies used matching doses of rituximab or obinutuzumab-gly and we still saw a benefit, again suggesting efficacy in the absence of glycomodification and this may reflect the type II nature of the antibody.

Based on these findings and the findings of others [122] we are satisfied that the differences between mouse IgG1 and IgG2a antibodies can be accounted for by their ability to elicit macrophage mediated ADCP and are not due to other mechanisms independent of FcγR such as CDC. This conclusion is supported by the fact that mice were able to deplete B cells in the absence of complement component C3 but were unable to deplete B cells once macrophages had been depleted using clodronate liposomes.

Recent work by Herter *et al* has demonstrated that obinutuzumab is superior to rituximab in the presence of competing IgG [248]. This would presumably

be due to obinutuzumab having a greater affinity for FcγRIIIa and out competing the surrounding IgG, therefore whereas we saw there to be minimal difference between obinutuzumab and obinutuzumab-gly it may be that *in vivo* where these antibodies work in the presence of circulating IgG obinutuzumab is in fact superior in its glycomodified form.

The redistribution of CD20 by rituximab into clustered caps at the cell surface has been proposed to enhance ADCC activity by NK cells [249]. Results presented here conflict with this assertion as it was found that type II antibodies which do not cluster CD20 into lipid rafts to the same extent are superior to rituximab at eliciting ADCC. An explanation for these different results may be that Rudnicka *et al*. used established B cell lines which have been shown not to modulate antibody to the same extent as primary B cells. Therefore although rituximab will induce capping which may facilitate ADCC any beneficial effects may be lost due to antigenic modulation. This hypothesis is supported by the fact that type I antibodies out performed type II antibodies in ADCP assays but this benefit was lost following antigenic modulation in as little as 2 hours. Therefore approaches to minimise the process of antigenic modulation would be useful. It has previously been shown that increased levels of FcγRIIb augment antigenic modulation by anti-CD20 antibodies [232]. Recent work has described such a treatment, blocking the activity of inhibitory FcγRIIb, using a mAb, which will not only reduce the level of antigenic modulation but will also act as an additional target for effector cells [250].

In conclusion, the work presented in this chapter demonstrates that antigenic modulation has a detrimental effect upon the known FcγR dependent mechanisms of killing mediated by NK cells and macrophages. This detrimental effect is biased towards the type I antibodies such as ofatumumab and rituximab which cluster CD20 into lipid rafts at the cell surface. Additionally, we show using a variety of mAb isotypes that ADCP is the dominant effector mechanism, at least in the mouse. This was demonstrated by the fact that human IgG1 antibodies were able to deplete B cells *in vivo*, however, they were unable to elicit ADCC when used with murine target and effector cells. In contrast human IgG1 antibodies were able to elicit equivalent levels of ADCP to that of the mouse IgG2a antibodies. These results would suggest that future research should investigate ways to block the detrimental

antigenic modulation process and also to enhance ways of eliciting macrophage mediated ADCP.

Chapter 4: Multiple FcγR are required for effective B cell depletion

4.1 Chapter Introduction

Monoclonal antibodies have become an established first line treatment for many diseases ranging from autoimmune conditions such as SLE and RA to cancers such CLL, DLBCL and FL. However, in many cases their precise mechanisms of action remain unknown. What has become clear over recent years is that for depleting antibodies such as rituximab Fc:FcγR interactions are critical to successful therapy [94, 95, 110, 111]. Furthermore, it has recently been demonstrated, at least in the mouse, that macrophages are the critical effector cell population responsible for target cell depletion [135, 136, 251, 252]. As described in chapter 1 macrophages are a highly heterogeneous population which express the full range of activatory and inhibitory FcγR [127] and there is some debate in the literature as to which of these activatory FcγR are more important to effective target cell depletion.

Some of the earliest work investigating the role of FcγR tested their contribution *in vivo* using mice that were deficient for FcγRI or FcγRIII and had FcγRIV blocked using the monoclonal antibody 9E9 [123, 128]. The monoclonal antibody 9E9 was first reported upon in 2005 where it was shown to bind specifically to mouse FcγRIV and block immune complex binding to this receptor. In these studies mice deficient for FcγRI and FcγRIII showed no reduction in mAb mediated platelet clearance. However, mice which had FcγRIV blocked using 9E9 showed a significant inhibition in the ability to clear platelets following mAb treatment [123]. Since 2005 there have been a number of publications demonstrating the importance of mouse FcγRI and FcγRIV whilst giving a redundant role to mouse FcγRIII. These experiments typically use FcγRI$^{-/-}$ mice in combination with 9E9 to block FcγRIV [123, 128, 135, 253, 254]. Hamaguchi *et al* used a B cell depletion, adoptive transfer model, to demonstrate that FcγRIV is critical to effective depletion of B cells by IgG2b and IgG2a antibodies [128]. More recently Gul *et al* highlighted the importance of macrophages as the dominant effector cell population and again they used the

combination of FcγRI$^{-/-}$ mice with 9E9 to show that macrophages are dependent upon FcγRI and FcγRIV to deplete target cells [135].

In this chapter the importance of each individual FcγR to B cell depletion was investigated. Furthermore, the effect of functionally excluding multiple FcγR upon depletion of B cells *in vivo* by anti-CD20 mAb Ritm2a was investigated.

4.2 Functional redundancy between multiple FcγR

Previous publications have shown that there is a loss of effector cell activity in response to depleting mAb when using γ chain deficient mice [110]. Further to this it has been established that there is a level of functional redundancy between FcγRs; particularly FcγRI and FcγRIV [135]. To determine whether systemic loss of one FcγR was sufficient to impact on depletion of hCD20 expressing B cells by type I antibody Ritm2a (mouse IgG2a isotype) adoptive transfer experiments were performed (**Figure 4-1**).

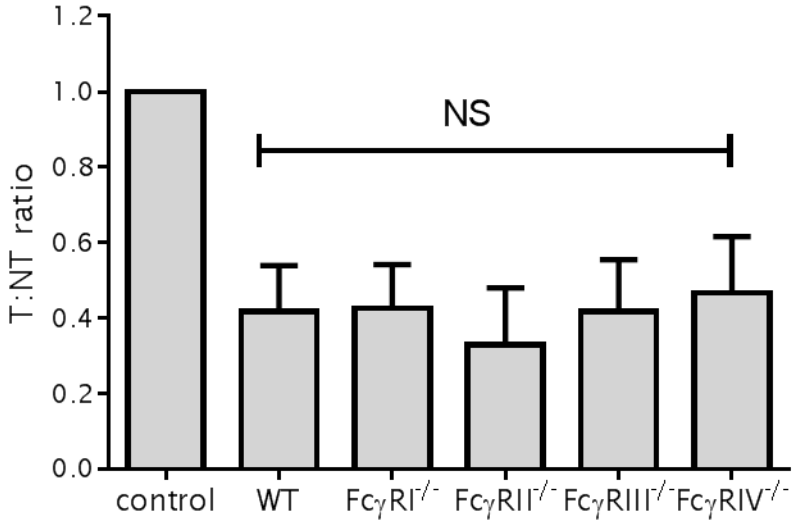

Figure 4-1 Adoptive transfer assay to determine the role of individual FcγR in B cell depletion

Splenocytes from WT or hCD20 BALB/c mice were stained with CFSE (WT-0.5μM) (hCD20-5μM). A 1:1 mixture of WT and hCD20 splenocytes ($5x10^6$ cells) were injected i.v. into recipient BALB/c WT or FcγRI - $FcγRIV^{-/-}$ mice. The following day (18-24hr) mice were injected i.v. with Ritm2a (50 μg). The following day (18-24 hr) spleens were harvested, dissociated and stained with anti-CD19-APC (1D3) before being acquired on a flow cytometer. N=7 +/- SD. Statistical analysis performed using one-way ANOVA.

From **Figure 4-1** it can be seen that there is no significant difference in B cell depletion between WT mice and individual $FcγR^{-/-}$ mice thus highlighting that at least in response to mouse IgG2a antibody there is functional redundancy between two or more activatory FcγR. There is a slight although not significant trend for B cell depletion to be improved in the $FcγRIIb^{-/-}$ mouse. After

establishing that some level of functional redundancy exists the effect of knocking out/blocking multiple FcγR was examined.

As in previous studies [135, 253] FcγRI$^{-/-}$ or FcγRIII$^{-/-}$ mice in combination with 9E9 were used in adoptive transfer assays looking at the depletion of hCD20 Tg B cells in response to Ritm2a. The previously established *in vivo* dose of 9E9 required to block FcγRIV is 400 µg [255]. To test the dose response of 9E9 needed to block FcγRIV in our system various amounts of 9E9 were administered to C57BL/6 mice and the amount of free FcγRIV on macrophages, monocytes and neutrophils was detected 24 hours later, by flow cytometry.

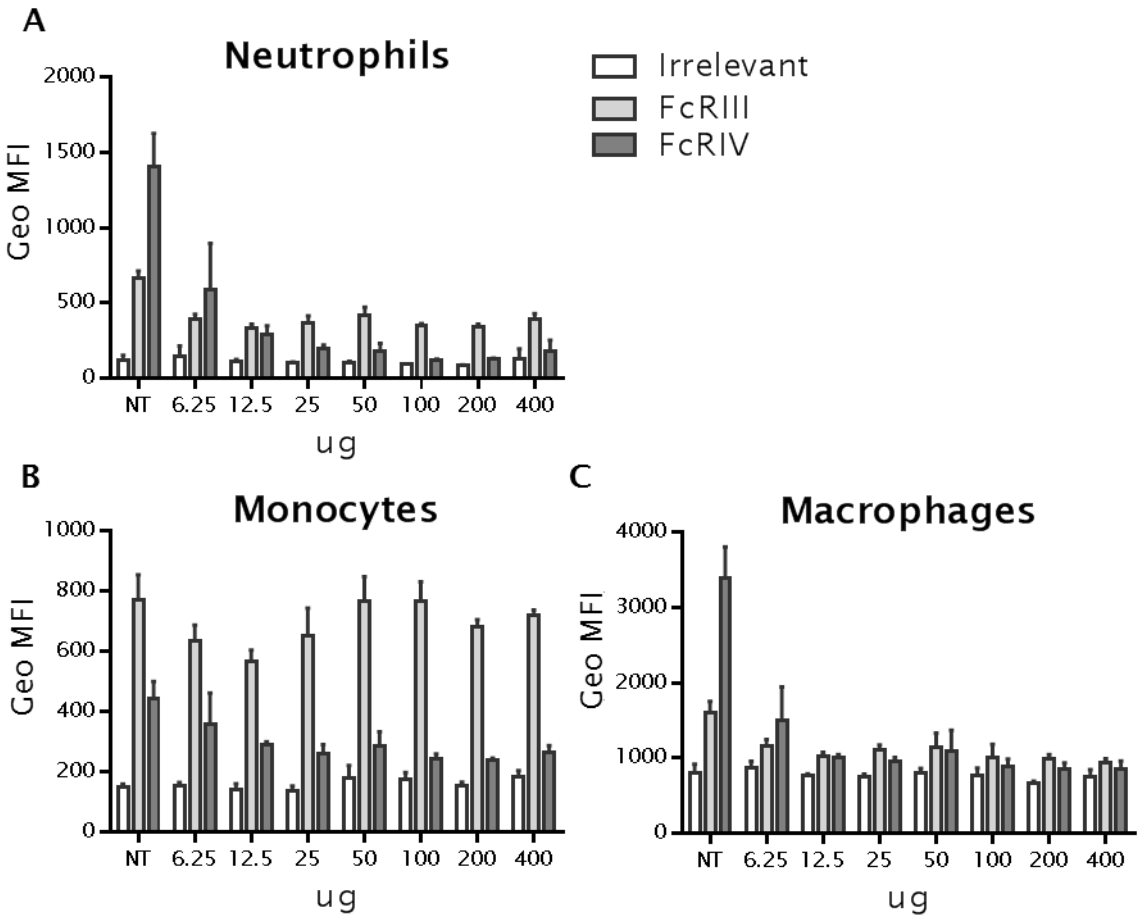

Figure 4-2 Detection of FcγRIII and FcγRIV following administration of 9E9

C57BL/6 mice were treated i.p. with various doses (400-6.25 µg) of anti-FcγRIV antibody 9E9. The following day mice were sacrificed and spleens harvested, the level of FcγRIII (AT152-4 F(ab)$_2$-FITC) (10 µg/ml) and FcγRIV (9E9-FITC) (10 µg/ml) were determined by flow cytometry. (**A**) Neutrophils, identified as CD11b$^+$, Ly6G^{Hi} and Ly6C^{int}. (**B**) Monocytes, identified as CD11b$^+$, Ly6G^{int} and Ly6C^{hi}. (**C**) Macrophage, identified as CD11b^{int}, F4/80^{hi}. N=3 +/-SD.

From **Figure 4-2** it can be seen that, as expected addition of 9E9 blocks detection of FcγRIV. Blocking of FcγRIV was observed when administering 9E9 at 400 µg down to 12.5 µg and was observed on all three cell populations investigated. Intriguingly, it also appeared that levels of FcγRIII were reduced following administration of 9E9, this was observed on neutrophils and macrophages but not monocytes. It is interesting that such low doses of 9E9 could be used to saturate FcγRIV on effector cells. However, since detection of cell surface receptor was achieved using fluorochrome conjugated mAb and not immune complex binding the physiologically relevant blocking of FcγRIII and FcγRIV following 9E9 administration could not be determined and so the widely used dose of 400 µg was taken forward in subsequent experiments.

4.2.1 Impact of silencing multiple activatory FcγR on B cell depletion

The removal of a single activatory FcγR had no impact upon B cell depletion in adoptive transfer assays (**Figure 4-1**), in response to a mouse IgG2a antibody. Therefore the effect of blocking and/or knocking out multiple FcγR was next investigated. This was achieved using 9E9 in combination with either FcγRI$^{-/-}$ or FcγRIII$^{-/-}$ mice in a similar fashion to that of previously published data [128, 135, 253] (**Figure 4-3**).

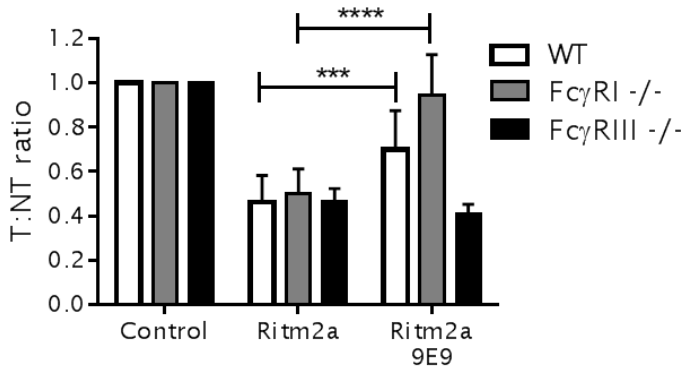

Figure 4-3 Adoptive transfer assays blocking multiple activatory FcγR

WT, FcγRI$^{-/-}$ or FcγRIII$^{-/-}$ mice on a BALB/c background were subjected to adoptive transfer assays with or without additional blocking of FcγRIV using mAb 9E9. Splenocytes from WT or hCD20 Tg mice were differentially stained with CFSE (WT-0.5µM, hCD20-5µM), they were then mixed together 1:1 and injected i.v. into recipient mice (5x10^6 cells). The following morning mice were injected i.p. with 9E9 (400 µg) this

was followed ~3-4 hours later with i.v. injection of Ritm2a (10 µg). The following day spleen was harvested, disassociated and opsonised with anti-CD19-APC (1D3) antibody. N=6+/- SD. Statistical analysis was performed using two-way ANOVA.

From **Figure 4-3** it can be seen that depletion of B cells in response to Ritm2a alone is the same for WT, FcγRI$^{-/-}$ and FcγRIII$^{-/-}$ mice. However, once FcγRIV is blocked with 9E9 there is a significant decrease in B cell depletion shown by the WT mouse and an almost complete block in B cell depletion shown by the FcγRI$^{-/-}$ mouse. Interestingly, the FcγRIII$^{-/-}$ mouse which had been blocked with 9E9 and so should only display FcγRI showed no attenuated B cell depletion.

Additional phenotyping was subsequently performed on the splenocytes harvested from the mice used to generate the data in **Figure 4-3**. The level of activatory FcγR displayed on the cell surface of the splenocytes following treatment with Ritm2a, +/- 9E9 was assessed (**Figure 4-4** - **Figure 4-6**).

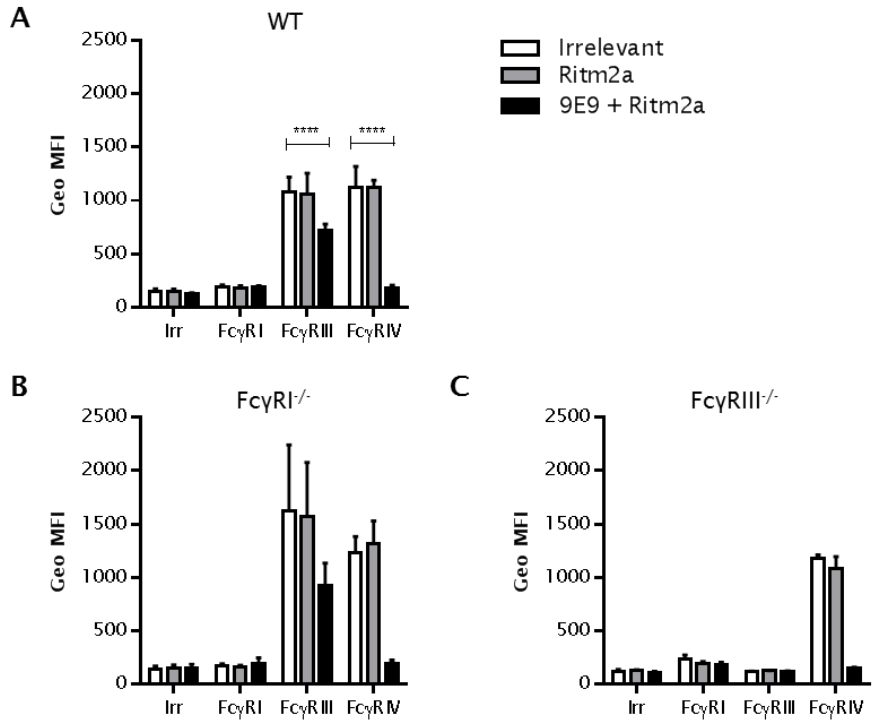

Figure 4-4 Detection of activatory FcγR on neutrophils following 9E9 blocking

BALB/c splenocytes were obtained from the experiment presented in **Figure 4-3**. Splenocytes from WT (**A**), FcγRI$^{-/-}$ (**B**) or FcγRIII$^{-/-}$ (**C**) mice were stained with CD11b, Ly6G and Ly6C to allow identification of neutrophils. Cells were additionally stained with FITC conjugated mAb detecting FcγRI (AT150-9 F(ab)$_2$), FcγRIII (AT154-2 F(ab)$_2$) or FcγRIV (9E9). Samples were stained on ice for 30 minutes. Red blood cells were then lysed and samples were acquired on a flow cytometer. N=6+/- SD. Statistical analysis performed using two-way ANOVA.

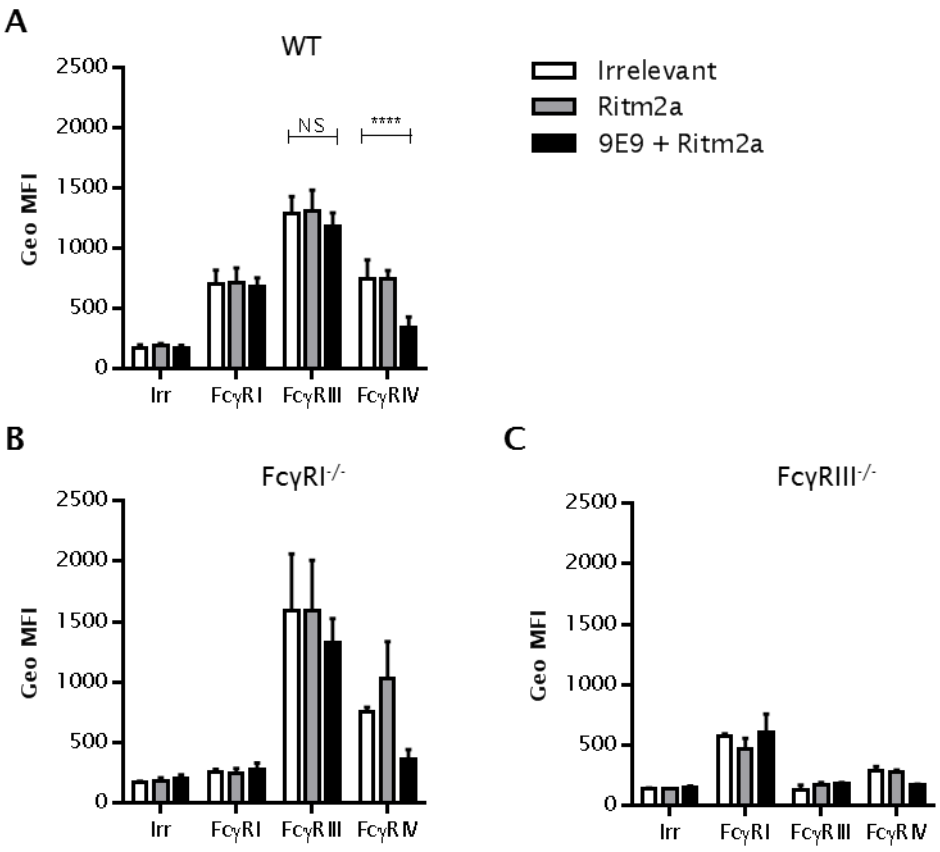

Figure 4-5 Detection of activatory FcγR on monocytes following 9E9 blocking

BALB/c splenocytes were obtained from the experiment presented in **Figure 4-3**. Splenocytes from WT (**A**), FcγRI$^{-/-}$ (**B**) or FcγRIII$^{-/-}$ (**C**) mice were stained with CD11b, Ly6G and Ly6C to identify monocytes. Cells were additionally stained with FITC conjugated mAb detecting FcγRI (AT150-9 F(ab)$_2$), FcγRIII (AT154-2 F(ab)$_2$) or FcγRIV (9E9). Samples were stained on ice for 30 minutes. Red blood cells were then lysed and samples were acquired on a flow cytometer. N=6+/- SD. Statistical analysis performed using two-way ANOVA.

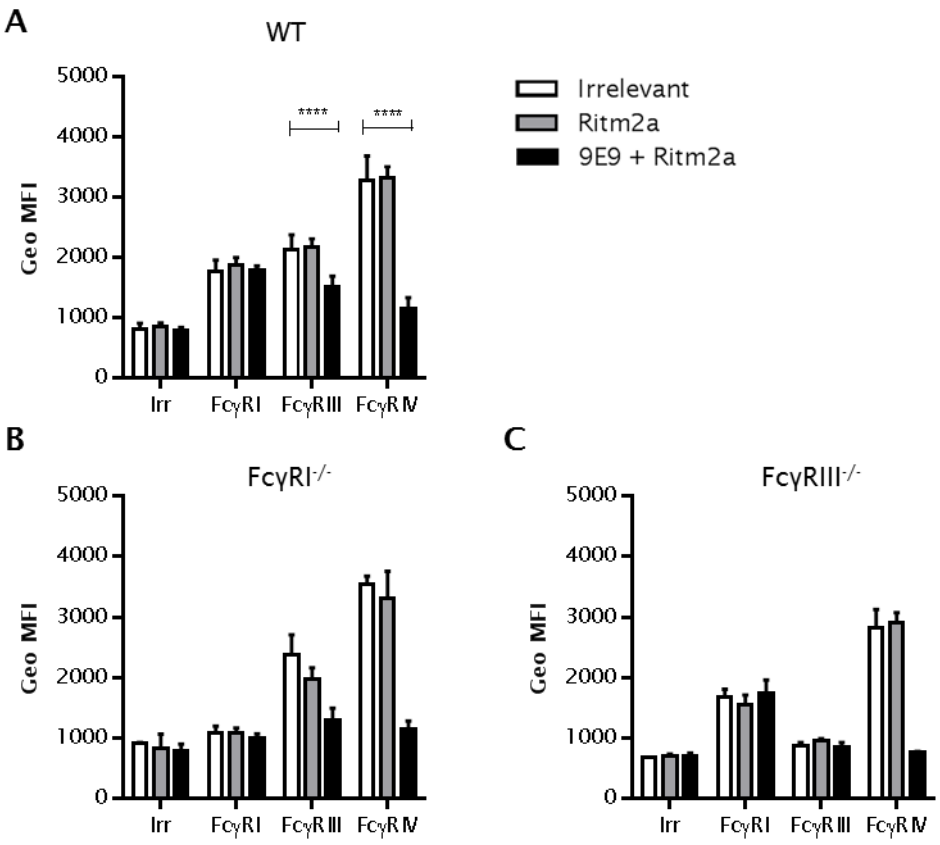

Figure 4-6 Detection of activatory FcγR on macrophages following 9E9 blocking

BALB/c splenocytes were obtained from the experiment presented in **Figure 4-3**. Splenocytes from WT (**A**), FcγRI$^{-/-}$ (**B**) or FcγRIII$^{-/-}$ (**C**) mice were stained with CD11b, and F4/80 to allow identification of macrophages. Cells were additionally stained with FITC conjugated mAb detecting FcγRI (AT150-9 F(ab)$_2$), FcγRIII (AT154-2 F(ab)$_2$) or FcγRIV (9E9). Samples were stained on ice for 30 minutes. Red blood cells were then lysed and samples were acquired on a flow cytometer. N=6+/- SD. Statistical analysis performed using two-way ANOVA.

Results from **Figure 4-4** confirm that FcγRI$^{-/-}$ and FcγRIII$^{-/-}$ mice did in fact not express these receptors. It was also demonstrate that WT neutrophils express low levels of FcγRI but relatively high levels of FcγRIII and FcγRIV. Importantly, it can again be seen that 400 µg of 9E9 was sufficient to completely saturate all FcγRIV on the neutrophil population making it undetectable by 9E9-FITC. Interestingly, blocking with 9E9 appeared to significantly reduce the level of detectable FcγRIII in the WT mouse. It can be seen in **Figure 4-5** that WT monocytes display high levels of FcγRIII and intermediate levels of FcγRI and FcγRIV. Again, it can be seen that blocking with 9E9 significantly reduced detectable levels of FcγRIV, however, on monocytes no associated decrease in

FcγRIII was observed when blocking with 9E9. Finally, from **Figure 4-6** it can be seen that macrophages have high background levels of fluorescence. However, it can be seen that WT macrophages display intermediate levels of FcγRI and FcγRIII with higher levels of FcγRIV. Blocking with 9E9 significantly decreased the amount of FcγRIV that could be detected, having no impact on FcγRI levels but again significantly reducing the amount of FcγRIII that could be detected. Representative histograms from the data presented in **Figure 4-4** - **Figure 4-6** can be found in (**Appendix 3** - **Appendix 5**).

Additional experiments were subsequently performed to block multiple FcγR using other anti-FcγR mAb. For these experiments FcγRIV$^{-/-}$ mice on a BALB/c background were used in combination with the mAb 2.4G2 F(ab)$_2$. This antibody has been shown to interfere with immune complex binding to FcγRIIb and FcγRIII and has been widely used as a blocking reagent [256]. Whole IgG preparations of 2.4G2 should also bind to and block FcγRI by virtue of high affinity Fc, cis, interactions [257, 258]. Using this combination of FcγRIV$^{-/-}$ mice and 2.4G2 F(ab)$_2$ mAb adoptive transfer studies were undertaken to look at the level of B cell depletion following treatment with Ritm2a (**Figure 4-7a**).

From **Figure 4-7a** it can be seen that FcγRIV$^{-/-}$ mice had an equivalent level of B cell depletion compared to WT mice. Blocking of FcγRIIb and FcγRIII in FcγRIV$^{-/-}$ mice was sufficient to completely inhibit any B cell depletion, whereas blocking in the WT mouse led to a decreased ability to deplete B cells but not complete abolition. These findings contrasted with those presented in **Figure 4-3** whereby FcγRIII$^{-/-}$ mice treated with 9E9, which will only have activatory FcγRI present, are readily able to deplete B cells. These finding demonstrate that FcγRIV$^{-/-}$ mice which have had FcγRIII blocked (and so only have FcγRI available) are unable to deplete B cells. A simple explanation for these results would be that the high blocking dose of 2.4G2 F(ab)$_2$ used (400 µg) will contain some whole IgG which will block FcγRI interactions. However, 2.4G2 F(ab)$_2$ was tested using HPLC and was found to contain no whole IgG contamination (**Appendix 6**). The fact that 2.4G2 F(ab)$_2$ also binds inhibitory FcγRIIb complicates matters and in an attempt to clarify these findings it was hypothesised that 2.4G2 F(ab)$_2$ will bind to FcγRIIb displayed by target B cells and that this may act to interfere with Ritm2a opsonisation on the B cell surface. To test this hypothesis adoptive transfer assays were performed whereby FcγRIIb$^{-/-}$ and

hCD20 x FcγRIIb$^{-/-}$ splenocytes were adoptively transferred into recipient WT or FcγRIV$^{-/-}$ mice (**Figure 4-7b)**.

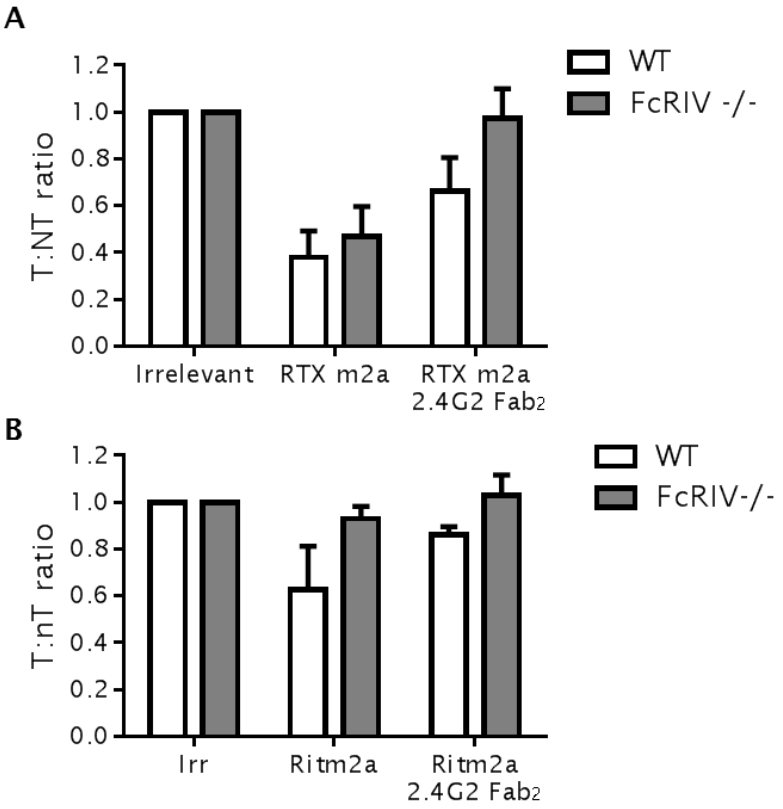

Figure 4-7 Adoptive transfer assays blocking activatory FcγR using 2.4G2 F(ab)$_2$

(**A**) Splenocytes from WT or hCD20 BALB/c mice were stained with CFSE (WT-0.5 μM, hCD20-5μM) and then injected (5x10^6 cells) i.v. into BALB/c WT or FcγRIV$^{-/-}$ mice. The following morning mice were treated i.p. with 2.4G2 F(ab)$_2$ (400 μg), 3-4 hours later mice were treated with Ritm2a (10 μg). (**B**) Splenocytes from FcγRIIb$^{-/-}$ or hCD20 x FcγRIIb$^{-/-}$ C57BL/6 mice were stained with CFSE (WT-0.5μM,hCD20-5μM) and then injected (5x10^6 cells) i.v. into C57BL/6 WT or FcγRIV$^{-/-}$ mice. The following morning mice were treated i.p. with 2.4G2 F(ab)$_2$ (400 μg), 3-4 hours later mice were treated with Ritm2a (10 μg). N=3+/- SD.

From **Figure 4-7b** it can be seen that FcγRIV$^{-/-}$ mice treated with Ritm2a showed a diminished ability to deplete B cells compared to the WT mouse treated with Ritm2a, although B cell depletion in WT mice was reduced compared to previous experiments (**Figure 4-7a**). Considering that FcγRIV$^{-/-}$ mice treated with Ritm2a showed this diminished response it is unsurprising that FcγRIV$^{-/-}$

mice treated with 2.4G2 $F(ab)_2$ also showed a drastically diminished ability to deplete B cells. WT mice treated with 2.4G2 $F(ab)_2$ prior to Ritm2a treatment did show an attenuated response compared to WT mice that had not received 2.4G2 $F(ab)_2$. Therefore the contrast between depletion studies using 9E9 and $Fc\gamma RIII^{-/-}$ mice and those using 2.4G2 $F(ab)_2$ and $Fc\gamma RIV^{-/-}$ mice remain unexplained and require further investigation.

4.3 De-glycosylation of 9E9 restores B cell depletion in FcγRI$^{-/-}$ mice

It was apparent from FcγR staining (**Figure 4-4** - **Figure 4-6**) that there was a significant decrease in the amount of FcγRIII that could be detected on neutrophils and macrophages when treating with 9E9. This led to speculation that the isotype of 9E9 (hamster IgG1) might have some level of affinity for FcγRIII leading to binding of this receptor through cis reactions on effector cells expressing both FcγRIV and FcγRIII. To test this hypothesis the binding affinity of 9E9 to FcγRI-IV was measured using SPR analysis (**Figure 4-8**).

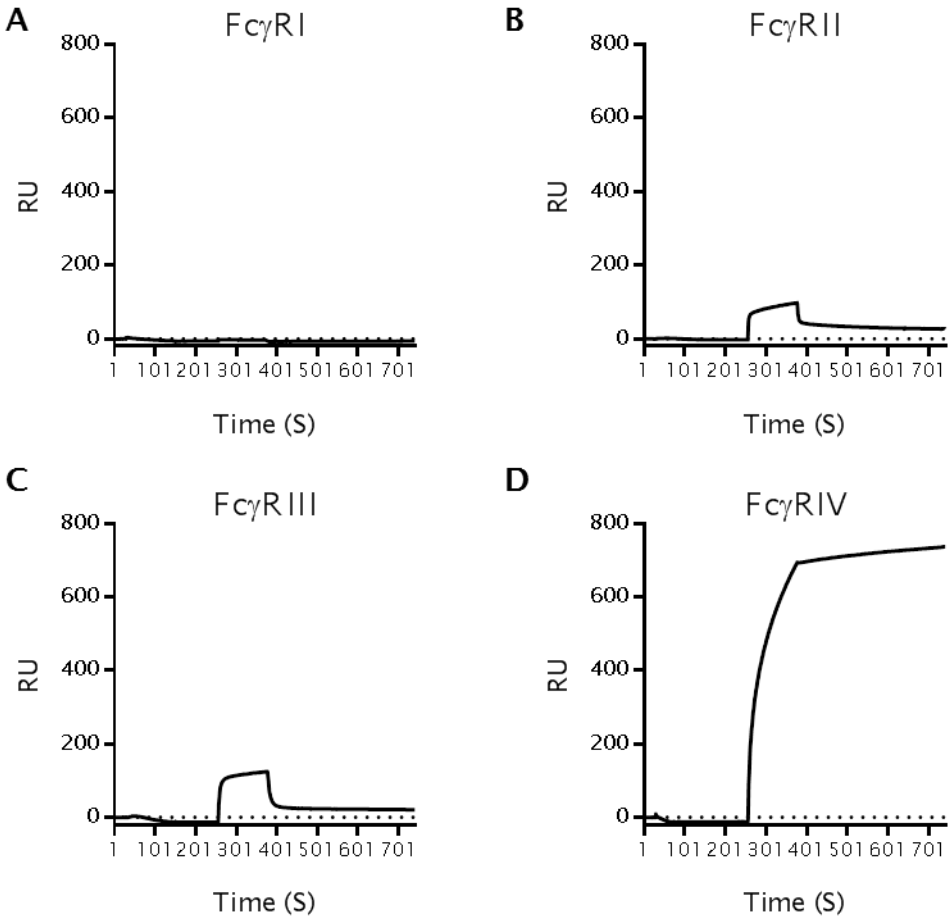

Figure 4-8 SPR analysis of binding affinity for 9E9 to murine FcγR

Soluble FcγR was bound to CM5 sensor chip, indirectly through binding to the His tag of immobilised anti-His antibodies. Following FcγR immobilisation 9E9 (200 nM) was passed through the flow cell, association was measured for 300 seconds and dissociation measured for 600 seconds.

As can be seen from **Figure 4-8** 9E9 was unable to bind to mouse FcγRI however this antibody had low affinity interaction with both FcγRIIb and FcγRIII, similar to that seen with mouse IgG1 antibodies [128, 259]. There was also a strong affinity interaction with FcγRIV which would be expected since this antibody binds to FcγRIV through its Fab regions. The observation that 9E9 had affinity for FcγRIII lent creed to the idea that the role of FcγRIII is perhaps being underplayed in reports using 9E9 to block FcγRIV.

To further investigate this issue a deglycosylated version of 9E9 was produced using the enzyme Peptide -N-Glycosidase F (PNGaseF) which will act to cleave sugar residues from Asn-297. This acts to prevent any Fc:FcγR interactions from occurring. The successful deglycosylation of 9E9 was confirmed using SDS Page gel analysis and the ability of deglycosylated 9E9 to bind to murine FcγRI-IV was assessed using SPR analysis (**Figure 4-9**).

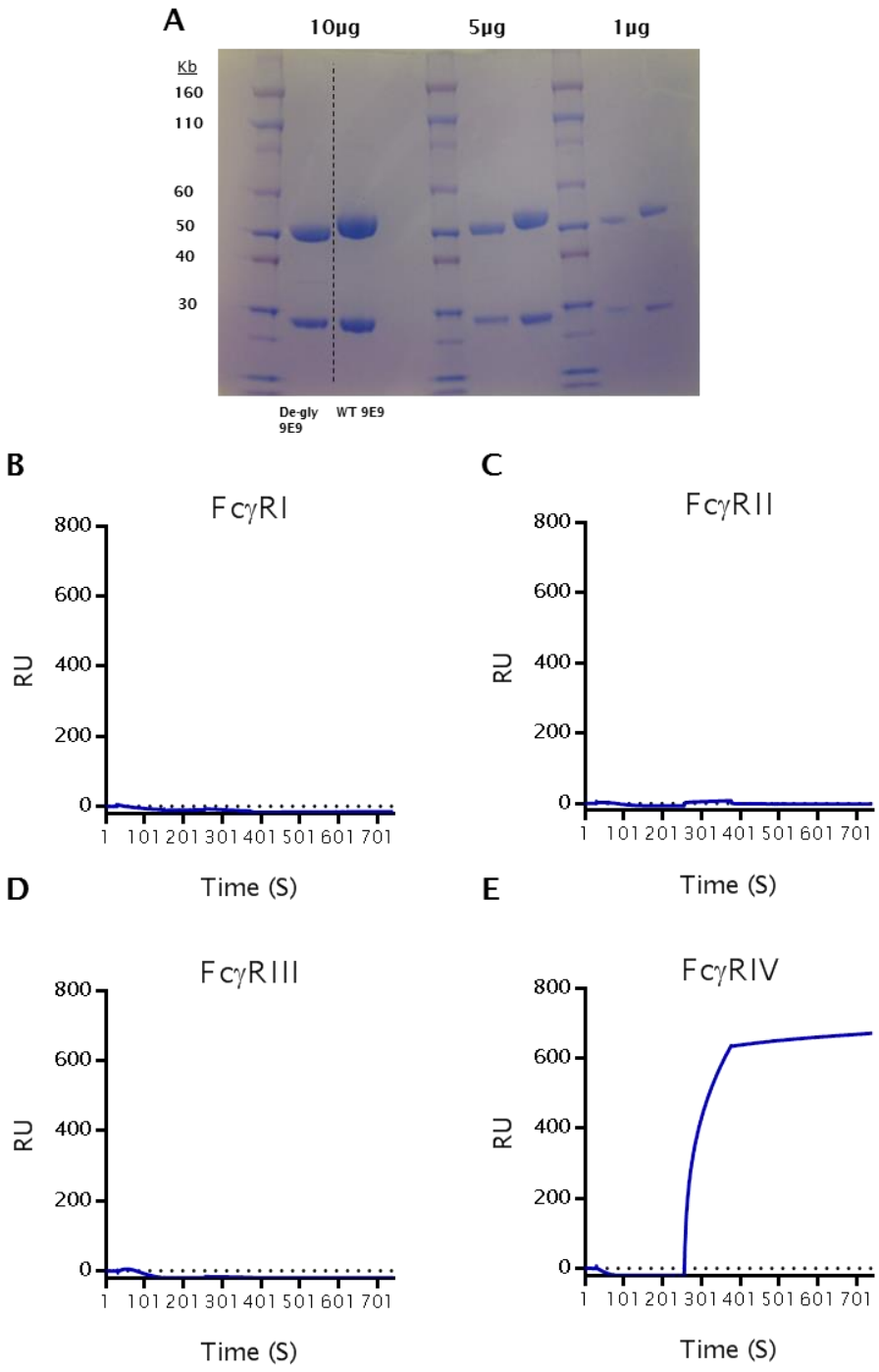

Figure 4-9 SPR analysis of binding affinity for deglycosylated 9E9 to murine FcγR

(**A**) Representative SDS gel. 9E9 or deglycosylated 9E9 (10-1 ng) were denatured and loaded onto a NuPage 10 % Bis Tris gel. Electrophoresis was performed at 220V for ~1 hour. The gel was then subject to staining with coomassie blue dye (**B-E**) Soluble FcγR was bound to CM5 sensor chip, indirectly through binding to the His tag of immobilised anti-His antibodies. Following FcγR immobilisation 9E9 (200 nM) was passed through the flow cell, association was measured for 300 seconds and dissociation measured for 600 seconds.

From **Figure 4-9** it can be seen that loading 5 µg of protein gave the best resolution when analysing deglycosylation status by SDS PAGE. It can be seen that the WT band had a slightly higher apparent molecular weight compared to the deglycosylated 9E9 band, suggesting that deglycosylation was successful. The successful deglycosylation of 9E9 was further shown by the SPR analysis profiles. It can be seen that deglycosylated 9E9 did not bind to mouse FcγRI and that whereas WT 9E9 bound with low affinity to FcγRIIb and FcγRIII the deglycosylated version of 9E9 showed no binding for these receptors. Finally the deglycosylated version of 9E9 retained its strong affinity for mouse FcγRIV. Having demonstrated the successful deglycosylation of 9E9 and its lack of affinity to FcγRIIb and FcγRIII, adoptive transfer assays were performed to investigate the level of B cell depletion in FcγRI$^{-/-}$ mice treated with deglycosylated 9E9 (**Figure 4-10**).

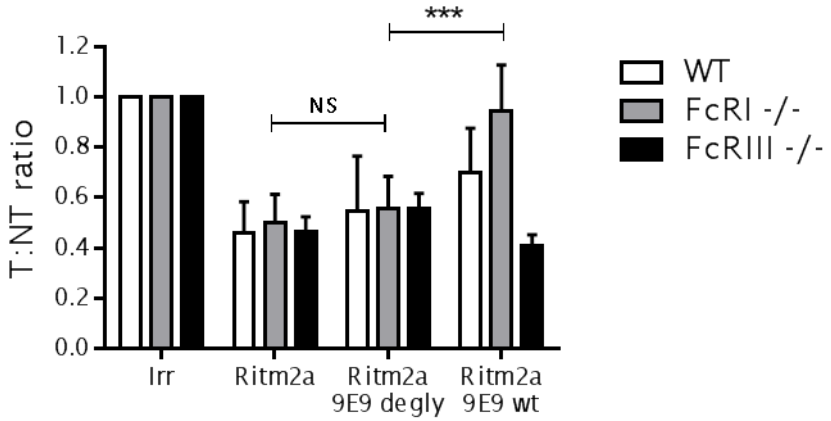

Figure 4-10 Adoptive transfer assays using deglycosylated 9E9 to block FcγRIV

WT, FcγRI$^{-/-}$ or FcγRIII$^{-/-}$ mice on a BALB/c background were subjected to adoptive transfer assays with or without additional blocking of FcγRIV using mAb 9E9 or deglycosylated 9E9. Splenocytes from WT or hCD20 Tg mice were differentially stained with CFSE (WT-0.5 µM, hCD20-5 µM), they were then mixed together 1:1 and injected i.v. into recipient mice (5x10^6 cells). The following morning mice were injected i.p. with 9E9 or deglycosytlated 9E9 (400 µg) this was followed ~3-4 hours later with i.v. injection of Ritm2a (10 µg). The following day spleen was harvested, disassociated and opsonised with anti-CD19-APC (1D3) mAb before being acquired on a flow cytometer. N=5+/- SD. Statistical analysis was performed using two-way ANOVA. NS=not significant.

From **Figure 4-10** it can be seen, as shown in **Figure 4-3**, that blocking with 9E9 resulted in an absence of B cell depletion in FcγRI$^{-/-}$ mice. However, if the deglycosylated version of 9E9 was used then there was a significant improvement in B cell depletion compared to mice treated with WT 9E9. This would suggest that the WT version of 9E9 is additionally blocking FcγRIII through cis reactions. The use of fully glycosylated 9E9 could be overstating the importance of FcγRI and FcγRIV whereas in fact there is functional redundancy between all activatory FcγR. In addition to the results presented in **Figure 4-4** - **Figure 4-6** additional experiments were undertaken investigating the cell surface expression of FcγR in the WT, FcγRI$^{-/-}$ and FcγRIII$^{-/-}$ mice treated with deglycosylated 9E9 (**Figure 4-11**- **Figure 4-13**).

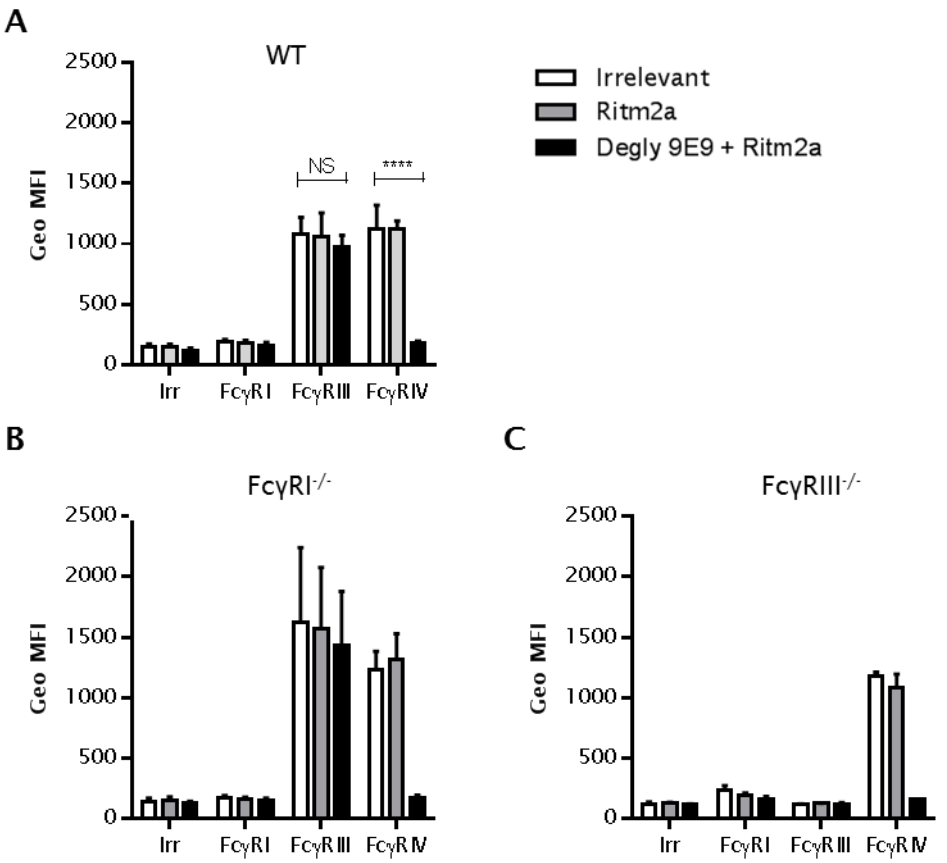

Figure 4-11 Detection of activatory FcγR on neutrophils following deglycosylated 9E9 blocking

BALB/c splenocytes were obtained from the experiment presented in **Figure 4-10**. Splenocytes from WT (**A**), FcγRI$^{-/-}$ (**B**) or FcγRIII$^{-/-}$ (**C**) mice were stained with CD11b, Ly6G and Ly6C to identify neutrophils. Cells were additionally stained with FITC conjugated mAb detecting FcγRI (AT150-9 F(ab)$_2$), FcγRIII (AT154-2 F(ab)$_2$) or FcγRIV (9E9). Samples were stained on ice for 30 minutes. Red blood cells were then lysed and samples were acquired on a flow cytometer. N=6+/- SD. Statistical analysis performed using two-way ANOVA.

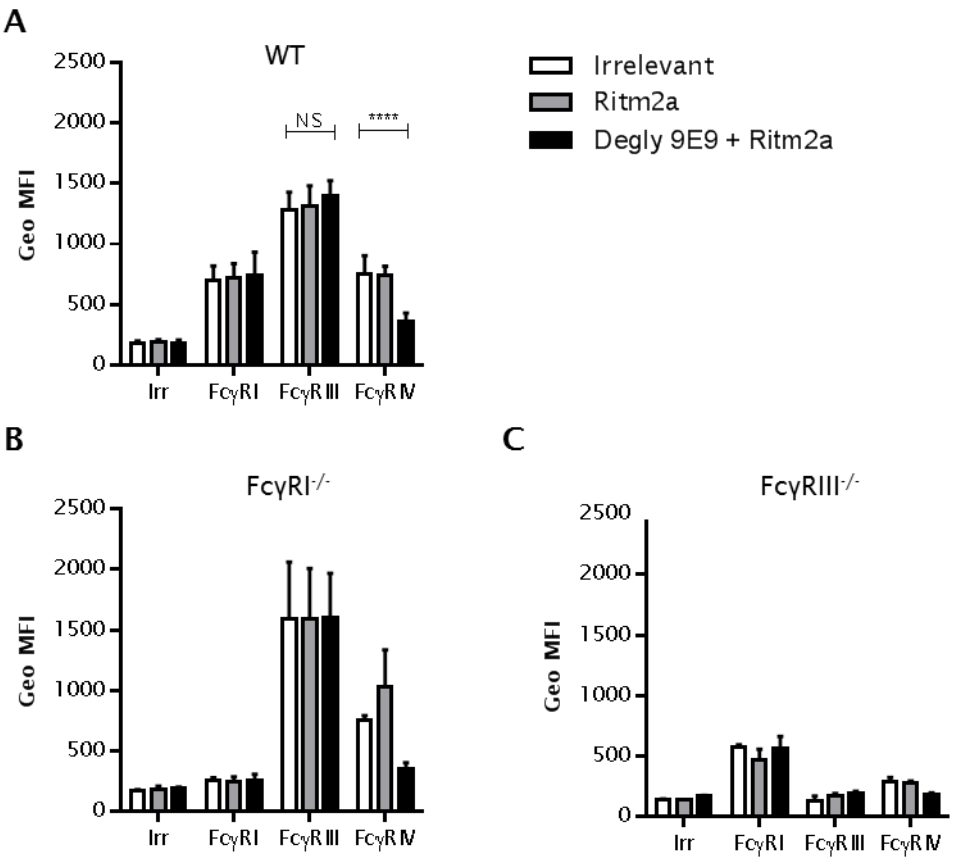

Figure 4-12 Detection of activatory FcγR on monocytes following deglycosylated 9E9 blocking

BALB/c splenocytes were obtained from the experiment presented in **Figure 4-10**. Splenocytes from WT (**A**), FcγRI$^{-/-}$ (**B**) or FcγRIII$^{-/-}$ (**C**) mice were stained with CD11b, Ly6G and Ly6C to identify monocytes. Cells were additionally stained with FITC conjugated mAb detecting FcγRI (AT150-9 F(ab)$_2$), FcγRIII (AT154-2 F(ab)$_2$) or FcγRIV (9E9). Samples were stained on ice for 30 minutes. Red blood cells were then lysed and samples were acquired on a flow cytometer. N=6+/- SD. Statistical analysis performed using two-way ANOVA.

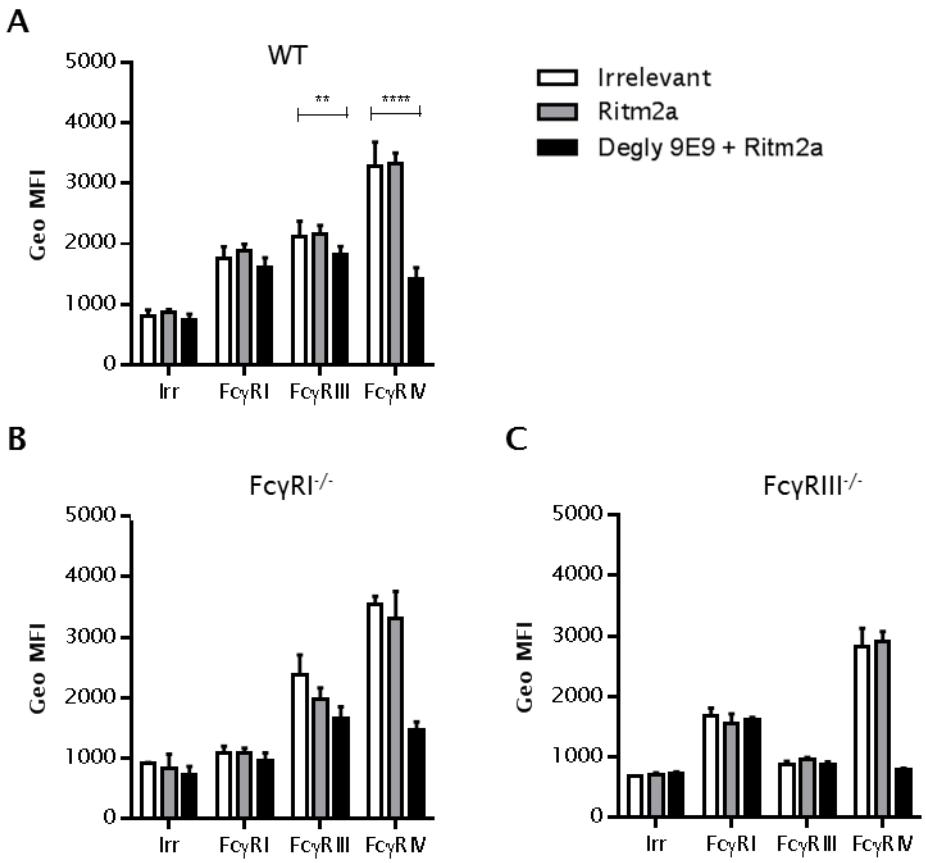

Figure 4-13 Detection of activatory FcγR on macrophages following deglycosylated 9E9 blocking

BALB/c splenocytes were obtained from the experiment presented in **Figure 4-10**. Splenocytes from WT (**A**), FcγRI$^{-/-}$ (**B**) or FcγRIII$^{-/-}$ (**C**) mice were stained with CD11b, and F4/80 to identify macrophages. Cells were additionally stained with FITC conjugated mAb detecting FcγRI (AT150-9 F(ab)$_2$), FcγRIII (AT154-2 F(ab)$_2$) or FcγRIV (9E9). Samples were stained on ice for 30 minutes. Red blood cells were then lysed and samples were acquired on a flow cytometer. N=6+/- SD. Statistical analysis performed using two-way ANOVA.

From **Figure 4-11** - **Figure 4-13** it can be seen that *in vivo* blocking with deglycosylated 9E9 did block detectable levels of FcγRIV to levels seen when using the native form of 9E9. However, in contrast to **Figure 4-4** where there was a significant reduction in the detectable amount of FcγRIII following treatment with 9E9, no such reduction was seen on neutrophils, in mice treated with the deglycosylated version of 9E9. With regards to detection of FcγR on monocytes treated with deglycosylated 9E9 in **Figure 4-12** similar results to those seen when blocking with the native 9E9 antibody were seen

(**Figure 4-5**) whereby treatment with deglycosylated 9E9 had no impact upon the level of FcγRIII but did block FcγRIV. Finally, FcγR staining results on macrophages (**Figure 4-13**) reveal that there is a modest but significant reduction in the amount of FcγRIII which can be detected on the macrophage cell surface following treatment with deglycosylated 9E9. Although significant the reduction of FcγRIII seen on macrophages in response to the native form of 9E9 was more severe than that seen with the deglycosylated form of 9E9. Representative histograms of the data presented in **Figure 4-11** - **Figure 4-13** can be found in (**Appendix 3** - **Appendix 5**).

4.4 Binding to FcγRIV is needed for cis blocking of FcγRIII

It is apparent that the WT form of 9E9 will interact via its Fc with low affinity to FcγRIII. Previous work investigating the isotype specific binding of this antibody [123] found no such interactions. However, this work looked at binding on cells expressing a single FcγR. Since SPR analysis found only low affinity for FcγRIII it would be expected that 9E9 would not exhibit monomeric binding to this receptor and that it is more likely that it will bind only in the form of immune complex. Further supporting this notion is the observation that monocytes which express low levels of FcγRIV did not show any reduction in FcγRIII levels upon treatment with 9E9. The hypothesis that engagement of FcγRIV by 9E9 is a prerequisite to FcγRIII binding was investigated next. Cell surface FcγR staining was carried out in WT and FcγRIV$^{-/-}$ C57BL/6 mice following treatment with 9E9 (**Figure 4-14**). Since 9E9 is unable to bind through its Fab regions in FcγRIV$^{-/-}$ mice the potential for monomeric 9E9 to bind to FcγRIII can be observed.

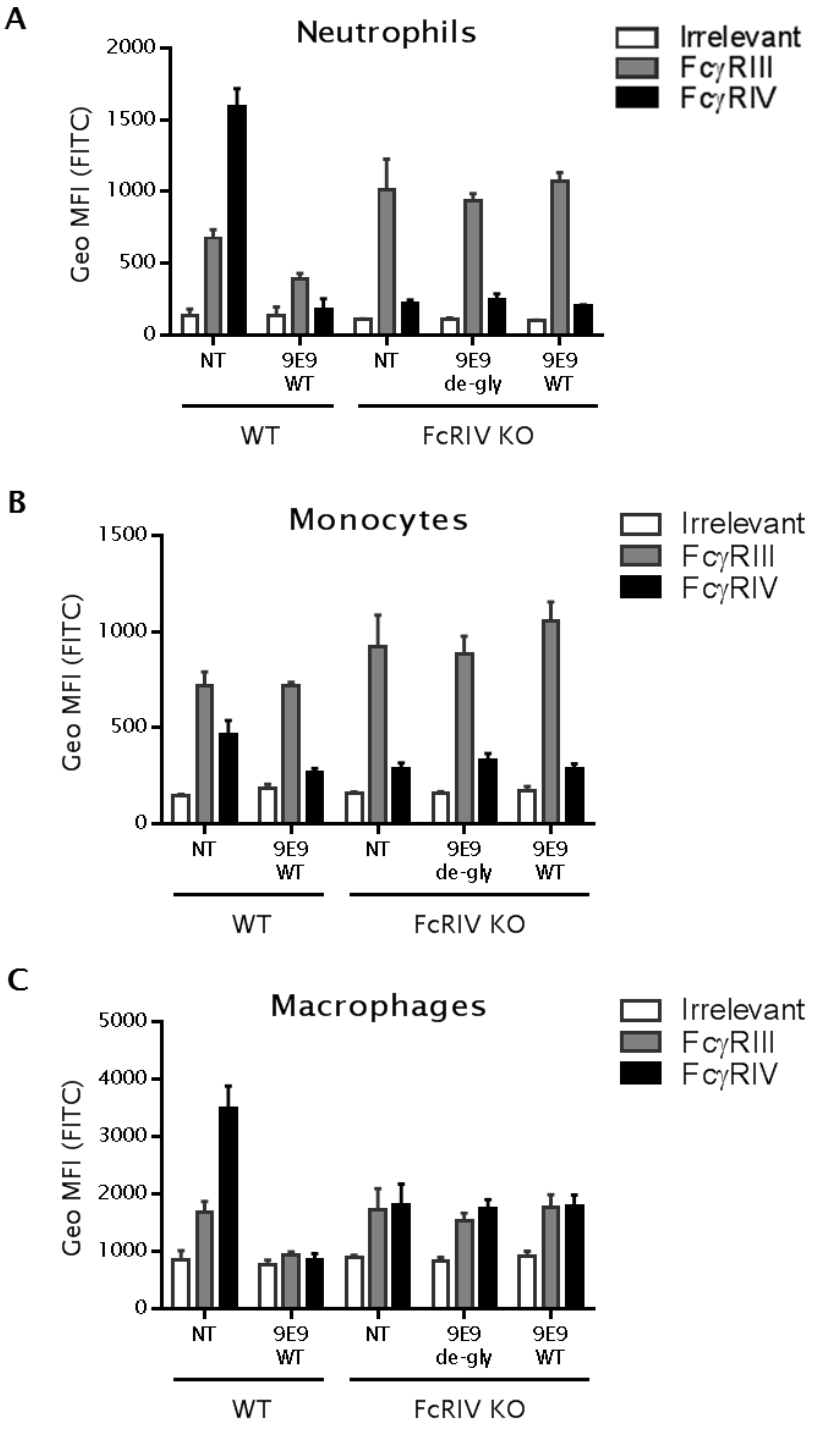

Figure 4-14 Detection of FcγRIII in FcγRIV$^{-/-}$ mice treated with 9E9

C57BL/6, WT or FcγRIV$^{-/-}$ mice were treated i.p. with blocking antibody 9E9 or deglycosylated 9E9 (50 µg). The following morning (16-20 hr) spleen was harvested, dissociated and stained with FITC conjugated antibodies (10 µg/ml) for mouse FcγRIII (AT154-2 F(ab)$_2$) and FcγRIV (9E9). Samples were stained on ice for 30 minutes and then red blood cells were lysed. Samples were acquired on a flow cytometer. (**A**) Neutrophils. (**B**) Monocytes and (**C**) Macrophages. N=3 +/- SD.

From **Figure 4-14** it can be seen that with regards to WT macrophages and neutrophils treated with 9E9 there was an absence in detectable FcγRIV and a reduction in FcγRIII levels as previously demonstrated (**Figure 4-4** - **Figure 4-6**). This was not true for monocytes, which showed a reduction in FcγRIV but no change in FcγRIII upon 9E9 treatment. Following administration of 9E9 to FcγRIV$^{-/-}$ mice it can be seen that as expected there is no detectable FcγRIV, however it can also be seen that there is no 9E9 associated reduction of FcγRIII levels. This was again true for the macrophage population, however background levels of FcγRIV were high. With regards to monocytes there was no change in FcγRIII levels following addition of 9E9 or deglycosylated 9E9.

4.5 Chapter Discussion

In this chapter it has been demonstrated that the specific depletion of one activatory FcγR alone is not sufficient to effect depletion of anti-CD20 mAb mediated depletion using an IgG2a isotype. Furthermore, it has been shown that in agreement with the published literature FcγRI$^{-/-}$ mice treated with 9E9 showed inhibition in B cell depletion following Ritm2a treatment [253]. The binding specificity of 9G8.1, one of the 3 original anti-FcγRIV clones having similar properties to 9E9, had been previously determined using CHO cells which had been stably transfected with individual FcγR, and showed sole specificity for FcγRIV [123]. In this chapter SPR analysis was used to show that 9E9 had low level affinity for murine FcγRIIb and FcγRIII with no detectable affinity for FcγRI. To determine if this was due to Fab or Fc interactions a deglycosylated version of 9E9 which is no longer able to engage FcγR through its Fc region was generated. This deglycosylated version of 9E9 was subjected to SPR analysis and this showed retention of FcγRIV specificity but an absence in detectable affinity for FcγRIIb and FcγRIII. Subsequent adoptive transfer studies demonstrated that using deglycosylated 9E9 to block FcγRIV in an FcγRI$^{-/-}$ mouse restored the ability for B cells to be depleted in response to Ritm2a. A schematic representation of the proposed mechanism by which 9E9 cross-blocks FcγRIII is shown in **Figure 4-15**.

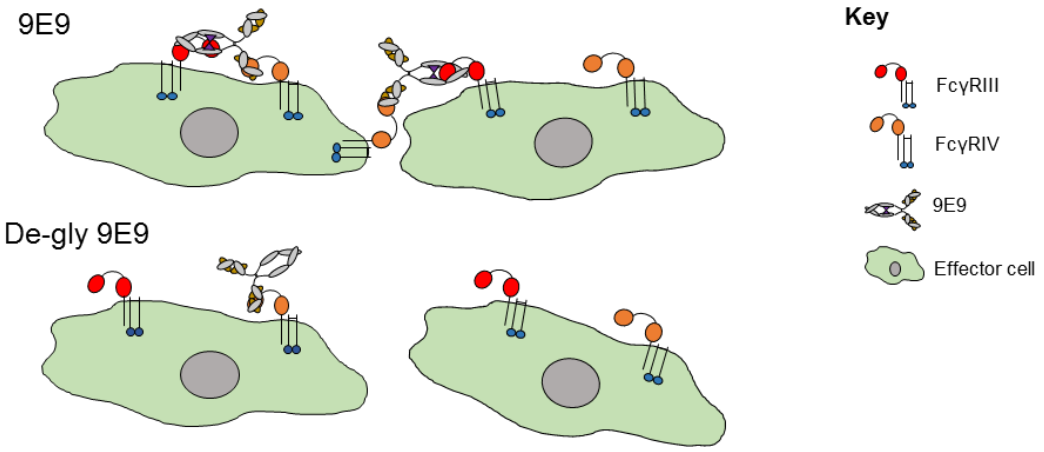

Figure 4-15 Schematic of the proposed mechanism by which 9E9 blocks FcγRIII function

WT 9E9 will bind to FcγRIV on the effector cell. This will cause clustering of FcγRIV on the cell membrane which will allow sufficient avidity for Fc regions to bind to and block FcγRIII, through cis or trans reactions, on the same or adjacent effector cell.

The original characterisation of 9G8.1 may not have detected this cross blocking effect as antibody would have been presented to FcγR in a monomeric fashion and so only high affinity Fc interactions would be observed. On myeloid effector cells which express multiple FcγR, such as macrophages and neutrophils antibody bound to FcγRIV would cluster and allow sufficient avidity to bind to and block FcγRIII, and although not investigated here, probably mouse FcγRIIb. Since in the FcγRI$^{-/-}$ mouse treated with 9E9 a complete block in B cell depletion was seen, this would again suggest that NK cells, which only express FcγRIII are not the dominant population responsible for IgG2a mediated depletion in the mouse. Again the fact that monocyte FcγRIII levels were not impacted upon by 9E9 blocking also suggests that this population may not be critical to effective IgG2a mediated depletion. How these responses would differ upon mouse IgG1 mediated depletion would be an interesting avenue of research. It has been shown that mouse IgG1 antibodies have no affinity for activatory FcγRI and FcγRIV but can still mediate ADCC through FcγRIII. This mediation of ADCC is not as impressive as that of IgG2a but still this demonstrates that FcγRIII is capable of facilitating ADCC and so it is perhaps no surprise that redundancy is seen between all activatory FcγR. Work by Minard-Colin *et al* assessed survival of mice in a B cell lymphoma model and found that at high tumour doses FcγRIV alone was not sufficient to confer significant survival and that either FcγRI or FcγRIII in combination with FcγRIV

was needed [108]. The work presented here suggests functional redundancy between all activatory FcγR receptors since FcγRI$^{-/-}$ mice treated with WT 9E9 were the only ones to show a complete block in B cell depletion. SPR analysis revealed that 9E9 has no affinity for FcγRI and so is incapable of interacting with it. Therefore in the WT mouse treated with 9E9 depletion can take place solely through FcγRI since 9E9 does not interact with it.

In our studies the amount of 9E9 needed to block FcγRIV detection was found to be very low, 12 μg was sufficient to block detection of FcγRIV ~24 hours after i.p. administration. This was a surprisingly low dose as the established literature typically uses 200- 400 μg to block FcγRIV [135, 253]. However, these results may not translate into applicable doses required to block immune complex binding since titration experiments seen in **Figure 4-2** used 9E9-FITC as the detection antibody whereas FITC labelled immune complex would have been a more physiologically relevant model of blocking FcγRIV function. Therefore, future experiments could look to titrate the amount of immune complex binding that can be seen following 9E9 blocking of FcγRIV.

Analysis of deglycosylated 9E9 by SPR revealed that there was low affinity binding to FcγRIIb and FcγRIII. This chapter was focussed on the cross-blocking of FcγRIII by the Fc of 9E9, however blocking of FcγRIIb is also a likely scenario and may go some way to explaining why FcγRIII$^{-/-}$ mice displayed good levels of B cell depletion. It may have been that in the absence of FcγRIII 9E9 was binding to FcγRIIb through cis interactions thus blocking this receptor and increasing the A:I ratio, allowing for B cell depletion. Similar, work by Kurlander used mAb against human Fc receptor antigens to block FcγR and then investigate the binding of labelled hIgG1 antibody. They show that pre-treatment with blocking antibody resulted in the absence of hIgG1 binding and that this was due to Fc blocking of FcγR [260]. Indirect evidence for cis over trans binding comes from the fact that data is obtained using flow cytometry where only single cells will be processed. Although, in reality the possibility of trans reactions taking place cannot be discounted and it is likely that both reactions contribute to some extent.

Additional experiments looked to block multiple FcγR using FcγRIV$^{-/-}$ mice in combination with the mAb 2.4G2. It was found that when FcγRIV$^{-/-}$ mice were treated with 2.4G2 F(ab)$_2$ and then with Ritm2a there was a complete block in B

cell depletion. These results are in contrast to adoptive transfer experiments shown in **Figure 4-3** where FcγRIIb$^{-/-}$ and 9E9 treated mice show good levels of B cell depletion in response to Ritm2a. In both of these cases it would be predicted that only FcγRI is being displayed by effector cells. A simple explanation would have been that whole IgG contaminants of 2.4G2 are binding to and blocking FcγRI, however, HPLC analysis showed 2.4G2 F(ab)$_2$ to be pure. Another hypothesis was that 2.4G2 F(ab)$_2$ is binding to FcγRIIb on the CFSE labelled targets which is preventing efficient opsonisation by Ritm2a. To test this hypothesis FcγRIIb$^{-/-}$ target and non-target cells were transferred into FcγRIV$^{-/-}$ mice. Mice were then treated with 2.4G2 F(ab)$_2$ and Ritm2a. These mice again showed a block in B cell depleting capacity (**Figure 4-7b**). However, very poor depletion of B cells was seen in the FcγRIV$^{-/-}$ mice that were treated in the absence of 2.4G2 F(ab)$_2$. The mice used in these experiments were on a C57BL/6 and not a BALB/c background and were elderly (~10 months old). These are factors which may have influenced these experiments.

In conclusion, it would appear that at least in the mouse there is functional redundancy between all activatory FcγR and that previous studies may have under-appreciated the role that FcγRIII plays *in vivo*. Furthermore, this highlights the potential issues that isotype interactions can cause when antibodies bind to cells with multiple FcγR.

Chapter 5: Impact of apoptosis on anti-CD20 therapy

5.1 Introduction

Circumvention of the apoptotic machinery has long been associated with tumorigenesis [2, 3]. The anti-apoptotic protein Bcl-2 was first implicated in such tumorigenesis through studies relating to the t14;18 translocation seen in FL [59]. However, when this translocation was mimicked in the Eμ-Bcl-2 mouse the time to tumorigenesis was lengthy and many of the resulting tumours were not follicular in nature [261]. What was clear is that for a malignancy to arise the dysregulation of other oncogenes was necessary, in the case of Eμ-Bcl-2 mice the dysregulation of the oncogene c-MYC was most common [261, 262]. Wider dysregulation of Bcl-2 throughout the haematopoietic system did result in FL like tumours. This was achieved through the generation of Vav Bcl-2 mice. In this case Bcl-2 was overexpressed throughout the haematopoietic compartment and the formation of splenic tumours was largely attributed to a dysfunctional T cell compartment aiding in B cell mutagenesis, presumably due to germinal centre reaction interactions [202].

Work by Beers *et al* produced preliminary data suggesting that dysregulated apoptosis such as that seen in the Vav Bcl-2 mouse detrimentally impacts upon depletion of B cells in response to anti-CD20 antibodies. In these experiments isolated hCD20 Tg x Vav Bcl-2 B cells were adoptively transferred into WT recipients, to determine if apoptosis resistant B cells could be depleted in response to anti-CD20 therapy. These hCD20 x Vav Bcl-2 B cells were effectively depleted in wild type mice and so apoptosis was excluded as an important effector mechanism for B cell depletion by anti-CD20 antibodies [122]. However, when hCD20 x Vav Bcl-2 mice were directly treated with anti-CD20 antibodies they were found to be unable to effectively deplete B cells. The increased cellularity seen in the Vav Bcl-2 mouse might have explained these results as it may have been that higher doses of therapeutic antibody were needed. However, doses 20 times lower than those administered to Vav Bcl-2 mice still effectively depleted B cells in the WT mouse (unpublished data).

Further evidence implicating the microenvironment of the Vav Bcl-2 mouse as being unable to facilitate mAb mediated depletion came from adoptive transfer studies whereby hCD20 target B cells were transferred into the Vav Bcl-2 recipient. Again, mice were unable to effectively deplete B cells when given therapeutic anti-CD20 antibody (unpublished data). These studies were the impetus for investigations into whether different rates of apoptosis will impact on B cell depletion in response to anti-CD20 antibodies and in what way reduced levels of systemic apoptosis, like those seen in the Vav Bcl-2 mouse will modulate FcγR expressing effector cells.

The studies in chapter 3 have placed clodronate sensitive FcγR expressing macrophages as being the dominant effector cell in response to anti-CD20 therapy. As described in Chapter 1 macrophages have high levels of plasticity and can be manipulated by a multitude of extracellular factors. We were therefore interested in the ability of apoptotic materials to polarise macrophages and whether dysregulated apoptosis in other mouse models was associated with a diminished ability to deplete anti-CD20 mAb opsonised B cells.

5.2 Apoptosis resistant mice show abrogated B cell depletion

Preliminary work by Beers *et al* showed the Vav Bcl-2 mouse to be inefficient at B cell depletion with Ritm2a. Subsequent analysis revealed that this was not due to an inherent defect in the B cell target but rather that there was something wrong with the microenvironment of the mouse. To investigate whether apoptosis dysregulation might affect antibody therapy, 3 model systems were chosen. Extremely low levels of systemic apoptosis were represented by Vav Bcl-2 mice whereas very high levels of B cell specific apoptosis were represented by Eμ Myc mice. WT mice were used to represent baseline levels of apoptosis. To verify that these models do have alternate levels of cell death an Annexin V/PI assay to determine cell viability was used. This assay detects both apoptosis and secondary necrosis as illustrated in **Figure 5-1**. Annexin V positive events reflect the state of cells which have increased expression of PS on their cell surface and so have engaged the apoptotic program but are not necrotic. In contrast, Annexin V and PI positive events reflect late stage apoptotic/necrotic events, with PI staining indicating that the cell membrane has lost its integrity.

In order to confirm the dysregulated cell death levels displayed by Vav Bcl-2 or Eμ Myc mice, splenocytes were harvested from mice, disassociated and cultured in six well tissue culture plates for three days (73 °C, 10 % CO_2). Each day the level of cell death was assessed using the Annexin V/PI assay. From **Figure 5-1b** it can be seen that splenocytes from Eμ Myc mice lost cell viability rapidly. In contrast, splenocytes from Vav Bcl-2 mice had high levels of viability following 3 days culture, confirming their apoptosis resistance. WT mice showed an intermediate level of cell death whereby the majority of cells had lost viability by Day 3. These results confirmed the apoptosis dysregulated status of the mice.

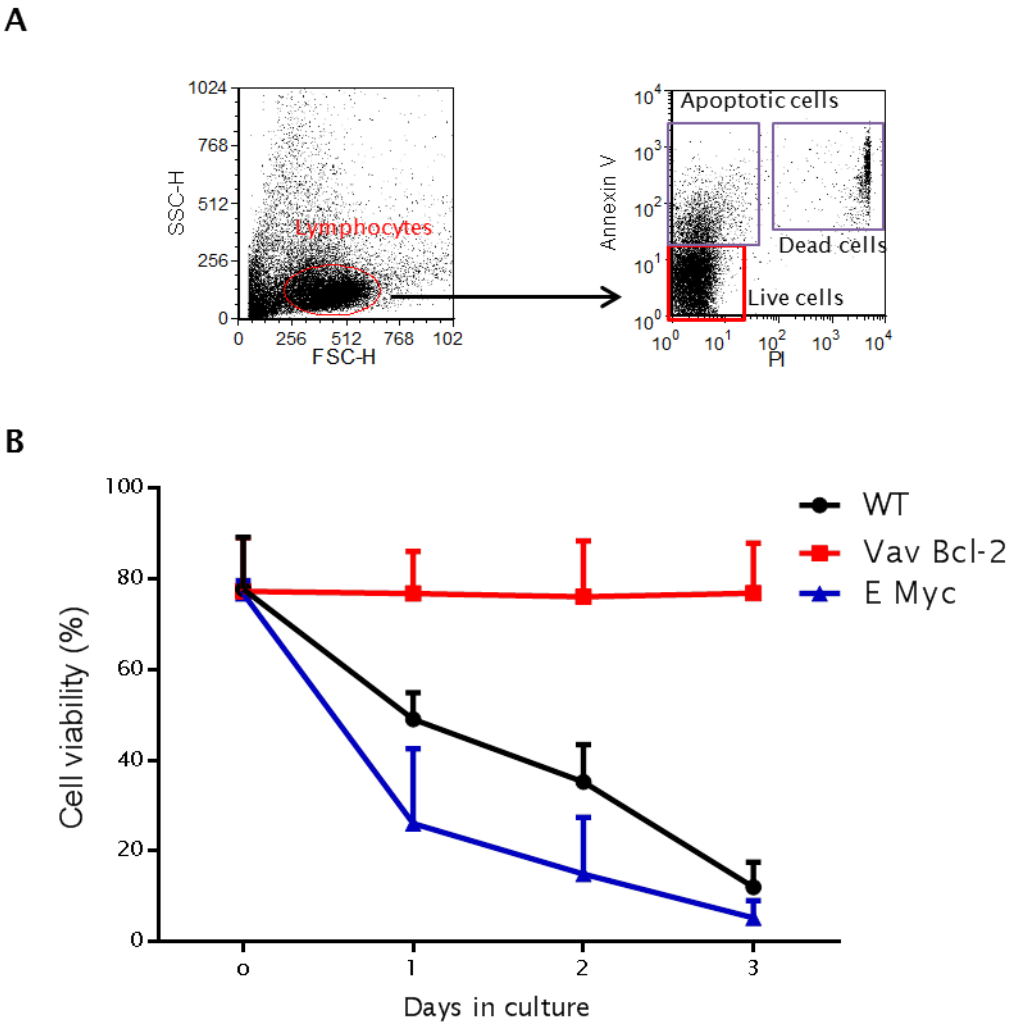

Figure 5-1 Annexin V/PI analysis to detect cell death

(**A**) Representative flow cytometry plots showing the FSC and SSC and the Annexin V/PI status of splenocytes acquired on the flow cytometer. Live cells are Annexin V and PI negative whereas early apoptotic and dead cells are Annexin V positive/PI negative and Annexin V positive/ PI positive respectively. (**B**) Splenocytes from apoptosis dysregulated mice were placed into six well tissue culture plates ($1x10^7$ cells/ml) and samples were incubated over three days at 37 °C (10 % CO_2). Each day cells were stained with Annexin V (1.6 µg/ml) and PI (9 µg/ml) before being acquired using a FACS calibre flow cytometer. Viability was measured as the percentage of cells that were both Annexin V and PI negative (red box). N=3 +/- SD.

After confirming the dysregulated state of cell death within Vav Bcl-2 and Eµ Myc mice the effect of dysregulated apoptosis on antibody therapy was investigated. Adoptive transfer assays were used to compare the efficiency of B cell depletion in WT, Vav Bcl-2 and Eµ Myc mice. Mice were injected with non-target WT and target hCD20 splenocytes stained with CFSE (WT- 0.5 µM or

hCD20- 5 μM, respectively) at a 1:1 ratio. 24 hours later mice were treated with either irrelevant (WR17) or Ritm2a (10 μg/ml) antibody. 24 hours following antibody infusion splenocytes were harvested and stained with CD19-APC (1D3). Samples were then acquired on a FACS calibre flow cytometer. The T:nT ratio was determined by dividing the percentage of hCD20 B cells by WT B cells. To better compare data sets from different experiments data was normalised. This was done by dividing ritm2a treated T:nT values by the irrelevant T:nT values (**Figure 5-2**).

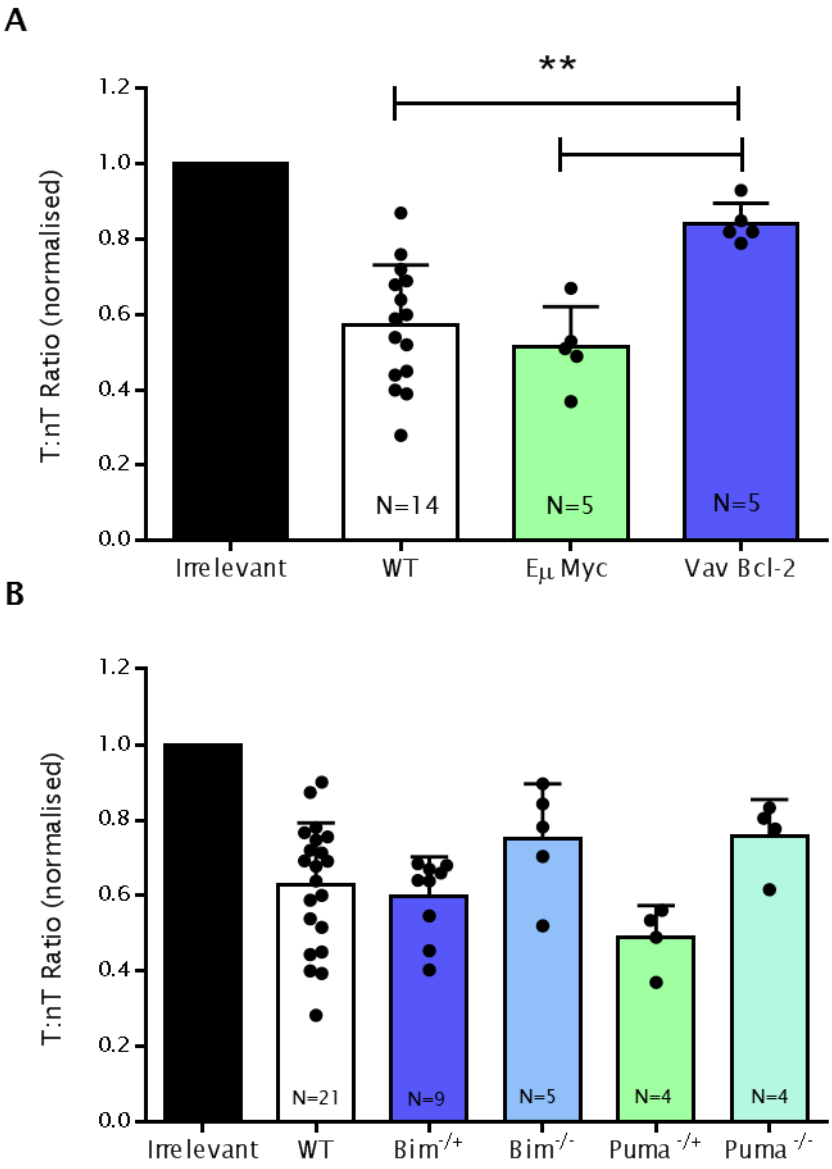

Figure 5-2: B cell depletion in apoptosis dysregulated mice

(**A**) WT, Vav Bcl-2 and Eμ Myc mice were injected i.v. ($5x10^6$ cells) with CFSE stained splenocytes (WT-0.5 μM, hCD20 5 μM). The following day mice were treated with irrelevant or Ritm2a mAb (10 μg). Splenocytes were harvested 24 hours post treatment with therapeutic mAb, splenocytes were stained with (2.5 μl) CD19-APC (1D3) and acquired on a FACS calibre flow cytometer. (**B**) Adoptive transfer experiments using Bim and Puma $^{-/-}$ and $^{-/+}$ mice performed as described in **A**. Statistical analysis performed using one-way ANOVA.

As can be seen in **Figure 5-2** Vav Bcl-2 mice showed significantly (P=<0.005) lower levels of B cell depletion compared to both the WT and Eμ Myc mice. It was found that Eμ Myc mice showed a trend of being more efficient than the

WT mouse at depleting B cells although this did not reach significance. Bim and Puma homozygous and heterozygous mice were examined in their ability to deplete B cells, since these mice will display intermediate levels of apoptosis. There was a trend for the homozygous knock out mice to have attenuated B cell depletion although this did not reach significance. These adoptive transfer experiments appear to show that low levels of systemic apoptosis act to disrupt anti-CD20 mAb mediated B cell depletion capacity. The reverse situation where high levels of apoptosis were seen in the Eμ Myc mouse, made no significant difference to B cell depletion.

One possible explanation for this observed B cell depletion defect in the Vav Bcl-2 mouse is that these mice have more lymphocyte cells in total. This increased cellularity displayed by the Vav Bcl-2 mouse would allow for enhanced antigenic modulation which would clear antibody from the system faster and so diminish B cell depletion capacity. To test this hypothesis hCD20 Tg mice were crossed onto the Vav Bcl-2 mouse and long term B cell depletions were performed using either the type I antibodies which undergo pronounced antigenic modulation or type II antibodies which do not undergo antigenic modulation to the same extent. Either hCD20 or hCD20 x Vav Bcl-2 mice were treated with Ritm2a (type I) or OBZm2a (type II) (250 μg) and sequentially bled over 56 days (**Figure 5-3**).

From **Figure 5-3** it can be seen that even with type II antibodies which do not undergo antigenic modulation there is still an inability to deplete B cells. hCD20 Tg mice were able to deplete B cells in response to both Ritm2a and OBZm2a with OBZm2a providing substantially more prolonged B cell depletion compared to Ritm2a, as seen in chapter 3. However, hCD20 x Vav Bcl-2 mice were unable to deplete B cells when given either type I or type II antibody suggesting that the B cell depletion defect seen is not due to enhanced levels of antigenic modulation.

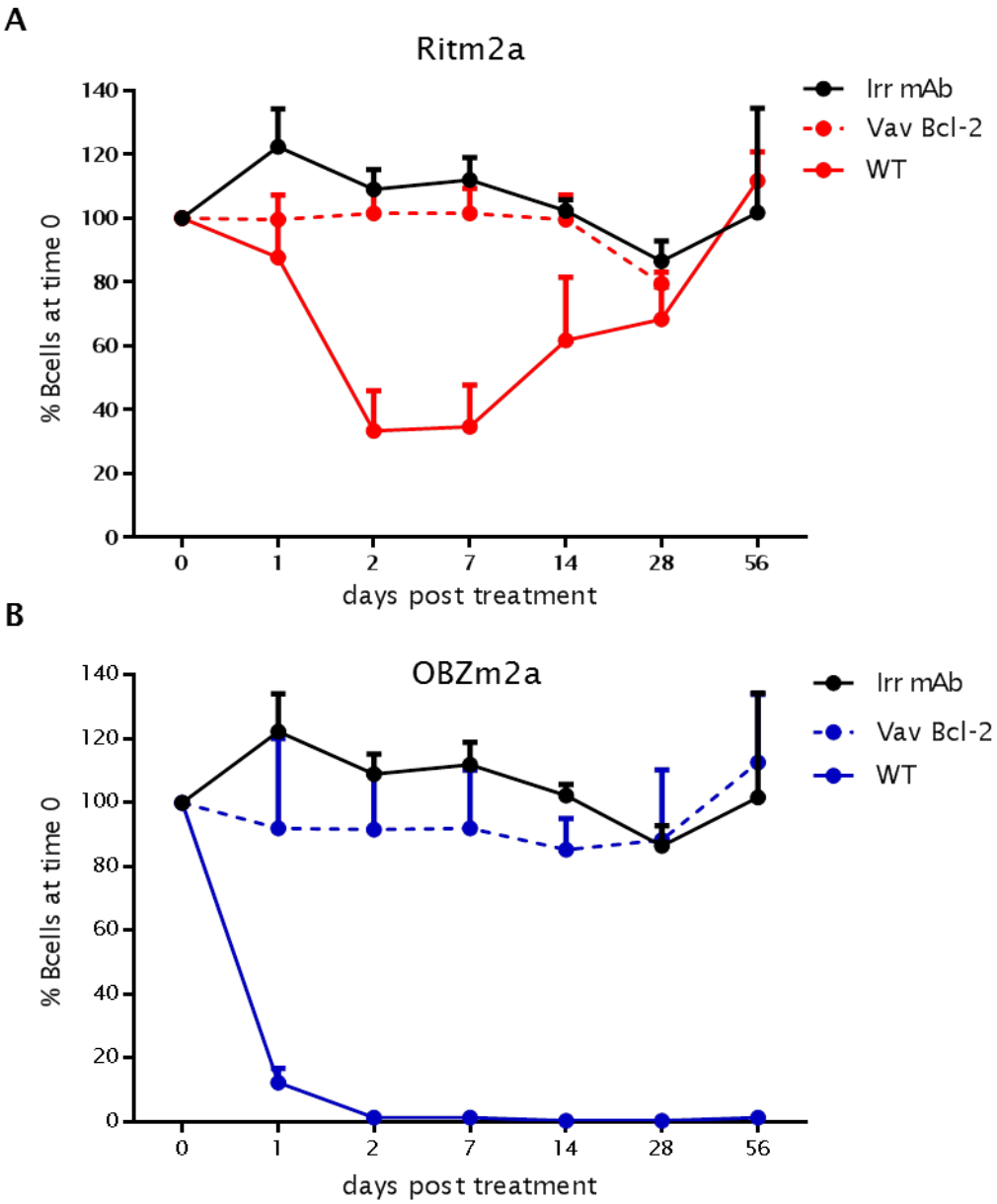

Figure 5-3 Long term B cell depletion studies in hCD20 x Vav Bcl-2 mice

C57BL/6 hCD20 Tg mice were crossed with C57BL/6 Vav Bcl-2 mice, Long term B cell depletions were performed over 56 days following i.v. injection of Ritm2a (**A**) or OBZm2a (**B**) (250 µg/ml). Peripheral blood was collected through tail vein puncture on days -1, 0, 1, 2, 7, 14, 28 and 56 post therapeutic mAb injection. Blood was stained on ice for 30 minutes with B220-PerCP and CD19 (1 µl). Red blood cells were lysed and samples were acquired on a flow cytometer. N=3+/- SD.

To more directly assess whether antigenic modulation could help explain the B cell depleting defect seen in the Vav Bcl-2 mouse, antigenic modulation assays were performed using isolated B cells from either hCD20 or hCD20 x Vav Bcl-2 Tg mice. B cells were isolated from splenocytes using a Miltenyi B cell isolation kit. Cells were then opsonised with either type I (Ritm2a) or type II (OBZm2a) antibody conjugated to Alexa 488, and incubated for 0.5-4 hours. Samples were then divided in 2, and half stained with an anti-Alexa 488 antibody. This antibody would bind to any anti-CD20 antibody still on the cell surface and quench its fluorescence. Therefore samples which have high levels of quenching will have high levels of primary antibody on the cell surface. In contrast, cells which are undergoing antigenic modulation will internalise antibody from the cell surface and will not be quenched by the anti-Alexa 488 mAb.

From **Figure 5-4** it can be seen that when either hCD20 or hCD20 x Vav Bcl-2 murine B cells were treated with Ritm2a the percentage of cell surface quenched antibody decreased over time indicating modulation from the cell surface. For appreciable levels of internalisation to occur B cells and antibody needed to be incubated together for 2 hours. Importantly, there was no difference between hCD20 B cells and hCD20 x Vav Bcl-2 B cells in terms of the amount of quenching that occurred with type I antibody. With regards to type II antibodies, for both hCD20 and hCD20 x Vav Bcl-2 B cells the amount of quenching that occurred over the 4 hour period remained consistent at around 80 percent and this suggests that little to no antigenic modulation occurred in response to opsonisation with the Type II antibody OBZm2a on both hCD20 and hCD20 x Vav Bcl-2 B cells. Together, this confirms that enhanced levels of antigenic modulation are not responsible for the reduced levels of B cell depletion seen in apoptosis resistant Vav Bcl-2 mice. From published data [122, 135] and the work presented in chapter 3 we know that macrophage mediated ADCP is likely the most important effector mechanism in the mouse therefore the ability of macrophages from either Vav Bcl-2 or Eμ Myc mice were assessed for their ability to orchestrate ADCP.

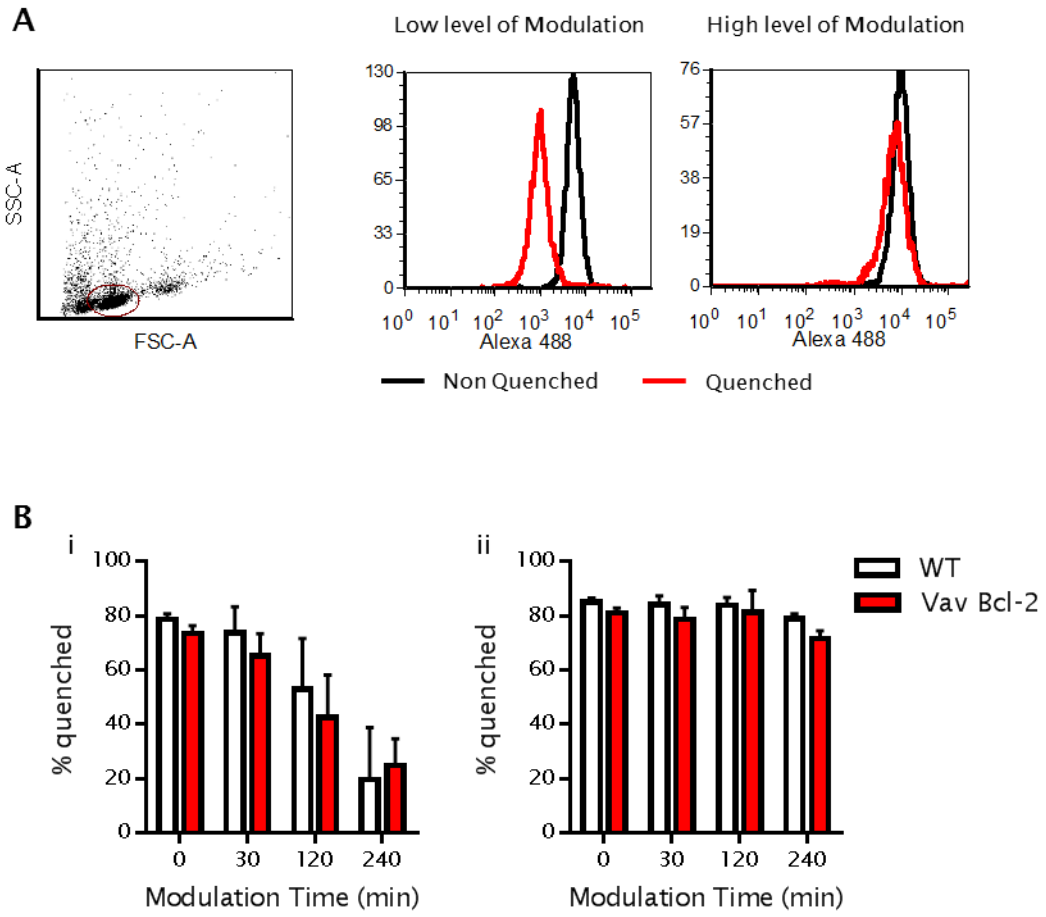

Figure 5-4 Quenching assay to look at the levels of antigenic modulation by WT and Vav Bcl-2 B cells

(**A**) Representative flow cytometry plots showing the typical FSC, SCC and Alexa 488 fluorescence, histograms were gated upon the circled B cell population. (**B**) C57BL/6, hCD20 or Vav Bcl-2 x hCD20 Tg B cells were opsonised with either Ritm2a (i) or OBZm2a (ii) (10 µg/ml) conjugated to Alexa 488. Cells were allowed to modulate for between 30 minutes to 4 hours at 37 °C (5 % CO_2). Samples were split and anti-Alexa 488 antibody (2 µl) was added to quench any remaining Alexa 488 fluorescence. Samples were stained on ice for 30 minutes. Samples were then washed in FACS wash and acquired on a flow cytometer. N=3 +/- SD.

5.3 Apoptosis resistant BMDMs are able to be polarised and can effectively phagocytose B cell targets

Thus far a general inability to deplete mAb opsonised B cells has been observed in apoptosis dysregulated mice. Studies by Beers *et al* have shown that abrogated B cell depletion in the Vav Bcl-2 mouse is not due to increased number of B cells and that there is not issue with the B cells as a target since they can be depleted in the wild type mouse when adoptively transferred [122]. It was hypothesised that increased cellularity would translate into increased levels of antigenic modulation. This was found not to be the case, since non modulating type II antibodies were again unable to deplete B cells in the Vav Bcl-2 mouse. Additionally, hCD20 and hCD20 x Vav Bcl-2 B cells were shown to undergo antigenic modulation to the same extent. Therefore, since macrophages and FcγR mechanisms have been shown to be key in the depletion of B cells the ability of WT, Vav Bcl-2 and Eμ Myc BMDMs to phagocytose B cell targets and to be polarised to either an M1 or M2 phenotype was investigated.

The ability of *in vitro* cultured BMDMs to phagocytose Ritm2a opsonised hCD20 target B cells was first investigated. This was done using BMDMs derived from C57BL/6 WT, Vav Bcl-2 or Eμ Myc mice that had typically been cultured for 7-11 days *in vitro*. Target hCD20 B cells were isolated from splenocytes, stained with CFSE (5 μM) and then opsonised with either irrelevant (WR17) or Ritm2a (10 μg/ml) antibodies. These target B cells were then incubated with effector BMDM cells for 30 minutes at 37 °C (5 % CO_2). Following co-culture samples were stained with F4/80-APC, to highlight the macrophage population and acquired on a FACS Calibre™ flow cytometer. Phagocytosis was measured as the percentage of $F4/80^+$, $CFSE^+$ events within the total number of $F4/80^+$ events. From **Figure 5-5** it can be seen that ~40 % of hCD20 B cells opsonised with Ritm2a were engulfed by effector BMDMs, whereas, hCD20 B cells opsonised with irrelevant antibody showed only 3 % phagocytosis. Importantly both Vav Bcl-2 and Eμ Myc BMDMs displayed equivalent levels of phagocytosis to that of wild type BMDMs.

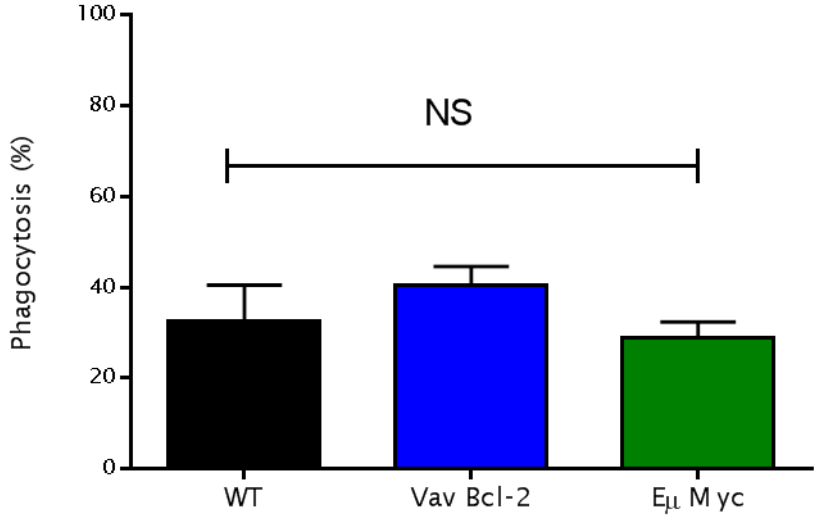

Figure 5-5 ADCP comparison between BMDM derived from different apoptosis dysregulated mice

Phagocytosis assays were performed using either WT, Vav Bcl-2 or Eμ Myc BMDMs. C57BL/6 hCD20 target B cells were stained with CFSE (5 μM) and then opsonised with either anti-hCD20 (Ritm2a) or irrelevant m2a (WR17) antibody (10 μg/ml). Opsonised target B cells were then co-cultured with effector BMDM (30 min, 37°c). Samples were then stained with F4/80-APC for 20 minutes at RT. Samples were washed in FACS wash and data was acquired on a FACS Calibre™ flow cytometer. N=3+/-SD. Statistical analysis performed using one-way ANOVA. NS=not significant.

Since equivalent levels of phagocytosis were seen between BMDM derived from apoptosis dysregulated and WT mice (**Figure 5-5**) it suggests that there is no inherent defect in the ability of macrophages from Vav Bcl-2 mice to phagocytose opsonised B cells. Since macrophage polarisation can dramatically affect the rate at which phagocytosis is undertaken it was decided that apoptosis dysregulated BMDMs from each of these mice would be tested for their ability to become M1 or M2 polarised. As described in chapter 1, macrophages have high levels of plasticity and can be polarised to a classically activated pro-inflammatory phenotype by IFNγ and LPS or to an anti-inflammatory alternatively activated macrophage by cytokines such as IL-4 and IL-13. To investigate the possibility that Vav Bcl-2 macrophages are impaired in their ability to become skewed to an M1 or M2 phenotype BMDMs were grown for 7 days and then skewed using cytokines as described in materials and methods (**2.6**). **Figure 5-6** highlights morphological changes in response to these polarising reagents. Initially, to determine suitable candidates for

skewing, WT BMDMs were isolated and cultured in complete media containing 20 % L929 for 7 days, on day 7 samples were stimulated with either M1 or M2 skewing reagents. Samples were incubated with these reagents for 24 hours before being observed using an Olympus CKX41 microscope. It can be seen that M1 polarising reagents result in cells that are slightly larger and have a number of dendrite-like projections. It also appears that there were a number of small rounder cells dispersed throughout. In contrast M2 and WT BMDMs appeared to be elongated and to not have as many projections.

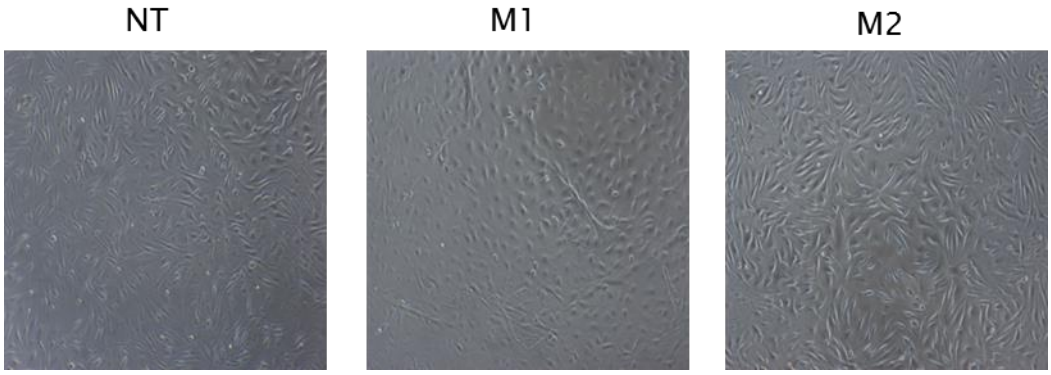

Figure 5-6: Micrographs of WT BMDMs polarised to an M1 or M2 phenotype

Representative micrographs of BMDM from a C57BL/6 mouse following 7 days culture. BMDMs were stimulated with either LPS (100 ng/ml) & IFNγ (2 ng/ml) (M1) or IL-4 (10 ng/ml) & IL-13 (10 ng/ml) (M2). Samples were cultured for 24 hours at 37 °C (5 % CO_2). Samples were analysed using an Olympus CKX41 microscope (10x magnification).

Having established these conditions and to test whether Vav Bcl-2 mice have an inherent defect in their ability to become polarised to either an M1 or M2 phenotype, BMDMs from WT, Vav Bcl-2 or Eμ Myc mice were polarised with either M1 skewing agents LPS, (100 ng/ml) & IFNγ (2 ng/ml) or M2 skewing agents IL-4 (10 ng/ml) & IL-13 (10 ng/ml) and the production of NO or arginase was measured. Results from these experiments are shown in **Figure 5-7** and demonstrate that M1 polarised BMDMs did display higher levels of NO and that these levels were similar between WT, Vav Bcl-2 and Eμ Myc BMDM. Arginase levels were variable but were generally found to be higher in M2 polarised BMDMs of WT, Vav Bcl-2 and Eμ Myc mice suggesting M2 polarisation was successful. Together these data confirm that apoptosis dysregulated BMDMs are responsive to typical polarising cytokines and 'skew' akin to WT BMDMs.

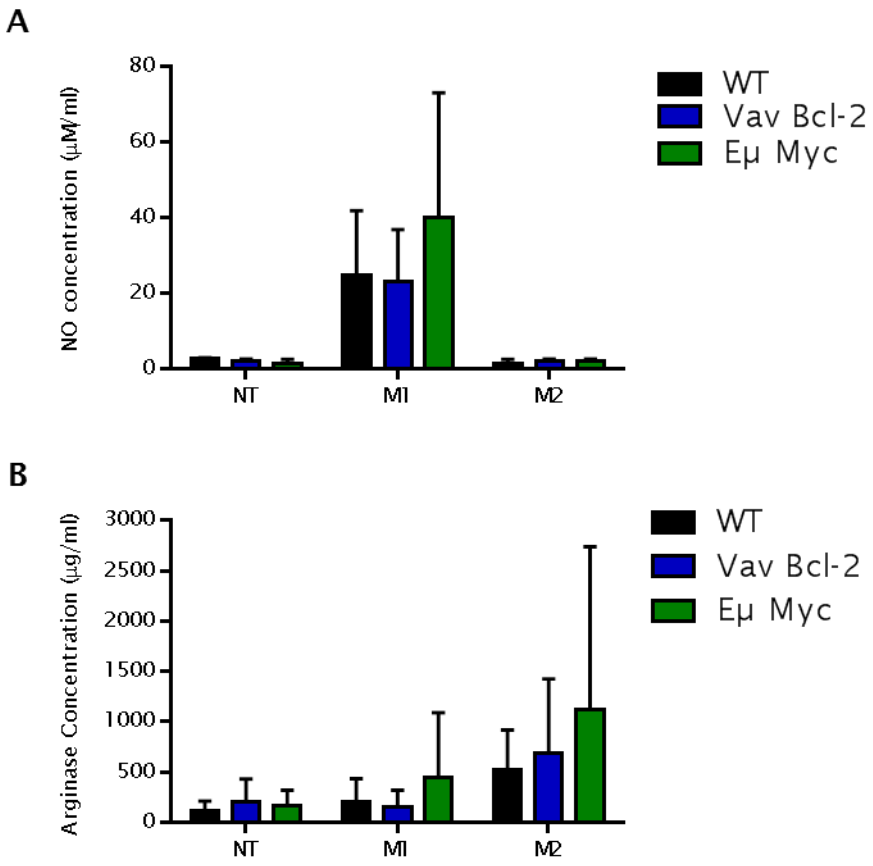

Figure 5-7 Analysis of BMDM polarisation by NO and Arginase production

BMDM (day 8) from C57BL/6 WT, Vav Bcl-2 or Eμ Myc mice were stimulated with either IFNγ (2 ng/ml)/LPS (100 ng/ml) or IL-4 (10 ng/ml)/IL-13 (10 ng/ml) for 24 hours to give an M1 or M2 macrophage phenotype respectively (**A)** The level of NO in 100 μl of cell culture supernatant was measured using a standard curve of $NaNO_3$ (250-0 μM). samples were incubated with NED (0.1 %) and sufanilamide (1 %) for 10 minutes at RT. Sample fluorescence was analysed using an EPOCH microplate (**B**) The level of Arginase was measured following lysis of BMDM of interest (~$1x10^6$ cells). Arginase was activated by $MnCl_2$ (10 mM) and incubation at 55 °C (10 minutes) followed by addition of 0.5 M L-arginase and incubation for 60 minutes at 37 °C. Arginase levels were detected indirectly by addition of 7% α-isonitroso-propiophenone and incubation at 100 °C for 45 minutes. Samples were analysed using an EPOCH microplate reader at 570 nm. N=3+/- SD.

Following confirmation that BMDMs from WT, Vav Bcl-2 or Eμ Myc mice were able to be polarised to an M1 or M2 phenotype similar experiments were performed to assess the ability of polarised BMDMs from WT, Vav Bcl-2 or Eμ Myc mice to phagocytose antibody opsonised hCD20 expressing B cells. To achieve this BMDM from WT, Vav Bcl-2 or Eμ Myc mice were generated and then

stimulated to an M1 or M2 phenotype overnight as described in materials and methods (**2.6**). The following day phagocytosis assays were conducted using hCD20 target B cells and type I (Ritm2a) anti-CD20 antibody (**Figure 5-8**).

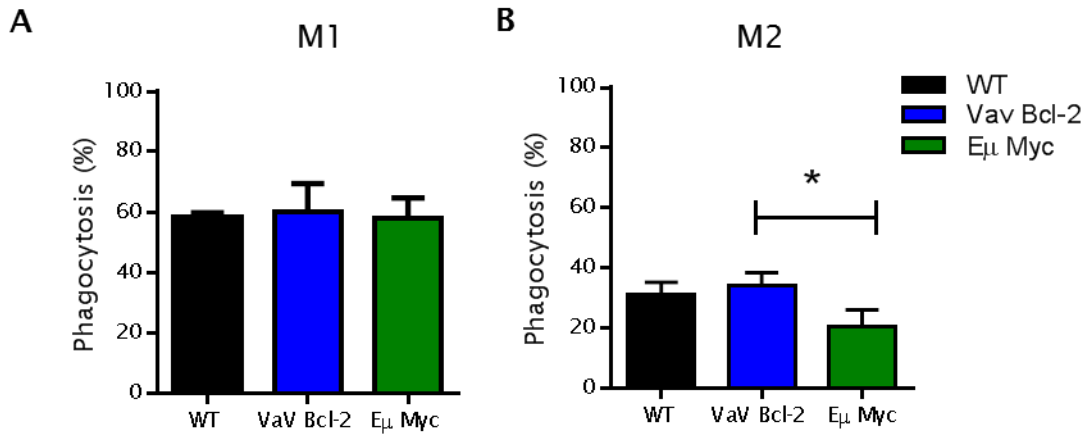

Figure 5-8 Phagocytic potential of apoptosis dysregulated BMDM following polarisation

BMDMs from C57BL/6 WT, Vav Bcl-2 or Eμ Myc mice were grown for 1 week. BMDMs were then polarised with M1 skewing cytokines IFNγ (2 ng/ml)/LPS (100 ng/ml) or M2 skewing cytokines IL-4 (10 ng/ml)/IL-13 (10 ng/ml) for 24 hours. Target hCD20 B cells were isolated, CFSE stained (5 μM) and opsonised with either irrelevant antibody or Ritm2a (10 μg/ml). Target cells were incubated with M1 or M2 skewed BMDMs at a 5:1 target to effector ratio for 30 minutes at 37 °C (5 % CO_2). Levels of phagocytosis were analysed on a BD FACS Calibre flow cytometer. N=3 +/- SD. Statistical analysis performed using a one-way ANOVA.

From **Figure 5-8a** it can be seen that M1 polarisation increases the level of phagocytosis seen to ~60 % and that there was no significant difference between WT, Vav Bcl-2 and Eμ Myc mice. With regards to M2 polarisation **Figure 5-8b** a general decrease in phagocytosis compared to NT BMDMs was seen although this decrease was only around 5-10 % and was not as striking as the increase in phagocytosis seen with M1 polarising reagents. Interestingly, there was a significant difference between Eμ Myc mice compared to either WT or Vav Bcl-2 mice, although this significance was modest (p=0.028). From these experiments it was concluded that BMDMs from apoptotic dysregulated mice had equivalent levels of phagocytosis and were able to become polarised to either an M1 or M2 phenotype akin to WT BMDMs. This suggested that the defective response to anti-CD20 therapy in the Vav Bcl-2 mouse is not due to

an inherent defect in the macrophage but likely a response to micro environmental cues. Therefore, the next sets of experiments were charged with investigating whether BMDMs could be polarised with apoptotic material to skew macrophages to a more suppressive phenotype.

5.3.1 Polarising BMDMs with apoptotic cells

These experiments aimed to examine whether BMDMs could be polarised by apoptotic material. To do this WT splenocytes were isolated and irradiated. Either irradiated splenocytes or apoptosis resistant Vav Bcl-2 splenocytes were incubated alongside WT BMDMs over their 8 day culture period. The phagocytic ability of these BMDMs was then assessed using the *in vitro* phagocytosis assays (**Figure 5-9**).

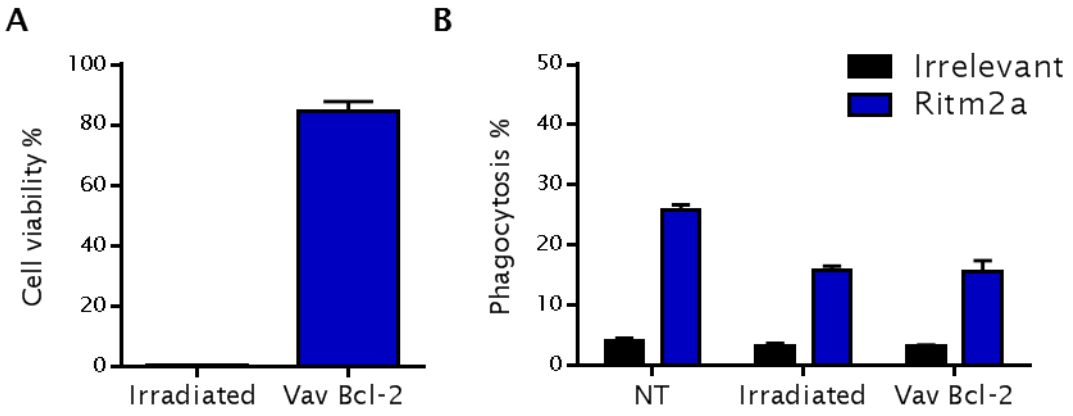

Figure 5-9 Phagocytosis assay following BMDM stimulation with apoptotic material

(A) C57BL/6 WT B cells were isolated and irradiated (40 Gy). Viability of splenocytes was then measured using Annexin V (1.6 µg/ml) and PI (9 µg/ml), samples were acquired on a flow cytometer and viable cells were identified as Annexin V and PI negative. **(B)** BMDMs were grown from a C56BL/6 mouse for 7 days and then co cultured overnight with either irradiated or Vav Bcl-2 isolated B cells ($1x10^7$ cells/ml). The following day hCD20 B cell targets were CFSE (10 µg/ml) stained and opsonised with either irrelevant (10 µg/ml) or Ritm2a (10 µg/ml) antibody then co-cultured with BMDMs. Samples were acquired on a flow cytometer, phagocytosis levels were measured as the percentage of $F4/80^+$ and $CFSE^+$ events. N=1, using triplicates +/- SEM.

From **Figure 5-9** it can be seen that irradiation of WT splenocytes resulted in negligible viability before co-culture with BMDMs, in contrast Vav Bcl-2

splenocytes showed ~80% viability before co-culture with BMDMs. It was found that co-culture with either cell source with BMDMs resulted in a reduced ability to phagocytose Ritm2a opsonised hCD20 B cells. Since results indicate that apoptotic material was unable to affect BMDM phagocytosis we next looked into whether serum from apoptosis dysregulated mice would polarise BMDMs to a more or less phagocytic state. Serum was isolated from C57BL/6 Vav Bcl-2, terminally bled mice and co cultured with BMDMs for 48 hours prior to phagocytosis assays (**Figure 5-10**).

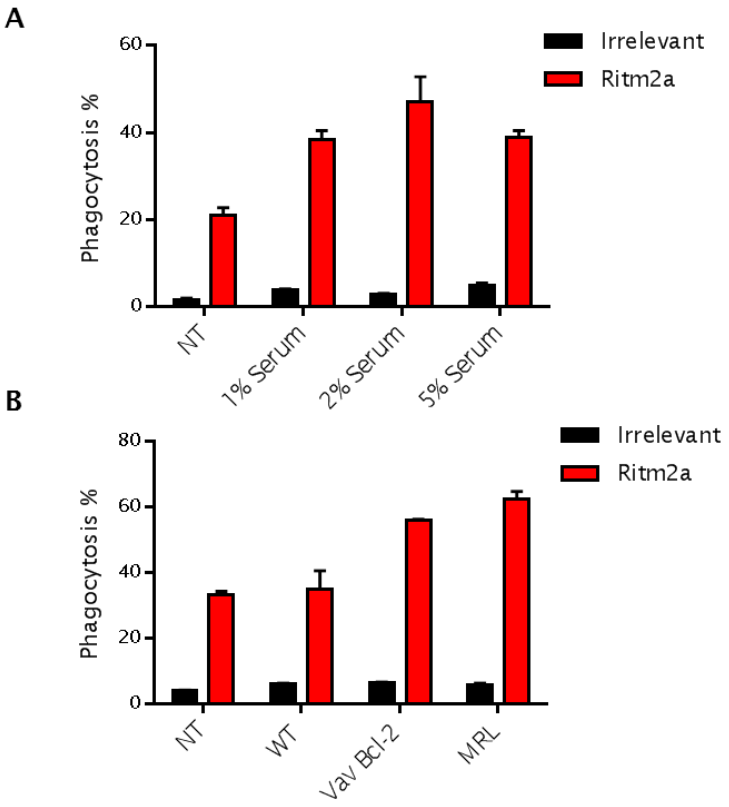

Figure 5-10 Phagocytosis assays following BMDM co-culture with serum from apoptosis dysregulated mice

Serum was isolated from C57BL/6, Vav Bcl-2, terminally bled mice and co-cultured with BMDMs 48 hours before phagocytosis assays were performed. Target C57BL/6 hCD20 Tg B cells were isolated and stained with CFSE (5 μM). Target B cells were opsonised with irrelevant mAb or Ritm2a (10 μg/ml) and were then co-cultured with BMDMs for 30 minutes at 37 °C (5 % CO_2). Samples were stained with F4/80-APC and acquired on a flow cytometer. (**A**) Vav Bcl-2 serum was co-cultured with BMDMs at various percentages (1, 2 and 5 %). (**B**) Serum from Vav Bcl-2 or MRL mice was co-cultured with BMDMs at 2%. N=1, using triplicates +/-SEM.

Results from **Figure 5-10** show that, perhaps unexpectedly, the addition of Vav Bcl-2 serum enhanced the BMDMs ability to phagocytose hCD20 opsonised target cells. Further to this, results from **Figure 5-10b** suggest augmented ability to undertake phagocytosis is restricted to apoptosis dysregulated mice since BMDMs co-cultured with WT serum showed no such increase in phagocytosis. The FcγR expression of these apoptosis dysregulated mice was next investigated since it has been well documented that the inhibitory receptor FcγRIIb will impact on antibody effector mechanisms and as others have reported upregulated FcγRIIb expression on B cells and myeloid cells [199].

5.4 Development of an 8 colour flow cytometry panel to investigate FcγR expression

5.4.1 Antigen and Fluorochrome selection

To understand how defective apoptosis could impact on ADCC/ADCP effector mechanisms there is a need to determine the FcγR expression level on the cell surface of effector leukocytes. To this end a multicolour flow cytometry panel was developed to detect FcγR expression on macrophages, monocytes and neutrophils all of which have been implicated in antibody mediated depletion and all express multiple FcγR. Rose *et al* developed a novel strategy to analyse the splenic myeloid compartment and formed the basis of the panel presented here [263]. The antigens chosen for this flow cytometry panel were; CD11b, F4/80, Ly6C and Ly6G. These antigens were used to detect neutrophils macrophages and Ly6C^{hi} monocytes. The lymphocyte markers CD3, CD19 and NK1.1 were selected to identify the key lymphocyte populations (NK cells, B cells and T cells). On each of these gated cell populations in house murine specific antibodies were used to detect FcγR expression. The antigen fluorochrome combinations chosen are listed in **Table 2**.

Table 2 List of antigen fluorochrome combinations

List of antigen fluorochrome combinations chosen for the detection of lymphoid and myeloid subsets along with the relevant clone names, antibody isotype and supplier.

Antigen	Fluorochrome	Clone	Isotype	Supplier
CD11b	PE	M1/70	Rat IgG2bκ	eBioscience
F4/80	APC	C1:A3/1	Rat IgG2aκ	In House
Ly6G	Pecy7	RB6—8C5	Rat IgG2bκ	eBioscience
Ly6C	PerCP Cy5.5	HK1.4	Rat IgG2cκ	eBioscience
CD19	APC eFlour 780	1D3	Rat IgG2aκ	eBioscience
CD3	BD Horizon 500	500A2	Rat IgG2aκ	BD
NK1.1	eFlour 450	pk136	Rat IgG2aκ	eBioscience
α-mFcγR	FITC	NA	NA	In House

To determine how these fluorochrome combinations would behave when used in combination Becton Dickinson spectral viewer software was used. This software gave predictions on fluorochrome emission after excitation from each of the three lasers available on the BD FACS Canto™ II. Importantly, this software also predicts any problems with fluorescence spill over which would need to be compensated for (**Figure 5-11**). From **Figure 5-11a** it can be seen that the 405 nm violet laser predominately excites Pacific Blue and BDV500 fluorochromes which are detected by the 450/50 nm and 510/50 nm band pass filters respectively. **Figure 5-11b** shows that excitation by the 488 nm blue laser will result in significant emissions by FITC, PerCP cy5.5, PE and PE cy7 fluorochromes which are detected by 530/30 nm, 670nm long pass (LP), 556 nm LP and 780/60 nm filters. Finally **Figure 5-11c** shows that the 688 nm red laser excites APC and APC cy7 fluorochromes and these are detected by 660/20 nm and 780/60 nm band pass filters respectively.

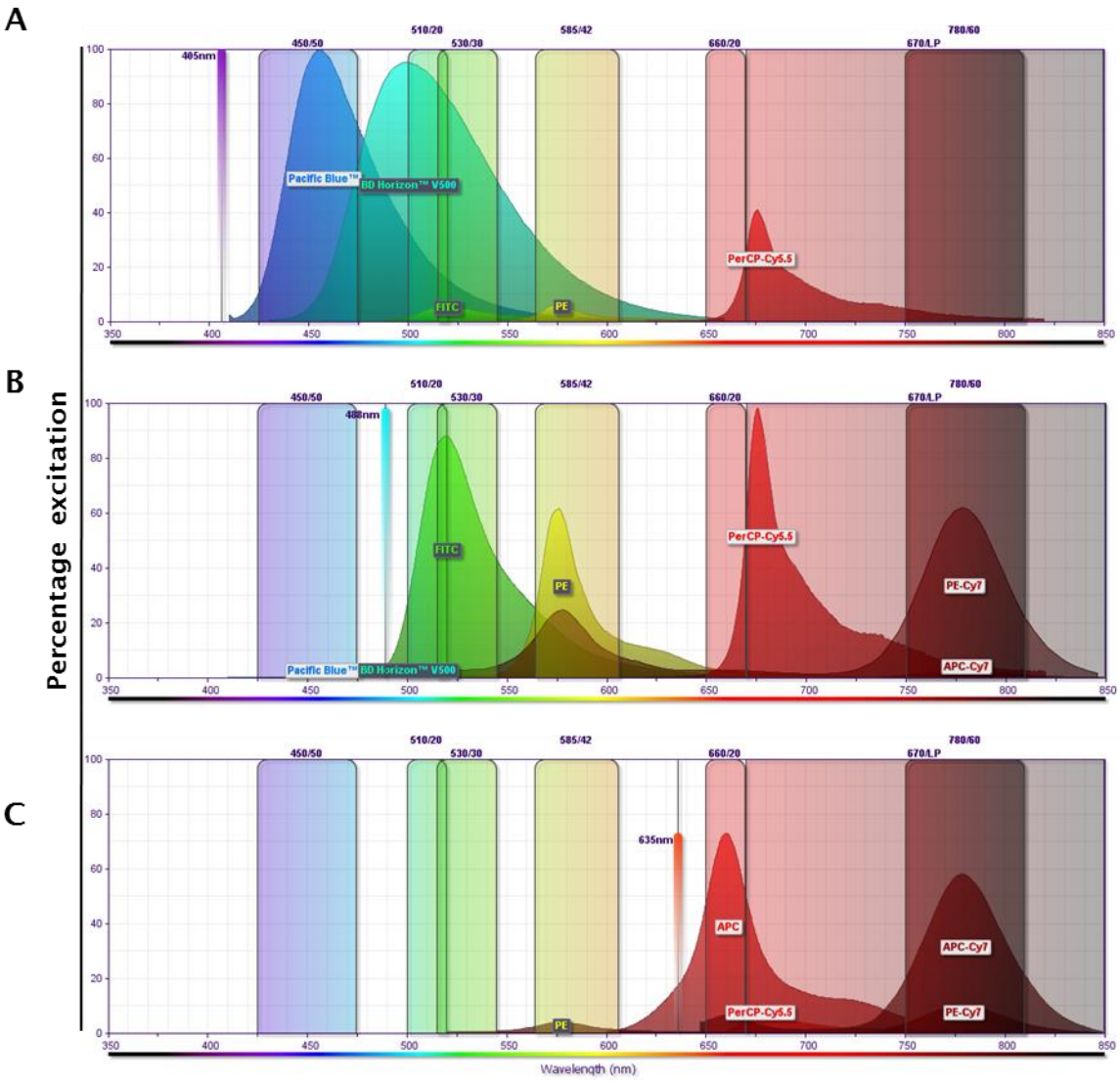

Figure 5-11 Spectral analysis to determine optimal antigen fluorochrome combinations

Becton Dickinson (BD) spectral viewer software was used to determine the amount of predicted fluorescence and fluorescence overlap between chosen fluorochromes when using the standard set up on the BD FCAS Canto™ II flow cytometer. (**A**) Fluorescence emission when excited by the 405 nm violet laser. (**B**) Fluorescence emission when excited by the 488 nm Blue Laser. (**C**) Fluorescence emission when excited by the 635 nm red laser.

Analysis by the BD spectral viewer also produced an estimate of the amount of emission spill over into undesired detectors which results in the need for compensation (**Table 3**). From **Table 3a** it can be seen that the 405 nm violet laser will excite Pacific blue, BD Horizon™ V500 and PerCP cy5.5 to above 10 %. PerCP cy5.5 emissions do not fall into either the Pacific blue or BD Horizon™ V500 band pass filters and so there is no need for compensation. However, 13 % of the predicted Pacific blue emissions fell into the BD Horizon™ V500 band pass filter and 38 % of the BD Horizon™ V500 emission fell into the Pacific blue band pass filter. **Table 3b** indicates that the fluorochromes FITC, PE, PerCP cy5.5 and PE cy7 are excited above 10 % by the 488 nm blue laser and that 26 % of the FITC emission spill over into the PE band pass filter whereas 53 % of the PE cy7 emissions fell into the PE band pass filters, due to the disassociation of tandem dye and it was this combination which required the most severe compensation adjustments.

Interestingly, 241% of PE cy7 emissions are expected to fall into the PerCP cy5.5 long pass filter, however this is not the case and these two fluorochromes can be used together successfully. This miscalculation is due to the way fluorescence emissions enter the set of detectors associated with the 488 nm laser. In this instance all emissions will first pass through a 735 nm long pass filter, allowing only PE cy7 emissions through to hit the 780/60 nm band pass filter and reflecting all other emissions towards the 670 nm long pass filter therefore successfully separating PerCP cy5.5 and PE cy7 emission. Finally **Table 3c** shows that APC and APC cy7 are significantly excited by the 635 nm red laser although PE cy7 and PerCP cy5.5 are moderately excited to ~10 %.

Table 3 Predicted spectral overlap between chosen fluorochromes

Using BD spectral viewer software the predicted spectral overlaps between the fluorochromes decided upon were determined. (**A**) Excitation by the 405 nm violate laser. (**B**) Excitation by the 488 nm blue laser. (**C**) Excitation by the 635 nm red laser.

A

	Fluorochrome	% Max	Ex	Em	Filters	FITC	PE	PerCP-...	PE-Cy7	APC	APC-Cy7	Pacific ...	V500
1	FITC	5.4		✓	530/30	47.0 %	0.6 %	--	5.7 %	--	--	9.3 %	114.6 %
2	PE	6.0		✓	585/42	26.8 %	70.4 %	--	53.6 %	0.4 %	--	1.7 %	38.5 %
3	PerCP-Cy5.5	40.9		✓	670/LP	--	3.6 %	91.9 %	241.2 %	100.6 %	123.3 %	--	--
4	PE-Cy7	0.0		✓	780/60	--	--	3.3 %	30.6 %	--	50.2 %	--	--
5	APC	0.0		✓	660/20	0.0 %	3.6 %	10.4 %	4.1 %	40.2 %	4.8 %	--	0.7 %
6	APC-Cy7	0.0		✓	780/60	--	--	10.5 %	197.8 %	--	77.8 %	--	--
7	Pacific Blue™	99.9		✓	450/50	--	--	--	--	--	--	61.9 %	38.1 %
8	BD Horizon™ V5...	95.1		✓	510/20	62.3 %	--	--	0.4 %	--	--	13.1 %	23.9 %

B

	Fluorochrome	% Max	Ex	Em	Filters	FITC	PE	PerCP-...	PE-Cy7	APC	APC-Cy7	Pacific ...	V500
1	FITC	88.0		✓	530/30	47.0 %	0.6 %	--	5.7 %	--	--	9.3 %	114.6 %
2	PE	61.6		✓	585/42	26.8 %	70.4 %	--	53.6 %	0.4 %	--	1.7 %	38.5 %
3	PerCP-Cy5.5	98.2		✓	670/LP	--	3.6 %	91.9 %	241.2 %	100.6 %	123.3 %	--	--
4	PE-Cy7	61.8		✓	780/60	--	--	3.3 %	30.6 %	--	50.2 %	--	--
5	APC	0.0		✓	660/20	0.0 %	3.6 %	10.4 %	4.1 %	40.2 %	4.8 %	--	0.7 %
6	APC-Cy7	3.3		✓	780/60	--	--	10.5 %	197.8 %	--	77.8 %	--	--
7	Pacific Blue™	0.1		✓	450/50	--	--	--	--	--	--	61.9 %	38.1 %
8	BD Horizon™ V5...	0.7		✓	510/20	62.3 %	--	--	0.4 %	--	--	13.1 %	23.9 %

C

	Fluorochrome	% Max	Ex	Em	Filters	FITC	PE	PerCP-...	PE-Cy7	APC	APC-Cy7	Pacific ...	V500
1	FITC	0.0		✓	530/30	47.0 %	0.6 %	--	5.7 %	--	--	9.3 %	114.6 %
2	PE	0.3		✓	585/42	26.8 %	70.4 %	--	53.6 %	0.4 %	--	1.7 %	38.5 %
3	PerCP-Cy5.5	10.4		✓	670/LP	--	3.6 %	91.9 %	241.2 %	100.6 %	123.3 %	--	--
4	PE-Cy7	10.0		✓	780/60	--	--	3.3 %	30.6 %	--	50.2 %	--	--
5	APC	72.8		✓	660/20	0.0 %	3.6 %	10.4 %	4.1 %	40.2 %	4.8 %	--	0.7 %
6	APC-Cy7	57.9		✓	780/60	--	--	10.5 %	197.8 %	--	77.8 %	--	--
7	Pacific Blue™	0.0		✓	450/50	--	--	--	--	--	--	61.9 %	38.1 %
8	BD Horizon™ V5...	0.0		✓	510/20	62.3 %	--	--	0.4 %	--	--	13.1 %	23.9 %

5.4.2 Experimental set up

Once the *in silico* analysis of fluorochrome combinations was complete, the experimental setup was established. To ensure that the correct volume of antibody is used so not to add excess or give sub optimal levels of staining each of the antibodies outlined in **Table 2** were titrated using whole splenocytes from C57BL/6 mice and 1 µl was found to give sufficient staining for $1x10^6$ cells (**Error! Reference source not found.**). Furthermore, the luorescence minus one (FL^{-1}) was obtained for each fluorochrome to ensure that compensation settings were adequate and that no undesired spill over was being misinterpreted as real staining. Once these quality control measures had been confirmed all colours were used in combination and analysis of data carried out (**Figure 5-12**).

As detailed in **Figure 5-12** doublets were first excluded by measuring the FSC-area vs. FSC-width. Any event which appears outside the blue box (**Figure 5-12a**) were discounted from further analysis. Macrophage were highlighted as being CD11b intermediate and F4/80 high events whereas neutrophils and monocytes were deemed as being CD11b positive and either Ly6G or Ly6C positive, respectively. Lymphocyte populations were broadly defined as CD3, NK1.1 or CD19 positive events which reflect T cells, NK cells and B cells, respectively. Upon each cell subset mentioned the level of FcγR was measured using in house antibodies conjugated to FITC. Expression level of FcγR are presented as either the geometric MFI (Geo-MFI) or the A:I ratio. This ratio was determined by multiplying the sum of Geo-MFI obtained for the activatory receptors and dividing the result by the inhibitory receptor FcγRIIb Geo-MFI. The resulting value for the non-treated control mouse was then divided by the values obtained for treated mice to give the A:I ratio relative to WT mouse.

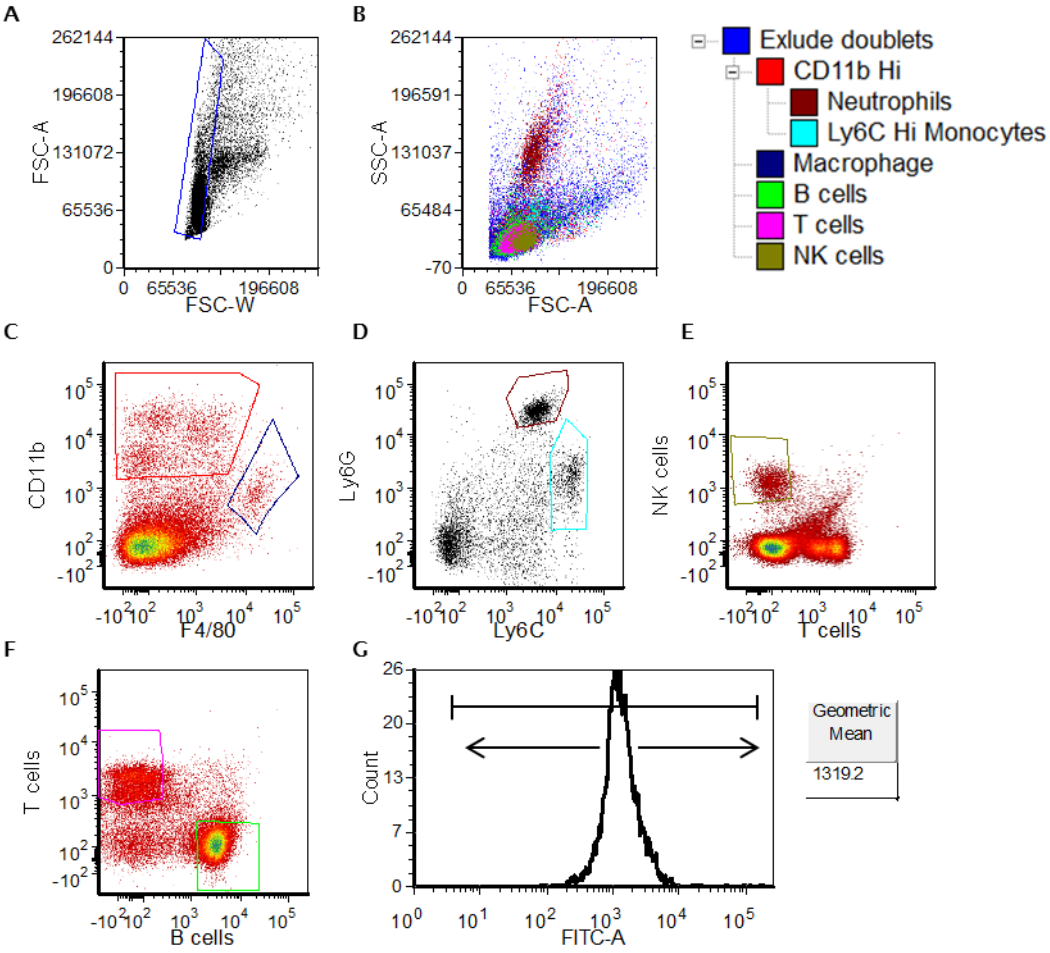

Figure 5-12 Multicolour flow cytometry panel to assess leukocyte FcγR expression

Representative FACS plots highlighting how data is interpreted once obtained using the flow cytometer. (**A**) FSC-Area and FSC-Width are used to gate out doublets. (**B**) Typical FSC vs SSC profile from a splenocytes population. (**C**) CD11b vs F4/80 highlighting the macrophage population (Blue box) and monocyte/granulocyte populations (Red box). (**D**) Ly6G vs Ly6C events gated from CD11b high events in C highlighting the neutrophil (Brown box) and Ly6C^{hi} monocytes (Blue box). (**E**) NK1.1 vs CD3 highlighting the NK cell population (Yellow box). (**F**) CD3 vs CD19 highlighting the T cell population (Pink box) and B cell population (Green box). (**G**) Upon each of the cell subsets defined, FcγR expression was measured using in house antibodies conjugated to FITC and expression reported as Geo-MFI.

5.4.3 Anti-mouse FcγR antibody validation

After successfully running this multicolour flow cytometry panel the ability to detect FcγR on each cell subset was investigated. In-house antibodies which had been conjugated to FITC were used. The specificity and binding ability was assessed on each of the cell populations investigated and compared against an FcγR null mouse which lacks all activatory and inhibitory FcγR. Staining was performed on whole splenocytes from C57BL/6 mice. Whole spleen was disassociated and opsonised with an antibody cocktail containing a mix of CD3, CD19, NK1.1, CD11b, F4/80, Ly6C and Ly6C plus the anti-FcγR antibody of choice or an irrelevant $F(ab)_2$ control. From **Figure 5-13** it can be seen that in-house antibodies show a good level of specificity when used against each of the cell types investigated. As reported in the literature B cells express only inhibitory mouse FcγRIIb and T cells as expected did not appear to express any FcγR. NK cells are reported to express mouse FcγRIII however staining here shows NK cells to express little of this receptor and data presented in chapter 3 shows resting NK cells to express little mouse FcγRIII. However, activation by IL-2 resulted in a marked increase in FcγRIII expression on mouse NK cells. Monocytes, macrophages and neutrophils were shown to express the full range of FcγR although it appears that both anti-mouse FcγRI (AT152-9 $F(ab)_2$) and FcγRIIb (AT130-2 N297A) show a small degree of off target specificity.

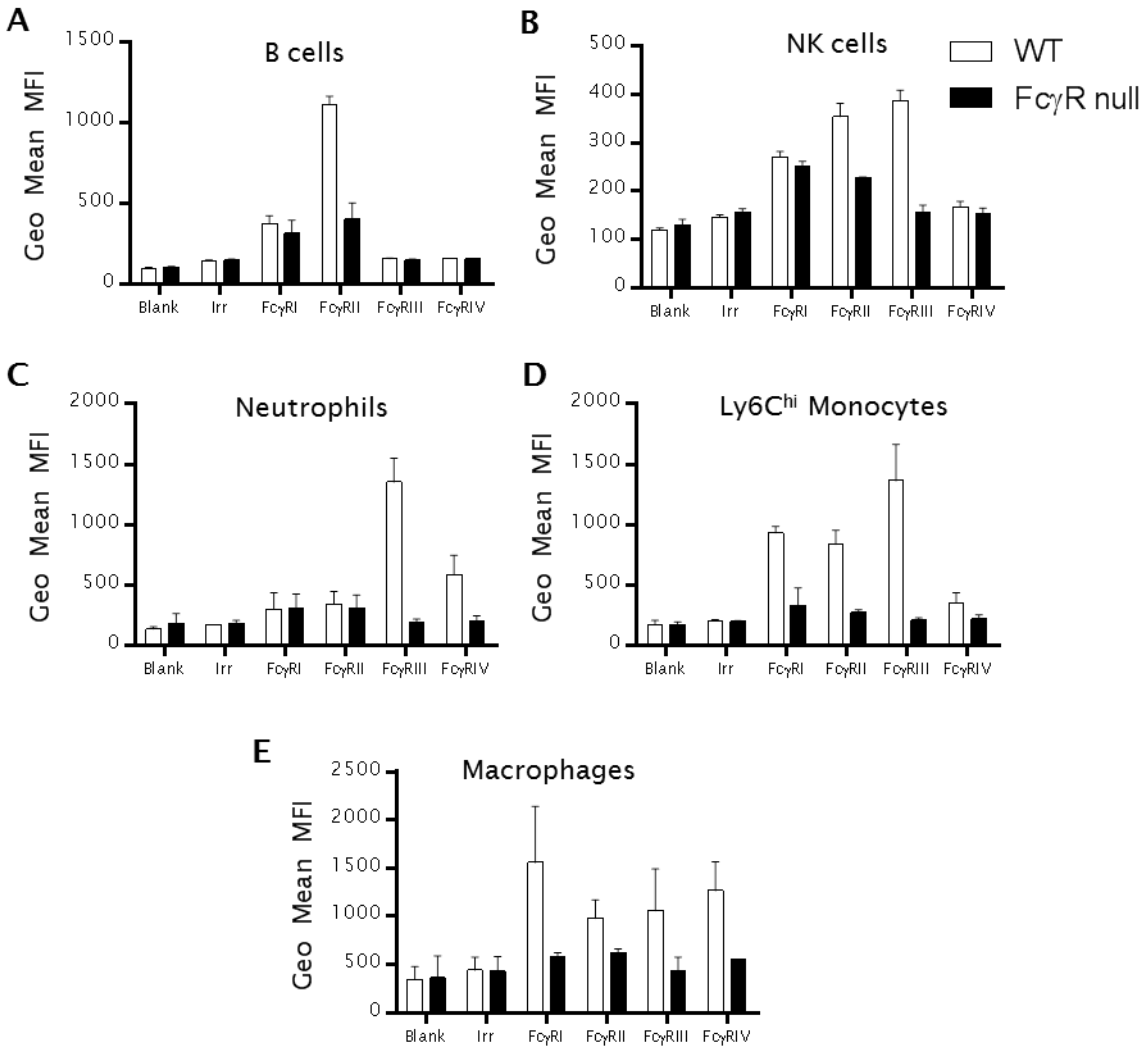

Figure 5-13 Validation of anti-mouse FcγR antibodies

Splenocytes from C57BL/6 WT (Clear bars) or FcγR null mice (Black bars) were disassociated and cell surface stained using a master mix of anti-CD3, CD19, NK1.1, CD11b, Ly6C, Ly6G and F4/89 antibodies (1 µl). Additionally, in house FITC conjugated anti-mouse FcγR antibodies (10 µg/ml) were used to determine the level of FcγRI (AT152-9), FcγRIIb (AT130-2 N297A), FcγRIII (AT154-2) or FcγRIV (AT137) on leukocyte subsets. Cells were stained on ice for 30 minutes. Red blood cells were lysed and samples were acquired on a BD FACS Canto™ II flow cytometer. (**A**) B cells were identified as $CD19^{+}$. (**B**) NK cells were identified as $NK1.1^{+}$ and $CD3^{-}$. (**C**) Neutrophils were identified as $CD11b^{+}$, $Ly6G^{hi}$ and $Ly6C^{low}$. (**D**) Monocytes were identified as $CD11b^{+}$, $Ly6G^{low}$ and $Ly6C^{hi}$. (**E**) Macrophages were identified as $CD11b^{int}$, $F4/80^{hi}$. N=2 +/- SD.

5.5 FcγR expression in apoptosis dysregulated mice

Having designed, generated and validated a robust flow cytometry panel for assessing FcγR expression patterns, on WT mice, the expression pattern on apoptosis dysregulated mice was also assessed. The literature relating to Vav Bcl-2 mice reported that there is an increased expression of the inhibitory receptor FcγRIIb on B cells and myeloid cells [199]. Here Lawlor *et al* looked to use Vav Bcl-2 mice in combination with models of collagen induced arthritis (CIA) and BxN serum transfer arthritis, both of which are antibody dependent. It was hypothesised that since a failure in the apoptosis of infiltrating leukocytes is often seen in rheumatoid arthritis (RA) and that overexpression of Bcl-2 in haematopoietic cells often results in autoimmunity, then the Vav Bcl-2 mouse will exemplify these models of RA. Conversely it was found that in fact, Vav Bcl-2 mice were protected against these models of RA and that this may have been in part down to increased expression of FcγRIIb on leukocytes. This paper demonstrated a direct link between defective apoptosis and FcγR expression. Since Fc:FcγR interactions are critical to effective antibody therapy and the expression of FcγR on effector cell can be modulated by the microenvironment, the expression of activatory and inhibitory FcγR on important leukocyte subsets was therefore investigated. Analysis on BM, blood and spleen was performed on WT and apoptosis dysregulated mice.

Analysis of splenocytes (**Figure 5-14**) revealed that there was significantly greater expression of inhibitory FcγRIIb on B cells, monocytes and macrophages from Vav Bcl-2 mice compared to WT or Eμ Myc mice. Additionally, macrophages from Vav Bcl-2 mice showed increased expression of activatory FcγRIV although there was variable expression which did not reach significance. Murine NK cells expressed very little FcγRIII and as expected T cells expressed no activatory FcγR but appeared to show a tendency of binding with the FcγRIIb mAb on Vav Bcl-2 B cells. Similar results to these were found when analysis of blood was carried out although as expected no macrophages were found in this compartment (**Figure 5-15**). With regards to the BM compartment only B cells, neutrophils and Ly6C High monocytes were clearly detectable in sufficient numbers and again B cells showed significantly increased expression of FcγRIIb. In contrast monocytes did not demonstrate an elevated level of FcγRIIb in the Vav Bcl-2 mouse and levels of this receptor were

generally elevated to the same extent in both WT and Eμ Myc mice (**Figure 5-16**).

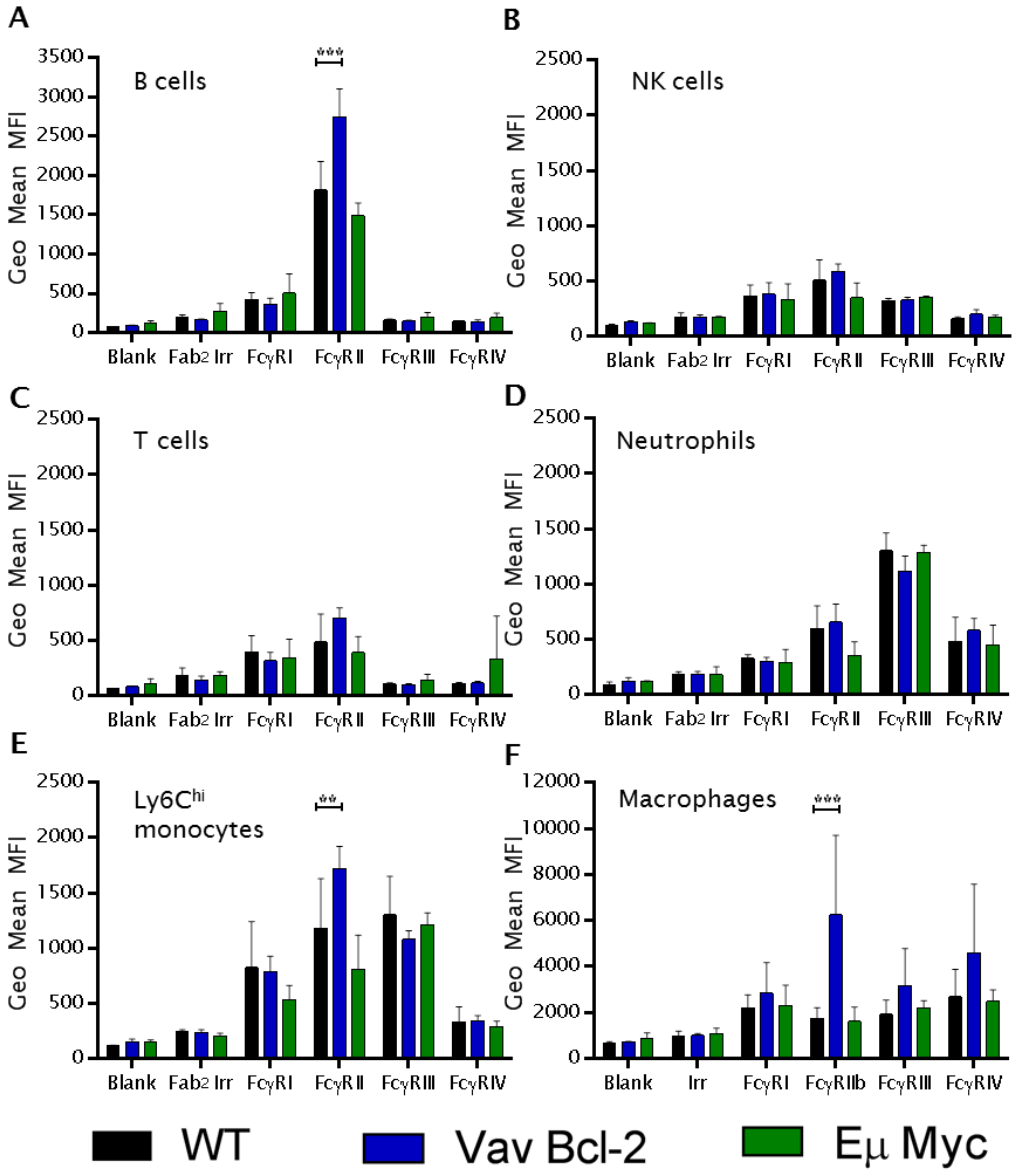

Figure 5-14 Comparison of murine FcγR expression on leukocyte subsets isolated from the spleen

Spleen was isolated from C57BL/6 WT, Vav Bcl-2 or Eμ Myc mice and disassociated. Splenocytes ($1x10^6$ cells) were stained with CD11b-PE, F4/80-APC, Ly6G PE cy7, Ly6C PerCP Cy5.5, CD19-APC Cy7 and NK1.1 Pacific Blue (1μl). Samples were also stained with anti-FcγRI (AT152-9 $F(ab)_2$) FcγRIIb (AT130-2 N297A), FcγRIII (AT152-9 $F(ab)_2$) or FcγRIV (AT137 $F(ab)_2$) mAb (10 μg/ml) for 30 minutes on ice. Red blood cells were lysed and samples were acquired on a FACS Canto™ II flow cytometer. Results reported as the Geo-MFI of FL-1 (FITC) N=3+/- SD. Statistical analysis performed using two-way ANOVA.

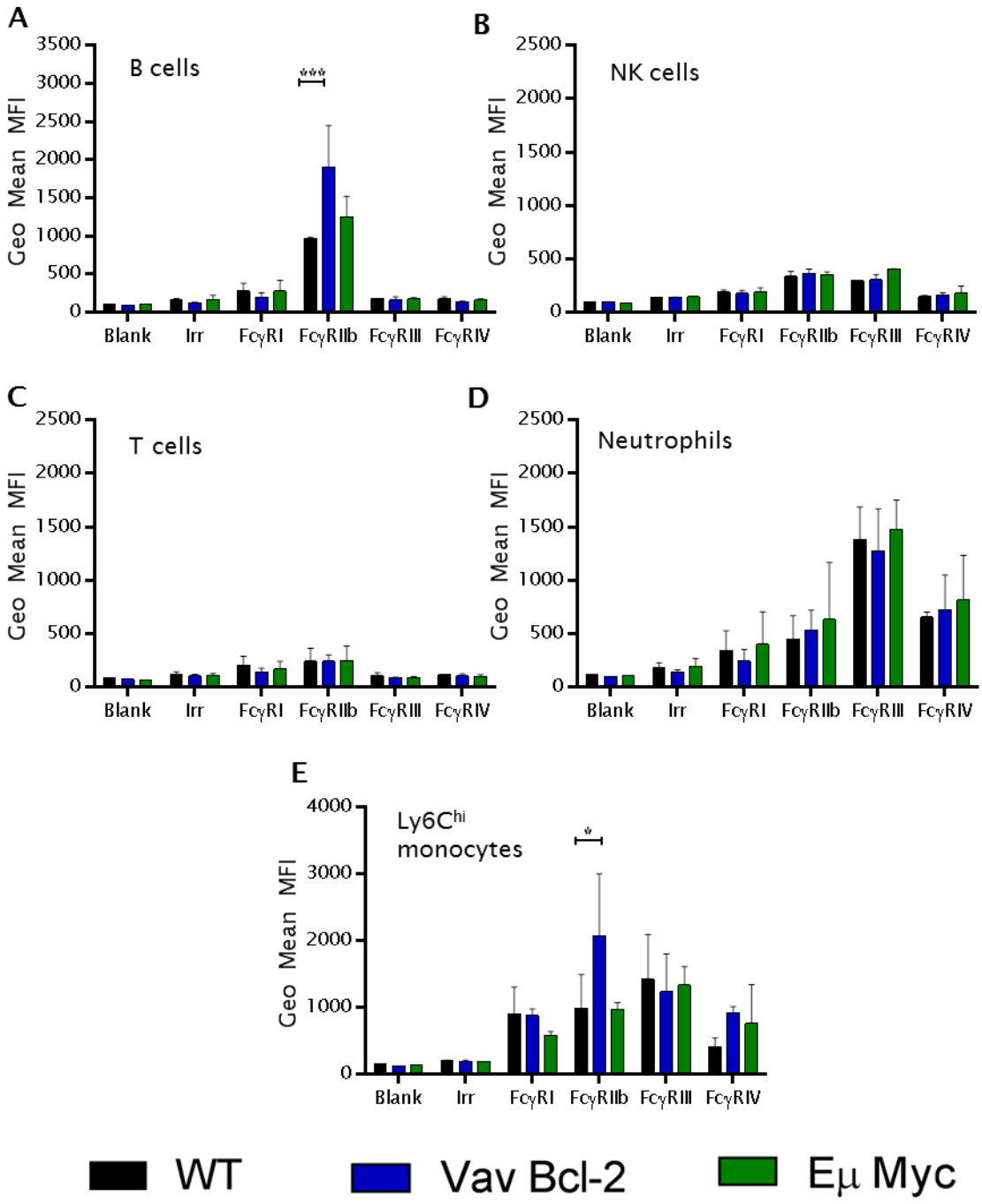

Figure 5-15 Comparison of murine FcγR expression on leukocyte subsets isolated from blood

Cardiac blood was isolated from C57BL/6 WT, Vav Bcl-2 or Eμ Myc mice. Blood (50 μl) was stained with CD11b-PE, F4/80-APC, Ly6G PE cy7, Ly6C PerCP Cy5.5, CD19-APC Cy7 and NK1.1 Pacific Blue (1μl). Samples were also stained with anti-FcγRI (AT152-9 $F(ab)_2$) FcγRIIb (AT130-2 N297A), FcγRIII (AT152-9 $F(ab)_2$) or FcγRIV (AT137 $F(ab)_2$) mAb (10 μg/ml) for 30 minutes on ice. Red blood cells were lysed and samples were acquired on a FACS Canto™ II flow cytometer. Results reported as the Geo-MFI of FL-1 (FITC) N=2+/- SD. Statistical analysis performed using two-way ANOVA.

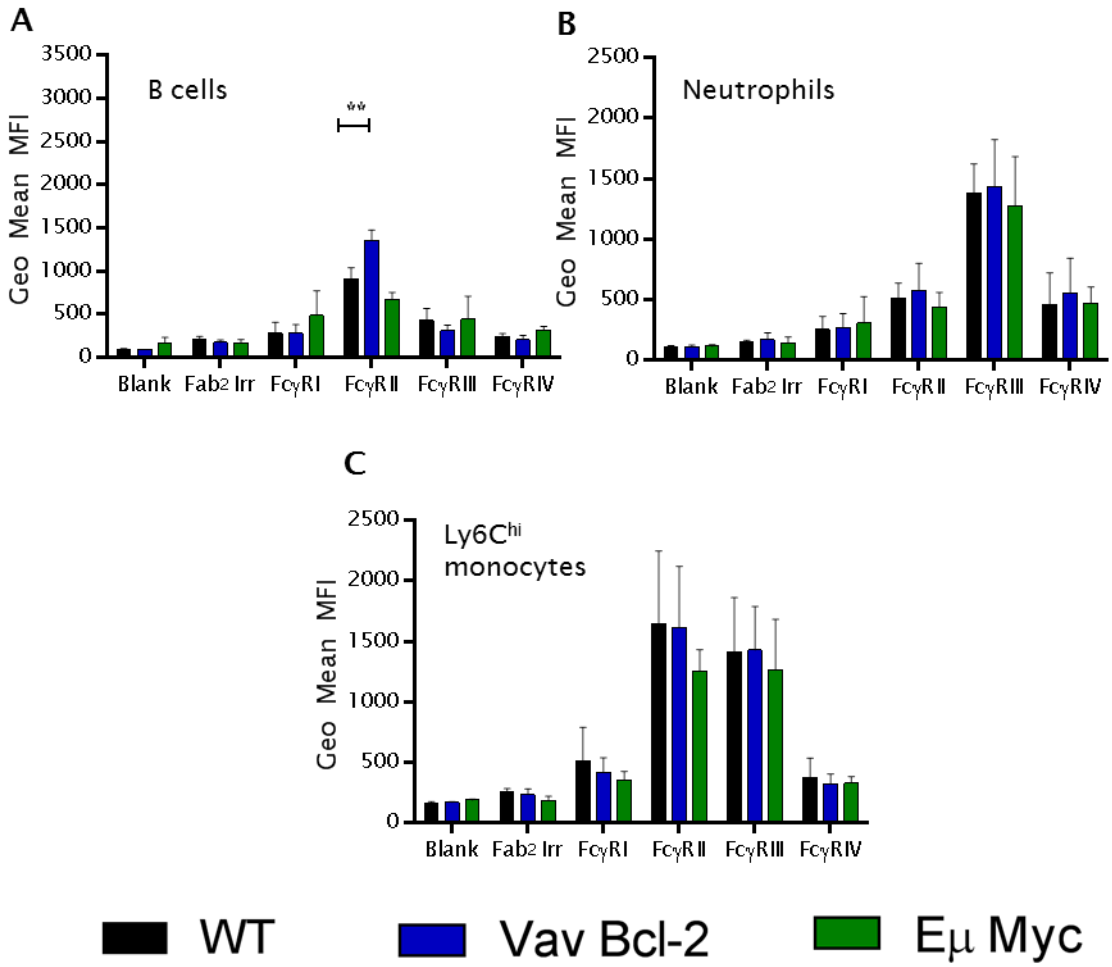

Figure 5-16 Comparison of murine FcγR expression on leukocyte subsets isolated from bone marrow

Bone marrow was isolated from the hind leg of C57BL/6 WT, Vav Bcl-2 or Eμ Myc mice. BM ($1x10^6$ cells) was stained with CD11b-PE, F4/80-APC, Ly6G PE cy7, Ly6C PerCP Cy5.5, CD19-APC Cy7 and NK1.1 Pacific Blue (1μl). Samples were also stained with anti-FcγRI (AT152-9 $F(ab)_2$) FcγRIIb (AT130-2 N297A), FcγRIII (AT152-9 $F(ab)_2$) or FcγRIV (AT137 $F(ab)_2$) mAb (10 μg/ml) for 30 minutes on ice. Red blood cells were lysed and samples were acquired on a FACS Canto™ II flow cytometer. Results reported as the Geo-MFI of FL-1 (FITC) N=2+/- SD. Statistical analysis performed using two-way ANOVA.

From **Figure 5-14** - **Figure 5-16** it can be seen that there is a general trend for increased expression of FcγRIIb on leukocyte subsets from Vav Bcl-2 mice. This is particularly prevalent on B cells, monocytes and macrophages. The overall A:I ratio for each cell subset investigated was next determined to see if these increased levels of FcγRIIb are likely to translate into a decreased ADCP potential in the Vav Bcl-2 mouse. From **Figure 5-17** it can be seen that the A:I

ratio of Vav Bcl-2 mice in the spleen is generally decreased and is particularly decreased on monocytes and macrophages which correlates with the increased expression of FcγRIIb and the decreased ability of these cells to deplete B cells *in vivo*. Interestingly, the A:I ratio in Eμ Myc mice was increased over that of WT mice even though there was no large increase in a single activatory FcγR or large decrease in inhibitory receptor. Similar results were seen in the blood. There was again a decrease in the A:I ratio of monocytes which correlates with effector function although no such increase in A:I ratio was observed in Eμ Myc cells. With regards to BM there was no difference in A:I ratio of neutrophils and monocytes of Vav Bcl-2 or Eμ Myc mice. Although there was a decrease in the level of FcγRIIb on B cells.

Overall it was clear that Vav Bcl-2 mice show an up-regulation of inhibitory FcγRIIb on both their myeloid and lymphoid subsets. Increased expression of FcγRIIb on myeloid cells will likely impact upon effector cell mechanisms, namely phagocytosis by macrophages. A strong preference for increased expression of FcγRIIb on B cells was also observed, which may have lent weight to the hypothesis that increased antigenic modulation is responsible for deficiencies in B cell depletions, although the experiments detailed herein indicate this not to be the case. The next set of experiments was aimed at examining in more detail the increased expression of FcγRIIb on B cells. Since there are many different B cell subsets, further phenotyping was performed on Vav Bcl-2 mice to see if there was a particular stage of B cell development which showed upregulated FcγRIIb or whether increased expression was seen throughout all B cell subsets.

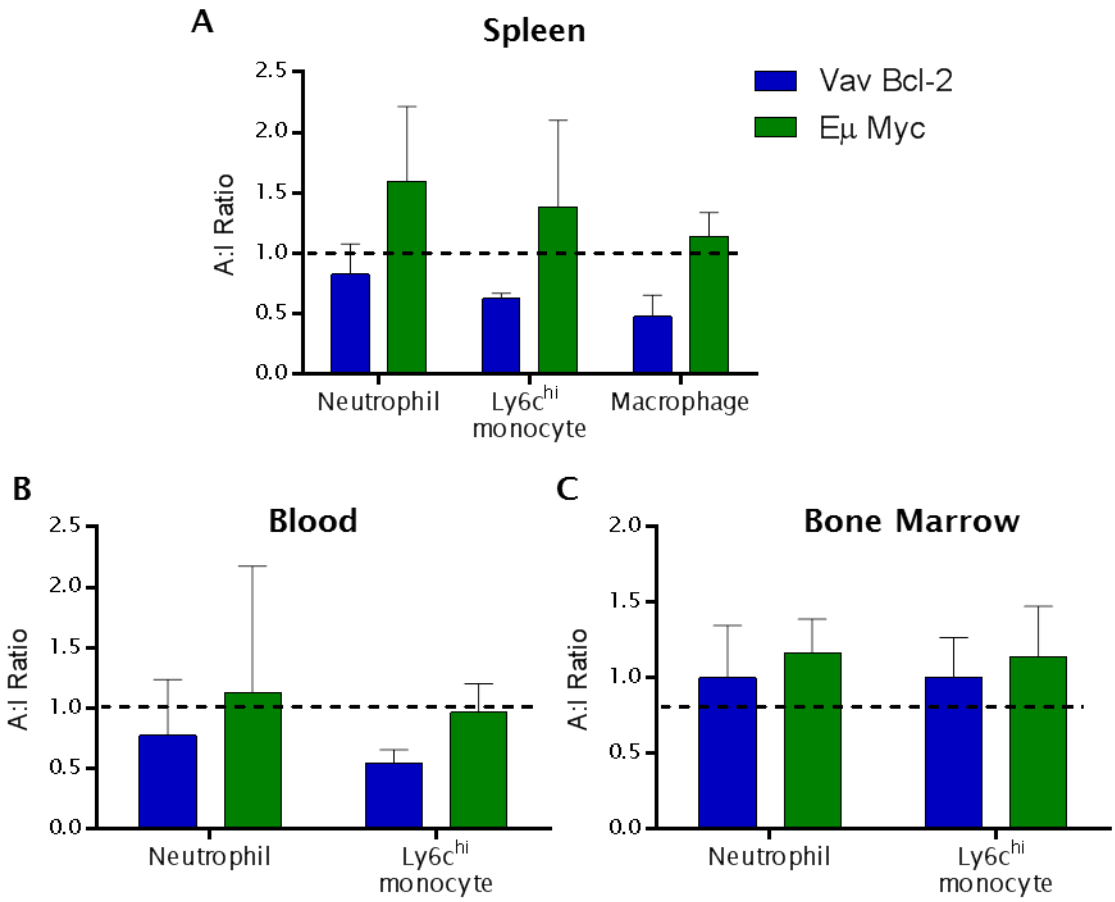

Figure 5-17 The A:I ratio from apoptosis dysregulated mice in different tissues and cell subset

The A:I ratio for Spleen (**A**), Blood (**B**) and BM (**C**) was calculated based on the Geo-MFI results obtained in **Figure 5-14** - **Figure 5-16**. The cell populations investigated were neutrophils, Ly6C^{hi} monocytes and macrophages. The A:I ratio was calculated by multiplying the Geo-MFI of activatory FcγRI, FcγRIII and FcγRIV together and then dividing this value by that of the Geo-MFI of inhibitory FcγRIIb [123]. To transform data so that it was relative to the WT mouse resulting values for apoptosis dysregulated mice were divided by the respective value for the WT mouse. Results are presented as the A:I ratio relative to WT mice. N=3+/-SD.

5.6 Phenotyping of B cells in Vav Bcl-2 mice

Vav Bcl-2 mice had increased expression of FcγRIIb within the B cell compartment. To determine if this was a generalised increase throughout all subsets or whether it was confined to a certain dysfunctional population immunophneotyping was carried out on spleen, blood and BM. Two staining panels were produced; the first looked at more mature B cells subsets and was used to investigate the spleen and blood whereas the other looked at the earlier stage B cell subsets and was used to investigate the BM.

The data presented in **Figure 5-18** shows the typical gating strategy used and staining pattern seen when using splenocytes or whole blood. Firstly B cells were identified as being CD19 and B220 positive and then T1, T2, follicular and marginal zone B cells were identified by CD21 vs CD23 staining and by CD38 vs IgM staining. T2 and follicular B cells are CD21 positive and CD23 intermediate as well as CD38 positive and IgM positive. T1 B cells were identified as being CD21 and CD23 low and CD38 and IgM positive. Finally, Marginal zone B cells were identified as being CD23 high and CD21 negative and CD38 and IgM positive events. Upon each gated population the expression of inhibitory FcγRIIb was measured using FITC conjugated antibodies previously described.

The data in **Figure 5-19** shows the typical gating strategy and staining pattern used to identify B cell populations in the murine BM. B cells were again identified based upon CD19 and B220 staining. Immature, pro and pre B cells were identified by gating upon the CD19 positive B220 low population and then comparing IgM vs IgD staining. Immature B cells were IgM positive whereas pro and pre B cells were IgM and IgD negative. Pro and pre B cells could be further differentiated based upon CD43 staining, pre B cells were CD43 high whereas pro B cells were CD43 intermediate. Mature B cells were identified as being CD19 positive B220 high events as well as IgM and IgD positive.

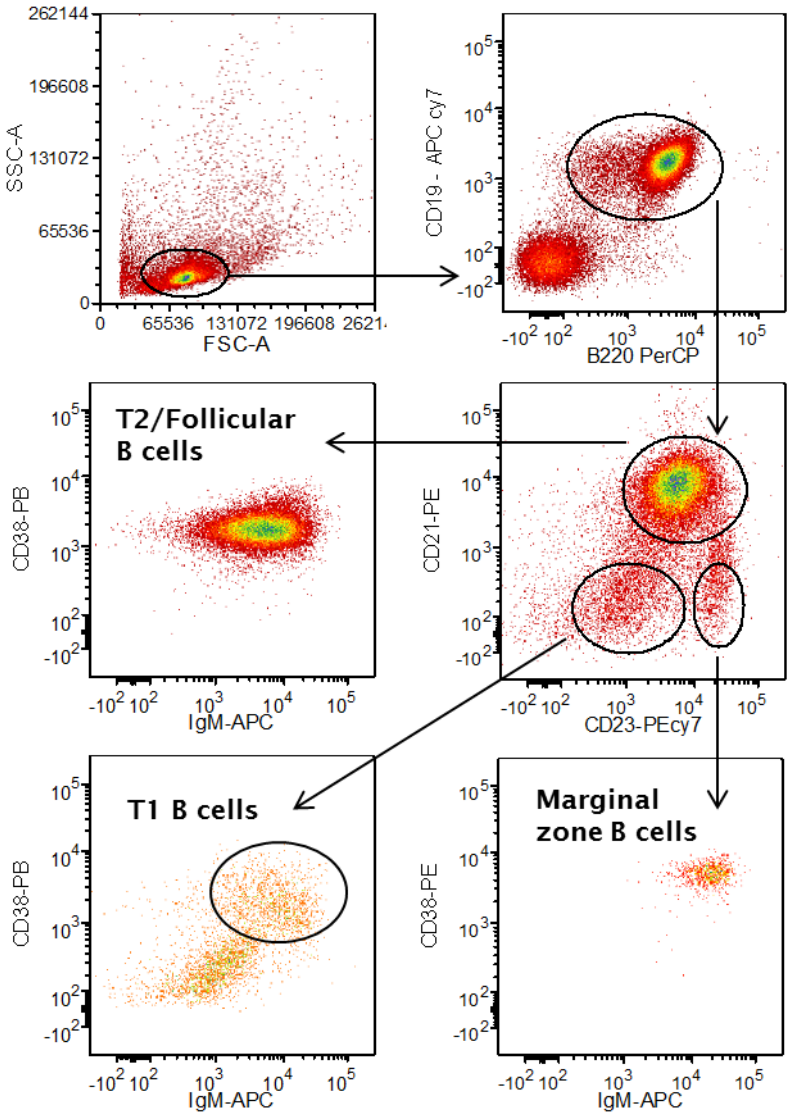

Figure 5-18 Gating strategy for phenotyping B cell subsets in the Blood and Spleen

Representative density plots showing staining of tissues from a C57BL/6 mouse. Peripheral whole blood or splenocytes were opsonised with antibodies to mouse CD19, B220, CD21, CD23, CD38, IgM (1 µl) and FcγRIIb (10 µg/ml). B cells were gated as being CD19 and B220 positive events. T1, T2/Folicular and Marginal zone B cells could be identified based upon CD21 vs CD23 staining. T1 B cells were CD21 and CD23 low, T2/Follicular B cells were CD21 positive CD23 intermediate events and marginal zone B cells could be identified as CD21 negative and CD23 high events.

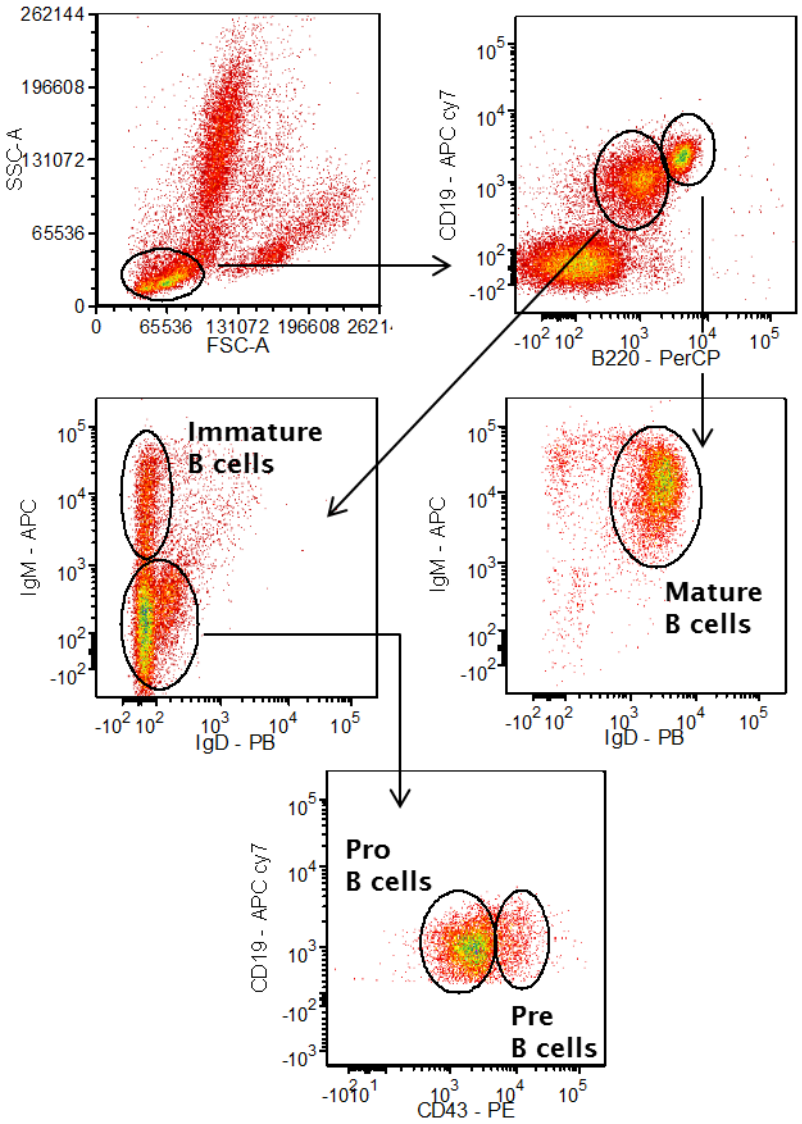

Figure 5-19 Gating strategy for phenotyping B cell subsets in murine Bone Marrow

Representative density plots showing staining of BM from a C57BL/6 mouse. Bone marrow was isolated from the hind legs of a C57BL/6 mouse and opsonised with antibodies against murine CD19, B220, IgM, IgD, CD43 (1 µl) and mouse FcγRIIb (10 µg/ml). B cells were identified as being CD19 and B220 positive events, upon the CD19 positive and B220 low events Immature B cells were identified as being IgM positive IgD negative events whereas Pro and Pre B cells were identified as being IgM and IgD negative. Pro and Pre B cells could be further distinguished based upon CD43 staining. Mature B cells were identified as being CD19 positive B220 high as well as IgM and IgD positive.

Using these B cell staining panels blood, spleen and bone marrow from WT and Vav Bcl-2 mice were compared and the percentages, cell numbers and FcγRIIb expression was analysed. Interestingly it was found that Vav Bcl-2 mice contained a B cell population that was B220 high, CD38 positive and IgM and IgD negative, this population was not detectable in the WT mouse (**Figure 5-20**). Further analysis revealed that this cell population was the most prevalent population found in the Vav Bcl-2 mouse (**Figure 5-21**).

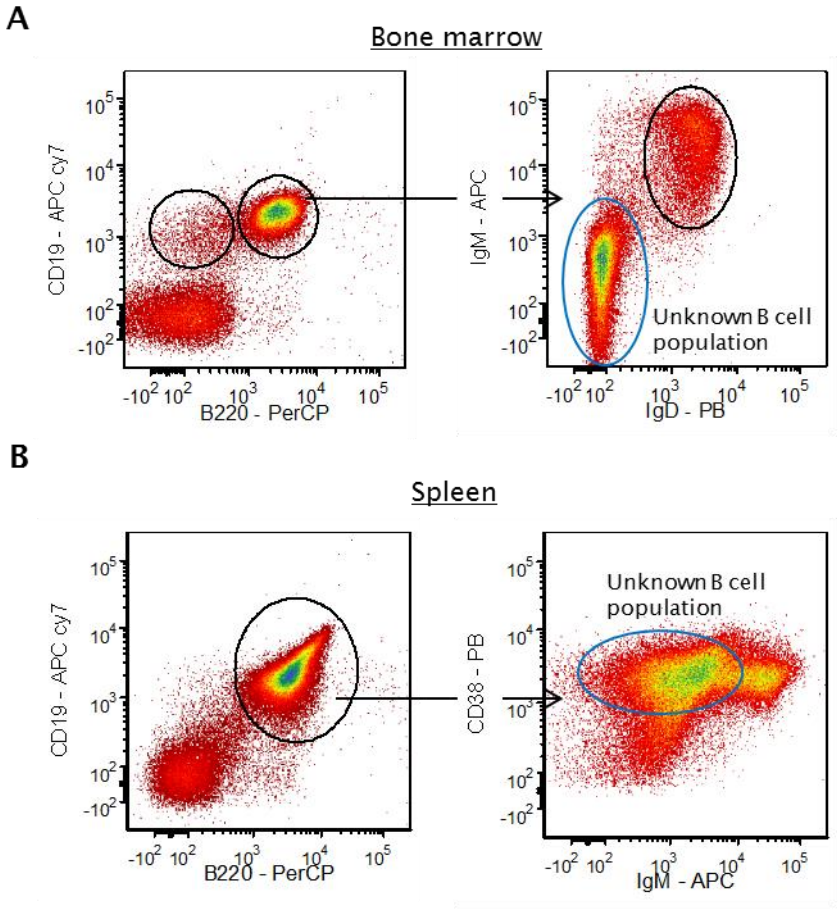

Figure 5-20 Identification of a dysregulated B cell population in Vav Bcl-2 mice

Representative density plots from a Vav Bcl-2 mouse from spleen and bone marrow tissue. Splenocytes were opsonised with an antibody cocktail containing CD19, B220, CD21, CD23, CD38, IgM (1 µl) and FcγRIIb (10 µg/ml). BM was opsonised with and antibody cocktail containing CD19, B220, IgM, IgD, CD43 (1 µl) and FcγRIIb (10 µg/ml). An unknown B cell population was identified as being B220 high, CD38 positive and IgM/IgD negative.

From **Figure 5-21** it can be seen that, in terms of total cell number, there are vastly more B cells in the Vav Bcl-2 mice compared to WT controls and that this is true for each B cell subset investigated. However, proportionally the percentages of T1, and germinal centre B cells remain the same between WT and Vav Bcl-2 mice and in fact there is a decrease in the percentage of MZ and T2/Follicular B cells. With regards to the BM interestingly there were similar numbers and percentages of early stage pro/pre, immature and mature B cells between WT and Vav Bcl-2 mice. Again Vav Bcl-2 mice displayed high levels of B220 high, CD38 positive and IgM/IgD negative B cell population in the BM. Additional analysis revealed that this unknown B cell population does not express CD138 indicating that they are not memory B cells but they are likely class switched indicated by being kappa chain positive but IgM negative (data not shown).

From these results it became apparent that the massive lymphadenopathy seen in the Vav Bcl-2 mouse largely results from late stage T2/follicular B cells as well as the ill-defined dysregulated B cell population with looks to be the source of elevated levels of FcγRIIb. Interestingly early stage B cells found in the bone marrow did not appear to be increased in number and expressed high levels, equivalent to this unknown B cell population, of FcγRIIb.

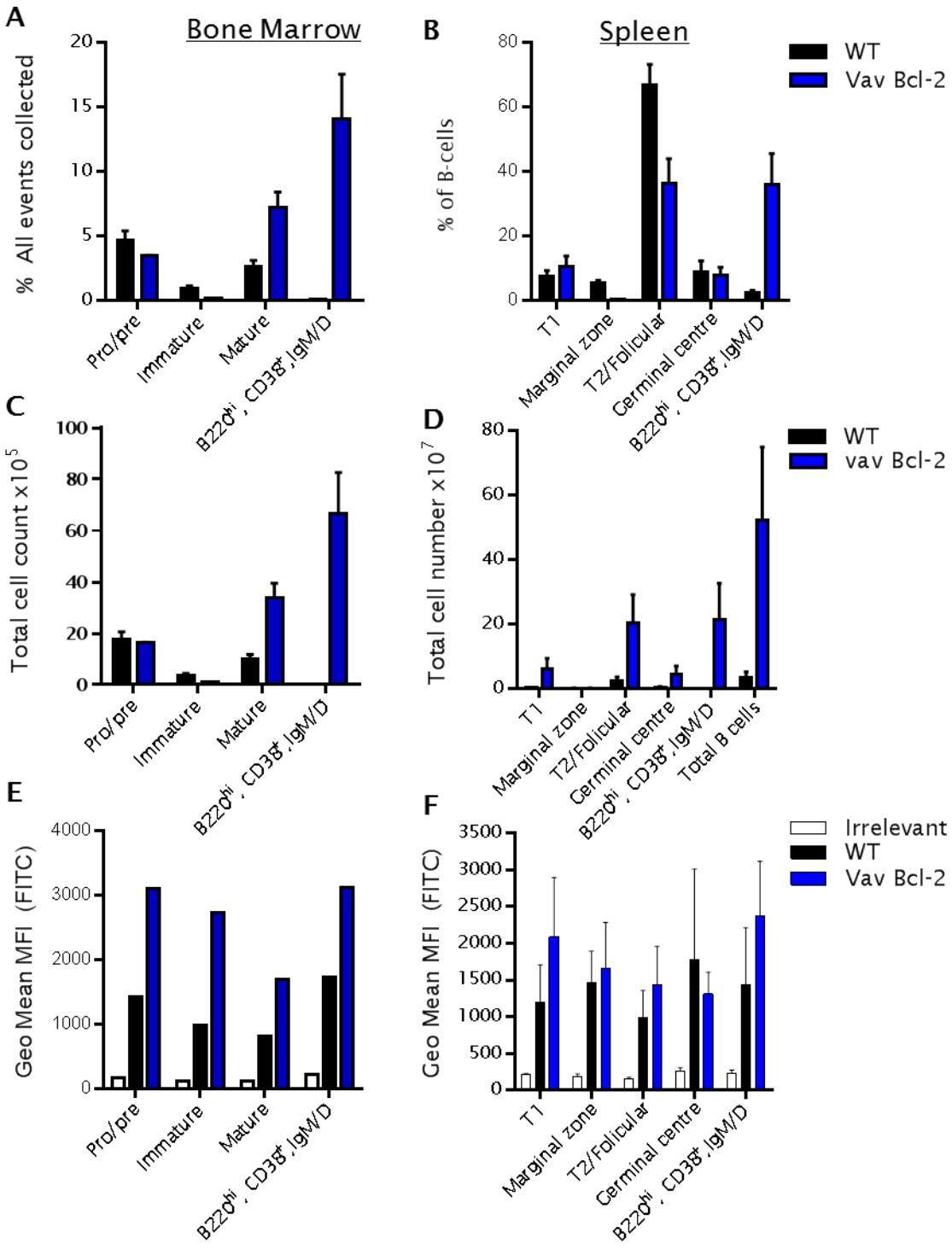

Figure 5-21 Analysis of B cell subsets in the Vav Bcl-2 mouse

Splenocytes and BM were harvested from C57BL/6 WT and Vav Bcl-2 mice. Cells ($1x10^6$) were stained with antibody as described in **Figure 5-18** and **Figure 5-19**. Samples were incubated for 30 minutes on ice. Red blood cells were lysed and samples were acquired on a FACS Canto™ II flow cytometer. N=3 +/-SD.

5.7 The impact of blocking mouse FcγRIIb on phagocytic potential in Vav Bcl-2 mice

The final set of experiments from this chapter were aimed at elucidating what effect the higher FcγRIIb expression in the myeloid compartment might have on depleting capacity in response to anti-CD20 antibodies. Recent work has demonstrated the therapeutic effect of blocking FcγRIIb on effector cells. Here, work by Roghanian *et al* found that antibody directed against FcγRIIb prevented internalisation of rituximab, resulting in enhanced antibody effector mechanisms. Also, it was found that anti-FcγRIIb antibody acted as an additional opsonin to further improve ADCC/ADCP mechanisms [250]. Based on these findings adoptive transfer experiments were performed which involved blocking inhibitory FcγRIIb on effector cells. In these experiments C57BL/6 Vav Bcl-2 or WT mice received a 1:1 mixture of CFSE stained hCD20 x FcγRIIb $^{-/-}$ target and FcγRIIb $^{-/-}$ non-target splenocytes, FcγRIIb$^{-/-}$ material was used to avoid any interactions that the FcγRIIb blocking antibody may have against target and non-target splenocytes. The following morning mice were injected with deglycosylated anti-mouse FcγRIIb (AT130-5) mAb. This antibody has been reported to be specific for FcγRIIb and to block immune complex binding [258]. Deglycosylated antibody was used to avoid any cis binding on multiple FcγR expressing effector cells and to avoid isotype binding on adoptively transferred target and non-target splenocytes. The impact of blocking FcγRIIb in the Vav Bcl-2 mouse became evident when administering anti-CD20 antibody (**Figure 5-22**).

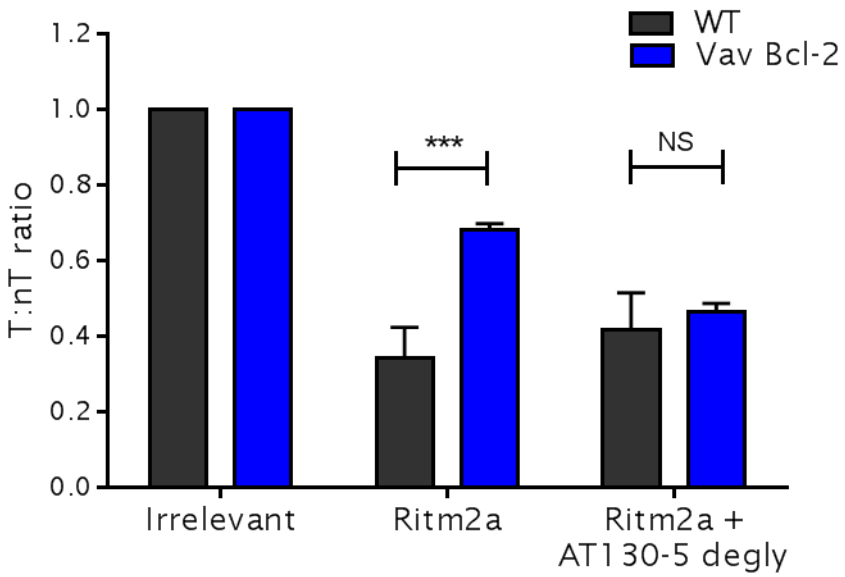

Figure 5-22 Adoptive transfer assay blocking mouse FcγRIIb in Vav Bcl-2 mice

Adoptive transfers were performed in C57BL/6 WT and Vav Bcl-2 mice. T:nT splenocytes were harvested from hCD20 x FcγRIIb$^{-/-}$ and FcγRIIb$^{-/-}$ mice respectively. Splenocytes were CFSE stained (5 μM), mixed 1:1 and injected (5x10^{6} cells) i.v. into recipient WT or Vav Bcl-2 mice. The following morning mice were injected i.p. with a deglycosylated version of AT130-5 (400 μg) ~3 hours before injection, i.v. of Ritm2a (50 μg). The following day splenocytes were harvested and stained with anti-CD19-APC (2.5 μl) on ice for 30 minutes. Red blood cells were lysed and samples were acquired on a FACS Canto™ II flow cytometer. N=3 +/-SD. Statistical analysis performed using two-way ANOVA.

From **Figure 5-22** it can be seen that WT mice when given Ritm2a depleted B cells to a T:nT ratio of 0.4 whereas Vav Bcl-2 mice showed significantly reduced ability to deplete B cells. In contrast when WT and Vav Bcl-2 mice were treated with AT130-5 prior to treatment with Ritm2a both mice were readily able to deplete target B cells to a similar level seen in the WT mouse treated with Ritm2a alone.

Next, to determine the effect of systemic loss of FcγRIIb on the Vav Bcl-2 mouse C57BL/6 Vav Bcl-2 mice were crossed onto a C57BL/6 FcγRIIb$^{-/-}$ background. The resulting offspring had no detectable FcγRIIb on endogenous B cells or effector cells. Adoptive transfer experiments were then performed whereby FcγRIIb expressing target and non-target splenocytes were adoptively

transferred into FcγRIIb$^{-/-}$ x Vav Bcl-2 mice and B cell depletion assessed following treatment with Ritm2a (**Figure 5-23a**).

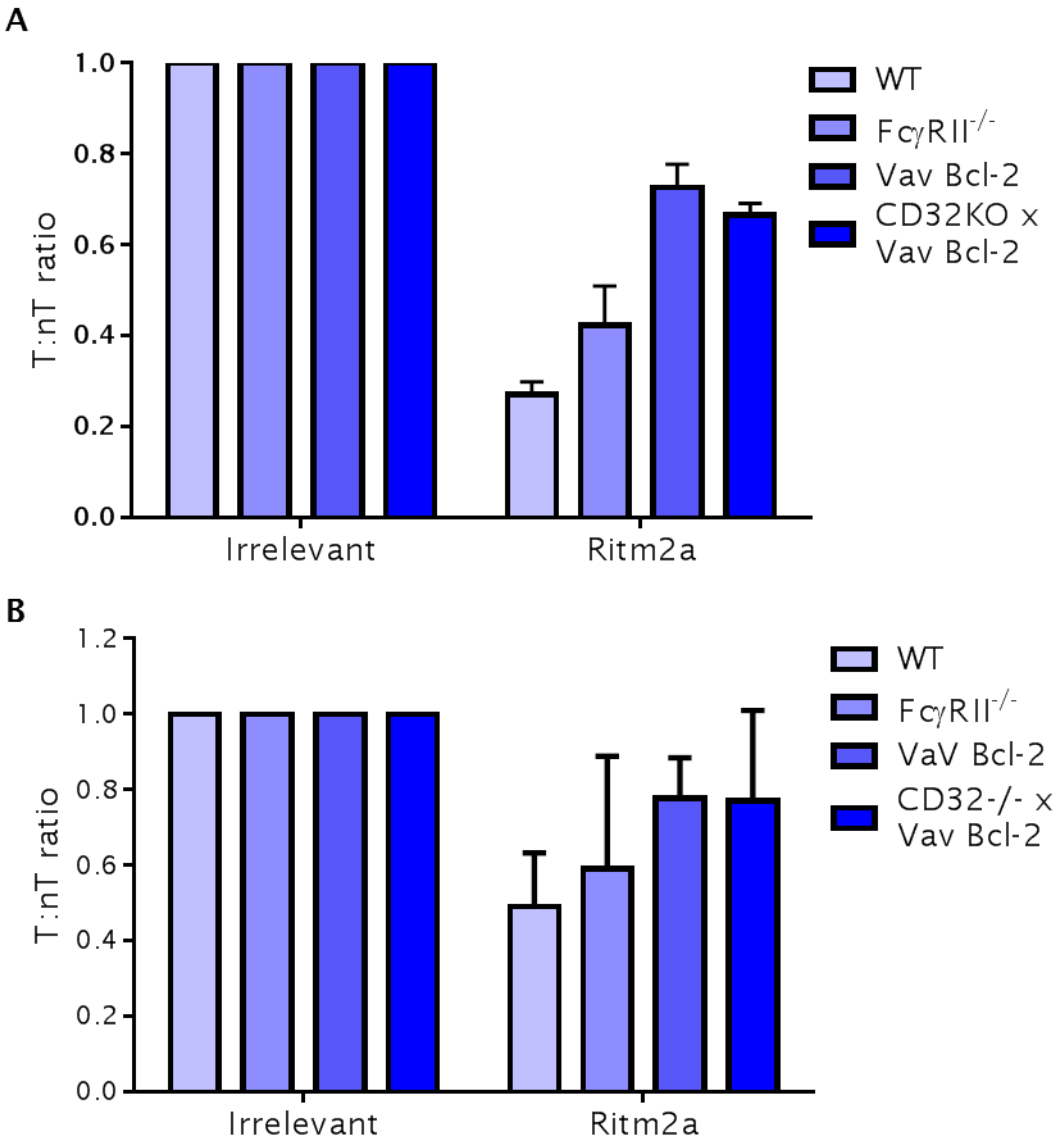

Figure 5-23 Adoptive transfer experiments using FcγRIIb$^{-/-}$ x Vav Bcl-2 mice

Adoptive transfers were performed in C57BL/6 WT, Vav Bcl-2, FcγRIIb$^{-/-}$ and FcγRIIb$^{-/-}$ x Vav Bcl-2 mice. (**A**) T:nT splenocytes were harvested from hCD20 and WT mice respectively. Splenocytes were CFSE stained (5 μM), mixed 1:1 and injected (5x10^6 cells) i.v. into recipient WT or Vav Bcl-2 mice. The following day mice were injected i.v. with Ritm2a (50 μg). The following day splenocytes were harvested and stained with anti-CD19-APC (2.5 μl) on ice for 30 minutes. Red blood cells were lysed and samples were acquired on a FACS Canto™ II flow cytometer. (**B**) Experiments were performed as in **A**, however, T:nT splenocytes were harvested from hCD20 x FcγRIIb$^{-/-}$ and FcγRIIb$^{-/-}$ mice respectively N=3 +/-SD.

From **Figure 5-23a** it can be seen that in contrast to the results seen in **Figure 5-22** the systemic depletion of FcγRIIb in the Vav Bcl-2 mouse did not result in an improved ability to deplete B cells in response to Ritm2a. Since in **Figure 5-23a** mice received FcγRIIb expressing target and non-target cells these differences could have been due to antigenic modulation occurring on the adoptively transferred material. To address this problem similar experiments to those shown in **Figure 5-23a** were performed however this time recipient mice received target and non-target cells which did not express FcγRIIb (**Figure 5-23b**). Again, from **Figure 5-23b** it can be seen that depletion of FcγRIIb in the Vav Bcl-2 mouse did not result in enhanced B cell depletion compared to the FcγRIIb expressing Vav Bcl-2 mouse. These results are conflicting with those presented in **Figure 5-22** and future experiments should look to explain these differences.

5.8 Chapter discussion

This chapter was designed to investigate whether rates of apoptosis could effect antibody therapy. Using three different mouse strains WT, Vav Bcl-2 and Eμ Myc, it was shown that Vav Bcl-2 mice have an inability to deplete B cells in the context of our adoptive transfer assays and systemic mouse experiments. Beers *et al* found that this was likely down to the effector components of the mouse since adoptively transferred Vav Bcl-2 x hCD20 B cells could be effectively depleted by WT mice [122].

Since it is well documented that Vav Bcl-2 mice have an increased cellularity [202] there is the potential that the increased numbers of B cell require higher doses of anti-CD20 mAb to see depletion. However, in our adoptive transfer assay only the target cells will be recognised by anti-human CD20 antibody, also, work by Beers *et al* has demonstrated that Ritm2a doses as low as 1 μg will effectively deplete target B cells in these assays [122]. The standard dose used in our adoptive transfer assays is 10 μg, although, future experiments should look to determine if doses greater than this will allow for B cell depletion in the Vav Bcl-2 mouse. Antigenic modulation was another possible cause for the B cell depletion defect seen in **Figure 5-3**. However we have ruled this out as a mechanism since type II antibody OBZm2a which does not undertake antigenic modulation to the same extent as the type I antibody Ritm2a also showed an inability to facilitate B cell depletion in the Vav Bcl-2 mouse when used in long term systemic depletions at a relatively high concentration (50 μg). Also, experiments looking into the detrimental effects of antigenic modulation found that B cells from WT or Vav Bcl-2 mice showed the same levels of antigenic modulation *in vitro*. These experiments appear to rule out antigenic modulation as the cause for the defective B cell depletion seen in the Vav Bcl-2 mouse. However, these antigenic modulation experiments did not take into account the enhanced cellularity seen in the Vav Bcl-2 mouse. Therefore, future experiments should aim to look at the levels of antigenic modulation and antibody consumption *in vivo*, perhaps indirectly by assessing the level of anti-CD20 mAb of Vav Bcl-2 mice by ELISA.

There is a large body of work demonstrating that FcγR mediated mechanisms are critical to effective mAb therapy [95, 110]. Furthermore, in response to mAb therapy, macrophages have been implicated as an important effector cell

population [135, 136]. Macrophages express multiple activatory and the inhibitory FcγR and the expression profile of FcγR will change depending on whether macrophages have been polarised to a classically activated M1 phenotype or alternatively activated M2 phenotype. The changed FcγR expression will result in an altered A:I ratio and this will effect the macrophages ability to phagocytose mAb opsonised targets. Therefore, if macrophages from Vav Bcl-2 mice had an inability to become polarised to an M1 phenotype this would partially explain their inability to deplete anti-CD20 opsonised B cells.

To investigate whether macrophages from apoptosis dysregulated mice had an inability to become polarised or to phagocytose anti-CD20 opsonised targets BMDMs were cultured from WT, Vav Bcl-2 and Eμ Myc mice and were assessed for their ability to undertake phagocytosis and become polarised *in vitro*. It was demonstrated that Vav Bcl-2 and Eμ Myc effector cells are capable of phagocytosis and at being polarised to an M1 or M2 phenotype therefore the defects in B cell depletion seen in the Vav Bcl-2 mouse are likely not due to an inherent defect in the macrophages of these mice. It was interesting to see that M2 polarisation was capable of enhancing phagocytosis to 60 % compared to baseline levels of 40 %. In contrast M2 polarisation only reduced phagocytosis by 5-10 %. The reason for this may be that M-CSF found in the L929 supernatant is polarising macrophages to an M2 like phenotype [264-266] and this may make results harder to interpret.

Since no inherent defect was found in the macrophages of apoptosis dysregulated mice the effect of exposure to apoptotic or non-apoptotic material was investigated. It was found that co-culture of BMDMs with highly apoptotic or apoptosis resistant material both resulted in slightly reduced levels of phagocytosis compared to the WT control. Un-expectantly, when BMDMs were co-cultured with the serum from apoptosis dysregulated mice there was an apparent increase in the level of phagocytosis compared to non-treated and BMDMs treated with WT serum. This result would merit further investigation but does not explain the B cell depletion defect.

Recent work has identified the BM as an area of low therapeutic IgG activity. In these studies Lux *et al* 2014 used humanised FcγR mice to show the level of B cell depletion varied greatly depending on anatomical location. Whereas B cells

in the spleen and periphery were readily depleted a great deal more antibody was needed to deplete targets in the BM [267]. Furthermore, this looked to be independent of the amount of CD20 expressed and mAb bound by the targeted B cells. This highlighted the BM as a niche with low therapeutic activity. Based on these results it would be interesting to examine the levels of B cell depletion in other anatomical compartments of the Vav Bcl-2 mouse, namely the blood, liver and BM and this could be achieved using adoptive transfer studies.

Over expression of Bcl-2 in the B cells of Vav Bcl-2 mice will lead to the survival and accumulation of B cells which otherwise would have undergone apoptosis and have been removed from the system. Some of these B cells will have had the potential to become autoreactive and it has been documented that Vav bcl-2 mice do show some autoimmune like symptoms [268]. Interestingly, Fukuyama, Nimmerjahn and Ravetch demonstrated that FcγRIIb modulates autoimmunity by limiting the accumulation of auto reactive B cells. Here they found that deletion of FcγRIIb in C57BL/6 mice resulted in an increase in anti-DNA, autoreactive, B cells. Typically FcγRIIb on B cells will limit the BCRs activatory response when these receptors are cross-linked together, as in the case of immune complex binding. To this end it was hypothesised that Vav Bcl-2 mice may have elevated levels of FcγRIIb on the B cell surface and so immunophenotyping studies were undertaken to assess the levels of FcγRIIb on key lymphocyte and granulocyte populations and what impact this would have on the A:I ratio. It was found that there were increased levels of FcγRIIb on B cells. This increased expression of FcγRIIb on B cells may be a mechanism by which B cells are limiting the accumulation and activation of autoreactive B cells. Interestingly, there was also an increase in FcγRIIb on monocytes and macrophages which resulted in these cells having a lower A:I ratio compared to the WT mouse. This lower A:I ratio would help explain the B cell depletion defect seen in the Vav Bcl-2 mouse. Lawlor *et al* found that Vav Bcl-2 mice rather than having a more aggressive response to serum transfer models of RA were in fact protected. This protection was attributed to an overexpression of FcγRIIb in the myeloid compartment of the mouse and so these results support those of our own [199].

After demonstrating that Vav Bcl-2 mice have increased levels of FcγRIIb on monocytes and macrophages we looked into the therapeutic potential of

blocking this inhibitory receptor. Adoptive transfer studies in figure **Figure 5-22** showed that blocking FcγRIIb in the Vav Bcl-2 mouse using a deglycosylated anti-FcγRIIb antibody (AT130-5) gave some therapeutic benefit. This suggested that elevated levels of FcγRIIb on monocytes and macrophages are responsible for the decreased B cell depletion seen in the vav bcl-2 mouse. However, the importance of antigenic modulation and/or abrogated phagocytosis still need to be clarified and future work should aim to investigate these mechanisms in the Vav Bcl-2 mouse. Since obinutuzumab is unaffected by antigenic modulation but still shows an inability to deplete B cells in the vav bcl-2 mouse it would suggest that defective phagocytosis is the key mechanisms being effected. However to further clarify the dominance of each mechanism, consumption of antibody in the WT compared to the vav bcl-2 mouse need to be ascertained.

The recent findings by Roghanian *et al* demonstrated that blocking FcγRIIb on the target B cell improved therapy by not only reducing antigenic modulation but also acting as an additional opsonin [250]. These studied demonstrate that the use of FcγRIIb blocking antibodies could also block FcγRIIb on the effector cells thus altering the A:I ratio and making effector cells more phagocytic. However, as demonstrated in chapter 4 the use of FcγR blocking antibodies with functional Fc regions may bind to and block activatory FcγR on multiple FcγR expressing cells and so the benefit of FcγRIIb blocking antibodies acting as an additional target vs. the potential problem of cross-blocking on effector cells should be further investigated.

To further confirm that the loss of FcγRIIb on effector cells would result in an improved ability to deplete target B cells the C57BL/6 Vav Bcl-2 mouse was crossed onto an FcγRIIb$^{-/-}$ background and the ability of these mice to deplete B cells was investigated. Surprisingly, it was found that these mice did not have any improvement in their ability to deplete anti-CD20 opsonised B cells. Future experiments should investigate this contradiction as it may be that the loss of FcγRIIb in these mice has led to a break in B cell tolerance, leading to more circulating immune complex which is blocking activatory FcγR. Alternatively it may be that the levels of activatory FcγR have been modulated on effector cells to compensate for the loss of FcγRIIb.

Chapter 6: The impact of immune complex on ADCP

6.1 Introduction

The results from chapter 5 reveal that the Vav Bcl-2 mouse has defective anti-CD20 mAb mediated B cell clearance and this may be in part due to dysregulated B cell development and enhanced FcγRIIb expression by myeloid effector cells. The Vav Bcl-2 mouse was developed as a model of follicular lymphoma [201, 202] however, these mice also display a tendency to develop autoimmune like symptoms and some succumb to kidney disease which has the histologic appearance of autoimmune glomerulonephritis [202]. It has also been documented that Eμ Bcl-2 mice can develop a similar lupus-like glomerulonephritis, indicating that this auto-immune disease is specifically due to dysregulated apoptosis [268]. Dysregulated B cell function and a break in tolerance are hallmarks of autoimmune disease such as systemic lupus erythromysis (SLE). Therefore Vav Bcl-2 mice can also be considered as a model showing SLE like symptoms. Patients suffering from autoimmune disease such as SLE will typically have high levels of circulating IgG and immune complex due to inappropriate B cell activation and proliferation [269].

SLE is an unpredictable disease with various origins and the typical treatment is the use of glucocorticosteroids and hydroxychloroquine but these treatments have undesired immunosuppressive side effects and safety concerns [270]. As a result, the B cell depleting capacity of rituximab has been investigated as a means to treat autoimmune conditions such as SLE but has thus far met with limited success. To date there have been two major trials investigating the use of rituximab in the treatment of SLE both of which concluded that there was no overall improvement in clinical symptoms [271, 272]. Interestingly the use of another monoclonal antibody, belimumab, has received clinical success in the treatment of SLE [273, 274]. Belimumab is not a depleting mAb but rather binds to soluble BAFF thus preventing it from interacting with its desired receptor on the B cell surface, BAFF-R [275]. As discussed in chapter 1 BAFF is involved in B cell survival and can regulate apoptosis of antibody secreting B cells. High levels of BAFF will reduce the threshold for B cell survival by

modulating levels of Bcl-2 protein, leading to an accumulation of autoreactive B cells. A similar situation is likely observed in the Vav Bcl-2 mouse, independently of BAFF, whereby forced expression of Bcl-2 will lead to a break in tolerance and accumulation of autoreactive B cells.

Insightful work by Ahuja *et al* 2011 picked up on the observation that rituximab, which is dependent upon Fc:FcγR showed limited success in autoimmune patients whereas depletion of B cells indirectly through use of belimumab did show clinical efficacy in the treatment of SLE. In these studies they found that serial transfer of serum from autoimmune MRL mice, which show a spontaneous SLE like phenotype, conferred a block in B cell clearance following anti-CD20 antibody therapy [276]. Here, by separating IgG and non-IgG components using a protein-G column they demonstrated that the active component inhibiting B cell depletion was serum IgG and that there was a block in mAb mediated ADCP mechanisms [276]. Further to this, recent investigations have revealed that mice persistently infected with virus exhibit a severe defect in FcγR mediated antibody effector mechanisms and that this was due to circulating immune complex [277, 278].

In this chapter, with relation to the Vav Bcl-2 mouse, investigations were made into the role that immune complexes play in the ability to modulate ADCP effector function. We demonstrate, using IgG ELISA, that Vav Bcl-2 mice display elevated levels of IgG in the serum and that heat aggregated IgG in the form of immune complex will specifically block the ability of BMDMs to undertake ADCP of anti-CD20 mAb opsonised B cells.

6.2 Apoptosis dysregulated Vav Bcl-2 mice have increased levels of circulating IgG

From the literature it appears that IgG and/or circulating immune complex block FcγR-mediated mechanisms [277, 278]. Therefore, since Vav Bcl-2 mice display a phenotype similar to that of SLE it was hypothesised that B cell depletion defects seen in the Vav Bcl-2 mouse might arise in part due to elevated levels of IgG and/or immune complex blocking activatory FcγRs. To investigate this hypothesis the circulating levels of total mouse IgG were measured by ELISA and compared to that of the congenic C57BL/6 WT mouse (**Figure 6-1**). Vav Bcl-2 mice and their aged matched litter mates were periodically bled between 5 and 25 weeks of age and serum was collected. Typically 150 - 250 µl of blood could be collected from each mouse per time point. Total IgG was measured using a standard sandwich ELISA as described in materials and methods. To minimise variability, all time points for each mouse were run together on a single 96 well microtitire plate. Results were analysed using Readerfit™ which generated a standard curve based on the plate standard OD values, then, using a non-weighted 4-paramater log fit curve test value OD was transformed into the resulting concentration (µg/ml). Microsoft Excel was used to multiply the resulting test value by its dilution factor. Upper and lower cut off points were determined by eye based upon where test values fell upon the standard curve, those falling within the linear range were accepted where as those falling into the upper or lower cut off points were rejected. The average of test values which fell within the linear region of the standard curve where then reported and displayed in GraphPad Prism software.

From **Figure 6-1c** it can be seen that from a very early age C57BL/6 Vav Bcl-2 mice display significantly ($P<0.0001$) elevated levels of total IgG. At 5 weeks of age these levels are at around 5 mg/ml, approximately 5 times greater than that of WT mice. By 10 weeks of age Vav Bcl-2 mice have even greater levels of IgG at ~ 10 mg/ml, around 10 times greater than that of WT mice. Total IgG levels in the Vav Bcl-2 mouse remained at 10 mg/ml until week 23 whereas total IgG levels in the WT mouse remained constant at around 1 mg/ml.

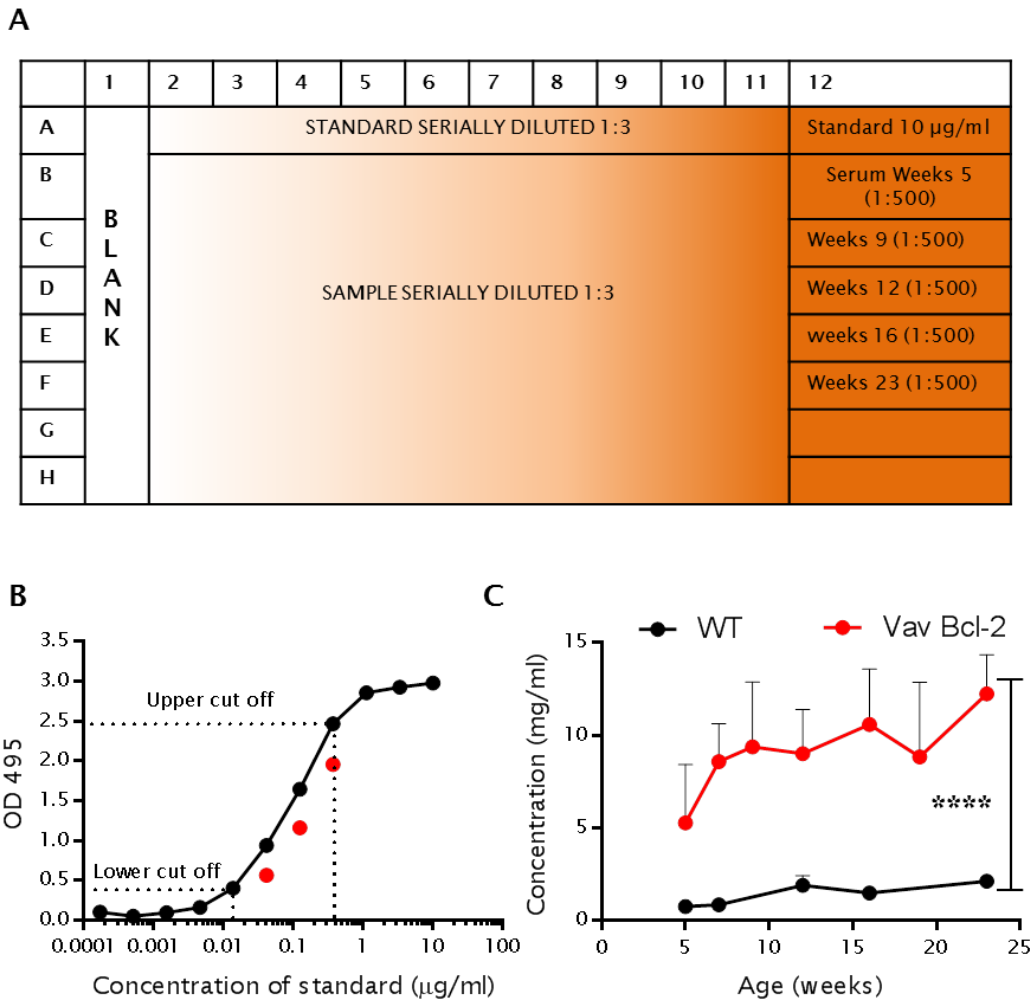

Figure 6-1 Immunoglobulin levels in Vav Bcl-2 mouse serum as measured by ELISA

(**A**) Typical 96 well microtitre plate layout highlighting how standards and samples were loaded. Standard at 10 µg/ml was loaded into well A12 and serially diluted 1:3 along the plate. Serum samples were diluted 1:500 and then loaded into wells B12-F12 these were then serially diluted 1:3 along the plate, column 1 was used to test background. (**B**) Typical analysis of results, standard curve was interpreted using Readerfit™ software and a 4-parameter log fit equation used to calculate test values. Manual upper and lower cut off values were used so that only test values reaching the linear part of the curve are reported. (**C**) Total levels of IgG were assayed for using WT and Vav Bcl-2 mouse serum, various weeks of age. Plates were coated with polyclonal Goat anti-mouse IgG (25 µg/ml) samples were detected using Goat anti-mouse IgG-HRP (1:4000). Samples were analysed using an EPOCH spectrophotometer (490 OD). N=4 +/- SD. Statistical analysis performed using two-way ANOVA.

It has been well documented that mouse IgG1 and IgG2a have different affinities for mouse FcγR [128]. Whereas IgG2a interacts with high affinity

towards mouse FcγRI and FcγRIV there is virtually no binding to these receptors when using a mouse IgG1 antibody. Therefore, since the mouse IgG isotype present in the mouse will have an effect on FcγR binding and interaction the amount of mouse IgG1, IgG2c and IgG2b in the Vav Bcl-2 mouse was analysed over time and compared to that of WT littermates (**Figure 6-2**).

Prior to this analysis the optimal concentrations and dilutions of primary and secondary antibody as well as the best standard concentrations and sample dilutions were investigated. Following optimisation, serum from **Figure 6-1** was analysed to detect levels of mouse IgG1, IgG2a or IgG2b. Standards were changed from polyclonal mouse IgG to a monoclonal antibody representing the isotype being tested. Results in **Figure 6-2** show that levels of all three IgG subclasses were significantly elevated in the Vav Bcl-2 mouse compared to WT littermates. However, it is apparent that the greatest increase was in IgG2c whereas in comparison the increase in mouse IgG1 was modest. Comparable to IgG2c the levels of IgG2b in the Vav Bcl-2 mouse also increased significantly from that of WT mice ($p<0.0001$). Overall the data shows that the increase in total IgG is largely down to an expansion of the IgG2c and IgG2b compartments.

Due to the observed ~10 fold increase in B cell number seen within the Vav Bcl-2 mouse [202] these results, perhaps unsurprisingly, demonstrate that there is also an ~10 fold increase in total circulating IgG. What is interesting is that this increase in total IgG predominantly comes from IgG2c and IgG2b compartments and this subclass has been shown to have high affinity for mouse FcγRI and FcγRIV [128]. Now that it had been ascertained that Vav Bcl-2 mice do show increased IgG levels it became important to determine how much if this IgG was in the form of immune complex.

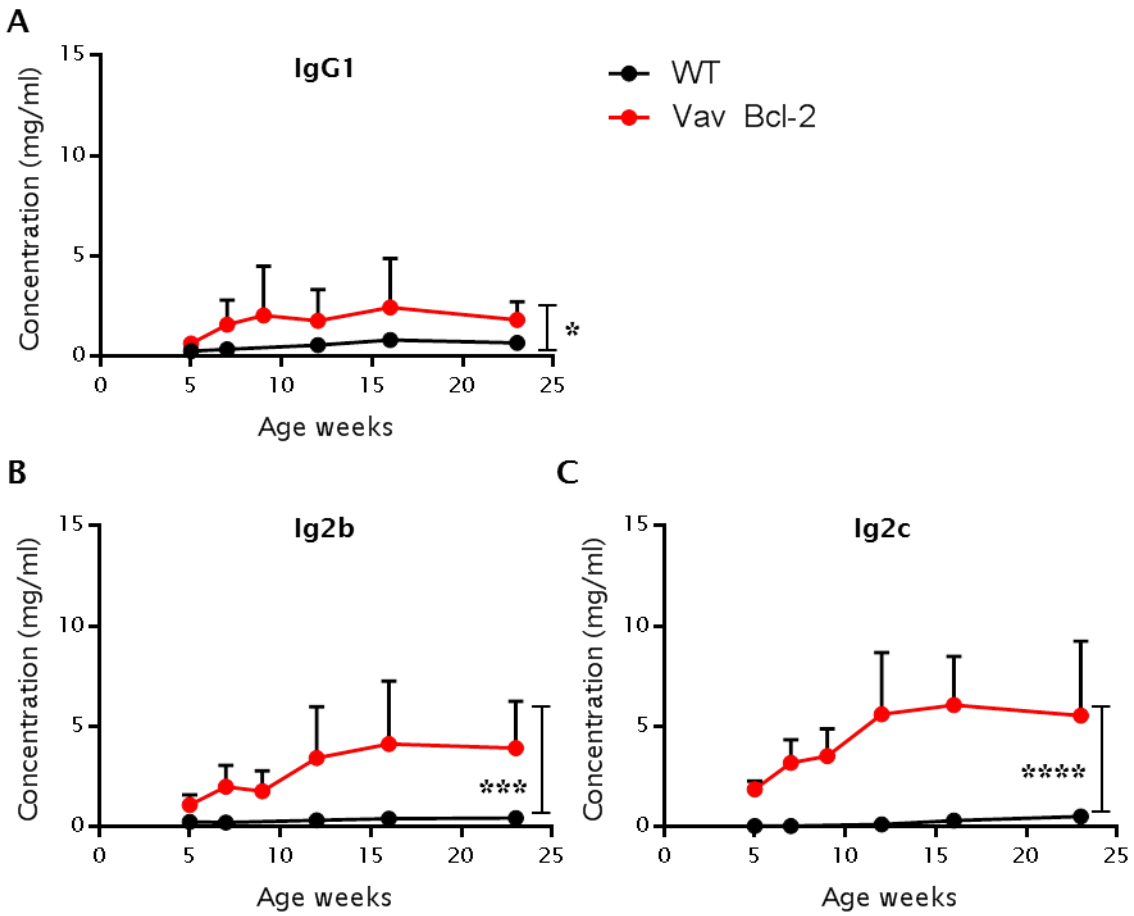

Figure 6-2 Immunoglobulin sub-class levels in Vav Bcl-2 mouse serum

IgG subclass levels were measured in WT and Vav Bcl-2 mouse serum using standard sandwich ELISA. (**A**) Mouse IgG1 levels were detected by coating a 96 well microtitre plate with goat anti-mouse IgG1 (2.5 µg/ml) antibody and detecting IgG1 levels using a goat anti-mouse IgG1-HRP antibody (1:10,000). As a standard the mouse IgG1 monoclonal antibody 3G8 was used at an initial concentration of 10 µg/ml. (**B**) Mouse IgG2b levels were detected by coating a 96 well microtitre plate with goat anti-mouse IgG2b (2.5 µg/ml) antibody and detecting IgG2b levels using a goat-anti mouse IgG2b-HRP antibody (1:10,000). As a standard the mouse IgG2b monoclonal antibody F2-2 was used at an initial concentration of 10 µg/ml. (**C**) Mouse IgG2c levels were detected by coating a 96 well microtitre plate with goat anti-mouse IgG2c (2.5 µg/ml) antibody and detecting IgG2c levels using a goat-anti mouse IgG2c-HRP antibody (1:10,000). As a standard the mouse IgG2c monoclonal antibody 18B12 was used at an initial concentration of 10 µg/ml. N=4 +/- SD. Statistical analysis was performed using two-way ANOVA.

6.2.1 Vav Bcl-2 mice do not show appreciable levels of immune complex

As Vav Bcl-2 mice display elevated levels of IgG, we hypothesised that this may lead to an increase in immune complex, capable of blocking Fc:FcγR interactions. Therefore to detect the presence of immune complex a C1q ELISA method was optimised for use. The C1q ELISA method was developed for use by Hunt *et al* in the 1980s, and involves coating a 96 well microtitre plate with C1q protein, probing with test serum then detecting immune complex binding with an anti-species IgG-HRP antibody [212]. Since monomeric IgG has low affinity for C1q ($K_D \sim 10^{-4}$ M) whereas immune complex has a greater affinity for C1q ($K_D \sim 10^{-8}$ M) only the aggregated components of the serum in the form of immune complex will bind to the coated C1q protein [213, 279, 280].

In order to optimise this assay for use a set of monomeric and aggregated immune complex standards were developed. Aggregated standard of a mouse IgG2a isotype were made through heat aggregation at 63 °C for 30 minutes followed by SEC [213, 281]. As can be seen from **Figure 6-3** the generation of immune complex was achieved by heating concentrated (>5 mg/ml) samples of mAb to 63 °C for 30 minutes. Samples were then successfully separated into their aggregated and monomeric fractions using SEC. The first peak in **Figure 6-3b** highlights the aggregated IgG fraction passing through the UV detector. Overall it takes about two hours for the aggregated fraction to be collected. This is followed by the monomeric IgG fraction about two hours later and again this takes around 1 ½ - 2 hours to be collected. In total the samples are run overnight for ~ 18 hours. The following morning all of the fractions containing aggregated sample were pooled and concentrated before being dialysed into PBS. This process of SEC was repeated for the monomeric IgG fractions. To confirm that fractions were indeed monomeric or aggregated, samples were subjected to HPLC analysis. Attempts were made to ascertain the size of the aggregated sample using HPLC and native PAGE gel analysis but these were unsuccessful due to the large size of aggregate. What was confirmed however is that aggregated samples were larger than IgM which is ~970 kDa.

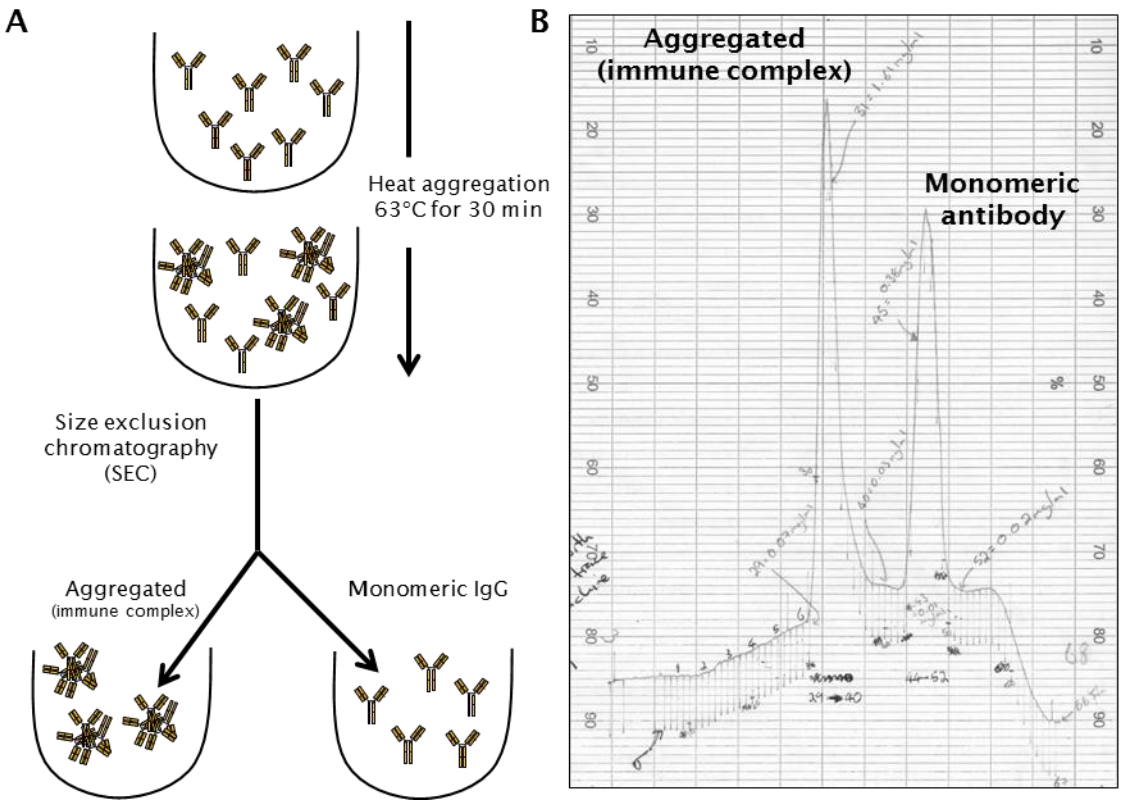

Figure 6-3 Generation of aggregated immune complex

(**A**) Schematic representation of how aggregated immune complex is generated from monoclonal antibody. Mouse IgG2a mAb (WR17) at a concentration of 5-10 mg/ml in PBS was heated to 63 °C and incubated for 30 minutes. Sample was then subjected to SEC, sample was passed through two superdex™ 200, 1.6 x 94.3 cm columns at a speed of 0.3 ml/min. the running buffer used was TE8. (**B**) Representative result following SEC, the first large peak contains the aggregated fractions of antibody and the smaller second peak contains the monomeric IgG fraction. Fractions were cut so as to contain the whole of the aggregated or monomeric peak. Samples were then concentrated and dialysed into PBS. Samples were stored long term at -20 °C, working stocks were kept at 4 °C to avoid freeze thawing.

Following the generation of aggregated and monomeric standards the C1q ELISA to detect immune complex in the serum of mice was undertaken. First, the ability to detect aggregated and monomeric IgG and the optimal dilution of secondary antibody was ascertained by serially diluting aggregated and monomeric antibody and then detecting bound immune complex using different dilutions of secondary Goat anti-mouse IgG-HRP antibody (**Figure 6-4**).

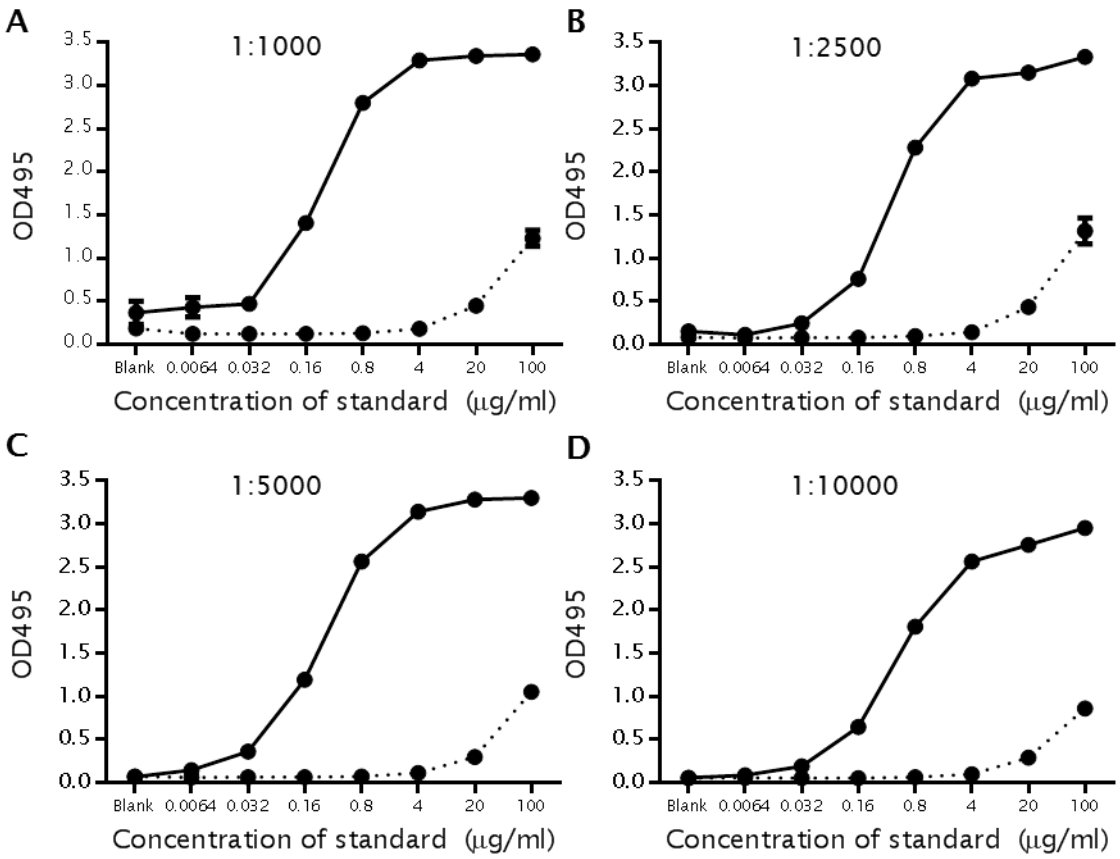

Figure 6-4 Detection of immune complex using a C1q ELISA assay

C1q ELISA was used to detect the level of immune complex in aggregated and monomeric IgG standards. Various dilutions of secondary goat anti-mouse IgG-HRP detection antibody were investigated. 96 well microtitre plates were coated overnight with C1q (1 µg/ml). Aggregated and monomeric standards (WR17) were added to pre coated ELISA plates (20 µg) at 100 µg/ml samples were than serially diluted 1:5 across the plate. Goat anti-mouse IgG-HRP detection antibody was used at various dilutions; (**A**) 1:1,000, (**B**) 1:2,500, (**C**) 1:5,000 and (**D**) 1:10,000 to determine the optimal dose response curve. Samples were incubated with secondary antibody for 90 minutes at RT. Samples were then washed and enzyme substrate added. Samples were incubated in the dark for 20 minutes (RT) and were then analysed by spectrophotometry at OD495.

From **Figure 6-4** it can be seen aggregated IgG was readily detected in this C1q ELISA assay, moreover a concentration of between 20 – 0.032µg/ml contained the linear part of the dose response curve, when coating ELISA plates with 1 µg/ml C1q. In contrast, monomeric IgG showed no response below 4 µg/ml. Beyond this concentration there was a slight response at 20 and 100 µg/ml but this background response was not near the saturating responses seen by aggregated IgG at these concentrations. With regards to the optimal dilution of

secondary goat anti-mouse IgG-HRP antibody there was little difference between using a 1:1,000 dilution or a 1:10,000 dilution therefore a 1:5,000 was taken forward for future experiments. It had now been determined that aggregated immune complex could be detected using this C1q ELISA assay and that monomeric antibody was not readily detectable. Next, the amount of immune complex in WT or Vav Bcl-2 mouse serum was investigated. Either WT or Vav Bcl-2 serum with a known amount of total IgG was probed for the level of immune complex. Further to this different dilutions of WT or apoptosis dysregulated mouse serum were assayed for the level of immune complex (**Figure 6-5**).

From **Figure 6-5** it can be seen that when WT or Vav Bcl-2 serum containing a known concentration of mouse IgG were assayed for immune complex there were no detectable levels. At all dilutions tested there was no response greater than that of the monomeric antibody control and no value was obtainable using the standard curve. Furthermore, when serum from WT or Vav Bcl-2 mice of unknown concentrations was used at various dilutions there was again no detection of immune complex. In contrast, artificially aggregated immune complex was readily detectable. Together this suggested that there are not elevated levels of immune complex in the Vav Bcl-2 mouse or at least these levels remain below 0.16 µg/ml. This data would also highlight that there are undetectable levels of immune complex circulating in the WT healthy murine blood.

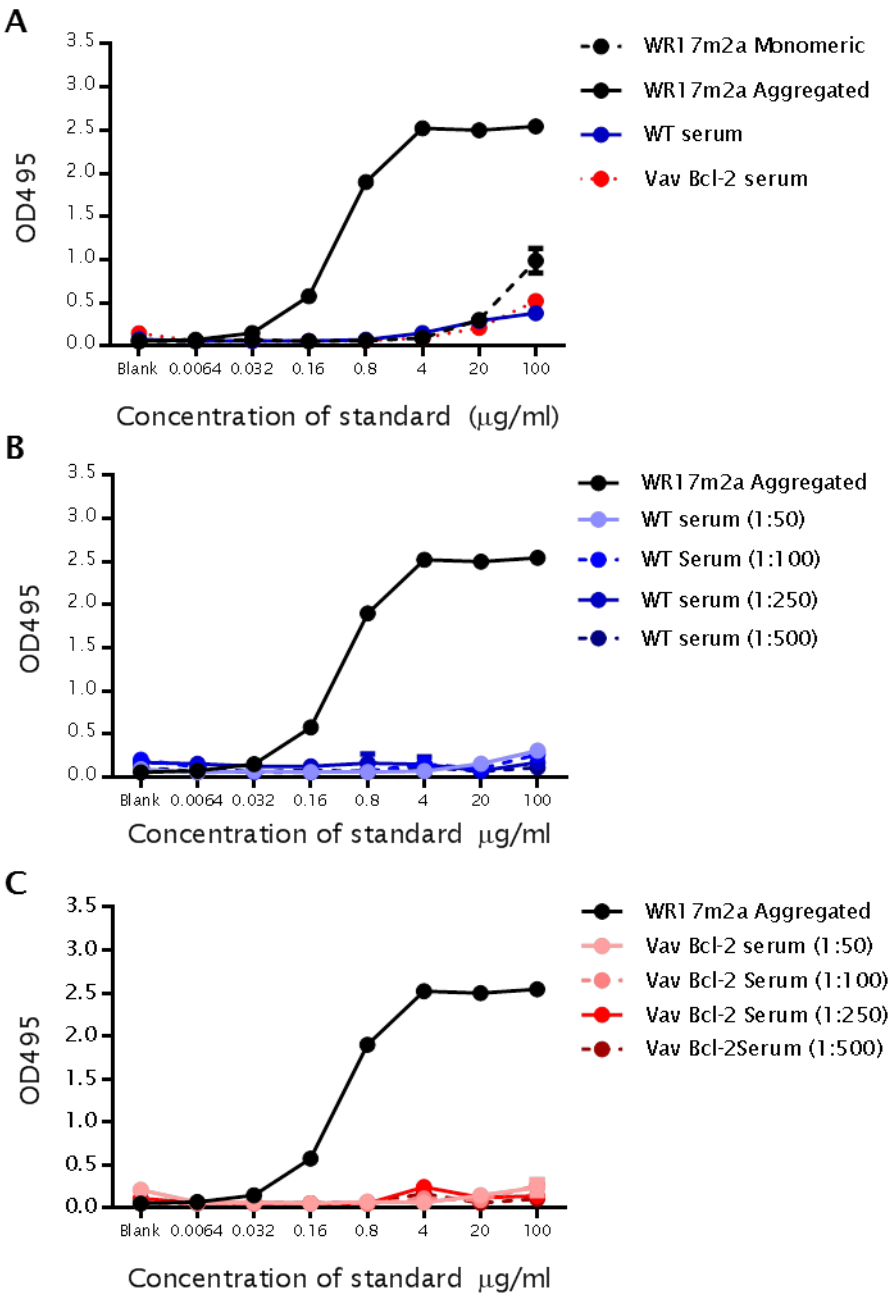

Figure 6-5 Detection of immune complex in WT and Vav Bcl-2 serum

Detection of immune complex was performed using C1q ELISA as described in **Figure 6-4**. Aggregated IgG (WR17m2a) was used as a standard and monomeric IgG (WR17) was used as a negative control (**A**) Serum from WT or Vav Bcl-2 mice was added to a 96 well microtitre plate, initially, at 500 µg/ml and serially diluted 1:3 across the plate. (**B-C**) WT or Vav Bcl-2 serum was added to a 96 well microtitre plate at various dilutions 1:50-1:500 and serially diluted across the plate (1:3).

It may be that factors such as C1q present in test serum have already bound immune complex and are preventing adequate detection in the serum. To test this hypothesis artificially aggregated IgG (WR17) was spiked into WT serum samples and the amount of detectable immune complex measured by ELISA. Therefore if C1q in the serum was neutralising immune complex detection in the assay then the levels of spiked immune complex would be lower than anticipated. It was also possible that the assay was not capable of detecting physiological IC. Previous publications have reported autoimmune MRL mice have circulating levels of immune complex therefore MRL mouse serum was also obtained and assayed for the levels of immune complex using this C1q ELISA format (**Figure 6-6**).

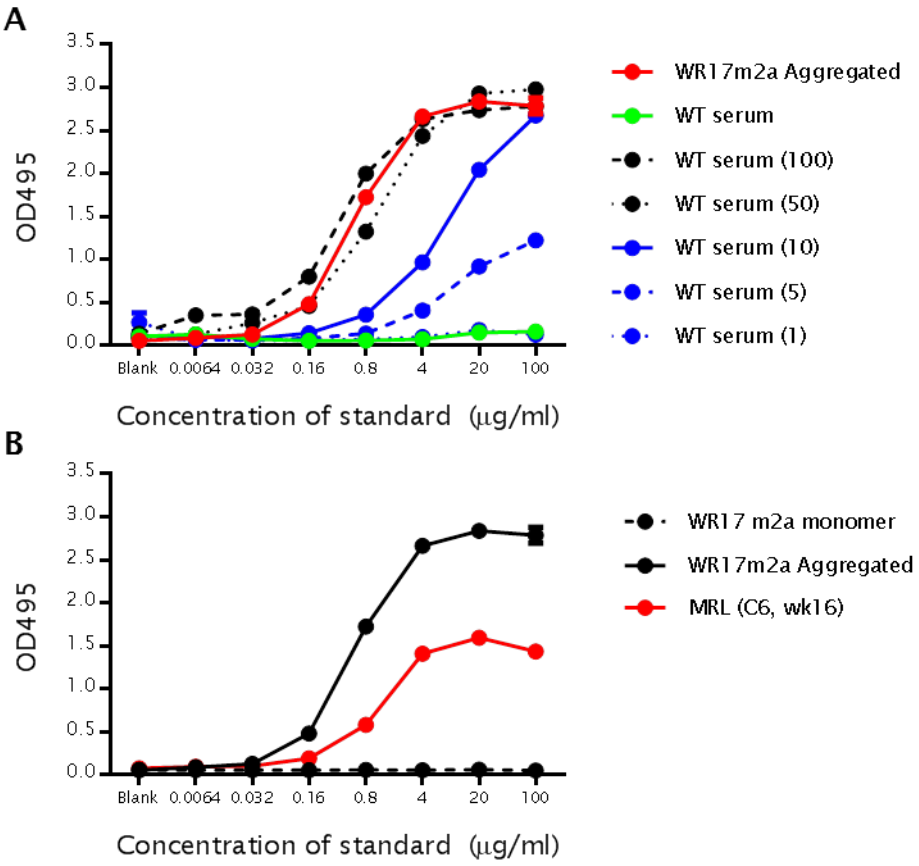

Figure 6-6 C1q ELISA to detect aggregated immune complex in mouse serum

Detection of immune complex was performed by C1q ELISA as described in **Figure 6-4** (**A**) Aggregated immune complex 1- 100 µg/ml (WR17) was spiked into WT C57BL/6 serum (**B**) MRL mouse serum was assayed for immune complex, starting dilution 1:50.

From **Figure 6-6** it can be seen that the aggregated IgG used to spike normal serum could be readily detected using this C1q ELISA format. Suggesting that C1q in the serum is not neutralising all of the immune complex present. Aggregated immune complex spiked into WT serum at 1 µg/ml were not detect by this assay suggesting that levels below this are not detectable using this ELISA format. Additionally, as it has been documented that autoimmune MRL mice have circulating immune complex we tested serum from these mice using the C1q ELISA format. It was found that Immune complex from these mice could be readily detected, demonstrating that this assay is capable of detecting physiological levels of immune complex. From these data it appeared that Vav Bcl-2 mice, although having higher levels of circulating IgG, do not have elevated levels of circulating immune complex.

6.3 Immune complex specifically block ADCP in vitro

It was hypothesised that Vav Bcl-2 mice which have an autoimmune like phenotype would display high levels of IgG and circulating immune complex. ELISA analysis revealed that these mice did indeed have high levels of circulating IgG and that this was specifically due to an increase in the IgG2c and IgG2b compartments. However, further analysis using a C1q ELISA revealed no detection of circulating immune complex in these mice. It has been previously documented that immune complex and the IgG compartment of autoimmune mice will inhibit ADCP effector mechanisms [276, 282]. Therefore, we next investigated the impact of aggregated and monomeric IgG on ADCP effector function. To do this BMDM of between 7-9 days old were co-cultured with various concentrations of either mouse IgG2a or IgG1 for 48 hours, so as to allow sufficient time for any polarising effects to take place. These BMDMs were then subjected to ADCP assays to determine the phagocytic response to anti-CD20 opsonised B cell targets (**Figure 6-7**).

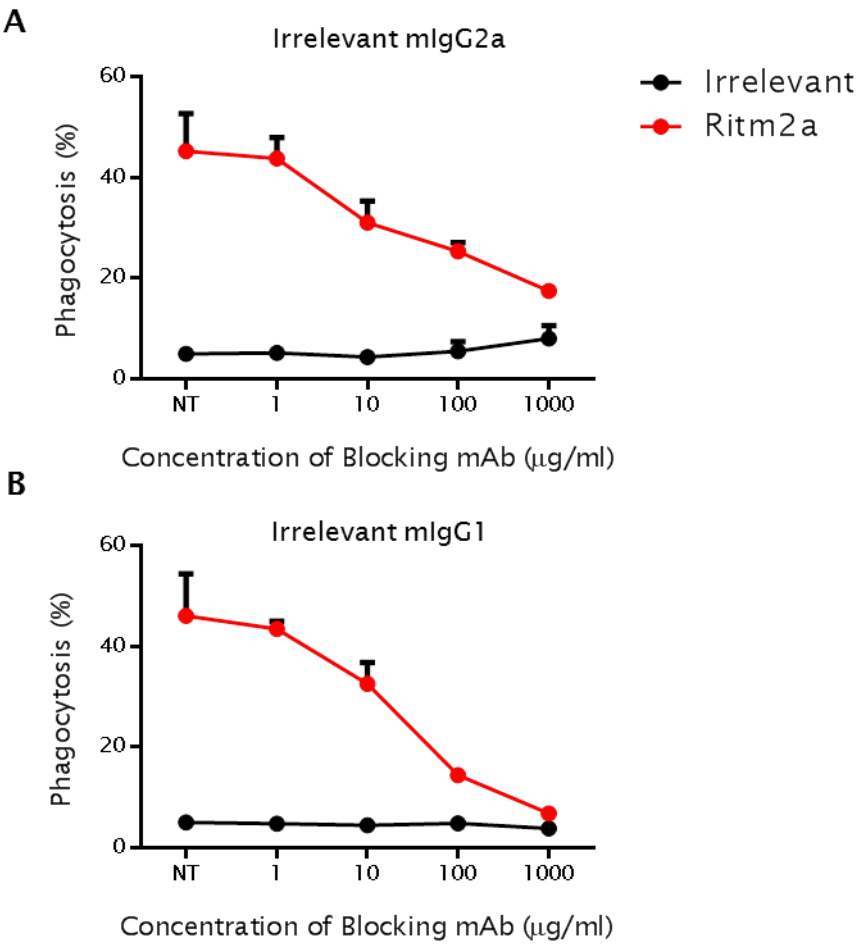

Figure 6-7 ADCP response to co-culture with irrelevant mAb

(**A**) C57BL/6 BMDMs (Day 7) were co-cultured with irrelevant mouse IgG2a (WR17) (1000-1 µg/ml) antibody for 48 hours at 37 °C (5 % CO_2). Target hCD20 B cells were isolated and stained with CFSE (5 µM). Target B cells ($2.5x10^6$) were opsonised with Ritm2a (10 µg/ml), then co-cultured with BMDMs ($5x10^4$ cells) for 30 minutes at 37 °C (5 % CO_2). Samples were then stained with F4/80-APC and then acquired on a FACS Calibre™ flow cytometer. (**B**) Samples were processed as in **A**, however, BMDMs were co-cultured for 48 hours with mouse IgG1irrelevant antibody (3G8). N=2 +/- SD.

From **Figure 6-7** it can be seen that irrelevant monoclonal antibodies of either a mouse IgG1 or IgG2a isotype are effective at blocking phagocytosis at high concentrations. For both mouse IgG1 and IgG2a antibodies, phagocytosis was inhibited at 10 µg/ml, severely inhibited at 100 µg/ml and completely blocked at 1 mg/ml. There was no difference in the level of phagocytosis when blocking with mouse IgG2a or mIgG1 antibodies.

From these experiments it appeared that high levels of monomeric antibody were indeed having a negative effect on ADCP. One possible cause for this may be that the preps of monoclonal antibody used may have had immune complex present. Therefore to test whether these differences in phagocytosis were due to monomeric antibody or were due to aggregated antibody, samples were subjected to HPLC analysis. Samples were analysed by HPLC prior to heat aggregation and following heat aggregation, but prior to SEC (**Figure 6-8**)

Figure 6-8 HPLC analysis of monoclonal antibody

Representative chart recording of irrelevant mouse IgG1 (3G8) antibody subjected to HPLC analysis before and after heat aggregation. Antibody was prepared at a concentration of 1.5 mg/ml in PBS and subjected to analysis by HPLC. Sample was then heat aggregated at 63 °C for 30 minutes. Sample was then again subjected to HPLC analysis.

From **Figure 6-8** it can be seen that mAb prior to heat aggregation show some small level of aggregate, which appears as a small peak/shoulder just before the large monomeric IgG peak. Following heat aggregation it can be seen that this aggregated peak has increased in size, although not to the same size as the monomeric peak and this may indicate that some of the larger aggregate is

not detectable by the column used and is lost in the void volume. Since it was apparent that there is some aggregate in the monomeric samples of IgG that were used in **Figure 6-7** investigations were made to better delineate the effects of monomeric and aggregated IgG on ADCP. Heat aggregated and re-purified monomeric fraction of mouse IgG2a and IgG1 antibody were therefore generated by SEC as previously described in **Figure 6-3** and these fractions were co-cultured with WT BMDM of between 7-9 days old. Following 48 hours co-culture ADCP assays were performed to assess the level of phagocytosis of hCD20 B cells in response to anti-CD20 antibody Ritm2a (**Figure 6-9**).

From **Figure 6-9** it can be seen that the aggregated fraction of IgG but not the monomeric fraction of IgG was inhibiting ADCP. With regards to both mouse IgG2a and IgG1there was no significant difference in the level of phagocytosis following co-culture with monomeric antibody at any of the concentrations tested. In contrast, the aggregated IgG2a fraction inhibited ADCP at concentrations as low as 1 µg/ml.

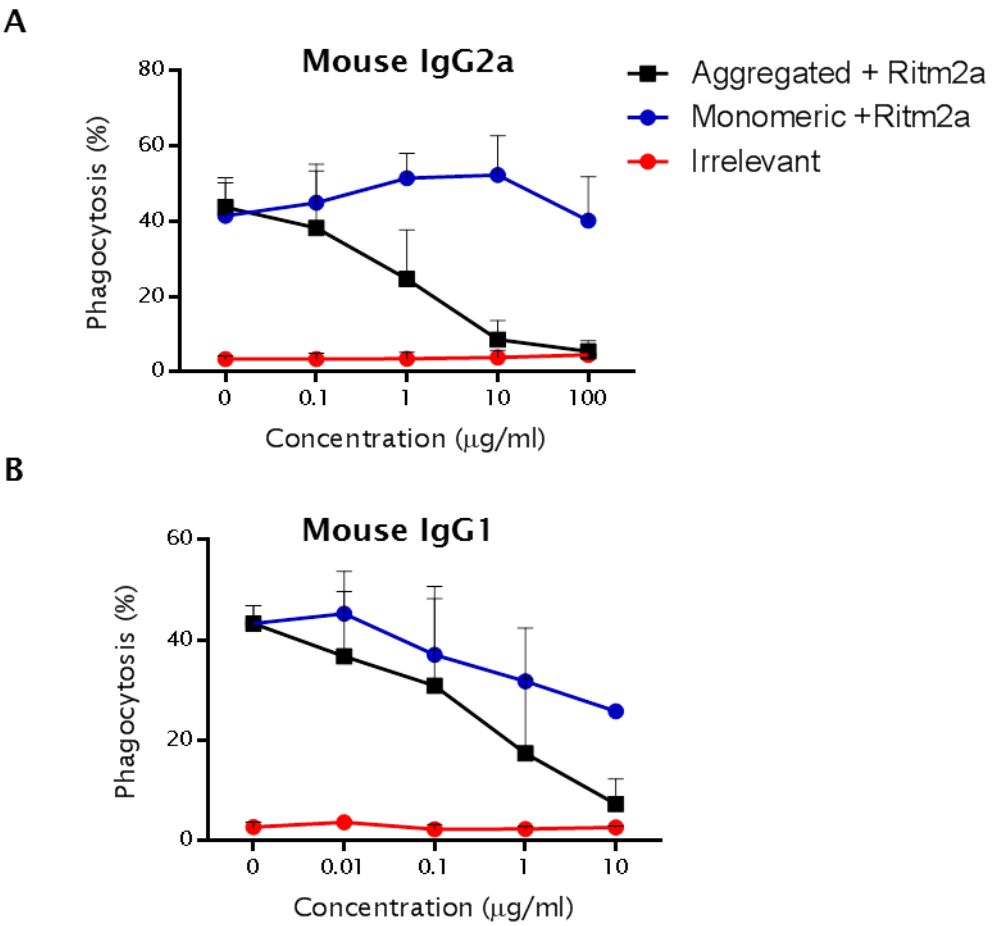

Figure 6-9 ADCP analysis in response to monomeric or aggregated IgG

Monoclonal antibodies of either a mouse IgG1 (3G8) or IgG2a (WR17m2a) were heat aggregated and the aggregated fraction was isolated based by SEC. Monomeric or aggregated mouse IgG2a or IgG1 fractions were co-cultured with BMDM at various concentrations for 48 hours prior to phagocytosis assays. Phagocytosis assays were performed as previously described, hCD20 Tg B cells were CFSE stained (5μM) and either irrelevant (WR17) or anti-CD20 (Ritm2a) (10 μg/ml) were used to deplete targets. N=3 +/- SD. Statistical analysis was performed using two-way ANOVA.

6.3.1 Does immune complex block or modulate FcγR expression

It was found that aggregated mouse IgG2a or IgG1 in the form of immune complex, but not monomeric, specifically inhibit phagocytosis. Next we wished to determine the mechanism of this inhibition. Experiments using either the monomeric or aggregated forms of antibody involved a long 48 hour co-culture with BMDM and therefore, it is unknown whether antibody is modulating the expression of FcγR or simply blocking Fc:FcγR interactions. To investigate whether modulation or blocking of FcγR occurs, BMDMs were incubated for 48 hours (modulating) or 30 minutes (blocking) with monomeric or aggregated IgG before ADCP assays looking at the ability to phagocytose hCD20 B cells opsonised with Ritm2a were performed (**Figure 6-10**).

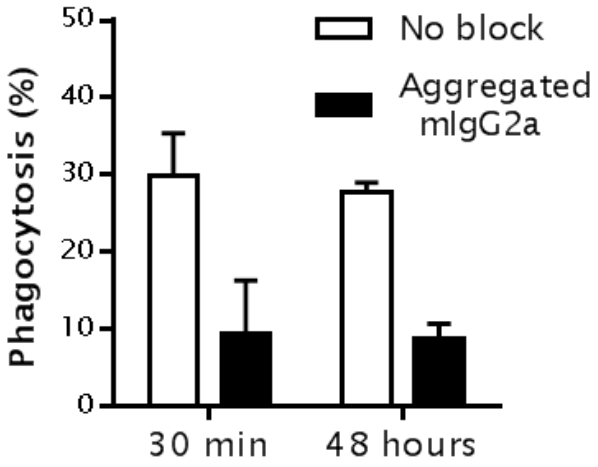

Figure 6-10 ADCP analysis of BMDM, long or short term block with aggregated IgG

Aggregated immune complex of a mouse IgG2a isotype (WR17) (10 µg/ml) was incubated with 8 day old BMDMs from C57BL/6 mice for 48 hours or 30 minutes at 37 °C (5 % CO_2). Target hCD20 B cells were isolated from C57BL/6 mice and stained with CFSE (5 µM). Target B cells were opsonised with Ritm2a (10 µg/ml) at 4 °C for 20 minutes. Target B cells (2.5 x10^6 cells) were then co-cultured with BMDMs (5x10^5 cells) for 30 minutes at 37 °C (5 % CO_2). Samples were then stained with F4/80-APC (2 µl) and acquired on a FACS Calibre™ flow cytometer. N=3+/-SD.

From **Figure 6-10** it can be seen that BMDMs co-cultured with aggregated IgG for 30 minutes or 48 hours both resulted in an equally diminished ability to phagocytose opsonised B cells. Suggesting that aggregated IgG is simply blocking Fc:FcγR interactions. To further address the ability of aggregated IgG to block or modulate FcγR expression qPCR was performed on BMDM lysates which had been incubated with either aggregated or monomeric antibody for 48 hours (**Figure 6-11**).

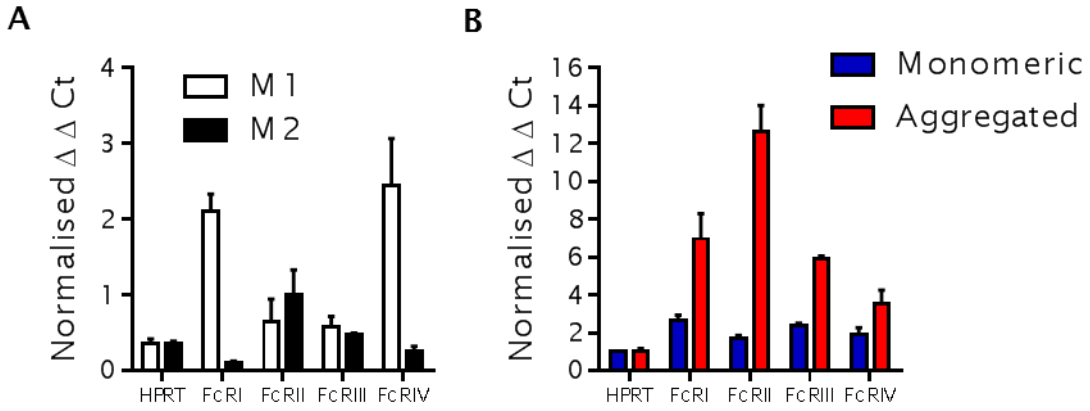

Figure 6-11 qPCR to assess the impact of aggregated IgG on FcγR expression

The level of mRNA transcripts following BMDM co-culture with aggregated or monomeric antibody was assessed using qPCR. (**A**) Following macrophage polarisation with classical M1 or M2 agonists. (**B**) Following polarisation with monomeric or aggregated IgG (m2a) for 48 hours at 37 °C (5 % CO_2).

From **Figure 6-11a** it can be seen that following polarisation with classical M1 or M2 reagents there was an increase in inhibitory FcγRIIb following polarisation with M2 skewing reagents. In contrast, following M1 polarisation there was an increase in FcγRI and FcγRIV transcripts. Following the validation of this assay using classical M1 and M2 skewing reagents the change in FcγR mRNA levels was determined following BMDM co-culture with monomeric or aggregated IgG2a (WR17) (**Figure 6-11b**). After polarisation with monomeric IgG it can be seen that there was a modest increase all FcγR, compared to non-treated controls. However, following co-culture with aggregated IgG it can be seen that in addition to an increase in FcγRI, FcγRIII and FcγRIV levels there was

a massive increase in inhibitory FcγRIIb. This data would suggest that co-culture of macrophages with immune complex is also capable of modulating FcγR expression.

6.4 Chapter discussion

From these studies it was found that the Vav Bcl-2 mouse, which displays an autoimmune like phenotype, also presents with increased levels of IgG and that this increase is predominantly due to an expansion of the IgG2c and IgG2b compartments. It is perhaps unsurprising that Vav Bcl-2 mice display 10 fold higher levels of total IgG since they present with a 10 fold greater number of B cells [202]. What is interesting is that this increase is primarily due to an expansion of the IgG2c compartment and to a lesser extent the IgG2b compartment. Mouse IgG2c (the ortholog of IgG2a, found in BALB/c mice) is traditionally seen as a pro-inflammatory isotype; it has greater affinity for activatory FcγR and is capable of activating complement, abilities which mouse IgG1 lacks [283]. It may be that the upregulation of mouse FcγRIIb described in chapter 5 is in part a response to these increased levels of IgG2c. Cross presentation of antigen via immune complex is known to enhance T cell responses, can lead to inflammation and is the major mechanism by which tumour immunoediting occurs. Work by Getahun *et al* showed how adoptive transfer of $CD4^+$ T cells specific for OVA followed by administration of IgG2a-OVA immune complex showed significantly increased T cell proliferation compared to OVA alone and that this process was enhanced in $FcγRIIb^{-/-}$ mice [284]. Indirectly this suggests that increased levels of FcγRIIb would have the reverse effect and would aim to dampen any inappropriate inflammation and damaging immune response. Evidence for this comes from findings that FcγRIIb is important in preventing the generation of autoreactive B cells [285]. Therefore, it would be interesting to further assess the T cell compartment in the Vav Bcl-2 mouse and to determine the levels of IgG in the Eμ Bcl-2 mouse, which does not have T cell help. We would hypothesise that since Eμ Bcl-2 mice do not have as much T cell help as Vav Bcl-2 mice, they will not present with as elevated levels of IgG and will not show increased levels of FcγRIIb on effector cell subsets since these B cells will not have undergone as prolific B cell activation in the germinal centre. Since increased levels of IgG in the vav bcl-2 mouse are likely a result of increased B cell number and dysregulated

activation, future work should aim to conduct functional studies to investigate the production of IgG by B cells from both WT and vav bcl-2 mice. ELISPOT analysis could be used to determine the numbers of active plasma cell in various tissue, this method could also be used to quantify amount of antibody produced by each cell [286].

After demonstrating that Vav Bcl-2 mice present with increased levels of IgG their levels of circulating immune complex was ascertained. To detect circulating immune complex a C1q ELISA assay was optimised for use, and using this assay it was demonstrated that Vav Bcl-2 mice have undetectable (<0.16 μg/ml) levels of circulating immune complex similar to that of the WT mouse. In contrast, autoimmune MRL mice had readily detectable levels of circulating immune complex. The lack of circulating immune complex in the Vav BCl-2 mouse was unexpected since these mice have heightened levels of IgG2c and display glomerulonephritis. It may be that Immune complex are readily cleared from the circulation or are deposited in tissue of these mice. If present immune complex would have provided a sufficient explanation as to why there is abrogated B cell depletion in this mouse, in that Fc: FcγR interactions are being blocked. However, the majority of B cell depletion takes place in the liver and not the spleen and so it would be important for future work to investigate this compartment in terms of macrophage FcγR expression, functional activity and presence of immune complex.

In vitro it was found that artificially made, heat aggregated, immune complex could readily block ADCP effector mechanisms whereas monomeric IgG had no effect on ADCP. This result adds to the work of Ahuja *et al* who found using protein G separation techniques that it was in fact the IgG compartment of the serum that was specifically conveying the block in B cell depletion seen in MRL autoimmune mice. It would appear that IgG in the form of immune complex is either blocking or modulating FcγRs. This is in agreement with recently published data demonstrating that mice chronically infected with lymphocytic choriomeningitis virus (LCV) had supressed FcγR function and that this was specifically due to immune complex inhibiting ADCP mechanisms and supressing antigen cross presentation [277, 278]. Therefore it would seem that in patients with high levels of circulating immune complex, mAb mediated target cell depletion methods independent of FcγR should be investigated, as

has been done with belimumab. Indeed, it has recently been shown that in a murine collagen-induced arthritis model, B cell inhibition through crosslinking of CD79b was preferential to depletion of B cells by rituximab [287]. To further investigate the role of immune complex in the Vav Bcl-2 mouse it would be important to recapitulate some of the experiments performed by Ahuja *et al* in terms of adoptively transferring serum and isolated the IgG.

It was hypothesised that since mouse IgG2a has greater affinity for activating FcγRI and FcγRIV, whereas IgG1 displays no affinity for this receptor, that IgG2a immune complex would be more potent at blocking Fc:FcγR interactions. However, this was not the case in our *in vitro* experiments and mouse IgG1 blocked ADCP just as potently as IgG2a. From these results it would be interesting to determine the binding affinity to of mouse IgG1 and IgG2a immune complex to activatory FcγR, using SPR analysis. The method used here to generate immune complex has been well established, however the size of these immune complex could not be easily determined, although it was known that they are larger than IgM. Future experiments should aim to better elucidate the size and range of these immune complex.

Efforts were made to determine if aggregated IgG was in fact blocking Fc:FcγR interactions of modulating FcγR expression on effector cells. **Figure 6-10a** showed that co-culturing BMDM with aggregated IgG for just 30 minutes was as effective as a 48 hour co-culture period. This suggested that aggregated IgG was blocking Fc:FcγR interactions. However, qPCR analysis of BMDMs co-cultured for 48 hours with immune complex showed a massive increase in FcγRIIb suggesting that over time immune complex also have the capacity to modulate FcγR expression on effector subsets.

Together these finding demonstrate clear mechanisms by which antibody therapy may be inhibited in patients with autoimmune disease and hypergammaglobulemia. Increased IgG production can not only directly block Fc:FcγR interactions but can also directly modulate the expression of FcγR on the cell surface creating a perfect storm to block ADCP effector response. Future research into this area could investigate either the targeting of B cells so as not to require Fc:FcγR interactions or targeting of circulating immune complex so as to make it unreactive to Fc:FcγR interactions. Using deglycosylating enzymes such as EndoS in combination with Endo S resistant

antibodies may be an ideal way of circumventing this problem in patients displaying hypergammaglobulemia, as has recently been reported [288].

Chapter 7: General discussion

Monoclonal antibody therapy is revolutionising the treatment of many different cancers. Some of the greatest success has come from the use of rituximab in the treatment of B cell malignancies. This success has been such that a number of next generation antibodies have been developed to take advantage of one or more of the proposed effector functions elicited by rituximab. This project aimed to better characterise and further elucidate some the FcγR mediated mechanism of action displayed by rituximab and these next generation antibodies. There was a particular interest in the type I and type II antibodies rituximab and obinutuzumab. Using a number of *in vivo* and *in vitro* models it has been confirmed here that the process of antigenic modulation has a significant impact upon antibody effector mechanisms, namely, macrophage mediated ADCP and NK cell mediated ADCC.

Previous comparisons between rituximab and obinutuzumab have shown obinutuzumab to provide a superior outcome compared to rituximab both in animal experimentation and in the clinical setting [131, 221, 243, 289]. This superior activity has been widely attributed to obinutuzumab having been glycoengineered so as to have enhanced affinity for FcγRIIIa (homolog to mouse FcγRIV). This is thought to translate into superior ADCC activity. These studies do not take into account the detrimental effects of antigenic modulation which have been shown here, in chapter 3, to significantly impact upon antibody dependent effector mechanisms. The ability for rituximab to undergo antigenic modulation has been well documented in this lab [109, 122, 232]. Importantly, rituximab is a type I antibody which displays high levels of antigenic modulation whereas obinutuzumab is a type II antibody which displays low levels of antigenic modulation. This translates into a fundamental difference in the kinetics of antibody loss from the cell surface and from the serum of treated mice. Therefore, it may well be that enhanced ADCC afforded by glycomodification does not account for the improved responses seen when using obinutuzumab in the clinic. Rather, it may simply be that the antibody half-life at the cell surface and in the serum of obinutuzumab is superior to rituximab by virtue of reduced levels of antigenic modulation. Over time this will leave more Fc available on the surface of target cells, which effector cells can interact with. Data from Herting *et al* supports these findings. Following

injection with the same dose (mg/kg) of rituximab or obinutuzumab this group measured the serum IgG levels of 4-8 week, female, SCID mice which had been injected with Z138 human MCL tumour cells. It was found that there was a reduced concentration of rituximab in the serum compared to obinutuzumab 5 and 8 days post infusion of mAb demonstrating that the serum half-life of obinutuzumab is superior to that of rituximab, in the mouse [243]. Interestingly, Bologna *et al* found that ADCP when using either rituximab or obinutuzumab, in combination with MDMs and primary CLL cells, was the same. This is in agreement with our findings that without taking into account antigenic modulation rituximab and obinutuzumab show similar levels of ADCP [289]. Work should continue to investigate whether obinutuzumab is superior to rituximab by virtue of its glycomodification or superior half-life, endowed by the type II nature of this antibody. As had been done for obinutuzumab it may be useful to make glycomodified versions of rituximab and see how these fair in head to head experiments in terms of the level of antigenic modulation, the plasma half-life and the ability to orchestrate ADCC/ADCP effector functions. This would help explain whether obinutuzumab is superior to rituximab by virtue of its glycomodification or its resistance to antigenic modulation.

It would also be important to determine the precise nature and mechanisms of antigenic modulation so as to develop better treatments for type I antibodies. There is some debate in the literature as to whether antigen: antibody complex is lost from the cell surface due to antigenic modulation or through the trogocytosis-like shaving reaction. Evidence for the shaving reaction comes from experiments using THP-1 monocytes and $CD20^+$ Z138 MCL cells. It was demonstrated that rituximab was readily lost from the surface of these B cell targets and could be detected on the surface of effector THP-1 cells [120]. It was later documented that this shaving reaction occurred rapidly and was dependent on FcγRs [241, 290]. Experiments performed here allowed opsonised B cells to undergo antigenic modulation in the absence of additional loss of antibody from the shaving reaction. Since type II antibodies do not undergo antigenic modulation to the same extent as type I antibodies it would be interesting to probe the levels of antibody:antigen loss through the shaving reaction when using type I and type II antibodies. It is difficult to demonstrate solely shaving by effector cells and not phagocytosis. Experiments have sought to control for this through the use of latex beads which can be taken up by

macrophages in a non FcγR mediated fashion. Bead saturated BMDMs do not have the ability to phagocytose opsonised B cells and removal of antibody by effector BMDMs can still be detected. Subsequent preliminary experiments in the laboratory indicate that both type I and II mAb are efficiently shaved. Therefore, as type II mAb are more potent *in* vivo and less effected by modulation we would propose that antigenic modulation is the major mechanism by which antibody: antigen complexes are removed from the target cell surface.

However, it is likely that both the shaving reaction and antigenic modulation contribute to the loss of antgen:antibody complex from the target cell surface. *In vitro* the precise mechanisms behind antigenic modulation are still unknown. What is known is that this process correlates strongly with the expression of FcγRIIb on the target cell surface, that the ITIM of FcγRIIb becomes phosphorylated following rituximab infusion and that cis binding is required to augment antigenic modulation [232]. The current working hypothesis on how rituximab is internalised is as follows: rituximab will bind to CD20 this will result in binding to FcγRIIb, through cis reactions. Phosphorylation of FcγRIIb occurs and antigen:antibody are internalised in a similar fashion to that of immune complex [291, 292]. However it was recently shown by Vaughan *et al* that FcγRIIb lacking the entire cytoplasmic domain, and so not able to signal through the ITIM domain, was still able to undertake antigenic modulation as effectively as the WT FcγRIIb, and this suggests that antigenic modulation is not dependent on FcγRIIb signalling [293].

There has been recent interest in FcγRIIb blocking antibodies as a co-therapeutic with rituximab. Roghanian *et al* demonstrated that blocking FcγRIIb resulted in improved therapeutic outcome when using rituximab or obinutuzumab in several mouse models [250]. Based on the literature and the results presented in chapter 3 it would seem that blocking FcγRIIb will prevent rituximab from binding through cis reactions, therefore reducing the level of antigenic modulation. This will leave more Fc available on the target cell surface to interact with FcγR on effector cells. If anti-FcγRIIb antibodies solely worked by reducing the level of antigenic modulation it would be surprising that in combination with type II obinutuzumab there is more efficient B cell depletion. However, Roghanian *et al* showed in both transgenic mouse and xenograph models in addition to blocking anti- FcγRIIb mAbs can also augment

B cell depletion by acting as an additional opsonin. Our experiments in chapter 4 demonstrate that blocking FcγR with mAb may result in additional cross blocking on multiple FcγR expressing cells. Therefore, the use of fully glycosylated FcγRIIb blocking antibody is preferable on the target cell but could be problematic if binding to FcγRIIb on multiple FcγR expressing effector cells, since it will leave them prone to depletion themselves or to blocking of their activatory FcγR through cross blocking via the Fc region.

Based upon the observation in chapter 3 that human IgG1 type II antibodies perform very poorly in murine ADCC assays but that they are able to deplete B cells *in vivo* and undertake ADCP to an equivalent level to that of mouse IgG2a it was concluded that macrophages are the dominant effector cell subset. A fundamental difference between mouse and human physiology is that murine NK cells express FcγRIII whereas human NK cells express FcγRIIIa, which is the homolog of mouse FcγRIV. Highlighting the difference that glycomodification of obinutuzumab makes to binding of murine FcγRs is SPR data in chapter 3 looking at the affinity of obinutuzumab for FcγRIV and which showed slightly reduced levels of disassociation. Meaning that obinutuzumab has a longer off rate, and increased affinity for this receptor. The differences between mouse and human FcγR physiology have recently been reviewed [115].

Recent investigations have taken advantage of the humanised mouse model which does not express murine FcγR but does expresses the full repertoire of human FcγR. Studies using these mice have again found that clodronate depleted macrophages results in reduced ability to delete antibody opsonised targets [252]. This is the first time that these kinds of experiment have shown that when using the human platform of FcγR expression, macrophages still appear to be the dominant cell subset. Interestingly, when using these humanised mice in combination with human IgG1 antibodies diminished levels of depletion were seen compared to when using a WT mouse with IgG2a antibody, and only human IgG1 antibodies with enhanced affinity for FcγRIIIa were able to sufficiently deplete targets in the humanised mouse [252]. Why this differs from the situation in humans where human IgG1 antibodies efficiently deplete B cells is not clear. Our findings, that macrophages appear to be the dominant effector cell subset, are in general agreement with the published literature [135, 136]. Although, there is debate over which is the

dominant granulocyte effector cell population and which FcγR are the most important to therapy. Macrophages, neutrophils and monocytes from various tissues have all been implicated and it may be that the effector cell orchestrating FcγR mediated depletion will vary depending on the tissue compartment, the antibody isotype and the targets being investigated.

Other groups have placed importance on NK cells and there has been some clinical success when using IL-2 as a co-therapeutic. Results from chapter 3 show that freshly isolated murine NK cells express very low levels of FcγRIII and it is only the addition of IL-2 that enhances this expression. Therefore, it may be that NK cells would be optimised if they received some kind of pro-inflammatory signal before addition of a depleting antibody. Recent work by Kohrt *et al* found that the level of a co-stimulatory cell surface protein on human NK cells, CD137 (41-BB), was increased in an FcγRIIIa dependent fashion upon addition of opsonised target cells. Additionally it was found that subsequent ligation of CD137 using a monoclonal antibody enhanced killing by NK cells both *in vitro* and *in vivo*. Similar results were also demonstrated using an anti-KIR antibody in the context of rituximab mediated depletion [227-229]. The work presented here would suggest macrophages to be the dominant effector cell subset. However, NK cells are capable of mediating ADCC and are likely contributing. Importantly, due to the differences in human and mouse FcγR physiology outlined, mouse studies may underplay the role of NK cells in the human setting.

Having established the importance of antigenic modulation and the key effector cells involved, we next wished to determine the principle FcγRs involved in B cell depletion. Much of the published literature has demonstrated FcγRIV to be a key receptor for pro-inflammatory IgG2a/c mediated activity. It has been confirmed here that, in agreement with the literature, FcγRI and FcγRIV are important to B cell depletion [128]. This evidence came from adoptive transfer data using FcγRI$^{-/-}$ mice in combination with the FcγRIV blocking antibody 9E9. However, we found that this model potentially underplays the role of FcγRIII in deletion since SPR analysis and FcγR staining suggest that 9E9 also interacts via its Fc region with FcγRIII, blocking it from facilitating antibody mediated activity. Interestingly, previous work looking into the depletion of platelets using the antibody 6A6-IgG2b found that when FcγRIV was blocked using 9E9 in the WT mouse there was a complete

abrogation in depletion, even though IgG2b immune complex bound to FcγRIII expressing cells *in vitro*. Binding of IgG2b immune complex to FcγRIII suggests that IgG2b opsonised targets should have access to this FcγRIII. The finding that 9E9 may bind FcγRIII through cis reactions could help explain why 6A6-IgG2b could not deplete platelets when 9E9 was used [254]. However, there are still some unresolved issues, for example in the WT mouse blocked with 9E9, 6A6-IgG1 antibody still maintained some depletion of platelets. This is difficult to reconcile as IgG1 will only engage FcγRIII or FcγRIIb as it has very low/no affinity for FcγRI or FcγRIV and since these WT mice will have been blocked using 9E9 it would suggest that in this context access to FcγRIII was still possible and cis blocking of FcγRIII by 9E9 did not occur. Potential explanations may be that since IgG1 has no affinity for FcγRIV it will bind to FcγRIII and sequester it away from FcγRIV, clustering and activating effector mechanisms. IgG2a/c and IgG2b antibodies would not do this as they will also be looking to bind FcγRIV. To test this hypothesis fluorescence microscopy could be used to detect clustering of FcγRIII and FcγRIV on the cell surface following blocking with 9E9 and addition of mouse IgG1 and IgG2a/c or IgG2b immune complexes in the form of opsonised B cell targets.

In this context, it would be interesting to look at B cell depletion using a mouse IgG1 version of rituximab, in the presence of FcγRIV blocking with 9E9 or deglycosylated 9E9. Data from our experiments would indicate that since 9E9 will block FcγRIII through cis binding that IgG1 would exhibit no effector response, however, data from the platelet model using 6A6-IgG1 antibody would suggest otherwise. Since FcγRIII is a low affinity receptor it is perhaps surprising that it would bind to the Fc of monomeric 9E9. Therefore, additional experiments in chapter 4 sought to clarify that in fact FcγRIV expression and Fab binding was a prerequisite for 9E9 blocking FcγRIII. The likely scenario is that effector cells expressing high levels of FcγRIV, will upon 9E9 binding display clustered FcγRIV on the cell surface thus allowing sufficient avidity to bind to and block FcγRIII on the same cell. This would explain why no cross blocking of FcγRIII was observed on Ly6C^{Hi} monocytes which express low levels of FcγRIV. It would be interesting to probe this hypothesis *in vitro* using fluorescence microscopy as suggested above. By using cells expressing differentially fluorescently tagged FcγRIII and FcγRIV, addition of 9E9 would be expected to cause clustering of FcγRIII and FcγRIV whereas addition of

deglycosylated 9E9 would only induce clustering of FcγRIV. However, the expression levels of FcγRIII and FcγRIV would need to be carefully considered.

There are wider applications for the use of deglycosylated antibodies as recent work has highlighted the importance of not ignoring inappropriate isotype interactions when it comes to flow cytometry analysis. It was found that mouse, hamster and rat isotypes were also prone to binding FcγRIV in a similar manner and so all FcγR should be blocked before using these isotypes [294]. These problems could be overcome by deglycosylating antibodies before conjugation with fluorescent fluorochrome, thereby removing the potential for unhelpful Fc: FcγR interactions. From the experiments in chapter 4 we would conclude that there is redundancy between all three activatory FcγR in the mouse. Coupled with our experiments in chapter 3 we would suggest that multiple FcγR expressing macrophages are critical to effective B cell depletion following antibody therapy.

Having established that there is functional redundancy between all activatory FcγR we next considered whether their expression may differ in various disease models. One such model is the Vav Bcl-2 mouse. These mice have forced expression of Bcl-2 under the control of the Vav promoter, resulting in over expression of Bcl-2, and therefore increased cell survival, throughout the haematopoietic system. Preliminary data generated in our lab found that apoptosis resistant Vav Bcl-2 mice showed an abrogated ability to deplete Ritm2a opsonised B cells. Furthermore it appeared that this block was due to the effector compartment of the mouse. This led to speculation that apoptosis may be impacting upon effector cell mechanism in response to antibody therapy. Results reported in chapter 5 demonstrated that there is no inherent difference between *in vitro* cultured BMDMs from mice with varying levels of apoptosis. Furthermore, BMDMs from mice displaying high or low levels of apoptosis were able to become polarised to either an M1 or M2 phenotype. This suggested that there was no underlying inherent defect in the functional ability of effector cells as a result of altered levels of apoptosis and suggests that there are direct micro environmental influences. However, BMDMs in these studies were grown *in vitro* for 8-10 days and the microenvironmental influences on these cells will be different to what is found *in vivo*. Therefore we next investigated the cell surface expression of FcγR on *ex vivo* splenocytes from Vav Bcl-2 mice. Since effective response to antibody therapy is reliant

upon activatory FcγR expression, efforts were undertaken to validate and optimise a panel of antibodies which would inform on the cell surface expression of activatory and inhibitory FcγR by flow cytometry. A number of different antibody clones were tested in WT and FcγR null mice to show specificity. The expression profiles of immune cells from Vav Bcl-2 mice were then acquired and compared with WT mice. It was found that Vav Bcl-2 mice have elevated levels of FcγRIIb on the surface of B cells and macrophages and that this specifically decreased the A:I ratio of macrophages to below what would be expected of those from a WT mouse.

Similar to our findings, the work of Lawler *et al* report upon an upregulation of FcγRIIb on the myeloid cell compartment in Vav Bcl-2 mice and interestingly this was ascribed to be the reason why these mice were surprisingly resistant to antibody dependent models of RA. It would be interesting if future experiments aimed to elucidate the mechanism behind this upregulated expression of FcγR. Namely is this upregulation due to defective apoptosis or is it more a response against the accumulation of autoreactive B cells. One interesting study provided a link between immune complex, FcγR and the regulation of apoptosis. Here, IL8 immune complex was shown to directly effect the level of apoptosis in neutrophils by binding to FcγRIIa which in turn modulated levels of Bcl-Xl in the cell, providing a clear link between FcγR engagement and the regulation of Bcl-2 protein levels [295]. Whether the reverse process of apoptosis protection augments FcγR expression remains to be determined.

With regards to apoptosis having a direct effect on macrophage polarisation it might be expected that high levels of systemic apoptosis would polarise macrophages to an anti-inflammatory phenotype, with a low A:I. Since apoptosis typically results in an anti-inflammatory, immunologically-silent response. Therefore, we would suggest that in the apoptosis defective Vav Bcl-2 mouse the increase in FcγRIIb may ensue from their autoimmune-like phenotype which is attempting to dampen any inappropriate activation by the B cell. However, our group has performed normal B cell depletion experiments in mice which have had a Bcl-1 lymphoma passaged into them, and so do not have an autoimmune phenotype. The result of these experiments again shows that mice with tumour respond poorly to B cell depletions and experiments are

currently underway to determine the mechanisms behind this depletion defect. There are a number of directions this work could take. Importantly, it was shown here that the rate of antigenic modulation between WT and Vav Bcl-2 B cells was the same however this does not take into account the ~10 fold greater number of B cells found in the Vav Bcl-2 mouse. Therefore, experiments should look into the half-life of rituximab in the Vav Bcl-2 mouse compared to the WT mouse and it would be expected to be worse in the Vav Bcl-2 mouse.

Additionally, further characterisation of FcγRIIb$^{-/-}$ x Vav Bcl-2 mice should be undertaken. It would be interesting to assess the levels of IgG in this mouse compared to the Vav Bcl-2 mouse, as the lack of FcγRIIb would be expected to impact on the B cells ability to regulate their activation status making it likely that this mouse would have more autoreactive B cells, immune complex and so higher levels of IgG. The use of the anti-FcγRIIb mAb, AT130-5, as a deglycosylated form showed some success in reversing the B cell depletion defect when used to block FcγRIIb on effector cells in the Vav Bcl-2 mouse. However, no such success was observed when treating Vav Bcl-2 mice with the fully glycosylated version of AT130-5. This could be due to a number of factors as it may have been that FcγRIIb expression on target and effector cells used in the Vav Bcl-2 mouse caused higher levels of antigenic modulation. Also it may well be that the FcγRIIb$^{-/-}$ x Vav Bcl-2 mouse has higher levels of immune complex and IgG which are interfering with effector cell mechanisms.

Based on the work the work of Ahuja *et al* it was hypothesised that Vav Bcl-2 mice which display an autoimmune like phenotype have diminished ability to deplete B cells due to elevated levels of IgG and immune complex blocking activatory FcγR activity. This hypothesis was further supported by the recent findings that in response to viral infection IgG immune complex can bind to and block activatory FcγR, preventing phagocytosis following antibody therapy [277, 278]. Data presented in chapter 6 demonstrate that the Vav Bcl-2 mouse does indeed have elevated levels of IgG and that this results largely from an expansion of the IgG2c and IgG2b pro-inflammatory compartment. Since this demonstrates there is likely to be a pro-inflammatory response occurring perhaps the elevated levels of FcγRIIb result from polarisation by regulatory B or T cells in response to chronic inflammation.

After optimising a C1q ELISA to detect immune complex, the levels of immune complex in Vav Bcl-2 mice were assessed. Perhaps surprisingly, no immune complex could be detected in Vav Bcl-2 mice whereas immune complex could readily be detected in autoimmune mice. Potentially the enhanced levels of FcγRIIb are preventing the formation of autoreactive B cells and the formation of immune complex. Alternatively, it could be that there are elevated levels of immune complex in the Vav Bcl-2 mouse but these are not detectable in the general circulation. Perhaps they are deposited on tissue or are occupied by FcγR, alternatively they may be too small to be detected with the C1q ELISA assay. It would be interesting if future experiments could perform analysis of immune complex on Vav Bcl-2 tissue in particular tissues prone to auto immunity such as the kidneys which see an auto immune like glomerulonephritis or the spleen which undergoes splenomegaly.

Additionally, in a manner similar to that of Ahuja *et al* it would be worth taking the serum of Vav Bcl-2 mice and attempting to recapitulate experiments where this serum is adoptively transferred into WT recipients to see if it is the serum fraction that conveys B cell depletion resistance in the Vav Bcl-2 mouse. Further to this it would be informative to separate the IgG fraction of the Vav Bcl-2 serum and specifically transfer this to recipient mice to see if it is the IgG fraction conveying resistance to B cell depletion. Additional analysis could then look at the glycosylation status of IgG and at the levels of pro and anti-inflammatory cytokines in the serum.

Even though we were unable to demonstrate that Vav Bcl-2 mice display higher levels of immune complex we were able to show that immune complex are capable of blocking ADCP using our *in vitro* phagocytosis assay. It was found that the immune complex specifically blocked phagocytosis with the monomeric fraction having minimal effect. Furthermore this block was potent, with immune complex, with levels as low as 10 μg/ml completely blocking phagocytosis. Additional experiments aimed to determine whether immune complex was simply blocking FcγR mediated activity or was directly modulating the expression of FcγR on the cell surface. Direct detection of FcγR by flow cytometry was difficult as FcγR would be engaged with immune complex and many anti-FcγR mAb bind in the Fc binding regions and are blocked by the presence of immune complex. Therefore qPCR analysis was used and results

showed that in response to 48 hours co culture with immune complex the level of FcγRIIb was massively increased suggesting perhaps a change to more anti-inflammatory M2 macrophages. The immune complex used in these studies was of the pro-inflammatory IgG2a type and the glycosylation status unknown and it may be that this increase is specific to IgG2a. Therefore the FcγR response to IgG1 immune complex would be interesting to also observe. Although IgG1 immune complex do block FcγR mediated activity in our ADCP assays. There was evidence that this was simply due to blocking of FcγR as only a 30 minute co-incubation provided just as much inhibitory activity as a 48 hour co-culture period. Therefore it may be that immune complex can both block and modulate FcγR expression on effector cell subsets. Work to take the results found in chapter 6 forward could look into the potential use of deglycosylating enzymes *in vivo* to prevent any immune complex binding to FcγR as described recently by Baruah *et al* [288]. This is an intriguing strategy whereby EndoS would be used to deactivate any circulating immune complex and an antibody resistant to EndoS would be employed to deplete target cells. This would also have implications for the treatment of autoimmune conditions where there are high levels of circulating immune complex.

An alternative explanation for the B cell depletion defect seen in the Vav Bcl-2 mouse is that the increased levels of circulating IgG are detrimental to the half-life of therapeutic antibody. This would be due to competition with the neonatal Fc receptor which is responsible for saving and recycling antibody from endosomal degradation. Due to increased levels of circulating IgG in the Vav Bcl-2 mouse this receptor is likely to be saturated. Therefore, less therapeutic antibody will bind, thus increasing antibody consumption and reducing B cell clearance. Therefore it would be extremely informative if future work compared the level of antibody consumption in hCD20 vs hCD20xVav Bcl-2 mice following treatment with Ritm2a.

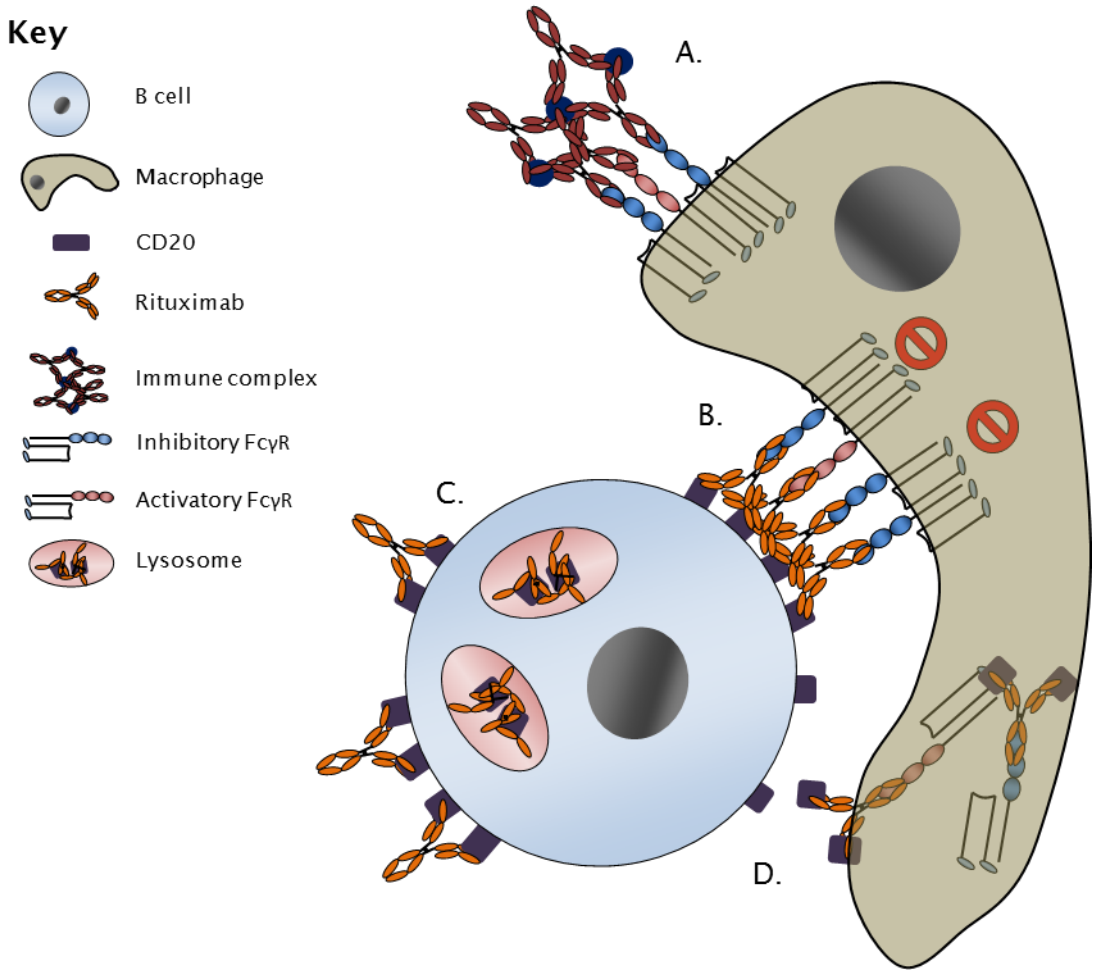

Figure 7-1 Proposed mechanisms behind defective B cell depletion in the vav bcl-2 mouse.

There have been a number of proposed factors which bring about a "perfect storm" in terms of defective B cell depletion. These mechanisms which reduces Fc:FcγR interactions and the macrophages ability to phagocytose opsonised cells are outlined here. A) Blocking FcγRs, immune complex will block activatory FcγR on effector cells. B) decreased A:I ratio, increased expression of FcγRIIb will inhibit the effector cells ability to phagocytose opsonised cells. C) Antigenic modulation, this will result loss of antigen antibody complex from the cell surface and reduced ability of effector cells to phagocytose. D) Trogocytosis, through the "shaving reaction" antigen antibody complex are again lost from the cell surface leading to reduced ability of effector cells to phagocytose.

In conclusion, we show here that the detrimental process of antigenic modulation has a significant impact of FcγR mediated mechanisms of action, namely the depletion of target cells by macrophages. Therefore, future antibody treatment and design should take this into account. Furthermore we

demonstrate that IgG immune complex will specifically inhibit phagocytosis and so patients being treated with depleting antibody therapy should be considered for the amount of immune complex they have in the circulation as it will impact on therapeutic outcome. This opens up future lines of research aimed at preventing immune complex from blocking FcγR mediated mechanism of action.

References

1. (WHO), W.H.O., *Cancer, Key facts. Accessed 14th March 2015 (http://www.who.int/mediacentre/factsheets/fs297/en/index.html).* 2013.
2. Hanahan, D. and R.A. Weinberg, *The hallmarks of cancer.* Cell, 2000. **100**(1): p. 57-70.
3. Hanahan, D. and R.A. Weinberg, *Hallmarks of cancer: the next generation.* Cell, 2011. **144**(5): p. 646-74.
4. research, L.a.L., *Patient information Acessed at http://leukaemialymphomaresearch.org.uk/ (12 March 2013).*
5. Freedman, A., *Follicular lymphoma: 2012 update on diagnosis and management.* Am J Hematol, 2012. **87**(10): p. 988-95.
6. Stevenson, F.K. and G.T. Stevenson, *Follicular lymphoma and the immune system: from pathogenesis to antibody therapy.* Blood, 2012. **119**(16): p. 3659-67.
7. Choi, J., S.T. Kim, and J. Craft, *The pathogenesis of systemic lupus erythematosus-an update.* Curr Opin Immunol, 2012. **24**(6): p. 651-7.
8. (WHO), W.H.O., *Cancer, Treatment of cancer, Accessed 24th April 2013, http://www.who.int/cancer/treatment/en/.* 2013.
9. Silverstein, A.M., *A history of immunology*1989, San Diego: Academic Press. xxi, 422 p.
10. Kantha, S.S., *A centennial review; the 1890 tetanus antitoxin paper of von Behring and Kitasato and the related developments.* Keio J Med, 1991. **40**(1): p. 35-9.
11. Nossal, G.J., *One cell-one antibody: prelude and aftermath.* Nat Immunol, 2007. **8**(10): p. 1015-7.
12. Cooper, M.D., M.L. Schwartz, and R.A. Good, *Restoration of gamma globulin production in agammaglobulinemic chickens.* Science, 1966. **151**(3709): p. 471-3.
13. Vaughan, A.T., A. Roghanian, and M.S. Cragg, *B cells--masters of the immunoverse.* International Journal of Biochemistry & Cell Biology. **43**(3): p. 280-5.
14. LeBien, T.W. and T.F. Tedder, *B lymphocytes: how they develop and function.* Blood, 2008. **112**(5): p. 1570-80.
15. Murphy, K., et al., *Janeway's immunobiology*. 8th ed2012, New York: Garland Science. xix, 868 p.
16. Busslinger, M., *Transcriptional control of early B cell development.* Annu Rev Immunol, 2004. **22**: p. 55-79.
17. Dal Porto, J.M., et al., *B cell antigen receptor signaling 101.* Mol Immunol, 2004. **41**(6-7): p. 599-613.
18. Gauld, S.B. and J.C. Cambier, *Src-family kinases in B-cell development and signaling.* Oncogene, 2004. **23**(48): p. 8001-6.
19. Market, E. and F.N. Papavasiliou, *V(D)J recombination and the evolution of the adaptive immune system.* PLoS Biol, 2003. **1**(1): p. E16.
20. Weigert, M., et al., *The joining of V and J gene segments creates antibody diversity.* Nature, 1980. **283**(5746): p. 497-9.
21. Gay, D., et al., *Receptor editing: an approach by autoreactive B cells to escape tolerance.* J Exp Med, 1993. **177**(4): p. 999-1008.

22. Tiegs, S.L., D.M. Russell, and D. Nemazee, *Receptor editing in self-reactive bone marrow B cells.* J Exp Med, 1993. **177**(4): p. 1009-20.
23. Goodnow, C.C., et al., *Altered immunoglobulin expression and functional silencing of self-reactive B lymphocytes in transgenic mice.* Nature, 1988. **334**(6184): p. 676-82.
24. Hartley, S.B., et al., *Elimination from peripheral lymphoid tissues of self-reactive B lymphocytes recognizing membrane-bound antigens.* Nature, 1991. **353**(6346): p. 765-9.
25. Liu, Y.J., *Sites of B lymphocyte selection, activation, and tolerance in spleen.* J Exp Med, 1997. **186**(5): p. 625-9.
26. Forster, R., et al., *A putative chemokine receptor, BLR1, directs B cell migration to defined lymphoid organs and specific anatomic compartments of the spleen.* Cell, 1996. **87**(6): p. 1037-47.
27. Cariappa, A., et al., *The recirculating B cell pool contains two functionally distinct, long-lived, posttransitional, follicular B cell populations.* J Immunol, 2007. **179**(4): p. 2270-81.
28. Rolink, A.G. and F. Melchers, *BAFFled B cells survive and thrive: roles of BAFF in B-cell development.* Curr Opin Immunol, 2002. **14**(2): p. 266-75.
29. Barrington, R.A., et al., *CD21/CD19 coreceptor signaling promotes B cell survival during primary immune responses.* J Immunol, 2005. **175**(5): p. 2859-67.
30. MacLennan, I.C., et al., *The changing preference of T and B cells for partners as T-dependent antibody responses develop.* Immunol Rev, 1997. **156**: p. 53-66.
31. Gatto, D. and R. Brink, *The germinal center reaction.* Journal of Allergy and Clinical Immunology, 2010. **126**(5): p. 898-907.
32. Cozine, C.L., K.L. Wolniak, and T.J. Waldschmidt, *The primary germinal center response in mice.* Curr Opin Immunol, 2005. **17**(3): p. 298-302.
33. Fanslow, W.C., et al., *Soluble forms of CD40 inhibit biologic responses of human B cells.* J Immunol, 1992. **149**(2): p. 655-60.
34. Allen, C.D., T. Okada, and J.G. Cyster, *Germinal-center organization and cellular dynamics.* Immunity, 2007. **27**(2): p. 190-202.
35. O'Shea, J.J. and W.E. Paul, *Mechanisms underlying lineage commitment and plasticity of helper CD4+ T cells.* Science, 2010. **327**(5969): p. 1098-102.
36. Radbruch, A., et al., *Competence and competition: the challenge of becoming a long-lived plasma cell.* Nat Rev Immunol, 2006. **6**(10): p. 741-50.
37. O'Connell, F.P., J.L. Pinkus, and G.S. Pinkus, *CD138 (syndecan-1), a plasma cell marker immunohistochemical profile in hematopoietic and nonhematopoietic neoplasms.* Am J Clin Pathol, 2004. **121**(2): p. 254-63.
38. Jacob, J., et al., *Intraclonal generation of antibody mutants in germinal centres.* Nature, 1991. **354**(6352): p. 389-92.
39. Laffleur, B., et al., *AID-induced remodeling of immunoglobulin genes and B cell fate.* Oncotarget, 2014. **5**(5): p. 1118-31.
40. Pereira, J.P., L.M. Kelly, and J.G. Cyster, *Finding the right niche: B-cell migration in the early phases of T-dependent antibody responses.* Int Immunol, 2010. **22**(6): p. 413-9.
41. Cogne, M., *Activation-induced deaminase in B lymphocyte maturation and beyond.* Biomed J, 2013. **36**(6): p. 259-68.
42. Stavnezer, J., *Immunoglobulin class switching.* Curr Opin Immunol, 1996. **8**(2): p. 199-205.

43. Litinskiy, M.B., et al., *DCs induce CD40-independent immunoglobulin class switching through BLyS and APRIL.* Nat Immunol, 2002. **3**(9): p. 822-9.
44. Kuppers, R. and R. Dalla-Favera, *Mechanisms of chromosomal translocations in B cell lymphomas.* Oncogene, 2001. **20**(40): p. 5580-94.
45. Tsujimoto, Y., et al., *The t(14;18) chromosome translocations involved in B-cell neoplasms result from mistakes in VDJ joining.* Science, 1985. **229**(4720): p. 1390-3.
46. Kerr, J.F., A.H. Wyllie, and A.R. Currie, *Apoptosis: a basic biological phenomenon with wide-ranging implications in tissue kinetics.* Br J Cancer, 1972. **26**(4): p. 239-57.
47. Yuan, J., et al., *The C. elegans cell death gene ced-3 encodes a protein similar to mammalian interleukin-1 beta-converting enzyme.* Cell, 1993. **75**(4): p. 641-52.
48. Liu, X., et al., *Induction of apoptotic program in cell-free extracts: requirement for dATP and cytochrome c.* Cell, 1996. **86**(1): p. 147-57.
49. Green, D.R., *Means to an end : apoptosis and other cell death mechanisms*2011, Cold Spring Harbor, N.Y.: Cold Spring Harbor Laboratory Press. xii, 220 p.
50. Galluzzi, L., et al., *Molecular definitions of cell death subroutines: recommendations of the Nomenclature Committee on Cell Death 2012.* Cell Death Differ, 2012. **19**(1): p. 107-20.
51. Goldstein, J.C., et al., *The coordinate release of cytochrome c during apoptosis is rapid, complete and kinetically invariant.* Nat Cell Biol, 2000. **2**(3): p. 156-62.
52. Zou, H., et al., *Apaf-1, a human protein homologous to C. elegans CED-4, participates in cytochrome c-dependent activation of caspase-3.* Cell, 1997. **90**(3): p. 405-13.
53. Li, P., et al., *Cytochrome c and dATP-dependent formation of Apaf-1/caspase-9 complex initiates an apoptotic protease cascade.* Cell, 1997. **91**(4): p. 479-89.
54. Yuan, S., et al., *Structure of an apoptosome-procaspase-9 CARD complex.* Structure, 2010. **18**(5): p. 571-83.
55. Tait, S.W. and D.R. Green, *Mitochondria and cell death: outer membrane permeabilization and beyond.* Nat Rev Mol Cell Biol, 2010. **11**(9): p. 621-32.
56. Tait, S.W. and D.R. Green, *Mitochondria and cell signalling.* J Cell Sci, 2012. **125**(Pt 4): p. 807-15.
57. Lamkanfi, M., et al., *Caspases in cell survival, proliferation and differentiation.* Cell Death Differ, 2007. **14**(1): p. 44-55.
58. McIlwain, D.R., T. Berger, and T.W. Mak, *Caspase functions in cell death and disease.* Cold Spring Harb Perspect Biol, 2013. **5**(4): p. a008656.
59. Vaux, D.L., S. Cory, and J.M. Adams, *Bcl-2 gene promotes haemopoietic cell survival and cooperates with c-myc to immortalize pre-B cells.* Nature, 1988. **335**(6189): p. 440-2.
60. Hockenbery, D., et al., *Bcl-2 is an inner mitochondrial membrane protein that blocks programmed cell death.* Nature, 1990. **348**(6299): p. 334-6.
61. Yang, J., et al., *Prevention of apoptosis by Bcl-2: release of cytochrome c from mitochondria blocked.* Science, 1997. **275**(5303): p. 1129-32.
62. Kluck, R.M., et al., *The release of cytochrome c from mitochondria: a primary site for Bcl-2 regulation of apoptosis.* Science, 1997. **275**(5303): p. 1132-6.

63. Chipuk, J.E., et al., *The BCL-2 family reunion.* Mol Cell, 2010. **37**(3): p. 299-310.
64. Korsmeyer, S.J., et al., *Bcl-2/Bax: a rheostat that regulates an anti-oxidant pathway and cell death.* Semin Cancer Biol, 1993. **4**(6): p. 327-32.
65. Oltvai, Z.N., C.L. Milliman, and S.J. Korsmeyer, *Bcl-2 heterodimerizes in vivo with a conserved homolog, Bax, that accelerates programmed cell death.* Cell, 1993. **74**(4): p. 609-19.
66. Chipuk, J.E. and D.R. Green, *How do BCL-2 proteins induce mitochondrial outer membrane permeabilization?* Trends Cell Biol, 2008. **18**(4): p. 157-64.
67. Letai, A., et al., *Distinct BH3 domains either sensitize or activate mitochondrial apoptosis, serving as prototype cancer therapeutics.* Cancer Cell, 2002. **2**(3): p. 183-92.
68. Willis, S.N., et al., *Proapoptotic Bak is sequestered by Mcl-1 and Bcl-xL, but not Bcl-2, until displaced by BH3-only proteins.* Genes Dev, 2005. **19**(11): p. 1294-305.
69. Guicciardi, M.E. and G.J. Gores, *Life and death by death receptors.* FASEB J, 2009. **23**(6): p. 1625-37.
70. Muzio, M., et al., *An induced proximity model for caspase-8 activation.* J Biol Chem, 1998. **273**(5): p. 2926-30.
71. Krammer, P.H., *CD95's deadly mission in the immune system.* Nature, 2000. **407**(6805): p. 789-95.
72. Micheau, O. and J. Tschopp, *Induction of TNF receptor I-mediated apoptosis via two sequential signaling complexes.* Cell, 2003. **114**(2): p. 181-90.
73. Li, H., et al., *Cleavage of BID by caspase 8 mediates the mitochondrial damage in the Fas pathway of apoptosis.* Cell, 1998. **94**(4): p. 491-501.
74. Luo, X., et al., *Bid, a Bcl2 interacting protein, mediates cytochrome c release from mitochondria in response to activation of cell surface death receptors.* Cell, 1998. **94**(4): p. 481-90.
75. Kohler, G. and C. Milstein, *Continuous cultures of fused cells secreting antibody of predefined specificity.* Nature, 1975. **256**(5517): p. 495-7.
76. Shukra, A.M., et al., *Production of recombinant antibodies using bacteriophages.* Eur J Microbiol Immunol (Bp), 2014. **4**(2): p. 91-8.
77. Teeling, J.L., et al., *Characterization of new human CD20 monoclonal antibodies with potent cytolytic activity against non-Hodgkin lymphomas.* Blood, 2004. **104**(6): p. 1793-800.
78. Fishwild, D.M., et al., *High-avidity human IgG kappa monoclonal antibodies from a novel strain of minilocus transgenic mice.* Nat Biotechnol, 1996. **14**(7): p. 845-51.
79. Clark, M.R., *IgG effector mechanisms.* Chem Immunol, 1997. **65**: p. 88-110.
80. Beurskens, F.J., et al., *Exhaustion of cytotoxic effector systems may limit monoclonal antibody-based immunotherapy in cancer patients.* J Immunol, 2012. **188**(7): p. 3532-41.
81. Stapleton, N.M., et al., *Competition for FcRn-mediated transport gives rise to short half-life of human IgG3 and offers therapeutic potential.* Nat Commun, 2011. **2**: p. 599.
82. Vidarsson, G., G. Dekkers, and T. Rispens, *IgG subclasses and allotypes: from structure to effector functions.* Front Immunol, 2014. **5**: p. 520.

83. Irani, V., et al., *Molecular properties of human IgG subclasses and their implications for designing therapeutic monoclonal antibodies against infectious diseases.* Mol Immunol, 2015. **67**(2 Pt A): p. 171-82.
84. Martin, R.M., J.L. Brady, and A.M. Lew, *The need for IgG2c specific antiserum when isotyping antibodies from C57BL/6 and NOD mice.* J Immunol Methods, 1998. **212**(2): p. 187-92.
85. Karsten, C.M. and J. Kohl, *The immunoglobulin, IgG Fc receptor and complement triangle in autoimmune diseases.* Immunobiology, 2012. **217**(11): p. 1067-79.
86. Jefferis, R. and J. Lund, *Interaction sites on human IgG-Fc for FcgammaR: current models.* Immunol Lett, 2002. **82**(1-2): p. 57-65.
87. Lood, C., et al., *IgG glycan hydrolysis by endoglycosidase S diminishes the proinflammatory properties of immune complexes from patients with systemic lupus erythematosus: a possible new treatment?* Arthritis Rheum, 2012. **64**(8): p. 2698-706.
88. Boross, P. and J.H. Leusen, *Mechanisms of action of CD20 antibodies.* Am J Cancer Res, 2012. **2**(6): p. 676-90.
89. Stashenko, P., et al., *Characterization of a human B lymphocyte-specific antigen.* J Immunol, 1980. **125**(4): p. 1678-85.
90. Nadler, L.M., et al., *A unique cell surface antigen identifying lymphoid malignancies of B cell origin.* J Clin Invest, 1981. **67**(1): p. 134-40.
91. Beers, S.A., et al., *CD20 as a target for therapeutic type I and II monoclonal antibodies.* Semin Hematol, 2010. **47**(2): p. 107-14.
92. Marcus, R., et al., *Phase III study of R-CVP compared with cyclophosphamide, vincristine, and prednisone alone in patients with previously untreated advanced follicular lymphoma.* J Clin Oncol, 2008. **26**(28): p. 4579-86.
93. Glennie, M.J. and J.G. van de Winkel, *Renaissance of cancer therapeutic antibodies.* Drug Discov Today, 2003. **8**(11): p. 503-10.
94. Lim, S.H., et al., *Anti-CD20 monoclonal antibodies: historical and future perspectives.* Haematologica, 2010. **95**(1): p. 135-43.
95. Glennie, M.J., et al., *Mechanisms of killing by anti-CD20 monoclonal antibodies.* Mol Immunol, 2007. **44**(16): p. 3823-37.
96. Ivanov, A., et al., *Monoclonal antibodies directed to CD20 and HLA-DR can elicit homotypic adhesion followed by lysosome-mediated cell death in human lymphoma and leukemia cells.* J Clin Invest, 2009. **119**(8): p. 2143-59.
97. Cragg, M.S. and M.J. Glennie, *Antibody specificity controls in vivo effector mechanisms of anti-CD20 reagents.* Blood, 2004. **103**(7): p. 2738-43.
98. Cragg, M.S., et al., *Complement-mediated lysis by anti-CD20 mAb correlates with segregation into lipid rafts.* Blood, 2003. **101**(3): p. 1045-52.
99. Byrd, J.C., et al., *The mechanism of tumor cell clearance by rituximab in vivo in patients with B-cell chronic lymphocytic leukemia: evidence of caspase activation and apoptosis induction.* Blood, 2002. **99**(3): p. 1038-43.
100. Stolz, C., et al., *Targeting Bcl-2 family proteins modulates the sensitivity of B-cell lymphoma to rituximab-induced apoptosis.* Blood, 2008. **112**(8): p. 3312-21.
101. Chan, H.T., et al., *CD20-induced lymphoma cell death is independent of both caspases and its redistribution into triton X-100 insoluble membrane rafts.* Cancer Res, 2003. **63**(17): p. 5480-9.

102. Dunkelberger, J.R. and W.C. Song, *Complement and its role in innate and adaptive immune responses.* Cell Res, 2010. **20**(1): p. 34-50.
103. Beers, S.A., M.S. Cragg, and M.J. Glennie, *Complement: help or hindrance?* Blood, 2009. **114**(27): p. 5567-8; author reply 5568.
104. Golay, J., et al., *The role of complement in the therapeutic activity of rituximab in a murine B lymphoma model homing in lymph nodes.* Haematologica, 2006. **91**(2): p. 176-83.
105. Wang, S.Y., et al., *Depletion of the C3 component of complement enhances the ability of rituximab-coated target cells to activate human NK cells and improves the efficacy of monoclonal antibody therapy in an in vivo model.* Blood, 2009. **114**(26): p. 5322-30.
106. Racila, E., et al., *A polymorphism in the complement component C1qA correlates with prolonged response following rituximab therapy of follicular lymphoma.* Clin Cancer Res, 2008. **14**(20): p. 6697-703.
107. Jin, X., et al., *Homozygous A polymorphism of the complement C1qA276 correlates with prolonged overall survival in patients with diffuse large B cell lymphoma treated with R-CHOP.* J Hematol Oncol, 2012. **5**: p. 51.
108. Minard-Colin, V., et al., *Lymphoma depletion during CD20 immunotherapy in mice is mediated by macrophage FcgammaRI, FcgammaRIII, and FcgammaRIV.* Blood, 2008. **112**(4): p. 1205-13.
109. Beers, S.A., et al., *Type II (tositumomab) anti-CD20 monoclonal antibody out performs type I (rituximab-like) reagents in B-cell depletion regardless of complement activation.* Blood, 2008. **112**(10): p. 4170-7.
110. Clynes, R.A., et al., *Inhibitory Fc receptors modulate in vivo cytotoxicity against tumor targets.* Nat Med, 2000. **6**(4): p. 443-6.
111. Uchida, J., et al., *The innate mononuclear phagocyte network depletes B lymphocytes through Fc receptor-dependent mechanisms during anti-CD20 antibody immunotherapy.* J Exp Med, 2004. **199**(12): p. 1659-69.
112. Albanesi, M., et al., *Cutting Edge: FcgammaRIII (CD16) and FcgammaRI (CD64) Are Responsible for Anti-Glycoprotein 75 Monoclonal Antibody TA99 Therapy for Experimental Metastatic B16 Melanoma.* J Immunol, 2012.
113. Wu, J., et al., *A novel polymorphism of FcgammaRIIIa (CD16) alters receptor function and predisposes to autoimmune disease.* J Clin Invest, 1997. **100**(5): p. 1059-70.
114. Weng, W.K. and R. Levy, *Two immunoglobulin G fragment C receptor polymorphisms independently predict response to rituximab in patients with follicular lymphoma.* J Clin Oncol, 2003. **21**(21): p. 3940-7.
115. Lux, A. and F. Nimmerjahn, *Of mice and men: the need for humanized mouse models to study human IgG activity in vivo.* J Clin Immunol, 2013. **33 Suppl 1**: p. S4-8.
116. Jilani, I., et al., *Transient down-modulation of CD20 by rituximab in patients with chronic lymphocytic leukemia.* Blood, 2003. **102**(10): p. 3514-20.
117. Kennedy, A.D., et al., *Rituximab infusion promotes rapid complement depletion and acute CD20 loss in chronic lymphocytic leukemia.* J Immunol, 2004. **172**(5): p. 3280-8.
118. Taylor, R.P. and M.A. Lindorfer, *Impact of low-dose rituximab on splenic B cells: evidence for the shaving reaction.* Transpl Int, 2010. **23**(1): p. 116-7.
119. Williams, M.E., et al., *Thrice-weekly low-dose rituximab decreases CD20 loss via shaving and promotes enhanced targeting in chronic lymphocytic leukemia.* J Immunol, 2006. **177**(10): p. 7435-43.

120. Beum, P.V., et al., *The shaving reaction: rituximab/CD20 complexes are removed from mantle cell lymphoma and chronic lymphocytic leukemia cells by THP-1 monocytes.* J Immunol, 2006. **176**(4): p. 2600-9.
121. Beurskens, F.J., et al., *Exhaustion of Cytotoxic Effector Systems May Limit Monoclonal Antibody-Based Immunotherapy in Cancer Patients.* The Journal of Immunology, 2012. **188**(7): p. 3532-3541.
122. Beers, S.A., et al., *Antigenic modulation limits the efficacy of anti-CD20 antibodies: implications for antibody selection.* Blood, 2010. **115**(25): p. 5191-201.
123. Nimmerjahn, F., et al., *FcgammaRIV: a novel FcR with distinct IgG subclass specificity.* Immunity, 2005. **23**(1): p. 41-51.
124. Bruhns, P., *Properties of mouse and human IgG receptors and their contribution to disease models.* Blood, 2012. **119**(24): p. 5640-9.
125. Brooks, D.G., et al., *Structure and expression of human IgG FcRII(CD32). Functional heterogeneity is encoded by the alternatively spliced products of multiple genes.* J Exp Med, 1989. **170**(4): p. 1369-85.
126. Veri, M.C., et al., *Monoclonal antibodies capable of discriminating the human inhibitory Fcgamma-receptor IIB (CD32B) from the activating Fcgamma-receptor IIA (CD32A): biochemical, biological and functional characterization.* Immunology, 2007. **121**(3): p. 392-404.
127. Jonsson, F., et al., *Neutrophils in local and systemic antibody-dependent inflammatory and anaphylactic reactions.* J Leukoc Biol, 2013. **94**(4): p. 643-56.
128. Hamaguchi, Y., et al., *Antibody isotype-specific engagement of Fcgamma receptors regulates B lymphocyte depletion during CD20 immunotherapy.* J Exp Med, 2006. **203**(3): p. 743-53.
129. Nimmerjahn, F. and J.V. Ravetch, *Antibodies, Fc receptors and cancer.* Curr Opin Immunol, 2007. **19**(2): p. 239-45.
130. Anthony, R.M., F. Wermeling, and J.V. Ravetch, *Novel roles for the IgG Fc glycan.* Ann N Y Acad Sci, 2012. **1253**: p. 170-80.
131. Goede, V., et al., *Obinutuzumab plus chlorambucil in patients with CLL and coexisting conditions.* N Engl J Med, 2014. **370**(12): p. 1101-10.
132. Bezbradica, J.S. and R. Medzhitov, *Role of ITAM signaling module in signal integration.* Curr Opin Immunol, 2012. **24**(1): p. 58-66.
133. Ravetch, J.V. and L.L. Lanier, *Immune inhibitory receptors.* Science, 2000. **290**(5489): p. 84-9.
134. Flannagan, R.S., V. Jaumouille, and S. Grinstein, *The cell biology of phagocytosis.* Annu Rev Pathol, 2012. **7**: p. 61-98.
135. Gul, N., et al., *Macrophages eliminate circulating tumor cells after monoclonal antibody therapy.* J Clin Invest, 2014.
136. Montalvao, F., et al., *The mechanism of anti-CD20-mediated B cell depletion revealed by intravital imaging.* J Clin Invest, 2013.
137. Taylor, P.R., et al., *Macrophage receptors and immune recognition.* Annu Rev Immunol, 2005. **23**: p. 901-44.
138. den Haan, J.M. and L. Martinez-Pomares, *Macrophage heterogeneity in lymphoid tissues.* Semin Immunopathol, 2013.
139. Geissmann, F., et al., *Development of monocytes, macrophages, and dendritic cells.* Science, 2010. **327**(5966): p. 656-61.
140. van Furth, R. and Z.A. Cohn, *The origin and kinetics of mononuclear phagocytes.* J Exp Med, 1968. **128**(3): p. 415-35.
141. Auffray, C., M.H. Sieweke, and F. Geissmann, *Blood monocytes: development, heterogeneity, and relationship with dendritic cells.* Annu Rev Immunol, 2009. **27**: p. 669-92.

142. Nerlov, C. and T. Graf, *PU.1 induces myeloid lineage commitment in multipotent hematopoietic progenitors.* Genes Dev, 1998. **12**(15): p. 2403-12.
143. Dai, X.M., et al., *Targeted disruption of the mouse colony-stimulating factor 1 receptor gene results in osteopetrosis, mononuclear phagocyte deficiency, increased primitive progenitor cell frequencies, and reproductive defects.* Blood, 2002. **99**(1): p. 111-20.
144. Schulz, C., et al., *A lineage of myeloid cells independent of Myb and hematopoietic stem cells.* Science, 2012. **336**(6077): p. 86-90.
145. Gomez Perdiguero, E., et al., *Tissue-resident macrophages originate from yolk-sac-derived erythro-myeloid progenitors.* Nature, 2015. **518**(7540): p. 547-51.
146. Hoeffel, G., et al., *Adult Langerhans cells derive predominantly from embryonic fetal liver monocytes with a minor contribution of yolk sac-derived macrophages.* J Exp Med, 2012. **209**(6): p. 1167-81.
147. Epelman, S., et al., *Embryonic and adult-derived resident cardiac macrophages are maintained through distinct mechanisms at steady state and during inflammation.* Immunity, 2014. **40**(1): p. 91-104.
148. Underhill, D.M. and H.S. Goodridge, *Information processing during phagocytosis.* Nat Rev Immunol, 2012. **12**(7): p. 492-502.
149. Jaumouille, V. and S. Grinstein, *Receptor mobility, the cytoskeleton, and particle binding during phagocytosis.* Curr Opin Cell Biol, 2011. **23**(1): p. 22-9.
150. Lemaitre, B., et al., *The dorsoventral regulatory gene cassette spatzle/Toll/cactus controls the potent antifungal response in Drosophila adults.* Cell, 1996. **86**(6): p. 973-83.
151. Medzhitov, R., P. Preston-Hurlburt, and C.A. Janeway, Jr., *A human homologue of the Drosophila Toll protein signals activation of adaptive immunity.* Nature, 1997. **388**(6640): p. 394-7.
152. Takeda, K. and S. Akira, *Toll-like receptors in innate immunity.* Int Immunol, 2005. **17**(1): p. 1-14.
153. Rock, K.L. and H. Kono, *The inflammatory response to cell death.* Annu Rev Pathol, 2008. **3**: p. 99-126.
154. Chen, C.J., et al., *Identification of a key pathway required for the sterile inflammatory response triggered by dying cells.* Nat Med, 2007. **13**(7): p. 851-6.
155. Scaffidi, P., T. Misteli, and M.E. Bianchi, *Release of chromatin protein HMGB1 by necrotic cells triggers inflammation.* Nature, 2002. **418**(6894): p. 191-5.
156. Kohl, J., *The role of complement in danger sensing and transmission.* Immunol Res, 2006. **34**(2): p. 157-76.
157. Shushakova, N., et al., *C5a anaphylatoxin is a major regulator of activating versus inhibitory Fc gamma Rs in immune complex-induced lung disease.* Journal of Clinical Investigation, 2002. **110**(12): p. 1823-1830.
158. Atkinson, J.P., *C5a and Fcgamma receptors: a mutual admiration society.* J Clin Invest, 2006. **116**(2): p. 304-6.
159. Hochreiter-Hufford, A. and K.S. Ravichandran, *Clearing the dead: apoptotic cell sensing, recognition, engulfment, and digestion.* Cold Spring Harb Perspect Biol, 2013. **5**(1).
160. Gregory, C.D. and J.D. Pound, *Cell death in the neighbourhood: direct microenvironmental effects of apoptosis in normal and neoplastic tissues.* Journal of Pathology, 2011. **223**(2): p. 177-194.

161. Krysko, D.V., K. D'Herde, and P. Vandenabeele, *Clearance of apoptotic and necrotic cells and its immunological consequences.* Apoptosis, 2006. **11**(10): p. 1709-1726.
162. Savill, J. and V. Fadok, *Corpse clearance defines the meaning of cell death.* Nature, 2000. **407**(6805): p. 784-8.
163. Truman, L.A., et al., *CX3CL1/fractalkine is released from apoptotic lymphocytes to stimulate macrophage chemotaxis.* Blood, 2008. **112**(13): p. 5026-36.
164. Lauber, K., et al., *Apoptotic cells induce migration of phagocytes via caspase-3-mediated release of a lipid attraction signal.* Cell, 2003. **113**(6): p. 717-30.
165. Peter, C., et al., *Migration to apoptotic "find-me" signals is mediated via the phagocyte receptor G2A.* J Biol Chem, 2008. **283**(9): p. 5296-305.
166. Elliott, M.R., et al., *Nucleotides released by apoptotic cells act as a find-me signal to promote phagocytic clearance.* Nature, 2009. **461**(7261): p. 282-6.
167. Bournazou, I., et al., *Apoptotic human cells inhibit migration of granulocytes via release of lactoferrin.* J Clin Invest, 2009. **119**(1): p. 20-32.
168. Fadok, V.A., et al., *Exposure of phosphatidylserine on the surface of apoptotic lymphocytes triggers specific recognition and removal by macrophages.* J Immunol, 1992. **148**(7): p. 2207-16.
169. Nakano, T., et al., *Cell adhesion to phosphatidylserine mediated by a product of growth arrest-specific gene 6.* J Biol Chem, 1997. **272**(47): p. 29411-4.
170. Hanayama, R., et al., *Identification of a factor that links apoptotic cells to phagocytes.* Nature, 2002. **417**(6885): p. 182-7.
171. Gardai, S.J., et al., *Cell-surface calreticulin initiates clearance of viable or apoptotic cells through trans-activation of LRP on the phagocyte.* Cell, 2005. **123**(2): p. 321-34.
172. Park, D., et al., *BAI1 is an engulfment receptor for apoptotic cells upstream of the ELMO/Dock180/Rac module.* Nature, 2007. **450**(7168): p. 430-4.
173. Kobayashi, N., et al., *TIM-1 and TIM-4 glycoproteins bind phosphatidylserine and mediate uptake of apoptotic cells.* Immunity, 2007. **27**(6): p. 927-40.
174. Elkon, K.B. and D.M. Santer, *Complement, interferon and lupus.* Curr Opin Immunol, 2012. **24**(6): p. 665-70.
175. Benoit, M.E., et al., *Complement protein C1q directs macrophage polarization and limits inflammasome activity during the uptake of apoptotic cells.* J Immunol, 2012. **188**(11): p. 5682-93.
176. Galvan, M.D., et al., *Complement component C1q regulates macrophage expression of Mer tyrosine kinase to promote clearance of apoptotic cells.* J Immunol, 2012. **188**(8): p. 3716-23.
177. Mills, C.D., et al., *M-1/M-2 macrophages and the Th1/Th2 paradigm.* J Immunol, 2000. **164**(12): p. 6166-73.
178. Mosser, D.M., *The many faces of macrophage activation.* J Leukoc Biol, 2003. **73**(2): p. 209-12.
179. Ezekowitz, R.A. and S. Gordon, *Alterations of surface properties by macrophage activation: expression of receptors for Fc and mannose-terminal glycoproteins and differentiation antigens.* Contemp Top Immunobiol, 1984. **13**: p. 33-56.

180. Dacosta, N.A. and S.G. Kinare, *Association of lung carcinoma and tuberculosis.* J Postgrad Med, 1991. **37**(4): p. 185-9.
181. Mantovani, A., et al., *Macrophage plasticity and polarization in tissue repair and remodelling.* J Pathol, 2013. **229**(2): p. 176-85.
182. Mantovani, A., et al., *The chemokine system in diverse forms of macrophage activation and polarization.* Trends Immunol, 2004. **25**(12): p. 677-86.
183. Leidi, M., et al., *M2 macrophages phagocytose rituximab-opsonized leukemic targets more efficiently than m1 cells in vitro.* J Immunol, 2009. **182**(7): p. 4415-22.
184. Stein, M., et al., *Interleukin 4 potently enhances murine macrophage mannose receptor activity: a marker of alternative immunologic macrophage activation.* J Exp Med, 1992. **176**(1): p. 287-92.
185. Sica, A. and V. Bronte, *Altered macrophage differentiation and immune dysfunction in tumor development.* J Clin Invest, 2007. **117**(5): p. 1155-66.
186. Gregory, C.D. and J.D. Pound, *Cell death in the neighbourhood: direct microenvironmental effects of apoptosis in normal and neoplastic tissues.* J Pathol, 2011. **223**(2): p. 177-94.
187. Allavena, P. and A. Mantovani, *Tumour-Associated Macrophages: undisputed stars of the inflammatory tumour micro-environment.* Clinical & Experimental Immunology, 2011: p. no-no.
188. Allavena, P. and A. Mantovani, *Immunology in the clinic review series; focus on cancer: tumour-associated macrophages: undisputed stars of the inflammatory tumour microenvironment.* Clin Exp Immunol, 2012. **167**(2): p. 195-205.
189. DeNardo, D.G., et al., *CD4(+) T cells regulate pulmonary metastasis of mammary carcinomas by enhancing protumor properties of macrophages.* Cancer Cell, 2009. **16**(2): p. 91-102.
190. Riss, J., et al., *Cancers as wounds that do not heal: differences and similarities between renal regeneration/repair and renal cell carcinoma.* Cancer Res, 2006. **66**(14): p. 7216-24.
191. Davies, L.C. and P.R. Taylor, *Tissue-resident macrophages: then and now.* Immunology, 2015. **144**(4): p. 541-8.
192. Zeisberger, S.M., et al., *Clodronate-liposome-mediated depletion of tumour-associated macrophages: a new and highly effective antiangiogenic therapy approach.* Br J Cancer, 2006. **95**(3): p. 272-81.
193. Fritz, J.M., et al., *Depletion of tumor-associated macrophages slows the growth of chemically induced mouse lung adenocarcinomas.* Front Immunol, 2014. **5**: p. 587.
194. Nimmerjahn, F. and J.V. Ravetch, *Antibodies, Fc receptors and cancer.* Current Opinion in Immunology, 2007. **19**(2): p. 239-245.
195. Nimmerjahn, F., *Fc-receptors and innate immune effector cells involved in IgG activity.* Immunology, 2011. **135**: p. 19-19.
196. Butchar, J.P., et al., *Reciprocal Regulation of Activating and Inhibitory Fc gamma Receptors by TLR7/8 Activation: Implications for Tumor Immunotherapy.* Clinical Cancer Research, 2010. **16**(7): p. 2065-2075.
197. Alas, S. and B. Bonavida, *Rituximab inactivates signal transducer and activation of transcription 3 (STAT3) activity in B-non-Hodgkin's lymphoma through inhibition of the interleukin 10 autocrine/paracrine loop and results in down-regulation of Bcl-2 and sensitization to cytotoxic drugs.* Cancer Res, 2001. **61**(13): p. 5137-44.

198. Alas, S., C. Emmanouilides, and B. Bonavida, *Inhibition of interleukin 10 by rituximab results in down-regulation of bcl-2 and sensitization of B-cell non-Hodgkin's lymphoma to apoptosis.* Clin Cancer Res, 2001. **7**(3): p. 709-23.
199. Lawlor, K.E., et al., *Bcl-2 overexpression ameliorates immune complex-mediated arthritis by altering FcgammaRIIb expression and monocyte homeostasis.* J Leukoc Biol, 2013.
200. Katzav, S., D. Martin-Zanca, and M. Barbacid, *vav, a novel human oncogene derived from a locus ubiquitously expressed in hematopoietic cells.* EMBO J, 1989. **8**(8): p. 2283-90.
201. Ogilvy, S., et al., *Constitutive Bcl-2 expression throughout the hematopoietic compartment affects multiple lineages and enhances progenitor cell survival.* Proc Natl Acad Sci U S A, 1999. **96**(26): p. 14943-8.
202. Egle, A., et al., *VavP-Bcl2 transgenic mice develop follicular lymphoma preceded by germinal center hyperplasia.* Blood, 2004. **103**(6): p. 2276-83.
203. Nilsson, J.A. and J.L. Cleveland, *Myc pathways provoking cell suicide and cancer.* Oncogene, 2003. **22**(56): p. 9007-21.
204. Harris, A.W., et al., *The E mu-myc transgenic mouse. A model for high-incidence spontaneous lymphoma and leukemia of early B cells.* J Exp Med, 1988. **167**(2): p. 353-71.
205. Adams, J.M., et al., *The c-myc oncogene driven by immunoglobulin enhancers induces lymphoid malignancy in transgenic mice.* Nature, 1985. **318**(6046): p. 533-8.
206. Michalak, E.M., et al., *Puma and to a lesser extent Noxa are suppressors of Myc-induced lymphomagenesis.* Cell Death Differ, 2009. **16**(5): p. 684-96.
207. Krysko, D.V., K. D'Herde, and P. Vandenabeele, *Clearance of apoptotic and necrotic cells and its immunological consequences.* Apoptosis, 2006. **11**(10): p. 1709-26.
208. Krysko, D.V. and P. Vandenabeele, *From regulation of dying cell engulfment to development of anti-cancer therapy.* Cell Death Differ, 2008. **15**(1): p. 29-38.
209. Taylor, P.R., et al., *A hierarchical role for classical pathway complement proteins in the clearance of apoptotic cells in vivo.* J Exp Med, 2000. **192**(3): p. 359-66.
210. Tutt, A.L., et al., *Development and Characterization of Monoclonal Antibodies Specific for Mouse and Human Fcgamma Receptors.* J Immunol, 2015. **195**(11): p. 5503-16.
211. Toomey, J.A., et al., *Cytokine requirements for the growth and development of mouse NK cells in vitro.* J Leukoc Biol, 2003. **74**(2): p. 233-42.
212. Hunt, J.S., et al., *A microplate adaptation of the solid-phase C1q immune complex assay.* J Immunol Methods, 1980. **33**(3): p. 267-75.
213. Stanilova, S.A. and E.S. Slavov, *Comparative study of circulating immune complexes quantity detection by three assays--CIF-ELISA, C1q-ELISA and anti-C3 ELISA.* J Immunol Methods, 2001. **253**(1-2): p. 13-21.
214. McLaughlin, P., et al., *Rituximab chimeric anti-CD20 monoclonal antibody therapy for relapsed indolent lymphoma: half of patients respond to a four-dose treatment program.* J Clin Oncol, 1998. **16**(8): p. 2825-33.

215. Coiffier, B., et al., *CHOP chemotherapy plus rituximab compared with CHOP alone in elderly patients with diffuse large-B-cell lymphoma.* N Engl J Med, 2002. **346**(4): p. 235-42.
216. Teeling, J.L., et al., *The biological activity of human CD20 monoclonal antibodies is linked to unique epitopes on CD20.* J Immunol, 2006. **177**(1): p. 362-71.
217. Dyer, M.J., *Safety and efficacy of ofatumumab in patients with fludarabine and alemtuzumab refractory chronic lymphocytic leukaemia.* Ther Adv Hematol, 2012. **3**(4): p. 199-207.
218. Wierda, W.G., et al., *Ofatumumab as single-agent CD20 immunotherapy in fludarabine-refractory chronic lymphocytic leukemia.* J Clin Oncol, 2010. **28**(10): p. 1749-55.
219. Mossner, E., et al., *Increasing the efficacy of CD20 antibody therapy through the engineering of a new type II anti-CD20 antibody with enhanced direct and immune effector cell-mediated B-cell cytotoxicity.* Blood, 2010. **115**(22): p. 4393-402.
220. Umana, P., et al., *Engineered glycoforms of an antineuroblastoma IgG1 with optimized antibody-dependent cellular cytotoxic activity.* Nat Biotechnol, 1999. **17**(2): p. 176-80.
221. Golay, J., et al., *Glycoengineered CD20 antibody obinutuzumab activates neutrophils and mediates phagocytosis through CD16B more efficiently than rituximab.* Blood, 2013. **122**(20): p. 3482-91.
222. Li, X., et al., *Allelic-dependent expression of an activating Fc receptor on B cells enhances humoral immune responses.* Sci Transl Med, 2013. **5**(216): p. 216ra175.
223. Cartron, G., et al., *Therapeutic activity of humanized anti-CD20 monoclonal antibody and polymorphism in IgG Fc receptor FcgammaRIIIa gene.* Blood, 2002. **99**(3): p. 754-8.
224. Gluck, W.L., et al., *Phase I studies of interleukin (IL)-2 and rituximab in B-cell non-hodgkin's lymphoma: IL-2 mediated natural killer cell expansion correlations with clinical response.* Clin Cancer Res, 2004. **10**(7): p. 2253-64.
225. Borgerding, A., et al., *B-lymphoma cells escape rituximab-triggered elimination by NK cells through increased HLA class I expression.* Exp Hematol, 2010. **38**(3): p. 213-21.
226. Kohrt, H.E., et al., *Targeting CD137 enhances the efficacy of cetuximab.* J Clin Invest, 2014. **124**(6): p. 2668-82.
227. Kohrt, H.E., et al., *CD137 stimulation enhances the antilymphoma activity of anti-CD20 antibodies.* Blood, 2011. **117**(8): p. 2423-32.
228. Houot, R., H. Kohrt, and R. Levy, *Boosting antibody-dependant cellular cytotoxicity against tumor cells with a CD137 stimulatory antibody.* Oncoimmunology, 2012. **1**(6): p. 957-958.
229. Kohrt, H.E., et al., *Anti-KIR antibody enhancement of anti-lymphoma activity of natural killer cells as monotherapy and in combination with anti-CD20 antibodies.* Blood, 2014. **123**(5): p. 678-86.
230. Albanesi, M., et al., *Neutrophils mediate antibody-induced antitumor effects in mice.* Blood, 2013. **122**(18): p. 3160-4.
231. Gong, Q., et al., *Importance of cellular microenvironment and circulatory dynamics in B cell immunotherapy.* J Immunol, 2005. **174**(2): p. 817-26.
232. Lim, S.H., et al., *Fc gamma receptor IIb on target B cells promotes rituximab internalization and reduces clinical efficacy.* Blood, 2011. **118**(9): p. 2530-40.

233. Vaughan, A.T., et al., *Inhibitory FcgammaRIIb (CD32b) becomes activated by therapeutic mAb in both cis and trans and drives internalization according to antibody specificity.* Blood, 2013.
234. Moga, E., et al., *Interleukin-15 enhances rituximab-dependent cytotoxicity against chronic lymphocytic leukemia cells and overcomes transforming growth factor beta-mediated immunosuppression.* Exp Hematol, 2011. **39**(11): p. 1064-71.
235. Chowdhury, F., et al., *Development of immunomonitoring of antibodydependent cellular cytotoxicity against neuroblastoma cells using whole blood.* Cancer Immunol Immunother, 2014. **63**(6): p. 559-69.
236. Neri, S., et al., *Calcein-acetyoxymethyl cytotoxicity assay: standardization of a method allowing additional analyses on recovered effector cells and supernatants.* Clin Diagn Lab Immunol, 2001. **8**(6): p. 1131-5.
237. Parker, A.K., et al., *Primary naive and interleukin-2-activated natural killer cells do not support efficient ectromelia virus replication.* J Gen Virol, 2008. **89**(Pt 3): p. 751-9.
238. Van Rooijen, N. and A. Sanders, *Liposome mediated depletion of macrophages: mechanism of action, preparation of liposomes and applications.* J Immunol Methods, 1994. **174**(1-2): p. 83-93.
239. Bichi, R., et al., *Human chronic lymphocytic leukemia modeled in mouse by targeted TCL1 expression.* Proc Natl Acad Sci U S A, 2002. **99**(10): p. 6955-60.
240. Taylor, R.P. and M.A. Lindorfer, *Fcgamma-receptor-mediated trogocytosis impacts mAb-based therapies: historical precedence and recent developments.* Blood, 2015. **125**(5): p. 762-6.
241. Beum, P.V., et al., *Loss of CD20 and bound CD20 antibody from opsonized B cells occurs more rapidly because of trogocytosis mediated by Fc receptor-expressing effector cells than direct internalization by the B cells.* J Immunol, 2011. **187**(6): p. 3438-47.
242. Rafiq, S., et al., *Comparative assessment of clinically utilized CD20-directed antibodies in chronic lymphocytic leukemia cells reveals divergent NK cell, monocyte, and macrophage properties.* J Immunol, 2013. **190**(6): p. 2702-11.
243. Herter, S., et al., *Preclinical activity of the type II CD20 antibody GA101 (obinutuzumab) compared with rituximab and ofatumumab in vitro and in xenograft models.* Mol Cancer Ther, 2013. **12**(10): p. 2031-42.
244. van Meerten, T., et al., *Complement-induced cell death by rituximab depends on CD20 expression level and acts complementary to antibody-dependent cellular cytotoxicity.* Clin Cancer Res, 2006. **12**(13): p. 4027-35.
245. Hirano, M., et al., *IgEb immune complexes activate macrophages through FcgammaRIV binding.* Nat Immunol, 2007. **8**(7): p. 762-71.
246. Ferrara, C., et al., *Unique carbohydrate-carbohydrate interactions are required for high affinity binding between FcgammaRIII and antibodies lacking core fucose.* Proc Natl Acad Sci U S A, 2011. **108**(31): p. 12669-74.
247. Lux, A., et al., *Impact of immune complex size and glycosylation on IgG binding to human FcgammaRs.* J Immunol, 2013. **190**(8): p. 4315-23.
248. Herter, S., et al., *Glycoengineering of therapeutic antibodies enhances monocyte/macrophage-mediated phagocytosis and cytotoxicity.* J Immunol, 2014. **192**(5): p. 2252-60.

249. Rudnicka, D., et al., *Rituximab causes a polarization of B cells that augments its therapeutic function in NK-cell-mediated antibody-dependent cellular cytotoxicity.* Blood, 2013. **121**(23): p. 4694-702.
250. Roghanian, A., et al., *Antagonistic Human FcgammaRIIB (CD32B) Antibodies Have Anti-Tumor Activity and Overcome Resistance to Antibody Therapy In Vivo.* Cancer Cell, 2015. **27**(4): p. 473-88.
251. Tipton, T.R., et al., *Antigenic modulation limits the effector cell mechanisms employed by type I anti-CD20 monoclonal antibodies.* Blood, 2015.
252. DiLillo, D.J. and J.V. Ravetch, *Differential Fc-Receptor Engagement Drives an Anti-tumor Vaccinal Effect.* Cell, 2015. **161**(5): p. 1035-45.
253. Otten, M.A., et al., *Experimental antibody therapy of liver metastases reveals functional redundancy between Fc gammaRI and Fc gammaRIV.* J Immunol, 2008. **181**(10): p. 6829-36.
254. Nimmerjahn, F. and J.V. Ravetch, *Divergent immunoglobulin g subclass activity through selective Fc receptor binding.* Science, 2005. **310**(5753): p. 1510-2.
255. Baudino, L., et al., *Differential contribution of three activating IgG Fc receptors (FcgammaRI, FcgammaRIII, and FcgammaRIV) to IgG2a- and IgG2b-induced autoimmune hemolytic anemia in mice.* J Immunol, 2008. **180**(3): p. 1948-53.
256. Biburger, M., et al., *Monocyte subsets responsible for immunoglobulin G-dependent effector functions in vivo.* Immunity, 2011. **35**(6): p. 932-44.
257. Kurlander, R.J., D.M. Ellison, and J. Hall, *The blockade of Fc receptor-mediated clearance of immune complexes in vivo by a monoclonal antibody (2.4G2) directed against Fc receptors on murine leukocytes.* J Immunol, 1984. **133**(2): p. 855-62.
258. Williams, E.L., et al., *Development and characterisation of monoclonal antibodies specific for the murine inhibitory FcgammaRIIB (CD32B).* Eur J Immunol, 2012. **42**(8): p. 2109-20.
259. White, A.L., et al., *Interaction with FcgammaRIIB is critical for the agonistic activity of anti-CD40 monoclonal antibody.* J Immunol, 2011. **187**(4): p. 1754-63.
260. Kurlander, R.J., *Blockade of Fc receptor-mediated binding to U-937 cells by murine monoclonal antibodies directed against a variety of surface antigens.* J Immunol, 1983. **131**(1): p. 140-7.
261. Strasser, A., A.W. Harris, and S. Cory, *E mu-bcl-2 transgene facilitates spontaneous transformation of early pre-B and immunoglobulin-secreting cells but not T cells.* Oncogene, 1993. **8**(1): p. 1-9.
262. Adams, J.M. and S. Cory, *The Bcl-2 apoptotic switch in cancer development and therapy.* Oncogene, 2007. **26**(9): p. 1324-37.
263. Rose, S., A. Misharin, and H. Perlman, *A novel Ly6C/Ly6G-based strategy to analyze the mouse splenic myeloid compartment.* Cytometry A, 2012. **81**(4): p. 343-50.
264. Hume, D.A. and K.P. MacDonald, *Therapeutic applications of macrophage colony-stimulating factor-1 (CSF-1) and antagonists of CSF-1 receptor (CSF-1R) signaling.* Blood, 2012. **119**(8): p. 1810-20.
265. Hume, D.A., *Differentiation and heterogeneity in the mononuclear phagocyte system.* Mucosal Immunol, 2008. **1**(6): p. 432-41.
266. Hume, D.A., *Macrophages as APC and the dendritic cell myth.* J Immunol, 2008. **181**(9): p. 5829-35.
267. Lux, A., et al., *A humanized mouse identifies the bone marrow as a niche with low therapeutic IgG activity.* Cell Rep, 2014. **7**(1): p. 236-48.

268. Strasser, A., et al., *Abnormalities of the immune system induced by dysregulated bcl-2 expression in transgenic mice.* Curr Top Microbiol Immunol, 1990. **166**: p. 175-81.
269. Spada, R., J.M. Rojas, and D.F. Barber, *Recent findings on the role of natural killer cells in the pathogenesis of systemic lupus erythematosus.* J Leukoc Biol, 2015.
270. Sciascia, S., et al., *Upcoming biological therapies in systemic lupus erythematosus.* Int Immunopharmacol, 2015.
271. Merrill, J.T., et al., *Efficacy and safety of rituximab in moderately-to-severely active systemic lupus erythematosus: the randomized, double-blind, phase II/III systemic lupus erythematosus evaluation of rituximab trial.* Arthritis Rheum, 2010. **62**(1): p. 222-33.
272. Rovin, B.H., et al., *Efficacy and safety of rituximab in patients with active proliferative lupus nephritis: the Lupus Nephritis Assessment with Rituximab study.* Arthritis Rheum, 2012. **64**(4): p. 1215-26.
273. Navarra, S.V., et al., *Efficacy and safety of belimumab in patients with active systemic lupus erythematosus: a randomised, placebo-controlled, phase 3 trial.* Lancet, 2011. **377**(9767): p. 721-31.
274. Furie, R., et al., *A phase III, randomized, placebo-controlled study of belimumab, a monoclonal antibody that inhibits B lymphocyte stimulator, in patients with systemic lupus erythematosus.* Arthritis Rheum, 2011. **63**(12): p. 3918-30.
275. Cancro, M.P., D.P. D'Cruz, and M.A. Khamashta, *The role of B lymphocyte stimulator (BLyS) in systemic lupus erythematosus.* J Clin Invest, 2009. **119**(5): p. 1066-73.
276. Ahuja, A., et al., *An acquired defect in IgG-dependent phagocytosis explains the impairment in antibody-mediated cellular depletion in Lupus.* J Immunol, 2011. **187**(7): p. 3888-94.
277. Yamada, D.H., et al., *Suppression of Fcgamma-receptor-mediated antibody effector function during persistent viral infection.* Immunity, 2015. **42**(2): p. 379-90.
278. Wieland, A., et al., *Antibody effector functions mediated by Fcgamma-receptors are compromised during persistent viral infection.* Immunity, 2015. **42**(2): p. 367-78.
279. Patel, R., et al., *IgG subclass specificity to C1q determined by surface plasmon resonance using Protein L capture technique.* Anal Biochem, 2015. **479**: p. 15-7.
280. Hughes-Jones, N.C. and B. Gardner, *Reaction between the isolated globular sub-units of the complement component C1q and IgG-complexes.* Mol Immunol, 1979. **16**(9): p. 697-701.
281. Filipe, V., et al., *Detection and characterization of subvisible aggregates of monoclonal IgG in serum.* Pharm Res, 2012. **29**(8): p. 2202-12.
282. Ahuja, A., et al., *Depletion of B cells in murine lupus: efficacy and resistance.* J Immunol, 2007. **179**(5): p. 3351-61.
283. Lux, A., et al., *The pro and anti-inflammatory activities of immunoglobulin G.* Ann Rheum Dis, 2010. **69 Suppl 1**: p. i92-96.
284. Getahun, A., et al., *IgG2a-mediated enhancement of antibody and T cell responses and its relation to inhibitory and activating Fc gamma receptors.* J Immunol, 2004. **172**(9): p. 5269-76.
285. Fukuyama, H., F. Nimmerjahn, and J.V. Ravetch, *The inhibitory Fcgamma receptor modulates autoimmunity by limiting the accumulation of immunoglobulin G+ anti-DNA plasma cells.* Nat Immunol, 2005. **6**(1): p. 99-106.

286. Sibley, L.S., et al., *ELISPOT Refinement Using Spot Morphology for Assessing Host Responses to Tuberculosis.* Cells, 2012. **1**(1): p. 5-14.
287. Bruhl, H., et al., *B-cell inhibition by cross-linking CD79b is superior to B-cell depletion with anti-CD20 antibodies in treating murine collagen-induced arthritis.* Eur J Immunol, 2015. **45**(3): p. 705-15.
288. Baruah, K., et al., *Selective deactivation of serum IgG: a general strategy for the enhancement of monoclonal antibody receptor interactions.* J Mol Biol, 2012. **420**(1-2): p. 1-7.
289. Bologna, L., et al., *Mechanism of action of type II, glycoengineered, anti-CD20 monoclonal antibody GA101 in B-chronic lymphocytic leukemia whole blood assays in comparison with rituximab and alemtuzumab.* J Immunol, 2011. **186**(6): p. 3762-9.
290. Boross, P., et al., *Both activating and inhibitory Fc gamma receptors mediate rituximab-induced trogocytosis of CD20 in mice.* Immunol Lett, 2012. **143**(1): p. 44-52.
291. Miettinen, H.M., et al., *Fc receptor endocytosis is controlled by a cytoplasmic domain determinant that actively prevents coated pit localization.* J Cell Biol, 1992. **116**(4): p. 875-88.
292. Budde, P., et al., *Tyrosine-containing sequence motifs of the human immunoglobulin G receptors FcRIIb1 and FcRIIb2 essential for endocytosis and regulation of calcium flux in B cells.* J Biol Chem, 1994. **269**(48): p. 30636-44.
293. Vaughan, A.T., et al., *Activatory and inhibitory Fcgamma receptors augment rituximab-mediated internalization of CD20 independent of signaling via the cytoplasmic domain.* J Biol Chem, 2015. **290**(9): p. 5424-37.
294. Biburger, M., I. Trenkwald, and F. Nimmerjahn, *Three blocks are not enough-Blocking of the murine IgG receptor FcgammaRIV is crucial for proper characterization of cells by FACS analysis.* Eur J Immunol, 2015.
295. Fudala, R., et al., *Anti-IL-8 autoantibody:IL-8 immune complexes suppress spontaneous apoptosis of neutrophils.* Am J Physiol Lung Cell Mol Physiol, 2007. **293**(2): p. L364-74.

Appendix

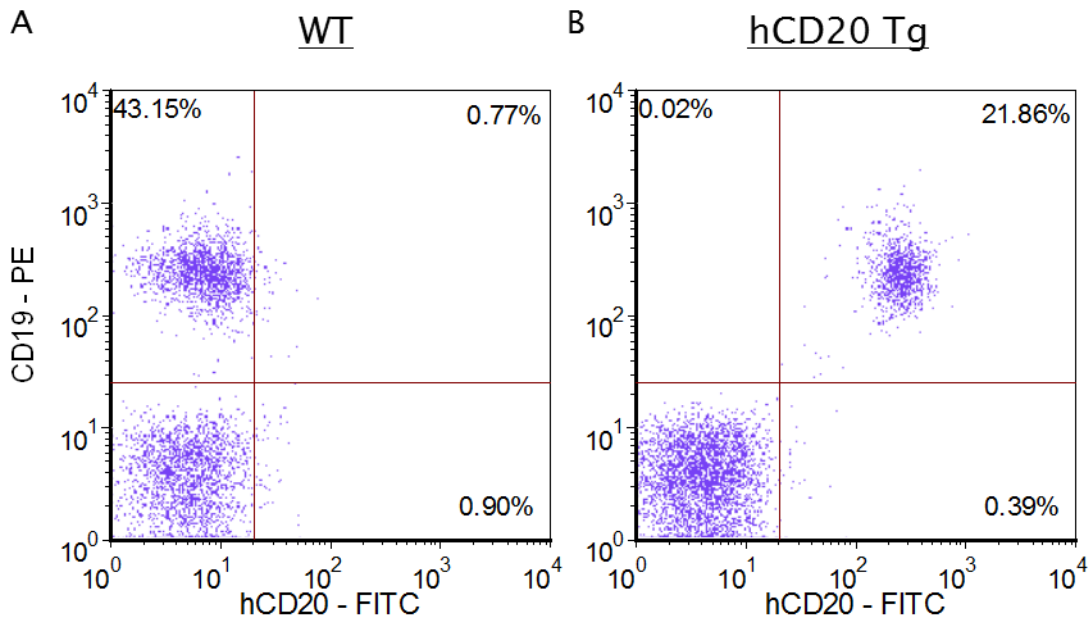

Appendix 1 Example of hCD20 Tg mouse phenotyping

Peripheral blood from hCD20, C75BL/6 mice was opsonised with anti-CD19 (1D3) and anti-human CD20 (Ritm2a) fluorescently conjugated antibodies. Following red blood cell lysis samples were acquired on a flow cytometer. WT mice were classified as being $CD19^{+}$, $CD20^{-}$ and hCD20 Tg mice were classified as $CD19^{+}$ and $CD20^{+}$.

A

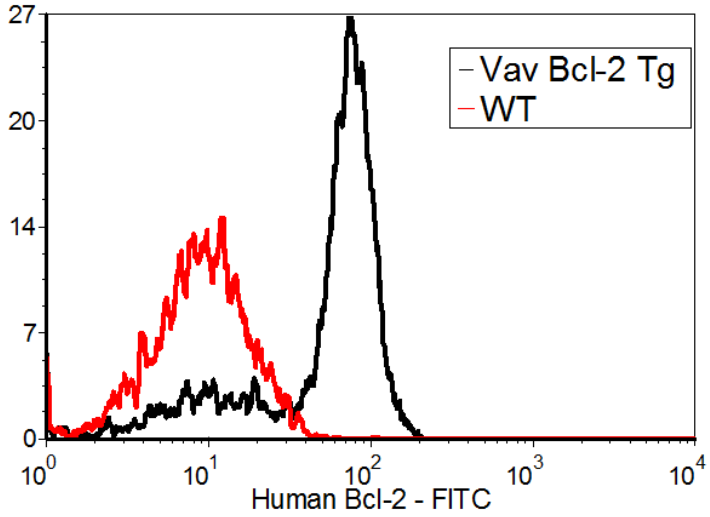

B

Cell count x10^6 cells/ml	
WT	Vav Bcl-2
~3	~12

Appendix 2 Intracellular staining for Vav Bcl-2

Peripheral blood from Vav Bcl-2 mice was fixed, permeabilised and stained with anti-human Bcl-2 conjugated to FITC. Samples were acquired on a flow cytometer and Vav Bcl-2 mice were identified as being FL-1 (FITC) positive.

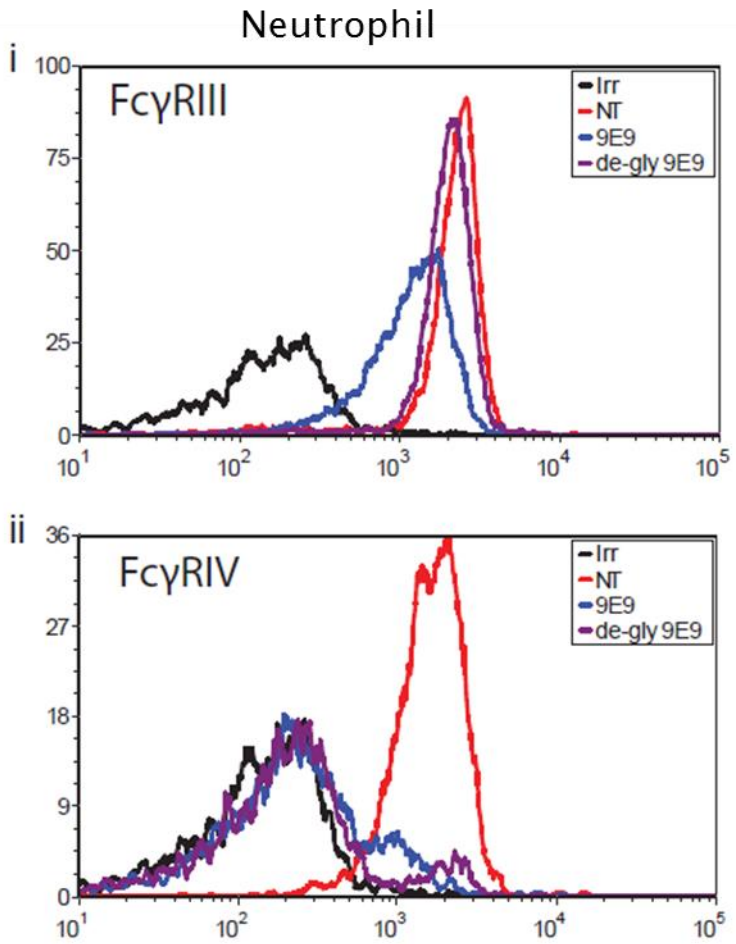

Appendix 3 Analysis of FcγR expression on neutrophils following blocking with 9E9

Representative FACS plots of FcγRIII and FcγRIV expression following *in vivo* blocking with 9E9 or deglycosylated 9E9. Mice were injected i.p. with 9E9 (400 µg). Splenocytes were obtained the following day. Neutrophils were highlighted by flow cytometry as being $CD11b^{+}$, $Ly6G^{hi}$ and $Ly6C^{int}$. Samples were additionally stained with anti- FcγRIII (AT154-2 $F(ab)_2$) or anti-FcγRIV (9E9) (10 µg/ml). Samples were acquired on a FACS Canto™ flow cytometer.

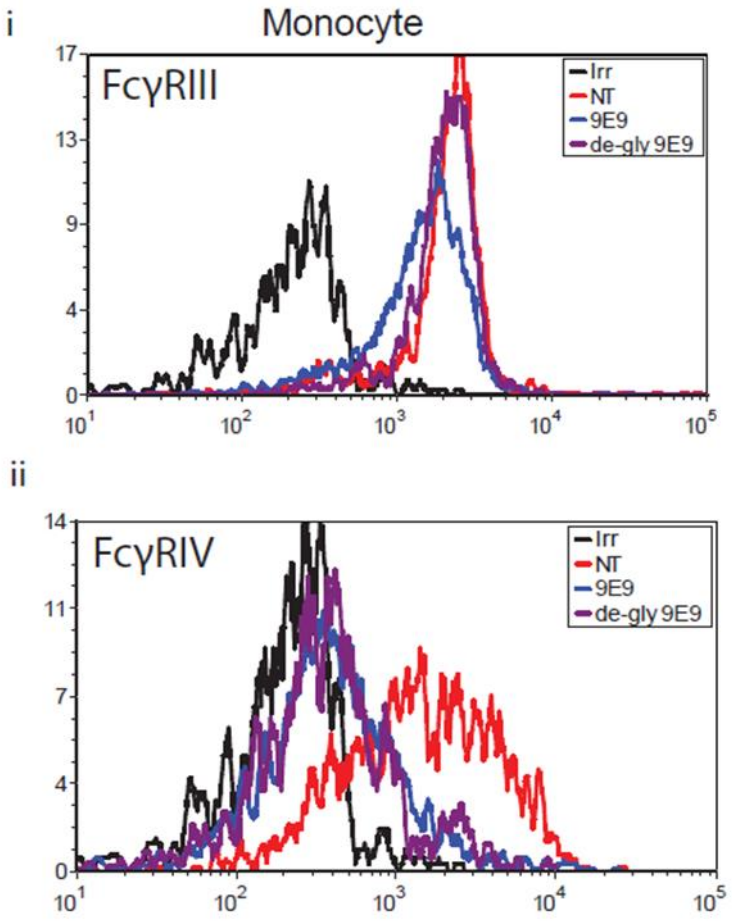

Appendix 4 Analysis of FcγR expression on neutrophils following blocking with 9E9

Representative FACS plots of FcγRIII and FcγRIV expression following *in vivo* blocking with 9E9 or deglycosylated 9E9. Mice were injected i.p. with 9E9 (400 µg). Splenocytes were obtained the following day. Monocytes were highlighted by flow cytometry as being $CD11b^{+}$, $Ly6G^{int}$ and $Ly6C^{hi}$. Samples were additionally stained with anti- FcγRIII (AT154-2 $F(ab)_2$) or anti-FcγRIV (9E9) (10 µg/ml). Samples were acquired on a FACS Canto™ flow cytometer.

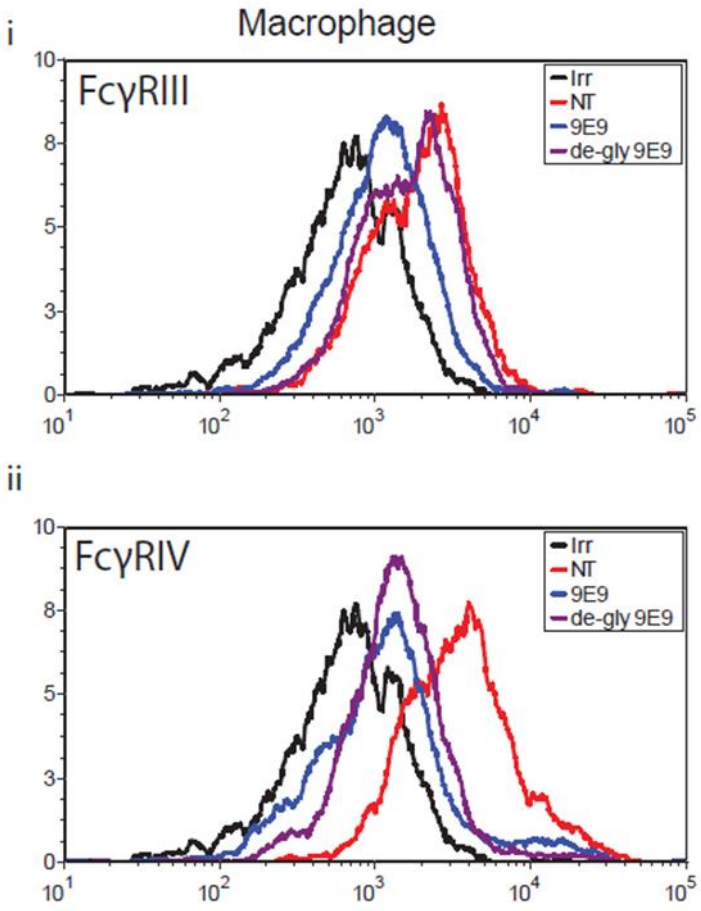

Appendix 5 Analysis of FcγR expression on neutrophils following blocking with 9E9

Representative FACS plots of FcγRIII and FcγRIV expression following *in vivo* blocking with 9E9 or deglycosylated 9E9. Mice were injected i.p. with 9E9 (400 µg). Splenocytes were obtained the following day. Macrophages were highlighted by flow cytometry as being $CD11b^{+}$, $F4/80^{hi}$. Samples were additionally stained with anti- FcγRIII (AT154-2 $F(ab)_2$) or anti-FcγRIV (9E9) (10 µg/ml). Samples were acquired on a FACS Canto™ flow cytometer.

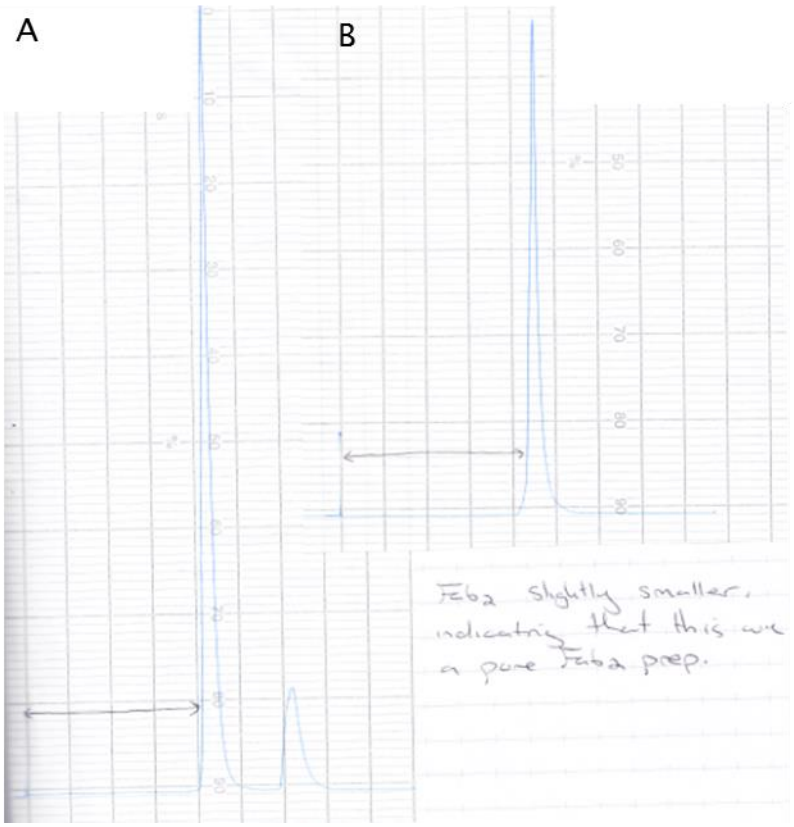

Appendix 6 HPLC analysis of 2.4G2 whole IgG and F(ab)$_2$

(**A**) HPLC analysis of 2.4G2 antibody. (**B**) HPLC analysis of 2.4G2 F(ab)$_2$. F(ab)$_2$ antibody has a slightly smaller size compared to whole IgG and so will come off the column slightly later.